

# **Mechanobiology of Adipocytes**

Anabela Ceba Areias

Supervised by Dr. Darryl Overby

Thesis submitted in fulfillment of the requirements for the award of Doctor  
of Philosophy and the Diploma of the Imperial College.

Department of Bioengineering

June 2019



## Abstract

The expansion of visceral adipose tissue (VAT) is considered to be the most life-threatening form of obesity. It is highly correlated with the risk of developing metabolic complications such as type 2 diabetes, cardiovascular diseases and hypertriglyceridemia. VAT is confined in the abdominal space where it experiences compressive stresses. Here we hypothesise that these compressive stresses act as a mechanoregulatory mechanism to inhibit further increase of intracellular lipids and consequently control visceral adiposity. Furthermore, we hypothesise that in obesity such feedback is disrupted due to an excessive increase of adipocyte size and compressive stress.

To test this hypothesis, we engineered a 3D adipose tissue model comprising of a collagen scaffold seeded with 3T3-L1 adipocytes. This model was subjected to compressive stress under static load. We validated that this engineered tissue withstands different loads, resulting in different levels of compression. We found a decrease of intracellular lipid content in a load-dependent manner, suggesting an increased lipolytic rate. This was associated with strong activation of the ERK pathway, that in turn activates important lipases, such as adipose triglyceride lipase (ATGL) and the hormone-sensitive lipase (HSL). Finally, overexpression of cavin-1 after compression suggests an altered adipocyte metabolism.

We then investigated how adipocyte hypertrophy influences the effectiveness of this mechanical sensing. We found that 3T3-L1 adipocytes treated with a fatty acid cocktail resulted in an opposite response to the compression, inhibiting the HSL activity. In line with these *in vitro* results, compression of the gonadal fat in overweight mice also led to an inhibition of the HSL activity.

Taken together our results indicate that compressive stress acts as a catalyst for lipolysis in normal adipocytes, suggesting a homeostatic feedback mechanism which prevents further adipocyte expansion. However, in overweight animals, compressive stress appears to deactivate the lipolysis, disrupting the proposed feedback mechanism. **(Word count: 297)**



Não sou nada.

Nunca serei nada.

Não posso querer ser nada.

À parte isso, tenho em mim todos os sonhos do mundo.

**Àlvaro de Campos, 15-01-1928**

Pseudonym of Fernando Pessoa



**To my grandmother**, for all her secret smiles looking at me, showing in silence that she was always proud of me.

**To my mum**, for all her support in every second since I arrived to London.

**To my dad**, for showing me the beauty of our nature. To teach me that within the forest, I could find myself.

**To Jacopo**, for all his patience and especially for his love.





## Acknowledgments

I would like to express my sincere gratitude to Dr. Darryl Overby for all his support since the start of this long journey. I would like to thank him for trusting me to start this new research line and for always being so positive towards new ideas and projects. I will bring with me not only his scientific advice, but also all energetic and creative moments that served as true inspiration to me.

My special thanks also go to,

Dr. Victoria Salem and Professor Kevin Murphy for their collaboration and support. It has been a great pleasure to learn with them. To Dr. Cristoforo Silvestri for his support throughout the investigation.

Dr. Tristan Rodriguez and his laboratory, especially to Dr. Ana Lima, Dr. Aida Pena and Dr. Salvador Montero. They all made me to feel as part of their group since the first day I asked their collaboration. A special thank you to Ana, not only for being a sister for me in London, but also for her enormous support. I will never forget the crazy hours working side by side, the moments when we discussed the science for hours... the pringles timeouts, when one of us failed an experiment and the expression 'isso e vida!'. Thank you Nokas!

Professor Molly Stevens and her group, for allowing me to use their facilities. A special thanks to Dr. Jennifer Puetzer for teaching me the hydrogel technique and to Dr. Lucia Mass, Liliana Brito and Maria Cruz for their friendship and support.

To all the Bioengineering staff, especially to Britta Ross for her help throughout the past years. I would also like to thank the FILM facility and flow cytometry staff, especially Jane Srivastava and Steve Rothery.

To my dear colleagues from the Overby laboratory for their positive spirit all the time and

for being a little family in London. Dr. Ester Reina thank you for bringing the peace and serenity to the office, for not letting me forget my Spanish and for sharing the Iberic spirit with me. To Dr. Michael Madekurozwa, for his kindness, friendship, knowledge, company... for everything! To Dr. Pei-Jung for her positive and genuine spirit. To Jack Bertrand, for all his companionship in the laboratory and hilarious discussions during the Friday drinks. To Alice Spenlehauer, for her sincere friendship and for being a great colleague along all these years. Thank you for the amazing moments we spent together inside and outside of the laboratory. For all our crazy dances, bagel times, karaokes and trips. We grew together during these years, and I was super lucky to have shared them with you. To Dr. Jason Chang for all the enormous support on the beginning of my PhD and for showing me London and for being the best sport mate. I would like to thank our adopted Overby member Dr. Anna Stejskalová for being the best housemate and for sharing the love for tissue engineering with me.

I would also like to thank my friends Joana de Rosa, Margarida Martins and Mariana Roriz for bringing me a bit of Esposende everyday. To Monica Marinho and Rita Pacheco for their unconditional love and for being always so proud of me. To my dear nephew Artur Esteven for making my days more colourful since he is born. To Raquel Neves, Marilia Nunes, Dr. Rita Nogueira, Dr. Iliona Wolfowicz and Pedro Sousa for being close to me. To Professor Senentxu Lanceros-Mendez for being such a great friend and mentor in my scientific life, since the moment I started my path in research. To the group of Caminhar em Antas for their amazing company during the months of my recover. To Hilde and Salvatore for all cheerfully moments along this journey.

I would also to thank my dear siblings Tiago and Mara for being the joy of my life. To Matilde and Carolina for being such rocking step-sisters. To Cristina for her never-ending support. To my lovely step-father for being a second father to me. Last but not least, I would like to thank my amazing mother and father as well as my dear future husband for trusting me and making this stage of my life possible.

## **Contribution Statement**

**Chapter 1** Dr. Pei-Jung Wu helped with the rheometry measurements. Ms. Ana Lima taught me the Western blot techniques. Dr. Jennifer Puetzer taught me how to prepare the collagen hydrogels.

**Chapter 3** Dr. Victoria Salem conducted the animal work. Dr. Michael Madekurozwa helped me to create the *in vivo* compression device.

**Appendix A** Dr. Bono helped with the simulations, and specifically with the analytical solution and force calculations.

## **Declarations**

\*Declaration of originality

I, Anabela Cepa Areias, declare that the studies presented in this thesis were originated by me, performed in Dr. Overby's laboratory between 2014 and 2019. Data acquired in collaborators laboratory have been referenced in the Contribution Statement section as well as contributions by other researchers. I certify that this thesis complies with copyright laws and does not contain any instance of plagiarism.

### **Copyright Declaration**

The copyright of this thesis rests with the author. Unless otherwise indicated, its contents are licensed under a Creative Commons Attribution-Non Commercial 4.0 International Licence (CC BY-NC). Under this licence, you may copy and redistribute the material in any medium or format. You may also create and distribute modified versions of the work. This is on the condition that: you credit the author and do not use it, or any derivative works, for a commercial purpose. When reusing or sharing this work, ensure you make the licence terms clear to others by naming the licence and linking to the licence text. Where a work has been adapted, you should indicate that the work has been changed and describe those changes. Please seek permission from the copyright holder for uses of this work that are not included in this licence or permitted under UK Copyright Law.

## Associated Publications

### Conference Presentations

#### *Podium Presentations*

Areias AC, Silvestri C, Overby DR (2018). "Effects of static compression on lipid accumulation and gene expression in 3T3-L1 adipocytes." *8th World Congress of Biomechanics*, Dublin, Ireland

#### *Poster Presentations*

Areias AC, Silvestri C, Overby DR (2016). "The Role of Compressive Load on Adipogenic Differentiation of 3T3-L1 Cells." *American Society of Cell Biology*, San Francisco, USA

Areias AC, Silvestri C, Overby DR (2017). "The Role of Compressive Load on Adipogenic Differentiation of 3T3-L1 Cells." *24th European Congress on Obesity*, Porto, Portugal



# Contents

<b>List of Figures</b>	<b>21</b>
<b>List of Tables</b>	<b>25</b>
<b>1 Introduction, Specific Aims and Background</b>	<b>31</b>
1.1 Introduction . . . . .	32
1.2 Specific aims . . . . .	33
1.3 Background . . . . .	35
1.3.1 Adipose depots and functions . . . . .	37
1.3.1.1 White adipose tissue . . . . .	39
1.3.1.2 Brown adipose tissue . . . . .	41
1.3.1.3 Beige adipose tissue . . . . .	41
1.3.2 Adipose tissue structure and microenvironment . . . . .	41
1.3.3 Adipose tissue expansion . . . . .	44
1.3.3.1 Hypertrophy . . . . .	44
1.3.3.2 Hyperplasia . . . . .	45
1.3.4 Adipogenesis . . . . .	46
1.3.5 Regulation of adipocyte size . . . . .	49
1.3.5.1 Lipogenesis . . . . .	50
1.3.5.2 Lipolysis . . . . .	51

1.3.6	Adipose tissue adaptation in response to obesity . . . . .	54
1.3.7	Relation between BMI and intra-abdominal pressure . . . . .	56
1.3.8	Mechanical forces controlling adipose tissue fate and function . . .	57
1.3.8.1	Tension studies . . . . .	59
1.3.8.2	Compression . . . . .	61
<b>2</b>	<b>3D <i>in vitro</i> model for static compression and main methods</b>	<b>65</b>
2.1	Introduction . . . . .	66
2.2	Materials and Methods . . . . .	68
2.2.1	Experimental design . . . . .	68
2.2.2	Cell culture . . . . .	68
2.2.2.1	3T3-L1 pre-adipocytes . . . . .	68
2.2.2.2	Adipogenic differentiation . . . . .	69
2.2.3	Cell-seeded collagen type I hydrogels . . . . .	69
2.2.3.1	Extraction and purification of rat tail collagen . . . . .	69
2.2.3.2	Hydrogel preparation . . . . .	71
2.2.4	Static compression . . . . .	71
2.2.4.1	Weights . . . . .	71
2.2.4.2	Region of interest . . . . .	74
2.2.4.3	Sample retrieval . . . . .	74
2.2.5	Quantification of strains . . . . .	74
2.2.5.1	Hydrogel deformation . . . . .	74
2.2.5.2	Cell deformation . . . . .	75
2.2.6	Immunofluorescence . . . . .	75
2.2.7	Protein quantification . . . . .	76
2.2.8	Gene Expression, RT-qPCR . . . . .	77



2.2.9	Lipid quantification by flow cytometry . . . . .	78
2.2.10	Cell Viability . . . . .	79
2.2.11	Statistical analysis . . . . .	80
2.3	Results . . . . .	81
2.3.1	Adipogenic differentiation of 3T3-L1 in 3D collagen hydrogels . . .	81
2.3.2	Deformation . . . . .	85
2.3.2.1	Hydrogel deformation . . . . .	85
2.3.2.2	Cell deformation in response to the static load . . . . .	86
2.3.3	Cell viability in response to static load . . . . .	88
2.4	Discussion . . . . .	92
<b>3</b>	<b>Effect of static compression on the lipid accumulation in adipocytes: 3D <i>in vitro</i> model</b>	<b>97</b>
3.1	Introduction . . . . .	98
3.2	Materials and Methods . . . . .	100
3.2.1	Experimental design and timeline . . . . .	100
3.2.2	Lipid quantification by flow cytometry . . . . .	101
3.2.3	Quantification of the surface area of adipocytes . . . . .	101
3.2.4	Protein expression . . . . .	101
3.2.5	Pathway Inhibitors . . . . .	102
3.2.6	Methyl- $\beta$ -cyclodextrin treatment . . . . .	102
3.2.7	Immunofluorescence . . . . .	103
3.3	Results . . . . .	103
3.3.1	Lipolysis is load-dependent under static compression . . . . .	103
3.3.2	Compression activates lipolytic players . . . . .	107
3.3.2.1	First step of lipolysis - ATGL . . . . .	108
3.3.2.2	Second step of lipolysis - HSL . . . . .	109

3.3.2.3	Effect of H89 and U0126 on ATGL protein expression. . . . .	117
3.3.3	Caveolae as sensors of compression . . . . .	117
3.4	Discussion . . . . .	123
<b>4</b>	<b>Effect of compression on lipolysis in adipocytes treated with fatty acids and in overweight animals</b>	<b>129</b>
4.1	Introduction . . . . .	130
4.2	Materials and Methods . . . . .	131
4.2.1	Cell culture . . . . .	131
4.2.2	Fatty acid treatment . . . . .	132
4.2.3	Lipid quantification . . . . .	132
4.2.4	Design of the compression device . . . . .	132
4.2.4.1	Animal Work . . . . .	134
4.2.5	Protein expression . . . . .	135
4.2.5.1	Statistical analysis . . . . .	135
4.3	Results . . . . .	135
4.3.1	Fatty acids treatment . . . . .	135
4.3.2	Attenuation of load-stimulated HSL activity . . . . .	136
4.3.3	Viability markers . . . . .	140
4.4	Discussion . . . . .	141
<b>5</b>	<b>Conclusions and Future Work</b>	<b>145</b>
5.1	Conclusions . . . . .	146
5.2	Future Work . . . . .	148
<b>6</b>	<b>Bibliography</b>	<b>153</b>
<b>7</b>	<b>Supplementary Information</b>	<b>169</b>

7.1	Supplementary Information Chapter 2 . . . . .	170
7.2	Supplementary Information Chapter 3 . . . . .	173
7.3	Supplementary Information Chapter 4 . . . . .	175
<b>A</b>	<b>Finite Element Model</b>	<b>181</b>
A.1	Rheological experiments . . . . .	182
A.2	Finite element analysis . . . . .	185
<b>B</b>	<b>Western-blots chapter 3</b>	<b>195</b>
<b>C</b>	<b>Permissions</b>	<b>227</b>



# List of Figures

1.1	Scientific publication and prevalence of obesity in the last years. . . . .	35
1.2	Obesity phenotypes and related pathologies. . . . .	36
1.3	Development of WAT and BAT depots. . . . .	39
1.4	AT depots distributions between humans and mice. . . . .	40
1.5	Adipose tissue morphology. . . . .	42
1.6	Modes of adipose tissue expansion. . . . .	44
1.7	Activation of lipolysis. . . . .	53
1.8	Mechanotransduction, extrinsic and intrinsic forces. . . . .	58
1.9	Cell stretching apparatus developed by Tanabe and Nakayama [2004] and Shoham et al. [2012]. . . . .	60
1.10	Compression apparatus in 2-dimensional cultures. . . . .	62
1.11	Mechanical compression of a hybrid decellularized tissue and peptite hydrogel developed by Pellegrinelli et al. [2014]. . . . .	63
2.1	Schematic representation of the adipogenesis timeline for 2D and 3D cultures.	69
2.2	Schematic representation of collagen extraction procedure. . . . .	70
2.3	Representation of the different loads and their corresponding mass, force and stress. . . . .	73
2.4	Schematic representation of the model. . . . .	73
2.5	3T3-L1 pre-adipocyte adipogenic differentiation in two and three-dimensional cultures. . . . .	82
2.6	mRNA levels of PPAR $\gamma$ and CEBP1 in two and three-dimensional cultures.	82

2.7	Cellular morphology during adipogenesis in two and three dimensional cultures. . . . .	84
2.8	Adipocyte functional proteins. . . . .	85
2.9	Hydrogel deformation. . . . .	86
2.10	Cell deformation in response to static compression. . . . .	87
2.11	Cell viability in response to the static compression. . . . .	90
2.12	Apoptosis and hypoxia markers. . . . .	91
3.1	Protocol timeline. . . . .	100
3.2	Schematic representation of the pathway inhibitors. . . . .	102
3.3	Lipid accumulation is affected by static mechanical compression. . . . .	106
3.4	Static mechanical compression decreases cell diameter. . . . .	107
3.5	Enhanced expression of ATGL in response to the load. . . . .	108
3.6	Expression of total HSL in response to the load. . . . .	109
3.7	Activity of HSL mediated by the AMPK phosphorylation site. . . . .	111
3.8	Activity of HSL mediated by PKA phosphorylation sites. . . . .	113
3.9	Activity of HSL mediated by ERK phosphorylation sites. . . . .	116
3.10	Effect of PKA and ERK inhibitors on load-mediated ATGL overexpression. . . . .	117
3.11	Decreased lipid content upon M $\beta$ CD treatment. . . . .	119
3.12	Increased PTRF protein expression and its nuclear translocation upon mechanical stimulation. . . . .	122
3.13	Proposed interactions between mechanical stimulation and decreased lipid content. . . . .	127
4.1	Schematic representation of the <i>in vitro</i> protocol. . . . .	132
4.2	Schematic representation of the <i>in vivo</i> protocol. . . . .	133
4.3	Effects of FA treatment on lipid content. . . . .	136
4.4	Effects of FA treatment on HSL activity. . . . .	137

4.5	Compression of gonadal fat leads to a decrease of HSL activity. . . . .	139
4.6	Results summary. . . . .	140
4.7	Cell apoptosis markers. . . . .	140
5.1	Hypothesis. . . . .	148
S1	LDH standard curve for 2D and 3D cultures. . . . .	170
S2	3D projections of adipocytes at day 8 in both 2D and 3D cultures. . . . .	171
S3	Full-length Western blot figures. . . . .	172
S4	Lipid accumulation is affected by static mechanical compression - 2nd data set. . . . .	173
S5	Effects of collagen concentration on lipid accumulation. . . . .	173
S6	Overtime protein expression of phosphorylated ribosomal S6 in loaded samples. . . . .	174
S7	Overtime protein expression of phospho-AMPK in loaded samples. . . . .	174
S8	Compression device drawings. . . . .	175
S9	Full-length Western blot figures, 30 seconds. . . . .	176
S10	Full-length Western blot figures, 10 seconds and 1 minute. . . . .	177
S11	Full-length Western blot figures, 1 and 10 seconds. . . . .	178
S12	Full-length Western blot figures, 3 minutes. . . . .	179
A.1	Strain and frequency sweep for the collagen type I hydrogel. . . . .	183
A.2	Storage modulus in function of collagen concentration. . . . .	185
A.3	Cross section of the simulated hydrogel. . . . .	187
A.4	Mesh convergence. . . . .	187
A.5	Relation between force and displacement. . . . .	189
A.6	Mean stress and strain in the ROI. . . . .	191
A.7	Stress and strain distributions in the ROI. . . . .	193





# List of Tables

1.1	Classification according to body mass index (BMI). . . . .	36
1.2	Adipocyte sizes in developing and adult humans versus in vitro culture. . .	54
1.3	Comparison of IAP among the different weight groups. . . . .	56
1.4	<b>Tension studies.</b> Studies evaluating the effect of tension on adipogenesis and lipid accumulation of adipocytes. . . . .	61
1.5	<b>Compression studies.</b> Studies evaluating the effect of compression on adipogenesis and lipid accumulation of adipocytes. . . . .	63
2.1	Experimental goals to establish the 3D compression model. . . . .	68
2.2	Oligonucleotide primers used for RT-qPCR analysis. . . . .	78



## List of Acronyms

<b>ACC</b>	Acetyl-CoA carboxylase
<b>ACS</b>	Acyl-CoA synthetases
<b>AKT</b>	Protein kinase B
<b>AMP</b>	Adenosine monophosphate
<b>AMPK</b>	5' AMP-activated protein kinase
<b>AT</b>	Adipose Tissue
<b>ATGL</b>	Adipose triglyceride lipase
<b>BAT</b>	Brown Adipose Tissue
<b>BMI</b>	Body mass index
<b>BMP</b>	Bone morphogenetic protein
<b>BSA</b>	Bovine serum albumin
<b>C/EBP</b>	CCAAT/enhancer binding protein
<b>CD36</b>	Fatty acid translocase
<b>CDC</b>	Centers for Disease Control and Prevention
<b>CGI58</b>	Comparative gene identification-58
<b>ChREBP</b>	Carbohydrate response element binding protein
<b>CIDEC</b>	Cell Death Inducing DFFA Like Effector C
<b>DAPI</b>	4-6-diamidino-2-phenylindole
<b>DGAT</b>	Diacylglycerol O-acyltransferase
<b>DMEM</b>	Dulbecco's Modified Eagle Medium
<b>DNA</b>	Deoxyribonucleic acid
<b>DNL</b>	<i>de novo</i> lipogenesis
<b>ECM</b>	Extracellular matrix
<b>EDTA</b>	Ethylenediaminetetraacetic acid
<b>ER</b>	Endoplasmatic reticulum
<b>ERK</b>	Extracellular signal-regulated kinases
<b>EthD-1</b>	Ethidium homodimer-1
<b>FA</b>	Fatty acids
<b>FAS</b>	Fatty acid synthase
<b>FATP</b>	Fatty acid binding and transport proteins
<b>FFA</b>	Free fatty acids
<b>FOXOs</b>	Forkhead proteins
<b>Fsp27</b>	Fat-specific protein 27
<b>HBSS</b>	Hank's Balanced Salt Solution
<b>HEPES</b>	4-(2-hydroxyethyl)-1-piperazineethanesulfonic acid

<b>HIF1<math>\alpha</math></b>	Hypoxia inducible factor 1 $\alpha$
<b>HPRT</b>	Hypoxanthine-guanine phosphoribosyltransferase
<b>hr</b>	hours
<b>HSL</b>	Hormone-sensitive lipase
<b>IAH</b>	Intra-abdominal hypertension
<b>IAP</b>	Intra-abdominal pressure
<b>IBMX</b>	3-isobutyl-1-methylxanthine
<b>IRS</b>	Insulin receptor substrate
<b>KLF5</b>	Kruppel like factor 5
<b>LD</b>	Lipid droplet
<b>LDH</b>	Lactate dehydrogenase
<b>LPL</b>	Lipoprotein lipase
<b>MAPK</b>	Mitogen-activated protein kinases
<b>MCP-1</b>	Monocyte chemoattractant protein-1
<b>MEK</b>	Mitogen-activated protein kinase kinase
<b>MEM</b>	Minimum Essential Medium
<b>MGL</b>	Monoacylglycerol lipase
<b>min</b>	minutes
<b>MMP</b>	Matrix metalloproteinases
<b>MSCs</b>	Mesenchymal stem cells
<b>mTOR</b>	Mammalian target of rapamycin
<b>NaOH</b>	Sodium hydroxide
<b>OXPHOS</b>	Oxidative Phosphorylation
<b>PARP</b>	Poly-ADP ribose polymerase
<b>PBS</b>	Phosphate buffered saline solution
<b>PDGFR</b>	Platelet derived growth factor receptor- $\alpha$ -positive cells
<b>PET</b>	Polyethylene terephthalate
<b>PFA</b>	Paraformaldehyde
<b>PI3K</b>	Phosphoinositide 3-kinases
<b>PPAR<math>\gamma</math></b>	Proliferator-activated receptor $\gamma$
<b>PRDM16</b>	PR domain containing 16
<b>PTRF</b>	Polymerase I and transcript release factor
<b>RNA</b>	Ribonucleic acid
<b>ROI</b>	Region of interest
<b>SAT</b>	Subcutaneous Adipose Tissue
<b>SE</b>	Sterol ester
<b>SREBP1c</b>	Sterol response element binding protein 1c
<b>TAG</b>	Triacylglycerols

<b>TNF-<math>\alpha</math></b>	Tumor necrosis factor $\alpha$
<b>TNF-<math>\beta</math></b>	Tumor necrosis factor $\beta$
<b>UCP-1</b>	Uncoupling protein-1
<b>VAT</b>	Visceral Adipose Tissue
<b>WAT</b>	White Adipose Tissue
<b>WNT</b>	Wingless integrated signalling
<b>ZFP</b>	Zinc finger proteins



# **Chapter 1**

## **Introduction, Specific Aims and Background**

## 1.1 Introduction

Obesity is a condition that affects 1 in 4 adults and 1 in 5 children in the UK ([www.nhs.uk](http://www.nhs.uk)). Generally, it results from an imbalance between low energy expenditure and excessive intake of calories (in particular fatty and sugary foods). This consequently leads to an abnormal or excessive fat accumulation in the white adipose tissue, either in the visceral and/or in subcutaneous depot. While subcutaneous adiposity is considered a healthy form of obesity, visceral adiposity is highly correlated with the risk of developing metabolic complications [Chouchani and Kajimura, 2019; Kwon et al., 2017]. The underlying mechanisms of such dysfunctions remain incompletely understood.

Increased adiposity results from an increased size or number of adipocytes. In adipocytes, the cell size is dictated by the accumulation of intracellular lipids. In lean individuals adipocyte size varies between 45 to 110  $\mu\text{m}$  diameter, whereas in obesity it almost doubles (ranging from 90 to 200  $\mu\text{m}$  diameter) [Pope et al., 2016]. This increase in volume is reflected in an increase in intra-abdominal pressure, which ranges from 0-7 mmHg in healthy individuals to 7-17 mmHg in obese [De Keulenaer et al., 2012]. Because, visceral adipocytes are confined within the abdominal cavity, they are exposed to compressive stresses that can vary depending on the level of adiposity of this tissue.

It is well established that pre-adipocytes and adipocytes are mechano-responsive. For example, adipocytes can sense their own size and consequently tune their cellular response, such as insulin signalling [Zhang et al., 2017]. It is therefore plausible to think that adipocytes within the cavity continuously sense compressive stresses which may regulate their size. Understanding the role of compressive stress in adipocyte function, such as lipolysis, could allow us to develop new strategies to combat obesity.



## Motivation of thesis

In our work, we propose that compressive stress acts as a feedback mechanism to further inhibit increase of adiposity within the abdominal compartment. In particular, **we hypothesise that adipocyte lipid metabolism, specifically lipolysis, is affected by compressive stress.** We believe that the interaction between compressive stress and lipid metabolism can regulate the adipocyte size. Therefore, the main goal of this thesis is to better understand the effect of compression on the lipid metabolism of adipocytes. We further formulated our strategy in the following three specific aims.

## 1.2 Specific aims

**Specific Aim 1: To engineer a static compression model of adipose tissue.** So far, the majority of the studies on mechanobiology of adipocytes have been conducted in two-dimensions. However, adipocytes are within a microenvironment composed by a three-dimensional network of extracellular fibers. Here, we aim to engineer a three dimensional microenvironment for adipocyte differentiation and maintenance, on which we can apply different levels of compression within a physiological range. To achieve this, we propose a combination of collagen scaffolds cultured with 3T3-L1 adipocytes, subjected to a range of static loads providing different strains to the mature adipocytes.

**Specific Aim 2: To determine the effects of compression on lipolysis in adipocytes.** We hypothesise that visceral adipocytes can sense the static compressive stress, in turn regulating the lipid metabolism. More specifically, we hypothesise that this type of stress inhibits further increase in lipid content by promoting lipolysis. To test this, we propose to mechanically stimulate mature adipocytes for different periods by using the system described in specific aim 1. We then plan to evaluate the effect of compression on the intracellular lipid accumulation. We also aim to investigate which cellular pathways are involved in the transduction of the compressive stimulus. For this, we plan to analyse the role of key lipolytic players

such as ATGL and HSL. Finally, since the plasma membrane of adipocytes contains a large amount of caveolae structures, we aim to investigate the involvement of caveolae.

**Specific Aim 3: To analyse the effects of compression on lipolysis in enlarged adipocytes.**

Obesity is characterised by a dysfunction of the lipid metabolism [Arner and Rydén, 2015; Chan et al., 2004]. Increased compressive stress as well as an increased adipocyte size may play a role in this dysfunction. Here we aim to study the effect of increased cell size. To test this we developed two approaches: (i) to investigate the effects of static compression on enlarge mature adipocytes *in vitro*; (ii) to investigate the effects of static compression on visceral fat pads of overweight mice.

### 1.3 Background

Adipose tissue (AT) has gained an increased interest due to a global rise in obesity. Supporting this is the sharp growth of the number of publications about obesity since 2000 (**Fig. 1.1a**). Obesity is a condition where a disproportionate ratio of body weight for height occurs as a result of an excessive accumulation of AT. This is usually accompanied by mild, chronic and systemic inflammation [González-Muniesa et al., 2017]. It is considered the 21st century epidemic, since the percentage of obese people has tripled since 1975 (**Fig. 1.1b**) [Abarca-Gómez, 2017; Han and Lean, 2016]. In 2016, the Centers for Disease Control and Prevention (CDC) in United States of America reported that approximately 40% of the adult population were overweight or obese ([www.cdc.gov/nchs/data/databriefs/db288.pdf](http://www.cdc.gov/nchs/data/databriefs/db288.pdf)) [Luong et al., 2019]. Furthermore, the projections indicate that the increase of the prevalence of the disease will not slow down [Abarca-Gómez, 2017].

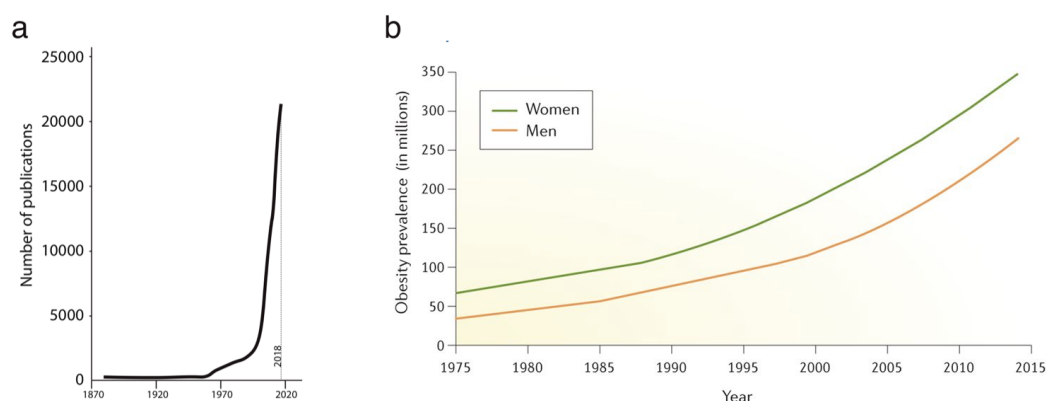


Figure 1.1: . **Scientific publication and prevalence of obesity in the last years.** (a) Number of scientific publications from 1870 to 2018 based on the pubmed data base for the word 'obesity'. (b) Global prevalence of obesity in woman and men since 1975. Figure reproduced with permission from [González-Muniesa et al., 2017].

To recognise whether someone is obese or not, the most simple method, but not very accurate, is to measure the patient's body mass index (BMI). The World Health Organisation classifies BMI as shown in **Table 1.1** [González-Muniesa et al., 2017].

BMI (kg/m <sup>2</sup> )	Classification
18.5 to 25	Normal
25 to 30	Overweight
30 to 40	Obese
≥ 40	Extremely obese

Table 1.1: Classification according to body mass index (BMI).

There are two obesity phenotypes, subcutaneous obesity and visceral obesity (**Fig. 1.2**). The former is associated with an expansion of subcutaneous fat, which is situated between the muscle and skin in the abdominal and gluteo-femoral area (**Fig. 1.2a**). The latter is a consequence of an increased mass of visceral adipose tissue (VAT) which is found only in the intra-abdominal cavity (**Fig. 1.2b**). These two phenotypes are often named as pear shape and apple shape body, respectively [Gesta et al., 2007].

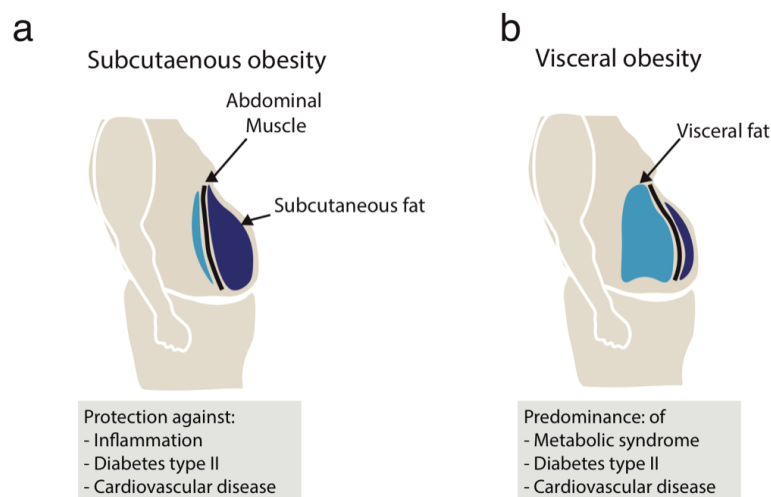


Figure 1.2: . **Obesity phenotypes and related pathologies.** (a) Subcutaneous obesity (b) Visceral obesity.

Despite their phenotypical similarities, the consequences of an increased adiposity differ greatly. In contrast with subcutaneous obesity, which is often referred to as a healthy obese phenotype, the visceral obesity is associated with many pathologies. In fact, there is a strong positive correlation between increased body weight and metabolic syndrome (MS) and with

some forms of cancer such as breast cancer [Argolo et al., 2018]. MS is a pathology where a clustering of conditions occur such as increased blood pressure, high blood sugar, abnormal cholesterol or triglyceride levels , leading to an increased risk of heart disease, stroke and type 2 diabetes [González-Muniesa et al., 2017]. However, obesity by itself is not the only driving force for metabolic dysfunction, since there are patients who suffer from MS and are not obese.

The reasons behind these correlations are still under investigation, and identifying the driving forces behind visceral obesity would be a step further towards prevention and new treatments. To date, it is known that the mode of AT expansion contributes to the development of inflammation and associated pathologies. However, it is unknown what drives the different forms of expansion. We hypothesise that mechanical forces may play a role in such fate and malfunctions.

Finally, it is well accepted that regardless of the type, obesity arises from genetic, environmental, behavioural and psychosocial factors that govern the energy regulation. The nervous and endocrine system, microbiota, stress or emotional factors and medications could trigger abnormal food intake, whereas poor physical activity, lack of sleep, thermal effect of nutrients, cold exposure and resting energy expenditure control the total energy expenditure. Furthermore, from the moment of conception until the individual reaches adulthood, there are several critical periods that influence later body composition [González-Muniesa et al., 2017].

In the next sections, we will explore the biology behind the AT in order to give the reader a good background for a better understanding of this thesis.

### **1.3.1 Adipose depots and functions**

Until the late 1940s, AT was considered as a form of connective tissue filled with lipid droplets [Rosen and Spiegelman, 2014]. Nowadays, it is known that adipose tissue plays

important roles apart from only accumulating lipids. It is the master regulator of energy balance and nutritional homeostasis in the body. In fact, AT communicates with other tissues, establishing a homeostatic feedback loop, which is mediated by secreting proteins and hormones [Frayn et al., 2003; Parimisetty et al., 2016]. For this reason, AT is considered as an important endocrine organ [Musi and Guardado-Mendoza, 2014].

AT is located in various depots in the body, that are believed to be originated from the neural crest and from the distinctive areas of the mesoderm (paraxial, intermediate, and lateral mesoderm) [Ali et al., 2013; Luong et al., 2019; Pope et al., 2016]. The two major classifications of AT are the white adipose tissue (WAT), associated with obesity, and the brown adipose tissue (BAT) (**Fig. 1.3**).

WAT and BAT differ not only in their phenotype but also in their functions. WAT is characterised by adipocytes with a large central unilocular lipid droplet, that occupies the entire cytoplasm of the cell. BAT presents a cytoplasm composed by multilocular lipid droplets, central nucleus and high abundance of cytochromes in the mitochondria. This last feature results in the brown appearance of BAT. WAT primary functions are energy storage, hormonal secretion and insulation [Rosen and Spiegelman, 2014; Trayhurn and Beattie, 2008]. Its secretome is also involved on the local regulation of immunity, inflammation, vasculogenesis and extracellular matrix remodeling. The main function of BAT is the heat generation which is mediated by the uncoupling protein-1 (UCP-1), a family of mitochondrial proteins responsible for uncoupling the respiratory chain and consequently generating heat instead of ATP [Nascimento et al., 2018]. The main focus of this thesis is WAT. Therefore we will describe it in more detail, while only giving a brief introduction on BAT and induced-BAT (iBAT).

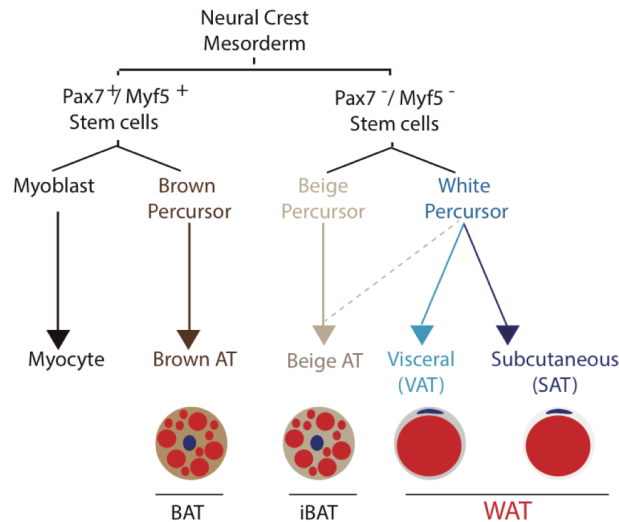


Figure 1.3: **Development of WAT and BAT depots.** AT is believed to have origin from the neural crest and from different areas of the mesoderm (paraxial, intermediate and lateral mesoderm). Brown adipocytes are originated in the paraxial mesoderm during embryonic development from precursors expressing Myogenic Factor 5, which are also involved in the origin of skeletal muscle [Su et al., 2018]. VAT arises from a *Wt1*-expressing cells lineage, which are derived exclusively from the lateral plate mesoderm [Chau et al., 2014; Pellegrinelli et al., 2016].

### 1.3.1.1 White adipose tissue

WAT starts to develop in late gestation and the rate of adipogenesis rapidly surges in response to increased nutrient availability, which culminates in a high postnatal expansion [Parlee et al., 2014]. WAT is the major responsible for the secretion of adipokines (AT cytokines), and adipocyte-derived lipids such as ceramides and sphingosines, that act as signalling molecules. The best known and studied adipokines are leptin and adiponectin. Leptin is involved in the process of suppressing food intake by interacting with the brain. It is also involved in energy expenditure, reproductive function and on the regulation of blood pressure. Leptin is a hormone secreted by adipocytes and also has angiogenic properties [Park et al., 2013]. In conditions such as obesity, leptin levels in the bloodstream are high, which consequently leads to a lack of the sensitivity to the hormone, known as leptin resistance. Therefore, mice overexpressing leptin show increased rate of diet-induced obesity [Ogus et al., 2003]. Adiponectin is known for its insulin-sensitising, anti-adipoptotic and

anti-inflammatory properties. Mice that overexpress adiponectin are protected against glucose intolerance and dyslipidaemia induced by a high-fat diet [Kim et al., 2007; Otabe et al., 2007].

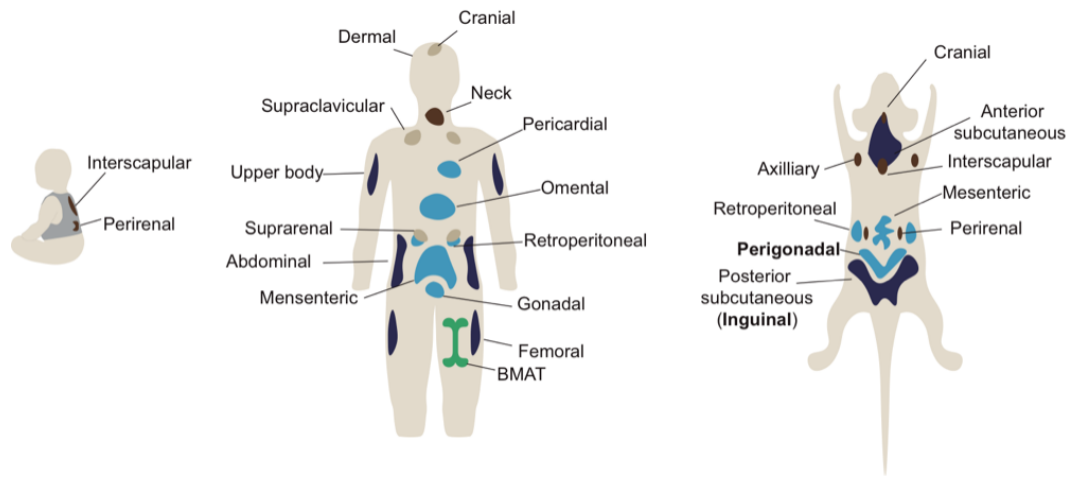


Figure 1.4: **AT depots distributions between humans and mice.** Dark blue: Subcutaneous adipose tissue; Light blue: Visceral adipose tissue; Brown and beige: Brown adipose tissue. Figures adapted with permission from [Choe et al., 2016; Peirce et al., 2014].

WAT is located in different depots giving rise to further sub-classification. The subcutaneous adipose tissue (SAT) is situated between muscle and skin in the abdominal and gluteo-femoral area, and visceral adipose tissue (VAT) is found only in the intra-abdominal cavity. The most predominant SAT and VAT depots in humans are the gluteofemoral and the omental depots, respectively. In mice, the inguinal adipose depot located around the groin and the gonadal depot are used as models of human subcutaneous and visceral adipose tissue, respectively [Ghaben and Scherer, 2019]. However, caution is needed when using animal studies to infer human AT properties, since there is a great divergence in the gene expression of the fat depots [Luong et al., 2019].

Apart from their phenotypic similarities, SAT and VAT differ on their metabolic profiles such as adipokine secretion, rate of lipolysis and response to external stimuli and pathologies [Karpe and Pinnick, 2015; Rosen and Spiegelman, 2014]. This seems to be a result of the genetic signature given by the derived population, and not only a consequence of the local



microenvironment.

### **1.3.1.2 Brown adipose tissue**

BAT is predominantly found during embryonic development and in newborn babies, where it is located in the interscapular and supraclavicular regions [Peirce et al., 2014]. The main function of BAT is the heat generation, which is crucial at birth. This is because after birth, newborns have to self-regulate their body temperature without relying on the mother. After infancy, BAT starts to decrease and is primarily found in the deep neck in adults [Lecoultrre and Ravussin, 2011; Leitner et al., 2017; Peirce et al., 2014]. Other features of BAT are high vascularisation, innervation by sympathetic nerves, and a centrally located cell nucleus [Lidell and Enerbäck, 2010].

### **1.3.1.3 Beige adipose tissue**

Finally, another minor group of AT is called beige adipose tissue also known as brite (brown in white), iBAT (induced BAT), recruitable BAT and wBAT (white adipose BAT). This results from the browning of WAT or its precursors [Harms and Seale, 2013; Peirce et al., 2014]. This is a result of increased UCP-1 expression as well as of a core set of BAT specific genes, when WAT is exposed to several types of stimuli such as  $\beta$ -adrenergic stimulation and exposition to cold environment for an extended period of time [Lidell and Enerbäck, 2010]. Because the thermogenic properties of BAT are associated with improved insulin sensitivity and stimulation of lipolysis, the process of browning has been described as a potential therapeutic for obesity-related conditions [Harms and Seale, 2013].

## **1.3.2 Adipose tissue structure and microenvironment**

The adipose tissue is arranged in lobules composed by adipocytes and other cells (macrophages, fibroblasts, pericytes, endothelial cells and pre-adipocytes) that constitute the stromal vascular fraction of this tissue [Tordjman, 2013]. These lobules are separated by septa of loose connective tissue, called interlobular septa (**Fig. 1.5**). Furthermore, each adipocyte is sur-

rounded by a thick layer of extracellular matrix (ECM), called the basement membrane. The ECM is a filamentous collagenous structure predominantly composed by collagen type IV [Comley and Fleck, 2010; Mariman and Wang, 2010; Young et al., 2011]. It is estimated that the AT ECM is composed by 25-35% of collagens, 15-22% of elastin and 0.2-0.8% of sulfate glycosaminoglycan [Pope et al., 2016]. Apart from collagen type IV, type I and VI are also expressed [Mariman and Wang, 2010]. Adipocytes self-produce collagens, but other cells from the stromal vascular fraction also contribute to this.

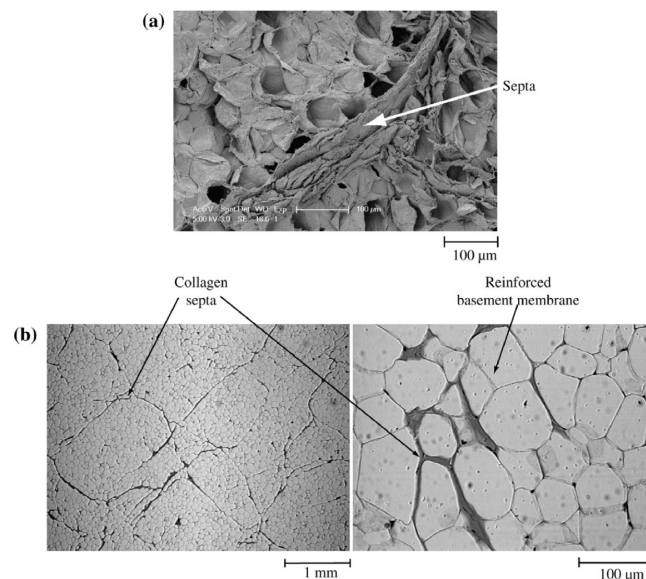


Figure 1.5: **Adipose tissue morphology.** Figure reproduced with permission from [Comley and Fleck, 2010].

This cellular microenvironment affects several biological functions such as proliferation, migration and differentiation. For example, the microenvironment of adipose tissue has been shown to regulate adipogenesis in obesity [Jeffery et al., 2016]. The ECM of AT directly affects the mechanical properties of the tissue. Subcutaneous and visceral AT present different stiffness, which could be a result of depot-specific ECM [Alkhouli et al., 2013].

The networks of fibronectin, laminin and collagen fibers serve as attachment points for integrins that are situated in the adipocyte membrane [Pope et al., 2016]. Integrins are heterodimers (alpha ( $\alpha$ ) and beta ( $\beta$ )) responsible for mediating extracellular stimuli into the

cell. During adipogenesis of 3T3-L1 pre-adipocytes, the expression of the integrin  $\alpha$  subunit changes from  $\alpha 5$  in pre-adipocytes to  $\alpha 6$  in mature adipocytes [Pope et al., 2016]. Accompanying this process, vimentin becomes up-regulated in order to ensure stability of the lipid droplets [Franke et al., 1987; Heid et al., 2014; Teichert-Kuliszewska et al., 1996]. In contrast, the expression of actin and tubulin decreases [Pope et al., 2016]. Other structures involved in the internalisation of extra-cellular stimuli are caveolae and ion channels on the adipocyte plasma membrane. Caveolae are plasma membrane invaginations. They are a special type of lipid raft where several membrane receptors are located such as receptors involved in lipid metabolism. These structures are involved on the regulation of both the physical and chemical composition of the plasma membrane and act as membrane reservoirs to rapidly buffer against changes in membrane tension [Mayor, 2011; Sinha et al., 2011]. Thus, caveolae can actin-controlled changes in tension by regulating multiple cellular pathways, including RhoA-driven actomyosin contractility [Echarri and Del Pozo, 2015]. Humans and mice that lack of these structures have small adipocytes and exhibit lipodystrophies and other physiological abnormalities [Pilch and Liu, 2011]. Stretch/mechano-sensitive ion channels presented at the plasma membrane of the adipocytes can also modulate signalling pathways acting on adipogenesis, fatty acid sensing, oxidative metabolism, inflammation and energy homeostasis [Zhang et al., 2017].

Adipocytes not only sense their environment, they are also linked together directly through gap-junctions. During differentiation the gap junction protein Connexin-43 is transiently activated via phosphorylation followed by its degradation. This process is vital for pre-adipocyte differentiation [Yeganeh et al., 2012].

In summary, the tissue microenvironment plays an essential role coordinating biological systems. Alterations in the expression of ECM proteins can lead to several pathologies. The effect of such alterations in the context of obesity will be discussed later in this chapter.

### 1.3.3 Adipose tissue expansion

Adipose tissue expansion is a complex process and the mode of expansion dictates the level of inflammation. There are two modes of adipose tissue expansion, an increase in the adipocyte size known as hypertrophy, and an increase in the adipocyte cell number, named hyperplasia (**Fig. 1.6**). The molecular control over those two modes is not fully understood. It is believed that SAT preferentially expands hypertrophically, while VAT can expand in both modes. In animals under prolonged high-fat diet the first WAT response is adipocyte hypertrophy, which is followed later by hyperplasia [Rosen and Spiegelman, 2014]. The number of adipocytes in a given depot is primarily determined early in life and it is mostly stable during adulthood. An estimation of the AT annual turnover is approximately 10% [Spalding et al., 2008].

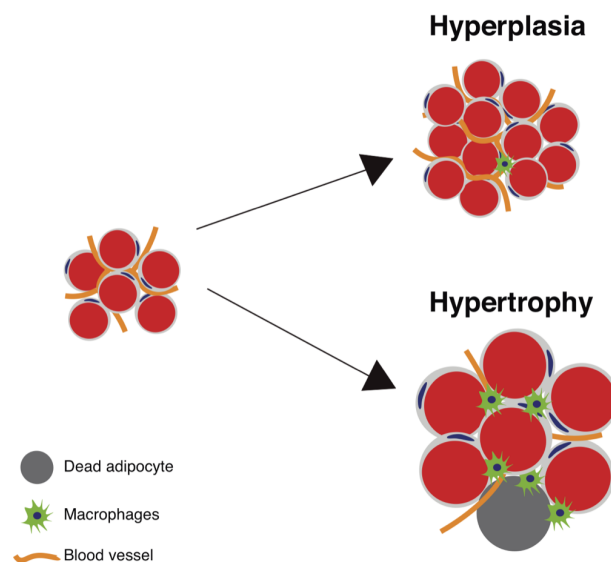


Figure 1.6: **Modes of adipose tissue expansion.** Hyperplasia refers to an increase of adipose tissue given by an increase in cell numbers. It is usually classified as a healthy expansion as the accompanied inflammation is not aggravated. Hypertrophy refers to a mode of expansion given by an increase of the cell sizes. This leads to elevated inflammation and tissue necrosis.

#### 1.3.3.1 Hypertrophy

Hypertrophic adipocyte growth results in an increased size of the existing adipocytes due to an intake of lipids, and consequently increased lipid droplet size. Hypertrophic growth is as-

sociated with several WAT dysfunctions and pathologies [Rutkowski et al., 2015]. Obese hypertrophic adipocytes show necrotic-like abnormalities, like the rupture of the plasma membrane, dilatation of the endoplasmic reticulum, and release of cell contents to the extracellular space. This leads to a secretion of pro-inflammatory cytokines, such as tumor necrosis factor  $\alpha$  and monocyte chemoattractant protein-1 (MCP-1), which culminates in an inflammatory state [Choe et al., 2016; Cinti et al., 2005].

A hypertrophic growth also results in hypoxia, since the tissue starts to lack in vasculature. Hypoxia-inducible factor (HIF)  $1\alpha$  serves as oxygen sensor in several cell types. Under normoxic conditions HIF- $1\alpha$  is ubiquitinated, whereas in hypoxia it translocates to the nucleus where it functions as a transcription factor. As a result, the genes involved in inflammatory responses become up-regulated. For example, hypoxia in WAT works as a catalyst for adipose tissue fibrosis [Lawler et al., 2016; Trayhurn, 2013; Trayhurn et al., 2008]. Furthermore, glycolytic metabolic programs take place in such conditions, altering the metabolism of the cell. Other features of hypertrophic growth are increased free fatty acid (FFA) release, which consequently causes ectopic lipid accumulation in the adjacent organs such as liver, and lipotoxicity. Impaired insulin-dependent glucose uptake and decreased expression of adiponectin are other characteristics of this mode of growth [Choe et al., 2016].

#### **1.3.3.2 Hyperplasia**

An increase in number of adipocytes, hyperplasia, requires that precursor cells differentiate into new adipocytes, a process called adipogenesis. Hyperplasia, in contrast to hypertrophy, is associated with a healthier metabolic profile. This is because *de novo* adipogenesis results in an adipocyte population with smaller cell sizes, characterised by low levels of fatty acid release, pro-inflammatory cytokines, immune cell recruitment, hypoxia and fibrosis [Choe et al., 2016]. Other features of this profile are the enhanced insulin sensitivity and adiponectin expression.

### 1.3.4 Adipogenesis

Adipogenesis requires two important steps. The first consists of the commitment of multipotent precursor cells into pre-defined adipocytes, and the second corresponds to the terminal differentiation of pre-adipocytes into a lipid-filled adipocyte [Cristancho and Lazar, 2011]. The entire process involves a complex rearrangement of cytoskeleton, signalling pathways and transcription regulators. In fact, there are chronological changes in the expression of specific genes that determine the adipocyte signature. The two key transcription factors that are central to the regulation of adipogenesis are the nuclear hormone receptor peroxisome proliferator-activated receptor- $\gamma$  (PPAR $\gamma$ ) and the CCAAT/enhancer binding protein family (C/EBP  $\alpha$ ,  $\beta$ ,  $\delta$ ) [Madsen et al., 2013]. During the different phases of adipogenesis, different stimuli will act downstream on the activation of both transcription factors. PPAR $\gamma$  is named as the master regulator of adipogenesis because it is essential for adipocyte differentiation both *in vivo* and *in vitro* [Chawla and Lazar, 1994; Peter et al., 1994; Rosen et al., 1999; Tontonoz et al., 1994]. It belongs to a group of nuclear receptor proteins that function as transcription factors, controlling the expression of key adipogenic genes as well as genes involved in lipid metabolism. C/EBP is a transcription factor family composed of six members that interact with the CCAAT (cytosine-cytosine-adenosine-adenosine-thymidine) box motif. Depending on the phase of adipogenesis, some of the family members are more predominantly expressed [Darlington et al., 1998]. C/EBP $\beta$  and  $\delta$  are transiently induced during the early stages of adipocyte differentiation. This is followed by C/EBP $\alpha$  up-regulation in the terminal stage where it also ensures normal adipocyte function.

The first step of adipogenesis is known as the commitment step. *In vitro* this step is characterised by the differentiation of mesenchymal stem cells (MSCs) into committed white pre-adipocytes upon adipogenic stimuli. Alternatively, MSCs can differentiate into myoblasts, chondrocytes and osteoblasts. *In vivo* the adipocyte niche is not yet completely understood because of the heterogeneous nature of precursors in the different depots of WAT. However, adipocytes tend to emerge in a tight association with blood vessels, since expanding adipose

tissue requires increased nutrient supply [Escobedo and Oliver, 2017].

The adipogenic stimuli that trigger the commitment step can arise from different mechanisms. It is known that bone morphogenetic protein 2 and 4 (BMP2 and BMP4, a group of growth factors/cytokines) are sufficient to drive adipocyte commitment by activating the SMAD signalling pathway [Ghaben and Scherer, 2019]. SMADs are a family of signal transducers for receptors of the transforming growth factor beta (TGF- $\beta$ ) superfamily. SMAD4 activation promotes adipocyte terminal differentiation by stimulating the transcription of PPAR $\gamma$ . Some zinc finger proteins, ZFP423, ZFP467 and KLF5, also enhance adipogenesis by activating BMP signalling, C/EBP $\alpha$  and PPAR $\gamma$ , respectively [Cassandri et al., 2017; Wei et al., 2013]. Other transcription factors either inhibit (GATA2, GATA3 and EGR1) or promote (ERG2) the commitment process.

The second step of adipogenesis, the differentiation of pre-adipocytes into a mature adipocytes, is stimulated either by signalling modulators that directly influence the expression of the master regulators, or by systemic physiological factors such as chronic inflammation, circadian rhythms and cold exposure [Aggarwal et al., 2017; Ghaben and Scherer, 2019].

Signalling hormones and ligands can originate from different extracellular stimuli. WNT (Wingless/Integrated) signalling is a group of signal transducers, that act through cell surface receptors. WNT can either inhibit or promote the adipogenesis, depending on the WNT ligand [Christodoulides et al., 2009]. The WNT10B ligand connects to the frizzled receptor at the plasma membrane activating the canonical pathway of WNT. This consists of the translocation of the  $\beta$ -catenin to the nucleus, activating WNT target genes, which are anti-adipogenic. The same effect is found in the non-canonical pathway when mediated by the ligand WNT5A. On the contrary, stimulation of the non-canonical pathway by WNT5B stimulates adipogenesis, since this ligand inhibits the nuclear translocation of  $\beta$ -catenin. The usual adipogenesis cocktails use compounds that inhibit the WNT10B ligand activation, for example cyclic AMP agonists.

Insulin is a peptide hormone produced by beta cells of the pancreatic islets and it is considered to be the main anabolic hormone of the body. When insulin binds to the insulin receptor tyrosine kinase (IR) at the plasma membrane, it mediates an insulin signalling cascade by activating consecutively IRS1, PI3K, AKT1 and AKT2 [Haeusler et al., 2017; Lowe et al., 2011]. From this activation, CREB, mTOR and forkhead proteins (FOXOs) also become activated and consequently activate the expression of PPAR $\gamma$  promoting adipogenesis. Knockouts of the insulin receptor and mTOR result in protection against obesity and inhibit adipose tissue development, respectively [Blüher et al., 2002; Shan et al., 2016].

BMP signalling also participates in the terminal differentiation of the adipocytes by the same mechanisms reported above [Ghaben and Scherer, 2019]. The Hedgehog family of ligands decreases adipogenesis by interfering with the BMP signalling pathway [Suh et al., 2006]. Moreover, glucocorticoids which are steroid hormones, act as pro-adipogenic molecules by up-regulating C/EBPs [Chapman et al., 1985; Hauner et al., 1987].

Finally, composition and stiffness of the extracellular matrix can also regulate adipogenesis by the RHO-family GTPases [Sordella et al., 2003]. Activation of RAC-GTP blocks terminal differentiation by not allowing the conversion of spindly fibroblasts to rounded adipocytes. This is a result from the formation of actinomyosin fibers [McBeath et al., 2004]. Inhibition of the members of the matrix metalloproteinases (MMPs), responsible for digesting the surrounding ECM and consequently regulating the ECM stiffness, lead to impaired adipogenesis *in vivo* [Lijnen et al., 2002].

### **Animal cell models to study adipogenesis**

Preadipocyte cell lines have been used over the last several years allowing to uncover important aspects of adipogenesis, adipocyte function and metabolism. Primary cultures of preadipocytes, mainly from murine origin, have been commonly used in the field. Their major advantageous are that they can derived from different adipose tissue depots from animals with specific ages and features allowing us to study a variety of condition-related problems.



However, due to difficult isolation procedures, inability of propagation and hard maintenance in culture, genetic variation due to animals different origin, as well as difficulties in DNA transfection, make them less advantageous compared to clonal cell lines such as 3T3-L1, 3T3-F44A, C3H10-T1/2 and OP9.

The 3T3-L1 cell lines were cloned and established from a heterogeneous population of 3T3 Swiss mouse embryo fibroblasts by Green and colleagues in the 70's [Green and Kehinde, 1974, 1975, 1976; Green and Meuth, 1974]. Since then this population has been widely used to study adipogenesis [Morrison and McGee, 2015; Ruiz-Ojeda et al., 2016]. 3T3-L1 differentiation can be triggered by pro-differentiation agents after growth arrest, which results in fully lipid filled adipocytes [Salazar-Olivo et al., 1995]. The main advantages of this cell line is its easy culture and low cost. It can maintain a homogeneous cell population even when the number of passages is high. However, because this cell line fails to recapitulate the characteristics of primary cell culture models [Morrison and McGee, 2015], obtained results can not be interpolated to depot specific responses. The 3T3-L1 gene expression profile and basal metabolism resembles WAT, but upon treatment with catecholamines, these cells increase their oxygen consumption in a UCP-1-dependent manner. This consequently increases the expression of genes enriched in brown adipocytes. Another clonal cell line similar to the 3T1-L1 is the 3T3-F44A. When compared to 3T3-L1, the 3T3-F44A main advantage is the higher efficiency of adipogenic commitment and lipid accumulation. Finally, a mouse stromal cell line named OP9 is been also used in the adipose tissue field. The main advantage of this cell line is the quick differentiation upon adipogenic stimuli corresponding to a time-scale of 72 hours. This feature makes this cell model suitable for high-throughput screening.

### **1.3.5 Regulation of adipocyte size**

Adipocyte size is regulated by the nutrient availability in the body. When the nutrients are in excess, the pancreas produces insulin that will promote the adipocytes to intake lipids

and glucose, and store them in the form of lipid droplets (LD), a process named lipogenesis [Chouchani and Kajimura, 2019]. Since the lipid droplet nearly fills the entire space of the cytosol, the adipocyte size is governed by the size of this organelle. Lipid droplets are mainly composed by a neutral lipid core consisting of triacylglycerols (TAGs) and sterol esters (SEs), which are characterised by their insolubility in water.

The opposite process of lipogenesis is lipolysis, which occurs in situations of nutrient deprivation. When the glucose levels in the blood drops, it stimulates the secretion of certain hormones (e.g. glucagon and noradrenaline) [Rutkowski et al., 2015]. As a result of the stimulation of these hormones, the stored triglycerides start to break down into free fatty acids (FFA) and glycerol. FFAs will then be released in the circulation and taken up by other organs.

#### **1.3.5.1 Lipogenesis**

From the moment of food intake until the lipid droplet formation, the dietary lipids undergo several transformation steps along the digestive system before being stored in the adipocytes. Prior to being released in the circulation (in both bloodstream and lymphatic systems), triglycerides have to be incorporated in structures composed by lipoproteins, because of the TAG hydrophobic properties. Examples of these structures are the chylomicrons, present in the gut, which transport exogenous TAGs (from the diet). Very-low-density lipoproteins (VLDL) transport endogenous triglycerides, cholesterol and apolipoproteins, which are assembled in the liver. Those structures interact with lipoprotein lipase (LPL) in the capillaries, where LPL hydrolyses the TAGs to fatty acids and monoacylglycerols, which are then taken in the adipocytes once they reach the plasma membrane.

The non-esterified fatty acid sequestration is mainly mediated by CD36 (also known as fatty acid translocase (FAT)) and fatty acid binding and transport proteins (FATP) [Thompson et al., 2010]. At the same time, insulin mediates the intake of glucose which will also result in the accumulation of triglycerides, a process named *de novo* lipogenesis (DNL) [Song et al.,

2018]. DNL requires two important proteins, the fatty acid synthase (FAS) and acetyl-CoA carboxylase (ACC). Those two enzymes are transcriptionally regulated by sterol response element binding protein 1c (SREBP1c) and carbohydrate response element binding protein (ChREBP).

At this point, fatty acids from both sources are esterified by Acyl-CoA synthetases (ACSs) at the endoplasmic reticulum (ER) between the leaflets of the ER bilayer, producing the nascent lipid droplet [Meyers et al., 2017]. Central players of the first steps are DGAT1 and DGAT2, which catalyze the conversion of diacylglycerol and fatty acyl-CoA to triacylglycerols. Subsequently, the accumulation of neutral lipids start to increase resulting in the formation of a lens. In order to stabilize these structures and facilitate the growth of the nascent lipid droplet, seipin and other lipid droplet biogenesis factors are recruited [Wang et al., 2018]. Once the newly synthesised TAG accumulation within the ER bilayer is sufficient, the budding of the droplet into the cytosol occurs.

The expansion of the LDs and generation of big lipid droplets can be a consequence of two processes [Olzmann and Carvalho, 2019]. The first process is named coalescence by which two LDs fuse instantaneously to form one larger LD. A second process is a gradual enlargement of one LD and the depletion of oil in the adjacent second LD. This process requires the help of lipid droplet-associated proteins such as Fsp27/CIDE-C, which are localised in contact zones between the two LDs and facilitate the slow transference of TAG from the smaller droplet to the big one [Gong et al., 2011; Sun et al., 2013].

#### **1.3.5.2 Lipolysis**

Lipolysis is a multi-step hydrolysis composed by several complex signalling cascades that are responsible for the activation and/or inhibition of the process. The main purpose of intracellular lipolysis in adipose tissue is to produce energy to fulfil the metabolic needs of the cell (endogenous FA) or to feed target tissues such as skeletal muscle, liver and pancreas (exogenous FA). The most predominant way that lipolysis is activated is by PKA, which

is triggered by fasting or cold exposure via increased release of nonrepinephrine from the sympathetic nervous system [Chouchani and Kajimura, 2019].

FAs are important for several cellular functions such as the formation of biological membranes. FAs also work as nuclear transcription factors (e.g. PPAR $\gamma$ ). The balance of fatty acid esterification and the triglyceride hydrolysis is key to prevent lipotoxicity. Increased non-esterified FAs could lead to harmful effects at the cellular level leading to impaired membrane functions, endoplasmatic reticulum (ER) stress, mitochondrial dysfunction, inflammation and cell death [Zechner et al., 2012].

The principal drivers behind the lipolytic process are enzymes called lipases. The best known lipases in adipose tissue are adipose triglyceride lipase (ATGL), hormone-sensitive lipase (HSL) and monoacylglycerol lipase (MGL). Together they compose a three-step process where triglycerides are converted into diglycerides, subsequently monoglycerides and finally glycerol (**Fig. 1.7a**). The activity of ATGL and HSL corresponds to the main part of TAG hydrolysis.

ATGL is a 54kDa TAG hydrolase, which was first described in 2004 and officially named PN-PLA2 [Villena et al., 2004; Zimmermann, 2004]. It contains a structure of 504 aminoacids. Several mechanisms can increase or decrease ATGL mRNA levels. As ATGL has an extensive post-translational regulation, the concentration of ATGL mRNA cannot be use as quantitative indicator of the lipase activity. An example of this, is the isoproterenol lipolysis stimulation, which does not increase mRNA levels but increases the ATGL phosphorylation.

The ATGL enzymatic activity is dependent on the C-terminal region of the lipase. Until recently, ATGL was thought not to be directly phosphorylated by protein kinase A (PKA) [Greenberg et al., 2001]. Currently, it is known that the catalytic points Ser406 and Ser430 on ATGL can be directly phosphorylated by cAMP-PKA [Kobayashi et al., 2008; Schweiger et al., 2008]. The PKA indirect activation of ATGL requires its co-activator, the comparative gene identification-58 protein (CGI-58). CGI-58 interacts with ATGL, and upon its phos-

phorylation by perilipin-1 (another important lipid droplet associated protein) on Ser517 it dissociates from ATGL, allowing the latter to translocate to the lipid droplet [Miyoshi et al., 2007].

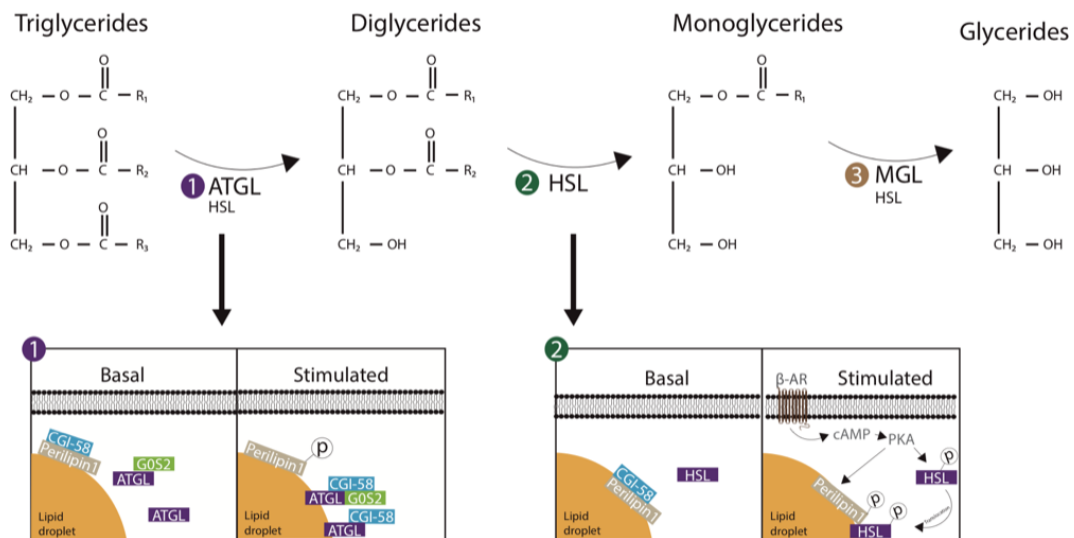


Figure 1.7: **Activation of lipolysis.** Triglycerides are broken down by the three lipases, ATGL, HSL and MGL (top). ATGL and HSL activity in basal and stimulated lipolysis in response to increased cAMP (bottom).

Another protein recently found to be involved in the inhibition of ATGL and its hydrolysis function is named GOS2. It binds directly on the patatin-like domain of ATGL through the hydrophobic domain of GOS2, which interestingly is the same site for CGI-68 binding [Heckmann et al., 2016; Yang et al., 2010]. As a result of this binding, an attenuation of the hydrolase activity is observed. Yang et al. proposed that at least a small fraction of ATGL is constantly in complex with GOS2 independently of lipolytic state (basal or stimulated) [Yang et al., 2010]. They showed that isoproterenol-stimulated translocation of this free fraction still allows for profound activation of lipolysis. The GOS2 expression fluctuates with the nutrient status. It is low during fasting and increases after feeding. A knockdown of endogenous GOS2 enhances basal and stimulated levels of lipolysis, while an overexpression decreases the lipolytic rate.

HSL is a protein mainly found in the cytoplasm (**Fig. 1.7a**). The mechanisms of HSL enzymatic control differs significantly from that of ATGL. Structurally, HSL has an NH<sub>2</sub>-terminal lipid-binding region and a  $\alpha/\beta$  hydrolase fold domain, which includes the (1) catalytic triad and (2) the regulatory module (where the phosphorylation sites are localized). A potent direct catalyst of HSL is PKA, which is well known to be induced by  $\beta$ -adrenergic stimulation. Other catalysts have been described in the literature: 5' AMP-activated protein kinase, extracellular signal-regulated kinase, glycogen synthase kinase-4 and Ca<sup>2+</sup>/calmodulin-dependent kinase. Apart from its high affinity for diglyceride hydrolysis, HSL is also able to breakdown other types of lipids at a lower rate. The mechanism of activation upon phosphorylation, consists of HSL translocation from the cytoplasm to the lipid droplet and subsequent binding to the NH<sub>2</sub> terminal region of perilipin-1 gaining access to the lipid droplets (**Fig. 1.7c**).

Finally, MGL is localised in the cell membranes, cytoplasm and in the LDs [Zechner et al., 2012]. It is responsible for the final step of the lipolysis converting monoglycerides into glycerol (**Fig. 1.7a**).

### 1.3.6 Adipose tissue adaptation in response to obesity

As mentioned before, the distribution of the excess of fat accumulation as well as the mode of the expansion predict the complications associated with obesity. Hypertrophic growth is associated with adipocyte dysfunction. During this growth, the adipocytes have a remarkable capacity of expansion, almost doubling their size (**Table 1.2**).

Cell Size	Subcutaneous and Visceral Fat			Subcutaneous Fat		Visceral Fat		2D Culture
	Fetus <sup>a</sup>	Neonate	Infant <sup>b</sup>	Lean	Obese	Lean	Obese	
Diameter range ( $\mu\text{m}$ )	40–50	50–80	90–130	50–130	90–270	45–110	90–200	30–70
Mean cell volume ( $\mu\text{m}^3$ )	48 000	144 000	697 000	382 000	3 054 000	244 000	1 596 000	65 000

Table 1.2: **Adipocyte sizes in developing and adult humans versus in vitro culture.** Table reproduced with permission from Pope et al. [2016].

A hallmark of obesity is the dysregulation of extracellular matrix proteins leading to a fibrotic state of the tissue. As a result, AT from obese people exhibits decreased tensile strength relative to healthy tissue [Lackey et al., 2014]. This seems to be a consequence of abnormal production of the different types of collagens, fibronectin and elastins, which physically restrain the AT expansion. As a result a lack of angiogenesis, hypoxia and infiltration of pro-inflammatory immune cells, such as M1 macrophages, is observed. The cellular population responsible for secreting pro-fibrosis ECM proteins in humans are still a target of investigation. Studies in rodents suggest that multiple cell lines in the AT depot could contribute to this state. M1 macrophages usually found in the inflammatory states in visceral obesity could contribute to a profound ECM remodelling [Dalmas et al., 2015; Pope et al., 2016].

Other well known effects associated with adipose tissue malfunction are the highly increased free fatty acid flux as well as increased levels of diacylglycerol and ceramides. It has been shown that weight gain is accompanied by high basal and low stimulated lipolysis, which seems to be linked to altered gene expression in insulin resistance [Arner et al., 2018]. High levels of circulating non-esterified fatty acids result in lipotoxicity in adjacent organs, that is, ectopic deposition of lipids in liver and skeletal muscle. This leads to mitochondrial dysfunction, particularly mitochondrial oxidative phosphorylation and biogenesis [de Mello et al., 2018; Zamora-Mendoza et al., 2018].

In obesity, pathological changes of adipocyte function also lead to increased expression of adipokines. Pro-inflammatory adipokines such as TNF- $\alpha$ , interleukin-6, angiotensinogen, monocyte chemoattractant protein-1 and resistin are elevated [Chouchani and Kajimura, 2019], enhancing the inflammatory response.

To conclude, obesity is a complex pathology where several biological changes occur at both cellular and tissue level. Compromising adipocyte function and its microenvironment could lead to disrupted cell-matrix interactions, cytoskeleton structures and membrane sensors, as well as inadequate adipogenesis and lipid metabolism.

### 1.3.7 Relation between BMI and intra-abdominal pressure

An interesting factor that is associated with visceral obesity is the increased intra-abdominal pressure (IAP). IAP is defined as a steady-state pressure located within the abdominal cavity, which results from the interaction between the abdominal wall and the viscera [Milanesi and Caregnato, 2016]. IAP is usually expressed in mmHg. Because the peritoneal cavity is a closed space, the IAP depends on the body position, muscle contraction and respiration [Niederauer et al., 2017]. Measurements of IAP are usually carried out at the end of expiration and in a supine position. This ensures that the abdominal muscle contractions are absent. It has been shown that the current techniques used to measure IAP can present some variance [Sugrue et al., 2015]. The most common techniques to measure IAP is manometry via the bladder or stomach. However, other techniques to assess IAP based on urine pressure, rectal pressure or inferior vena cava pressure have also been used [Malbrain, 2004]. However, the range between healthy and obese is considerable. Indeed, in healthy individuals it ranges between 0 and 7 mmHg and in over-weighted and obese individuals the pressure increases to values ranging between 7 and 17 mmHg [De Keulenaer et al., 2012], see **Table 1.3**. This increase leads to a diminished abdominal wall compliance. An IAP greater than 10 mmHg is considered intra-abdominal hypertension (IAH). An increase of IAP in obesity is likely caused by an increased visceral mass [Smit et al., 2016].

	Study characteristics		IAP (mean ± SD) according to BMI		
	N (observations)	Normal	Overweight <sup>c</sup>	Obese <sup>b</sup>	Morbidly obese <sup>c</sup>
Sanchez [30]	77 (231) <sup>d</sup>	5.0 ± 2.9	6.3 ± 2.9	8.9 ± 3.5	8.4 ± 2.5
Sugerman [31]	84 (84)	5.1 ± 1.2	NA	NA	13.2 ± 0.5
Sugerman [59]	15 (15)	NA	NA	7.4 ± 0.7	NA
Lambert [32]	45 (45)	0 ± 1.5	NA	NA	8.8 ± 0.6
Vasquez [47] <sup>e</sup>	45 (675)	6.5 (4.5–8.5)	11.2 (7.7–14.6)	13.7 (11.4–16.0)	NA
Arfvidsson [33]	15 (15)	6.2 ± 1.2	NA	NA	14 ± 3
Sugerman [34]	6 (6)	NA	NA	12.5	16.2 ± 2.2

<sup>a</sup> BMI 25.0–29.9 kg/m<sup>2</sup>

<sup>b</sup> BMI 30.0–39.9 kg/m<sup>2</sup>

<sup>c</sup> BMI ≥ 40

<sup>d</sup> IAP observations

<sup>e</sup> Data expressed as mean with 95% CI

Table 1.3: **Comparison of IAP among the different weight groups.** Table reproduced with permission from De Keulenaer et al. [2012].

To our knowledge, the direct relationship between the IAP and adipose tissue function and



fate has never been studied, neither in healthy or obese individuals. Understanding the adipocyte behaviour in response to pressure could advance current insights on the development of obese-related diseases.

### **1.3.8 Mechanical forces controlling adipose tissue fate and function**

Forces are present at all levels of the biological systems, from the subcellular to the microscopic level, at any time and space. Some of these forces are relevant in the regulation of several processes, ranging from embryonic development to tissue function. They can trigger intracellular pathways and subsequently regulate transcription in order to ensure a proper tissue/cell homeostasis. Defects in this sensory process, known as mechanotransduction, could lead to a number of diseases such as fibrosis or various types of cancer [Uhler and Shivashankar, 2017].

The mechanosensing of forces is mediated by membrane receptors, which are responsible for transducing the signals to the nucleus. This step is mediated throughout the cytoskeleton networks of actin and microtubules, and regulatory molecules. Once the signals reach the nucleus, these signals regulate the three-dimensional organisation of the chromosomes, and consequently affect the gene expression [Uhler and Shivashankar, 2017] (**Fig. 1.8**).

Cellular forces are generally divided in two main groups, the intrinsic forces (also named cell-generated) and external forces [Vining and Mooney, 2017] (**Fig. 1.8**). The former, as the name indicates, are generated as a result of the interaction between cells (such as cell-cell junctions), or by cell-matrix interactions. Therefore, physical properties of the ECM, such as its rigidity, governs how these intrinsic forces are transduced.

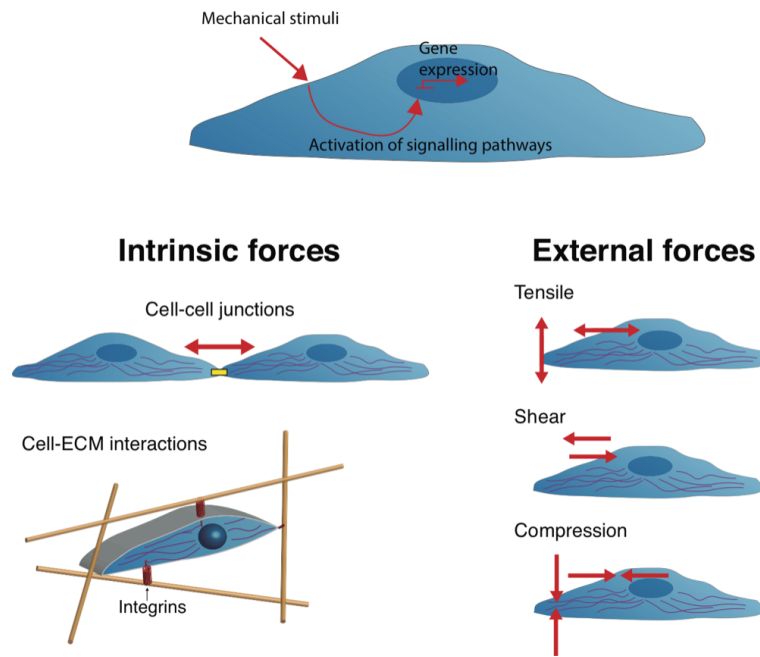


Figure 1.8: **Mechanotransduction, extrinsic and intrinsic forces.** Schematic of mechanotransduction pathway (top). Different intrinsic and extrinsic forces (bottom).

The external forces, such as shear, tension and compression are a consequence of mechanical actions such as blood flow the loading of the bones or even how the organism moves around.

Recently, the adipose tissue has gained some interest in the mechanobiology field. In the last decade multiple studies have surged in this field, starting from the work of Tanabe and Nakayama [2004], showing that tension inhibits adipogenesis, to the work of Zhang et al. [2017] more than 10 years later, showing for the first time that adipocytes could sense their own size by the mechanical-sensitive ion channel SWELL1 ([Tanabe, 2004; Tanabe et al., 2008; Tanabe and Nakayama, 2004; Zhang et al., 2017]). However, altogether the studies are still scarce, and they present several seemingly contradictory results (**Table ??**). Cells respond differently to the same mechanical stimuli depending on their micro-environment, and therefore changes in culturing substrata, magnitude of the stimuli and differently derived cell lines may explain these discrepancies. Nonetheless, there is widespread evidence that adipose tissue is mechano-responsive, and that mechanical forces influence its development. In the following sections we will give an overview of studies on tension and compression

affecting adipocytes.

### **1.3.8.1 Tension studies**

#### **Adipogenesis**

The pioneering work on mechanobiology of adipocytes was performed by Tanabe [2004]; Tanabe et al. [2008]; Tanabe and Nakayama [2004]. In their work, the authors cultured 3T3-L1 adipocytes in elastic silicon membranes coated with a mixture of collagen type I and IV. Seeded cells were then challenged for 45 hours during the commitment period with a uniaxial cyclic stretching of 110-175% of the initial length of the membrane (10% to 75% of strain). The authors found that cyclic stretching inhibited adipocyte differentiation, a result of reduced expression of PPAR $\gamma$ 2, which was mediated by activation of the ERK/MAPK system [Tanabe and Nakayama, 2004].

Shoham and Gefen A. reported that 3T3-L1 adipocytes exposed to static mechanical stretching during the whole period of culture had a significantly faster differentiation than the non-stretched controls [Shoham et al., 2012]. This result was linked with the activation of MEK/MAPK signalling pathway. However, PPAR $\gamma$  inhibition did not change the observed trend, ruling out the possible pathway MEK/MAPK - PPAR $\gamma$ . Furthermore, in an associated report, the authors mentioned that the magnitude of the stretch was key in the augmented adipogenesis. Strains of 6%, 9% and 12% were capable of triggering faster adipogenesis, whereas 3% did not [Levy et al., 2012].

These results by the Gefen group are at odds with the results found by the Tanabe group. Differences in the type of stretching (uniaxial versus biaxial as well as cyclic versus static) could be the reason for the discrepancies between their findings (**Fig.1.9 a and b**).

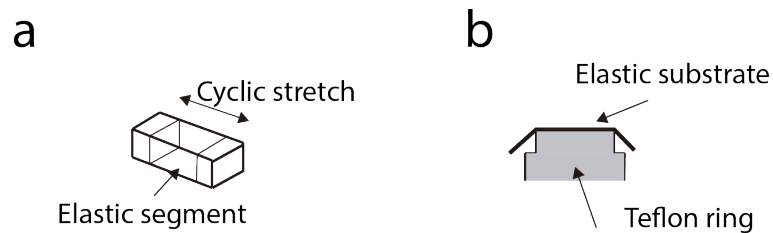


Figure 1.9: **Cell stretching apparatus developed by Tanabe and Nakayama [2004] and Shoham et al. [2012]**. Representation of the models described. (a) Uniaxial stretching. (b) Biaxial stretching.

The discussed works used pre-adipocytes as cell lines. Another study used MSCs for differentiation into adipocytes under cyclic mechanical strains [Sen et al., 2008]. In this work, the authors cultured cells on BioFlex collagen-I coated plates using a Flexcell FX-4000 system to apply 2% of strain. This resulted in inhibition of adipogenesis via  $\beta$ -catenin signal and consequently decrease of PPAR $\gamma$ . These results are consistent with Tanabe and Nakayama [2004].

### **Lipogenesis and lipolysis**

Later studies also reported that static compression could mediate an increase in lipid accumulation. Cells cultured under constant 12% strain during 30 days, led to differentiated adipocytes with bigger lipid droplets in relation to the controls [Levy et al., 2012; Shoham et al., 2012]. Furthermore, Shoham et al. have shown that during 3T3-L1 adipogenesis, the adipocyte stiffness changes with an increase in lipid droplet content, since the lipid droplet was shown to be stiffer than the adipocyte cytoplasm [Shoham et al., 2014]. Therefore, an increasing accumulation of LDs will lead to changes in the cytoskeleton arrangement, and potentially alter the tissue level stiffness. In the end, this will result in the activation of different mechanotransduction pathways. The same group showed by finite element simulations that the effectiveness of external forces on the plasma membrane and cell body does not only depend on the adipocyte maturation (lipid droplet accumulation) but also on the cell structure and dimensions [Katzengold et al., 2015].

Finally, another study using the Flexcell system, showed that 3T3-L1 cells differentiated and cultured under cyclic stretching increased their lipid production by a factor of 1.4 [Lustig et al., 2018].

Author, Year	Cell Line	Model	Mechanical Stimuli	Duration of loading	Results
<b>Adipogenesis</b>					
[Tanabe et al., 2008; Tan-abe and Nakayama, 2004]	3T1-L1 pre-adipocytes	2D	uniaxial cyclic stretching 10% to 75% of strain	45 hours	↓Adipogenesis
[Sen et al., 2008]	C3H10T1/2 MSC	2D	uniaxial cyclic stretching 2% of strain	6hrs per day for 5 days	↓Adipogenesis
[Levy et al., 2012] [Shoham and Gefen, 2012]	3T1-L1 pre-adipocytes	2D	static stretching 6%, 9% and 12% of strain	12 days	↑Adipogenesis
<b>Lipogenesis and Lipolysis</b>					
[Shoham and Gefen, 2012]	3T1-L1 pre-adipocytes	2D	static stretching 12% of strain	30 days	↑Lipid accumulation
[Lustig et al., 2018]	3T1-L1 pre-adipocytes	2D	uniaxial cyclic stretching 12% of strain	19 days	↑Lipid accumulation

Table 1.4: **Tension studies.** Studies evaluating the effect of tension on adipogenesis and lipid accumulation of adipocytes.

### 1.3.8.2 Compression

#### Adipogenesis

The effect of compression on adipogenesis was evaluated by Hossain et al. [2010]; Li et al. [2013] in two dimensional systems. Hossain M. and co-authors used a human pre-adipocyte cell line seeded in a 2D surface, and placed glass cylinders on top of the cells, creating a mechanical stress of 226 Pa (**Fig.1.10a**). The stimulus was applied for 12 hours, either before or after adipogenic induction. After 13 days of culture, the authors found that only cells mechanically stimulated for 12 hours before induction had decreased adipogenesis. This was confirmed by a decrease of mRNA expression of PPAR $\gamma$ 2 and C/EBP $\alpha$  in a COX-2 dependent manner.

Li G., et al. used a 2D culture of mouse adipose-derived stem cells (ASCs) in a four-point

bending mechanical device (**Fig. 1.10b**) [Li et al., 2013]. With this device, cells were stimulated with a uniaxial compressive force for 2 and 6 hours after adipogenic induction, leading to 0.2% deformation. The authors found that the adipogenic genes, PPAR $\gamma$ 1 and adiponectin (APN) were down-regulated. Together these data suggest effective inhibition of adipogenesis when mesenchymal stem cells and pre-adipocytes seeded on 2D surfaces are exposed to static and cyclic compression, respectively.

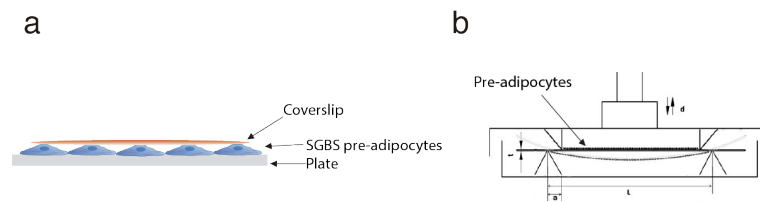


Figure 1.10: **Compression apparatus in 2-dimensional cultures.** (a) Representation of the experimental procedure described in [Hossain et al., 2010], and (b) four-point bending mechanical device developed by Li et al. [2013]. Panel b reproduced with permission.

### Lipogenesis and lipolysis

The aforementioned studies by Hossain et al. [2010]; Li et al. [2013] observed a reduction of lipid droplets in cells statically compressed. However, in both studies the authors did not investigate the possibility of this result being a consequence of lower number of differentiated cells.

To our knowledge, Pellegrinelli et al. [2014] was the only study on the effect of mechanical forces on adipocytes in 3D. The main focus of this work was to understand how adipocytes behave in fibrotic tissues and therefore the authors used decellularized adipose tissue from lean and obese in combination with a peptide gel (**Fig. 1.11a**). Cells were mechanically compressed with a similar device represented in **Fig.1.11b** reaching almost 10% of cellular deformation. The authors found that under simultaneous static compression and  $\beta$ -adrenergic stimulation, adipocytes presented lower rates of lipolysis. However, neither the duration of this stimulation as well as the potential mechanisms behind the reduced lipolysis were presented.

Author, Year	Cell Line	Model	Mechanical Stimuli	Duration of loading	Results
<b>Adipogenesis</b>					
[Hossain et al., 2010]	SGBS pre-adipocytes	2D	Static compression 226 Pa	12 hours	↓Adipogenesis
[Li et al., 2013]	Mouse adipose stem cells	2D	Cyclic compression 0.2% of deformation	2 or 6 hours	↓Adipogenesis
<b>Lipogenesis and Lipolysis</b>					
[Hossain et al., 2010]	SGBS pre-adipocytes	2D	Static compression 226 Pa	12 hours	↓Lipid accumulation
[Li et al., 2013]	Mouse adipose stem cells	2D	Cyclic compression 0.2% of deformation	2 or 6 hours	↓Lipid accumulation
[Pellegrinelli et al., 2014]	Human mature adipocytes	3D	Static compression 10% deformation	Not reported	↓Stimulated lipolysis

Table 1.5: **Compression studies.** Studies evaluating the effect of compression on adipogenesis and lipid accumulation of adipocytes.

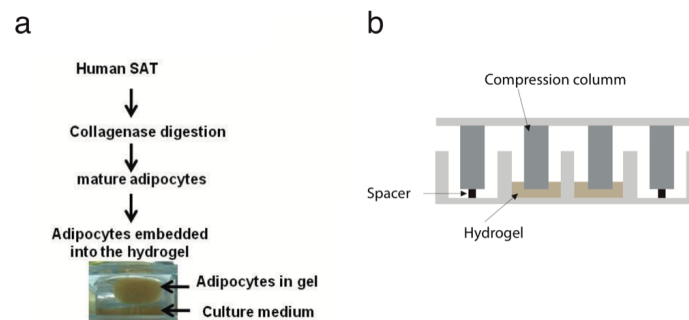


Figure 1.11: **Mechanical compression of a hybrid decellularized tissue and peptide hydrogel developed by Pellegrinelli et al. [2014].** (a) Hybrid hydrogel reproduced with permission from Pellegrinelli et al. [2014]. (b) Representation of the experimental procedure described in [Pellegrinelli et al., 2014].

## Other studies

Finally, recent research carried out by Jansson J. and colleagues in 2017, investigate the effect of body weight on the regulation of fat mass in rats and mice [Jansson et al., 2017]. The authors implanted capsules that weigh 15% of the animal body weight in the animals abdomen, and found that after 2 days of the implantation under high fat diet, the biological body weight decreased in relation to the controls. This observation was accompanied by a

remarkable decrease in WAT observed by MRI. The controls received the same dimensional capsules but without load. This capsule caused an equal reduction of food intake in both cases, ruling out this behaviour as a cause of the different weight loss. Therefore the authors hypothesis that the body weight itself acts as a homeostatic mechanism. Strikingly, they found that this mechanism was dependent on osteocytes of the weight-bearing bones that potentially communicate with the brain to decrease fat mass. This was confirmed by mice depleted of osteocytes, for which this body weight-reducing effect was lost.

To conclude, adipocytes are mechanosensitive cells that seem to respond to various stimuli. However, most of the studies have been carried out in two dimensional cultures that lack the three dimensional environment in which adipocytes usually are. Therefore, more research is needed to elucidate how mechanical stimuli are transmitted and the effect they have on the modulation of adipocyte gene expression.



## **Chapter 2**

### **3D *in vitro* model for static compression and main methods**

## 2.1 Introduction

Recently, adipose tissue has gained a strong interest due to an increase in the rate of obesity. Adipose tissue is a soft tissue, primarily composed by adipocytes, which are embedded in a basement membrane rich in type VI collagen. Surrounding this collagen mesh is a predominantly type I collagen fiber network termed the interlobular septum [Comley and Fleck, 2010]. Other cells, such as fibroblasts and immune cells, are also located within the tissue, where they play important roles on the development of obesity. *In vitro* studies of adipose tissue have been primarily performed using two-dimensional cultures. While such studies provide important insights, they do not reflect the interactions between cells and their microenvironment encountered *in vivo*. Therefore, we aimed to implement a tissue engineering approach.

Engineering a tissue requires the integration of three core principles, which are an appropriate choice of cells, scaffolds and signals. Clonal and primary cell lines are the usual choices for the first. The most commonly investigated adipogenic cell lines are 3T3-L1, 3T3-F442a and Ob17 murine cell lines [Flynn and Woodhouse, 2008]. Their ability to be cultured *in vitro* for long periods of time, associated with the maintenance of a well-defined identity, makes them a reliable tool to study adipogenesis and adipocyte function. Moreover, other studies have also shown that 3T3-L1 presented good ability to be cultured into three dimensional cultures [Gentleman et al., 2006; Louis et al., 2017]. The second aspect, the choice of the scaffold, is inspired by the microenvironment of the tissue. This requires appropriate materials that offer similar mechanical and structural properties to the native tissue. The scaffold should promote cell attachment and migration, facilitate cell-cell and cell-matrix interactions [Boudreau and Weaver, 2006; Gomillion and Burg, 2006]. A large range of materials (natural, synthetic and decellularized) have been used in AT engineering [Flynn and Woodhouse, 2008]. However, due to the collagenous nature of AT, collagen scaffolds have been pointed out as being good candidates to develop these three-dimensional models. Ev-

idence for this is the maintenance of adipocyte phenotype and depot specific characteristics for long term cultures, when primary mouse adipocytes, pre-adipocytes or human adipose-derived stem cells are cultured within these collagen hydrogels [Emont et al., 2015; Louis et al., 2019]. Other advantages of these scaffolds are tunable mechanical properties, direct cell encapsulation and low cost.

The last aspect, the signals, covers several cues that regulate cell fate and function. Examples of these cues are mechanical and electrical cues. In this work we are interested in mechanical cues. In the field of adipose tissue, models involving mechanical stimulation are scarce. The approaches reported are usually based on varying the substrate stiffness wherein the cells are seeded, applying tension on the substrate membranes, or applying static weights on top of the two-dimensional monolayers [Hossain et al., 2010; Katzengold et al., 2015; Levy et al., 2012; Shoham et al., 2012, 2015] (see previous chapter). To our knowledge, Pellegrinelli et al. was the first to use plastic lids to apply static compression to 3D cultures of primary adipocytes [Pellegrinelli et al., 2014]. However, the main focus of their work was to study the effect of fibrosis on AT.

In this chapter, we present a three-dimensional model of adipose tissue enabling static compression with different levels of strain, without compromising the cell viability. To achieve this, we pursued three goals. The first consists of the differentiation of the 3T3-L1 pre-adipocytes into mature functional adipocytes within a 3D environment. The second is to develop a method to statically compress the cells providing different levels of strain. The last goal is to evaluate whether the compression causes cellular damage. In summary, in this chapter we provide an overview of the model used for the *in vitro* studies as well as a detailed description of the main methodology.

## 2.2 Materials and Methods

### 2.2.1 Experimental design

In the table below we present the three goals of this chapter, as well as the strategies to investigate them. A more detailed description of each assessment follows.

Goal	Assessment
3D differentiation of 3T3-L1 pre-adipocytes into 3T3-L1 adipocytes and comparison with 2D	<ul style="list-style-type: none"> <li>- Percentage of differentiation (In relation to 2D)</li> <li>- Expression of the master regulators of adipogenesis (PPAR<math>\gamma</math> and C/EBP mRNA expression)</li> <li>- Expression of adipocyte functional proteins (perilipin-1, vimentin and caveolin-1 expression)</li> <li>- Cell morphology (lipid filled cell, round shape)</li> </ul>
Mechanical compression of cell-seeded hydrogels	<ul style="list-style-type: none"> <li>- Quantification of the hydrogel deformation (change in hydrogel thickness after the loading)</li> <li>- Cell deformation within the hydrogel (quantification of cell aspect-ratio under load )</li> </ul> <p>Appendix 1: Stress and strain distributions under the loads - Finite Element Analysis.</p>
Cell viability under compression	<ul style="list-style-type: none"> <li>- Necrosis (Live and Dead assay, LDH assay)</li> <li>- Apoptosis (expression of Cleaved caspase-3)</li> <li>- Hypoxia (expression of Hif1-alpha protein)</li> </ul>

Table 2.1: **Experimental goals to establish the 3D compression model.**

### 2.2.2 Cell culture

#### 2.2.2.1 3T3-L1 pre-adipocytes

3T3-L1 cells were provided by Dr. Cristoforo Silvestri and cultured following Silvestri et al. [2013]. Briefly, 3T3-L1 (from ATCC) were cultured in ‘growth’ medium (high glucose DMEM, Gibco™Life Technologies) supplemented with 1% of Penicillin-Streptomycin (Gibco™Life Technologies) and 10% of Fetal Bovine Serum (Gibco™10270), in a incubator

at 37° and with 5% of CO<sub>2</sub>. Cells were passaged once reaching 80% of confluence.

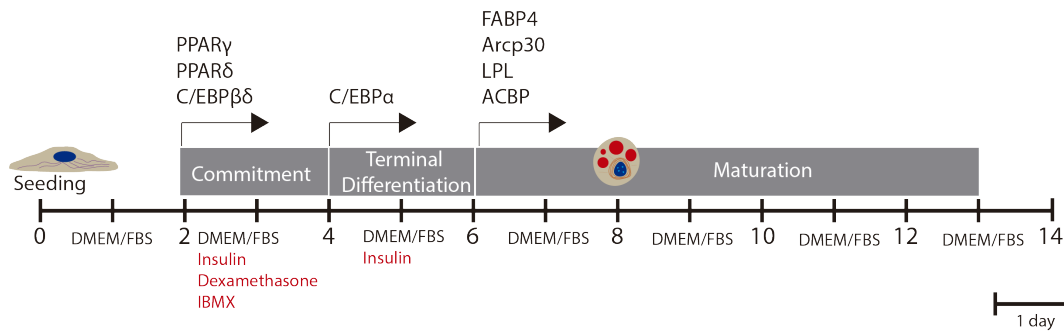


Figure 2.1: **Schematic representation of the adipogenesis timeline.** Adipogenesis is induced by an adipogenic cocktail composed by insulin, dexamethasone and IBMX. The cocktail induces the expression of the two masters regulators of adipogenesis, PPAR $\gamma$  and C/EBP $\alpha$ . After commitment, adipocytes start to express important genes involved in the adipocyte function.

### 2.2.2.2 Adipogenic differentiation

To induce adipogenesis either in 2D or 3D, cells were seeded at a concentration of  $5.3 \cdot 10^4$  cells/cm<sup>2</sup> and  $3 \cdot 10^5$  cells/ml, respectively, and cultured for 2 days with growth medium. After two days, the medium was switched to a ‘differentiation’ medium composed by high glucose DMEM supplemented with 0.5 mM of 3-isobutyl-1-methylxanthine (IBMX, Sigma), 1  $\mu$ g/ml of insulin (Sigma), 0.25 mM dexamethasone (Dex, Sigma) and 1% Penicillin-Streptomycin and 10% FBS for two days, corresponding to the commitment phase on **Fig. 2.1**. On day 4, cells were incubated for another 2 days with growth medium only supplemented 1  $\mu$ g/ml of insulin, corresponding to the terminal differentiation step on **Fig. 2.1**. Finally, during the maturation period, cells were fed with growth medium without supplements for the rest of the experiment, changing the medium every 2 days.

## 2.2.3 Cell-seeded collagen type I hydrogels

### 2.2.3.1 Extraction and purification of rat tail collagen

Type I collagen solutions were performed following an adaption of the protocol from Rajan et al. [2007]. Briefly, rat tails from Sprague Dawley rats (purchased from Sera Laboratories

International, LTD) were rinsed with 70% ethanol, and placed in a sterile glass petri dish under a laminar flow cabinet. The skin of the rat tails was peeled off using the hemostat and forceps, exposing the tendon bundles (**Fig. 2.2b**). Tendons were removed, rinsed with ethanol 70%, weighted and placed in 0.1% of sterile acetic acid (Sigma-Aldrich), at a concentration of 150 ml per gram of tendon (**Fig. 2.2c**). The collagen was allowed to stabilise for at least 48 hours at 4°C. Once stabilised, the solution was centrifuged at 9000 rpm for 90 minutes at 4°C (**Fig. 2.2d**). The clear supernatant was collected, frozen at -80°C overnight and lyophilized (Freeze Dryer, Labconco) for at least 48 hours (**Fig. 2.2e and f**).

The final collagen product was reconstituted in 0.2% sterile acetic acid (Sigma-Aldrich) at the desired concentration and stored at 4°C until use. Four collagen stock solutions were prepared: 1.25 mg/ml, 2.5 mg/ml, 5 mg/ml and 10 mg/ml.

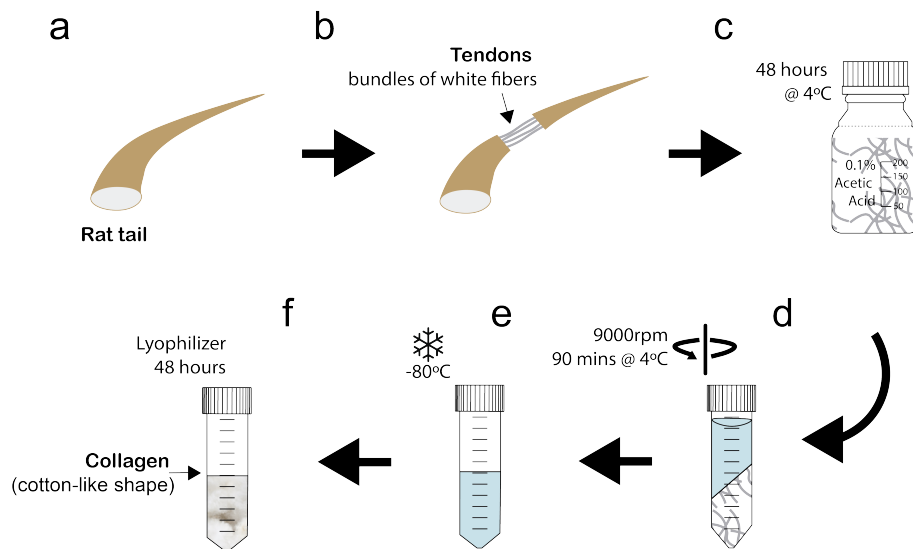


**Figure 2.2: Schematic representation of collagen extraction procedure. (a-b)** The skin of the rat tail was removed allowing to retrieve the rat tail tendons. **(c)** Tendons were exposed to 0.1% of acetic acid solution for 48 hours allowing the collagen to dissolve. **(d-e)** The solution resulted in step c was centrifuged and the supernatant was collected and subsequently frozen at -80°C. **(f)** The frozen supernatant was lyophilized resulting in a pure collagen mass.

### 2.2.3.2 Hydrogel preparation

All collagen hydrogels prepared in this work were produced by the following protocol. To produce collagen hydrogels at a final concentration of 1 mg/ml, 2 mg/ml, 4 mg/ml and 8 mg/ml, 8 parts of the respective stock solution (see previous section) was mixed with 1 part of 0.34 N NaOH, 1 part of 10x MEM and 1:400 of HEPES (Sigma-Aldrich). Once the pH was brought to approximately 7-7.4, 10  $\mu$ l of DMEM with or without cells was added and mixed with the collagen solution. The pH neutralisation corresponds to the first step of polymerization of the collagen hydrogels.

A 270  $\mu$ l of the solution was directly pipetted into 12-well culture inserts (0.4  $\mu$ m PET Transwells<sup>TM</sup>, Corning) that were previously brought at 37°C in the incubator. This resulted in a 2.39 mm thickness, which was calculated by

$$h = \frac{V}{\pi \cdot r^2} \quad (2.1)$$

where  $V$  is the volume of the solution and  $r$  the radius of the culture insert.

Immediately after pouring the hydrogel solution in the wells, the culture inserts were placed in the incubator at 37°C for 30 minutes to allow for the second step of the hydrogel polymerization. After gelation, fresh growth media was added to the wells.

The 1mg/ml and 4mg/ml hydrogels were used in the main research of this work whereas the 2mg/ml and 8mg/ml were used for supplementary analysis.

## 2.2.4 Static compression

### 2.2.4.1 Weights

To compress the collagen hydrogels, different cylindrical weights (diameter of 10 mm) were created from a glass ceramic rod ( $\rho = 2520\text{kg}/\text{m}^3$ , Macor<sup>TM</sup>Machinable Glass Ceramic,

RS). A schematic representation of the loads is shown in **Fig. 2.3**. A cover-slip of the same diameter was used to impose a similar transport barrier to the hydrogel without applying strain. The mass of each weight was measured using an analytical balance **Fig. 2.3**. As the weights were submerged when applied to the hydrogel, we accounted for the buoyancy force using the following equation:

$$F_b = g \cdot m_o \left(1 - \frac{\rho_f}{\rho_o}\right) \quad (2.2)$$

where,  $F_b$  is the buoyancy force,  $m_o$  is the true mass of the weight,  $\rho_f$  is the surrounding fluid density and  $\rho_o$  is the material density. We considered the density of the culture medium to be the same as water. Since the cells are experiencing this buoyancy force, we will use these values throughout this work.



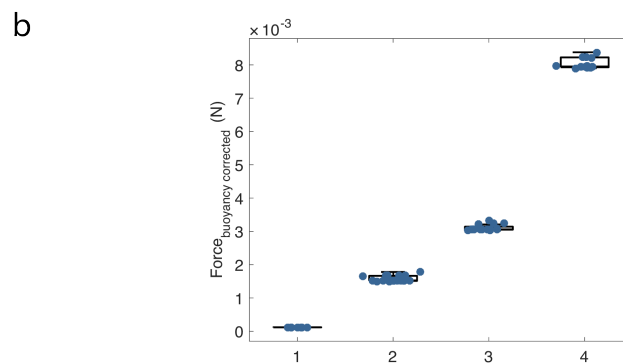
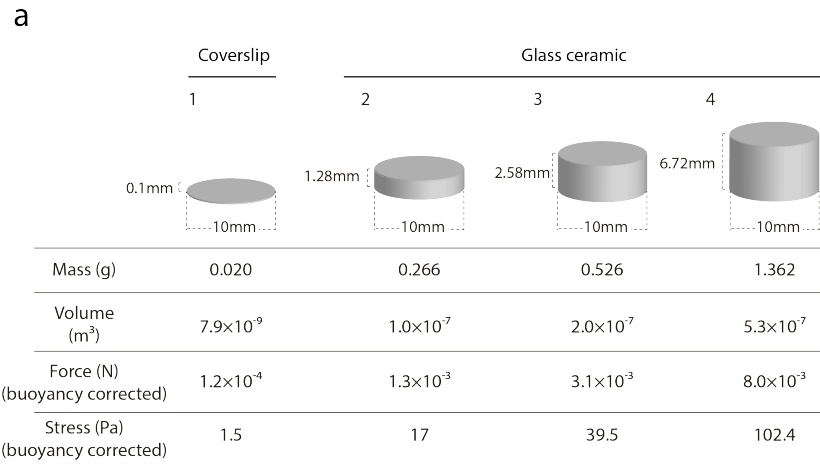


Figure 2.3: **Representation of the different loads and their corresponding mass, force and stress.** (a) Representation of the weights with their corresponding measured mean mass (g), volume (m<sup>3</sup>), force (N) and stress (Pa). (b) Individual force (buoyancy corrected) for all loads used.

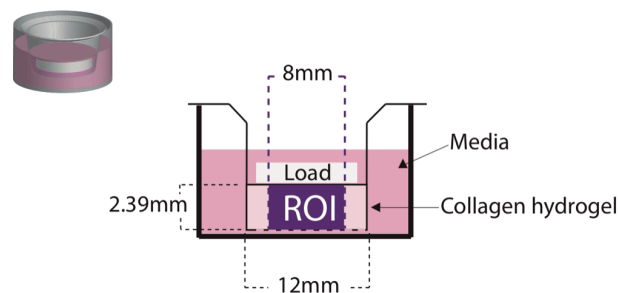


Figure 2.4: **Schematic representation of the model.** Collagen hydrogel casted in a 12 mm diameter culture insert. Predicted height of the casted hydrogel was 2.39 mm. A region of interest (ROI) in the center of the hydrogel was selected to study the effect of static compression on the cell behaviour (purple region). This ROI was retrieved by a 8mm diameter biopsy punch.

#### 2.2.4.2 Region of interest

The loads were placed on the center of the culture insert (see **Fig. 2.4**, grey zone). The region under the weight was extracted using a 8 mm diameter biopsy punch. This region was considered the region of interest (ROI) used for further experiments (**Fig. 2.4**, purple zone).

#### 2.2.4.3 Sample retrieval

**Cell suspensions.** Collagenase digestion was performed to liberate the cells from the collagen hydrogels to obtain single cell suspensions. Briefly, the ROI of the hydrogels (loaded and non-loaded) were placed into a collagen digestion buffer composed by 0.05 mg/ml of collagenase from *Clostridium histolyticum* ( $\geq 800$  CDU/mg, Sigma-Aldrich) dissolved in Hank's Balanced Salt Solution (HBSS, from Gibco) and 3% of bovine serum albumin (BSA, Sigma-Aldrich). This buffer was supplemented with 1 mM calcium chloride and 1 mM magnesium chloride (both from Sigma-Aldrich). The ROI samples were incubated in the digestion buffer at 37°C degrees for 30 minutes to obtain complete digestion of the collagen hydrogel. Immediately after, the cell suspension was filtered using a 100  $\mu\text{m}$  pore size cell strainer. The cell suspension was either kept in ice until further use or fixed with 2% of PFA in 1x PBS.

**Sample fixation in 3D.** For analysis of the cells embedded in the collagen hydrogels, the ROI was washed with 1x PBS for 30 minutes in constant agitation and fixed with 4% PFA overnight.

### 2.2.5 Quantification of strains

All the compression studies were performed at day 8 of the timeline (**Fig. 2.1**).

#### 2.2.5.1 Hydrogel deformation

Hydrogel deformation for the different loads was measured in the 1mg/ml and 4mg/ml collagen hydrogels. We used the loads corresponding to 0 Pa, 1.5 Pa, 17 Pa, 39.5 Pa and 102.4

Pa stress for 24 hours. The height of hydrogels (loaded and non-loaded) were measured by quantifying the distance between the initial and the last focal plane containing cells in the  $z$ -axis using a confocal microscope (10x magnification objective, Leica SP8 inverted confocal microscope). We analysed the ROI zone by taking five measurements per hydrogel. To ensure the hydrogel shape, we fixed it immediately after compression and we did not punch the ROI.

### **2.2.5.2 Cell deformation**

Cell deformation resulting from the highest load, 816mg, was quantified by measuring changes in the cell dimensions ( $x, y, z$  and aspect-ratio  $\frac{z}{\sqrt{xy}}$ ). Controls and 24 hours mechanically stimulated samples were fixed overnight with 4% of PFA immediately after removing the load and washed in 1x PBS three times, 10 minutes each. HCS CellMask<sup>TM</sup>Deep Red (ThermoFisher Scientific), a label that stains the entire cell, was used at a concentration of 2  $\mu\text{g/mL}$  for 15 minutes. Samples were washed three times with 1x PBS and kept in 1x PBS at 4°C until used. For each sample, 5 images composed by several stacks were acquired by confocal microscopy (Leica SP8 inverted confocal microscope). Images were analysed by Volocity 3D image analysis software. Briefly, cuboid shapes were automatically generated by the software around each cell. The  $x, y$  and  $z$  dimensions of each cuboid was exported and analysed in Matlab. To avoid artefacts detected by the software, cell volumes smaller than 400  $\mu\text{m}^3$  were excluded from the analysis as well as cuboids with at least one dimension ( $x, y$  or  $z$ ) smaller than 5  $\mu\text{m}$ .

### **2.2.6 Immunofluorescence**

All the immunofluorescence stainings performed in this thesis followed the standard procedures. Briefly, at the corresponding timepoint, cell culture media was aspirated, and the hydrogels were washed for 30 minutes with 1x PBS in constant agitation. The 1x PBS solution was aspirated and samples were fixed with 4% of PFA overnight in the fridge to ensure proper diffusion of the solution. Next day, samples were washed 3 times for 1 hour, and

blocked with blocking buffer containing 1x PBS, 5% of normal serum from the same species as the secondary antibody and 0.3% of TritonX-100, in agitation. After blocking, samples were incubated overnight at 4°C under constant agitation with primary antibodies diluted in antibody dilution buffer composed by 1x PBS, 1% of BSA and 0.3% of Triton X-100. The concentration used for primary antibodies was 1:200 for anti-rabbit IgG Perilipin-1, 1:100 for anti-rabbit IgG Caveolin-1, 1:200 for Vimentin. Samples were then washed 3 times for 1 hour, and incubated with the corresponding secondary antibodies diluted in the antibody dilution buffer (Goat anti-mouse IgG1 Cross-Adsorbed Secondary Antibody, Alexa Fluor 488 and goat anti-rabbit Secondary Antibody, Alexa Fluor 633) for 2 hours at room temperature, in continuous agitation in the dark. Samples were then rinsed three times with 1x PBS for 10 minutes each and stained with DAPI (1:1000) diluted in 1x PBS for 20 minutes in the dark. This last step was repeated to stain with LipidTox (1:1000). Finally, two washes of 15 minutes with 1x PBS were performed. All these last steps were performed under agitation. Samples were kept in 1x PBS until been imaged by confocal microscopy (Leica SP8 inverted confocal microscope).

To study cell morphology, phalloidin (ThermoFisher Scientific), a highly bicyclic selective peptide that binds to all variants of actin filaments, was used. In this work, phalloidin with different fluorophores (488, 568 and 647 nm) was used, depending on the aim. Briefly, after fixation with 4% of PFA the cells were permeabilised with Tween-20. Cells were stained with 20  $\mu$ l/ml during 30 minutes at room temperature in constant agitation using a shaker. Hydrogels were rinsed with 1x PBS, three times for 10 minutes in agitation. Samples were kept in 1x PBS at 4°C until usage.

### **2.2.7 Protein quantification**

Western-blots were performed following standard procedures. Briefly, hydrogels were punched with a biopsy punch in the ROI, as described previously. The punched section was washed in ice-cold 1x PBS for approximately 30 minutes in constant agitation to ensure proper wash-

ing out of the media and PBS inside of the hydrogel. Cells within the hydrogel were then lysed using RIPA buffer (Thermo Scientific™Pierce™) supplemented with 1X protease and phosphatase inhibitors and 5 mM EDTA (Halt™Protease and Phosphatase Inhibitor Cocktail (100X), ThermoFisher Scientific). The lysis procedure had a total duration of 30 minutes. During this period samples were in ice and vortex every 5 minutes. Lysates were quantified by BCA assay followed the protocol provided by the manufacturer (Pierce™BCA Protein Assay Kit, ThermoFisher Scientific). Each sample was diluted to the same protein concentration, followed by a denaturation step at 95°C for 10 minutes. A 15 µg of lysate was loaded per lane on a 12% polyacrylamide gels (XT MOPS, BioRad) and transferred into a nitrocellulose membrane. Membranes were blocked during 1 hour at room temperature with skim milk (Sigma-Aldrich). After blocking, the membranes were incubated with the primary antibody overnight at 4°C in constant agitation and washed before incubation with horseradish-peroxidase (HPR)-conjugated secondary antibody for 1 hour at room temperature. Finally, membranes were washed and rinsed with 1x PBS and incubated for 1 minute with ECL Western Blotting Substrate (Promega) and developed in film (GE Healthcare Life Sciences). The following primary antibodies were used at the specified concentrations: HIF1 $\alpha$  (1:500, Abcam), caspase-3 (1:1000, Cell Signalling), cleaved caspase-3 Asp175 (1:1000, Cell Signalling), cleaved PARP Asp214 (1:1000, Cell Signalling),  $\beta$ -actin (1:1000, Cell Signalling).

## **2.2.8 Gene Expression, RT-qPCR**

To extract RNA from the 3D hydrogels and 2D cultures, cells were initially homogenized in TRIzol™(Thermofisher Scientific). Subsequently RNA isolation and purification was performed using PureLink RNA Mini Kit (Thermofisher Scientific) according to the protocol provided by the manufacturer. cDNA was synthesized using Superscript reverse transcriptase (Invitrogen) and analysed using SYBER green technology (Fisher Scientific). The reverse transcription-quantitative PCR with gene-specific primers (**Table 2.2**, purchased from Sigma-Aldrich) was performed with QuantStudio 6 Flex Real-Time PCR System. Gene expression levels were calculated by normalization to hypoxanthine-guanine phosphoribosyl-

transferase (HPRT) by the  $\Delta\Delta C_T$  method. The mean cycle threshold ( $C_T$ ) was converted to a relative expression value by the  $2^{-\Delta\Delta C_T}$  method, and the range was calculated by the  $2^{(-\Delta\Delta C_T + \text{Standard deviation of } \Delta\Delta C_T)}$  method.

Table 2.2: Oligonucleotide primers used for RT-qPCR analysis.

Gene ID	R' Sequence	F' Sequence
HPRT	5'-GCCTGTATCCAACACTTCG	5'-TTGACACTGGTAAAACAATGC
PPAR $\gamma$ 2	5'-GTGATTTGTCCGTTGTCTTTCC	5'-ATGTCTCACAATGCCATCAGG
C/EBP $\alpha$	5'-TGAGTATCCAAGGCACAAGG	5'-GCGTCTAAGATGAGGGAGTC

## 2.2.9 Lipid quantification by flow cytometry

Intracellular lipid droplets can be measured by lipophilic reagents such as Nile red stain (AdipoRed<sup>TM</sup>, Lonza). Nile red becomes fluorescent in a hydrophobic environment and therefore lipid droplets can be detected at 530nm. Conventionally, the method is used in 2D cultured and the signal is measured by standard plate readers. However, due to the nature of a 3D assay, this method was adjusted to be used in flow cytometry. We first liberated the cells from the hydrogel using a collagenase solution, as described in the previous section. A gate strategy was established in order to select only the differentiated adipocyte population. Briefly, after collagenase digestion, samples were filtered with a 100  $\mu$ m cell strainer and fixed with 1% of PFA. Samples were stained with 0.1% v/v of AdipoRed<sup>TM</sup>. Quantification in the flow cytometer (BD Fortessa) was performed after 30 minutes of cell staining. Compensation controls (unstained cells and cells stained only with AdipoRed<sup>TM</sup>) were used in each experiment. The AdipoRed<sup>TM</sup> negative population corresponding to the undifferentiated population was used as a negative control. When combining different experiments in the same analysis, we used normalised flow cytometry data.

### **2.2.10 Cell Viability**

Cell viability in the hydrogels was investigated using the assays presented below. For all assays, we used 1 mg/ml collagen hydrogels.

#### **Live and Dead by flow cytometry**

Cell viability was assessed by Live and Dead Viability/Cytotoxicity Kit, which is based on the simultaneous determination of live and dead cells by intracellular activity and plasma membrane integrity. The assay provides two-colour fluorescence cell staining, calcein-AM for live and ethidium homodimer-1 for dead. These intensities were measured using flow cytometry. Green fluorescence emission (calcein-AM, 530/30 bandpass) was detected after 488 nm excitation, red fluorescence emission (ethidium homodimer-1, 610/20 bandpass) was detected after 528 nm excitation. For the sample preparation, the manufacturer's instructions were followed. Briefly, non-loaded and loaded cells were released from the hydrogels by collagenase digestion, as described previously, and stained with 1  $\mu$ M of calcein and 1  $\mu$ M of EthD-1 for 15 minutes at room temperature. Positive control for dead cells was achieved by treating the samples with saponin (Sigma-Aldrich). During acquisition, samples were kept in ice along the entire procedure. Compensation was performed by the DIVA software using samples without stains and samples with single stains. This avoids false positives, by detecting auto-fluorescence as well as spectral overlap between the two emission spectra.

#### **LDH assay**

Lactate dehydrogenase (LDH) is a common calorimetric assay, which quantifies the amount of endogenous LDH activity of the cells. Damaged or dead cells with compromised membranes have an increased LDH signal, allowing to use LDH quantification as an indicator of cell death. The assay was performed following the manufacturer's instruction with only an adaptation of the volumes, since we used a three dimensional model instead of two dimensional cultures. To validate this alteration, we performed two standard curves: a control in

two-dimensional cultures (which corresponds to the usual procedure), and a new standard curve for the three dimensional cultures (hydrogels).

The experimental procedure was performed as follows: at time points 0, 24 and 48 hours, 100  $\mu\text{l}$  of pure water was added to the non-loaded samples (negative control) and loaded samples. For positive controls, 100  $\mu\text{l}$  of lysis buffer was added. After 40 minutes of incubation at 37°C, 50  $\mu\text{l}$  of the supernatant of each sample was added to 50  $\mu\text{l}$  of the substrate (containing the enzyme) and incubated at room temperature for 30 minutes. In the end, a stop solution was added and the absorbance was measured at 490 nm and 680 nm in the SpectraMax M5 plate reader. The LDH activity was given by the subtraction of the 680 nm absorbance value from the 490 nm absorbance and the cell death was calculated following equation 2.3. All standard curves and the corresponding procedure are presented in supplementary section of this chapter.

$$\% \text{Cell death} = \frac{\text{Loaded sample LDH activity} - \text{Spontaneous LDH activity}}{\text{Maximum LDH activity} - \text{Spontaneous LDH activity}} \cdot 100 \quad (2.3)$$

### **Protein expression of HIF1 $\alpha$ and cleaved caspase-3**

To assess hypoxia and apoptosis we measured the protein expression of HIF1 $\alpha$  and cleaved caspase-3. See section 2.2.7 for details.

#### **2.2.11 Statistical analysis**

Samples were tested for normality before statistical analysis (Shapiro-Wilk test). For data normally distributed the following statistical methods were used. For comparing one or two normally distributed samples the *t*-test was used. For more than two samples the ANOVA test was used. To compare a set of samples where at least one set of samples was non-normally distributed, the Kruskal-Wallis test was used. To compare full distributions, the



Kolmogorov-Smirnov test was used. For a few cases when the number of N was equal to 2, no statistics were performed since the statistical power is too low.

All the analysis was performed in Matlab.

## **2.3 Results**

Our main goal in this chapter is to create a three dimensional scaffold supporting adipogenesis and adipogenic functions, as well as allowing various levels of compression of the cultured cells without damaging them.

### **2.3.1 Adipogenic differentiation of 3T3-L1 in 3D collagen hydrogels**

We used collagen type I hydrogels because of their resemblance to the natural environment of adipocytes. Accordingly, our first step was to evaluate whether 3T3-L1 pre-adipocytes were capable of differentiating in the same way as seen in the two dimensional cultures. To test this, we cultured the 3T3-L1 pre-adipocytes in culture plates (2D) and in hydrogels (3D). We then challenged the cells with an adipogenic cocktail. After 14 days of culture, the adipogenic differentiation was evaluated by quantifying the percentage of differentiated cells by flow cytometry (**Fig. 2.5**). No significant changes were found between the two conditions (two-sample t-test,  $p > 0.05$ ).

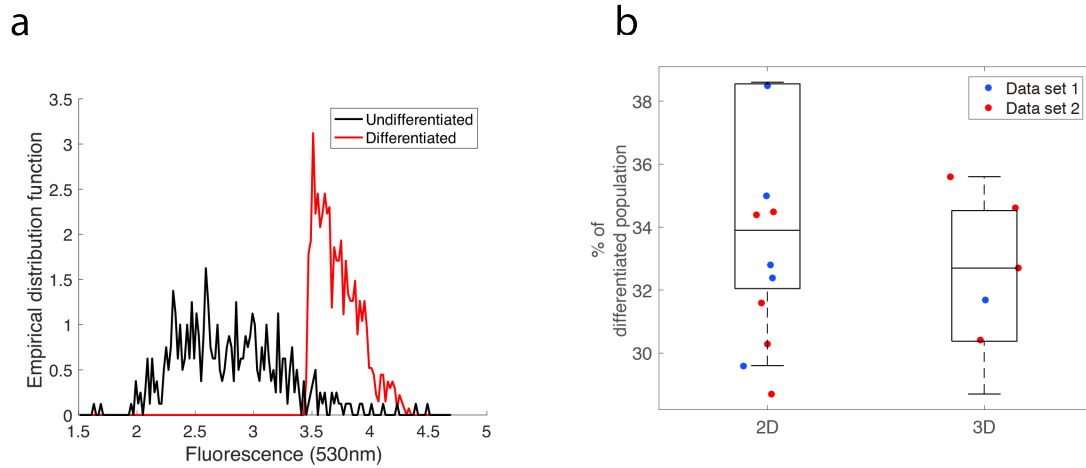


**Figure 2.5: 3T3-L1 pre-adipocyte adipogenic differentiation in two and three-dimensional cultures.** (a) An example of flow cytometry data for undifferentiated (black) and differentiated (red) populations. (b) 3T3-L1 adipocytes were cultured in 2D (plate) and 3D (1mg/ml hydrogel). Mature adipocyte counting was performed by flow cytometry by measuring the positive signal for AdipoRed<sup>TM</sup> as shown in panel a. Counts were normalised by the mean count of differentiated cells in two-dimensional cultures. No significant changes were found (two-sample t-test,  $p > 0.05$ ). Each data point correspond to one technical replicate from two experimental sets.

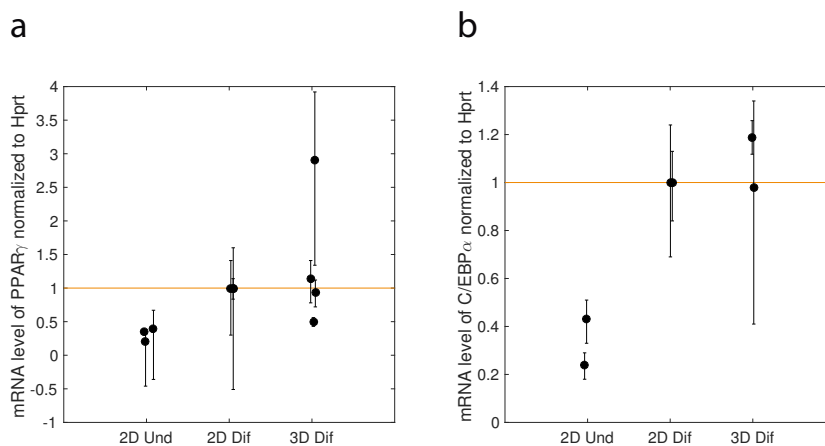


**Figure 2.6: mRNA levels of PPAR $\gamma$  and C/EBP $\alpha$  in two and three-dimensional cultures.** mRNA levels of undifferentiated and differentiated 3T3-L1 pre-adipocytes cultured in plate and differentiated in hydrogels (1 mg/ml) were measured at the 14 day. Error bars denote 1 standard deviation over three technical replicates.

At day 14, we also evaluated the expression of the two master regulators of the adipogenesis, PPAR $\gamma$  and C/EBP $\alpha$  (**Fig. 2.6a** and **b**). An undifferentiated sample, consisting of 3T3-L1

pre-adipocytes cultured for 14 days in 2D without adipogenic induction served as negative control for differentiation. The mRNA levels between the differentiated populations in 2D and 3D were similar. This was in line with our previous result, where we found a similar percentage of differentiation by flow cytometry.

Our next step was to evaluate the morphological changes that accompany the adipogenic differentiation. Remodelling of actin stress fibers into cortical fibers is a hallmark of adipogenesis [Nobusue et al., 2014]. Therefore, we analysed whether this process also occurs in the hydrogels. In **Fig. 2.7**, we show the 3T3-L1 morphology during the time in which adipogenesis occurs for both models. At day 2, both cultures show fibroblast-like morphology, characterised by long stress fibers. On day 4, after the samples were treated with the adipogenic cocktail, these fibers start to remodel. At day 8, it is possible to observe fully differentiated adipocytes, filled with lipids.

Despite the fact that both models qualitatively show the same remodelling pattern, we observed a more flattened phenotype in 2D cultures (**Supp. Fig. S2**).

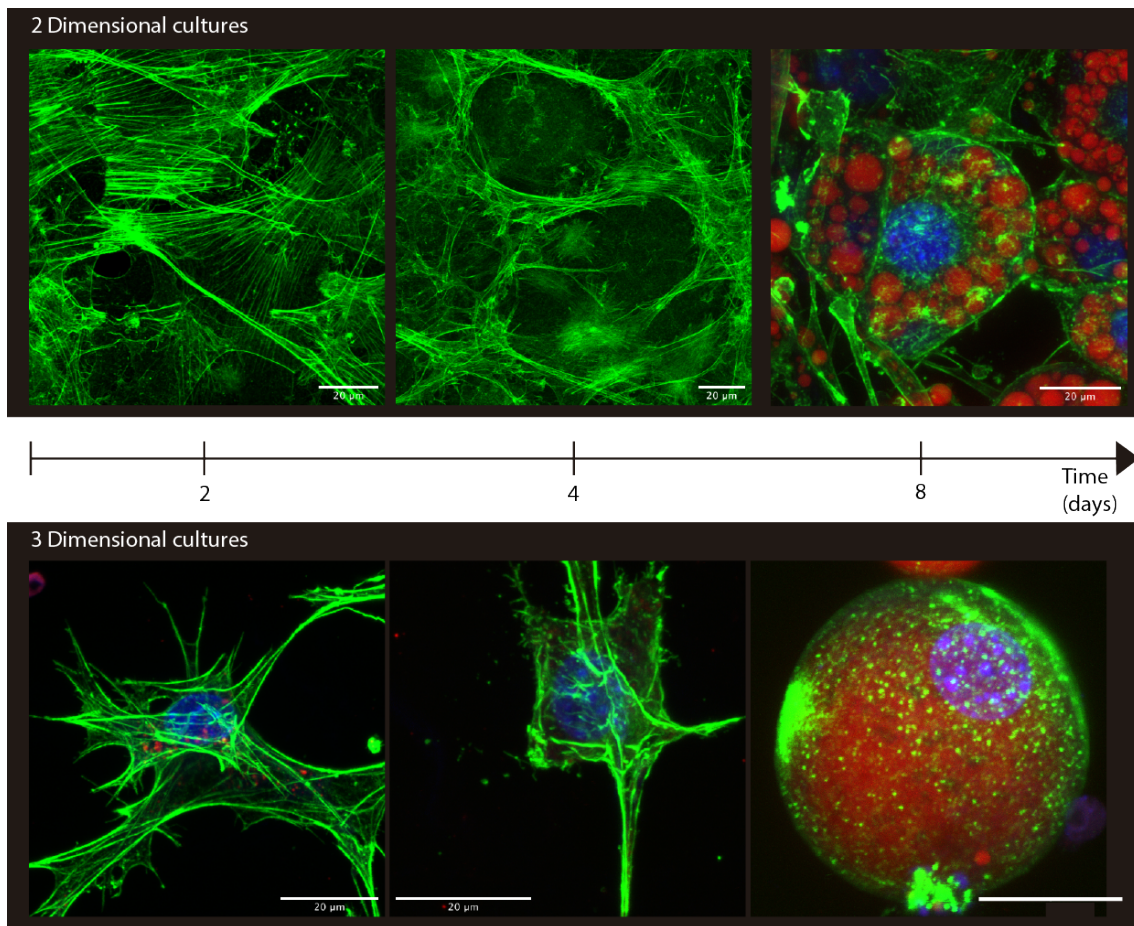


Figure 2.7: **Cellular morphology during adipogenesis in two and three dimensional cultures.** Green: F-actin (phalloidin); Red: lipids (LipidTox<sup>TM</sup>); Blue: nucleus (DAPI).

Finally, we investigate whether three important functional proteins of the adipocytes are expressed. The investigated proteins are vimentin, perilipin-1 and caveolin-1, which are involved in fatty acid transport and lipid droplet stability [Franke et al., 1987; Pilch and Liu, 2011; Shen et al., 2010; Sztalryd and Brasaemle, 2017]. We stained 3T3-L1 adipocytes differentiated in 4 mg/ml collagen hydrogels at day 8 for these proteins. We found that all of them were present, suggesting that the adipocytes not only differentiate in the three-dimensional collagen scaffolds but are also capable of expressing important functional proteins (**Fig. 2.8**). Taken together, these results show that collagen hydrogels can successfully accommodate pre-adipocytes and sustain their differentiation into fully mature adipocytes.

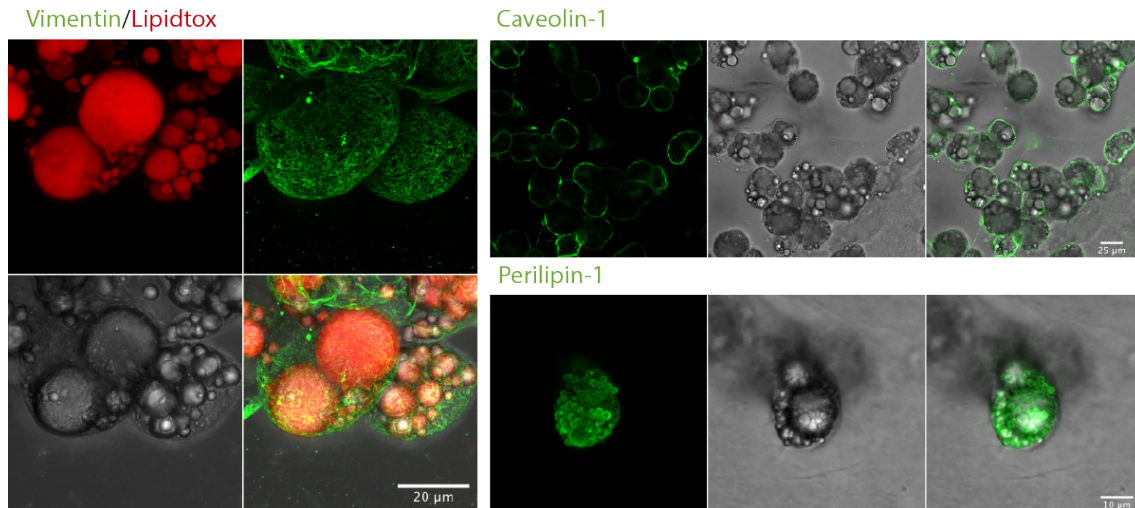


Figure 2.8: **Adipocyte functional proteins.** Immunofluorescence results of cultured 3T3-L1 adipocytes in collagen hydrogel. (Left) Vimentin and lipid. (Top right) Caveolin-1. (Bottom right) Perilipin-1.

## 2.3.2 Deformation

### 2.3.2.1 Hydrogel deformation

In order to understand which deformations the loads impose on the hydrogels, we measured changes in the height in unloaded and loaded samples. This was performed by confocal microscopy, by measuring the distance between the initial focal plane and the last. The stress and strain relationship is shown in **Fig. 2.9** for the different loads used. In 1 mg/ml hydrogels, the amount of strain was similar for all applied stresses (33%, 37% and 45% for 1.5 Pa, 17 Pa and 39.5 Pa, respectively). The highest load 102.4 Pa was not used for 1 mg/ml hydrogels due to time constrains. All loads were significantly different from the control, 0 Pa (two-sample t-test,  $p < 0.005$ ). However, they were not significantly different between themselves (two-sample t-test,  $p > 0.05$ ). For the 4mg/ml collagen hydrogels the strain increased with the stress (22%, 48% and 69% for 17 Pa, 39.5 Pa and 102.4 Pa, respectively). The first applied stress, 1.5 Pa, was not significantly different from the control. However, all other stresses resulted in significantly different strains compared to the control, as well as compared to

each other ( $p < 0.005$ ). These results demonstrate that, unlike 1mg/ml hydrogels, 4mg/ml hydrogels are capable of sustaining different amounts of strains.

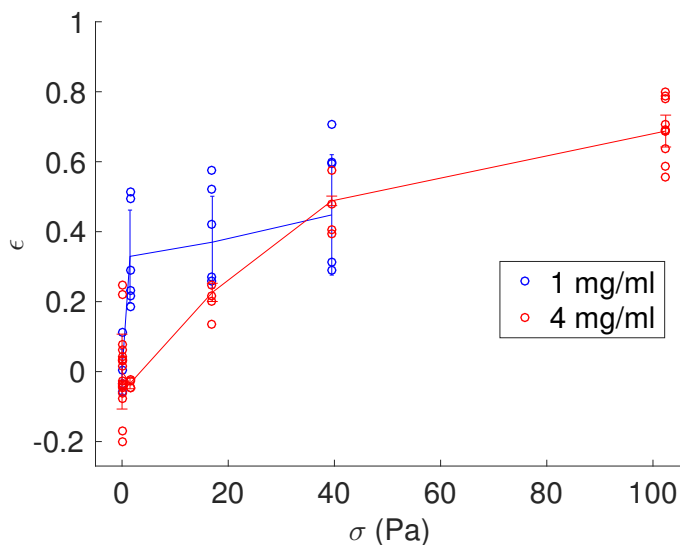


Figure 2.9: **Hydrogel deformation.** Strains in 1mg/ml and 4mg/ml collagen hydrogels in response to the different loads.

### 2.3.2.2 Cell deformation in response to the static load

Finally, we wanted to understand whether the static compression created a cellular deformation underneath the load. To understand how cells deform in response to applied load, we stained 102.4 Pa loaded the cells in 4 mg/ml hydrogels with a whole-cell dye and imaged the compressed region with a confocal microscope after fixation. The z-stack of each sample was then reconstructed. The smallest possible boundary box was generated around each cell using the Volocity software (**Fig. 2.10a**). The cumulative distributions of the different dimensions ( $x$ ,  $y$ ,  $z$ ) of each box are represented in **Fig. 2.10c**. We observed that cells under our highest load (corresponding to 102.4 Pa stress) showed a shift of 20% towards lower values in the  $z$  dimension, but no significant changes were observed in  $x$  and  $y$  dimensions (**Fig. 2.10c**). This was also reflected in a lower aspect ratio for loaded samples compared to controls (**Fig. 2.10b**). This indicates that the cell was effectively compressed along the vertical dimension, consistent with the direction of our applied stress.

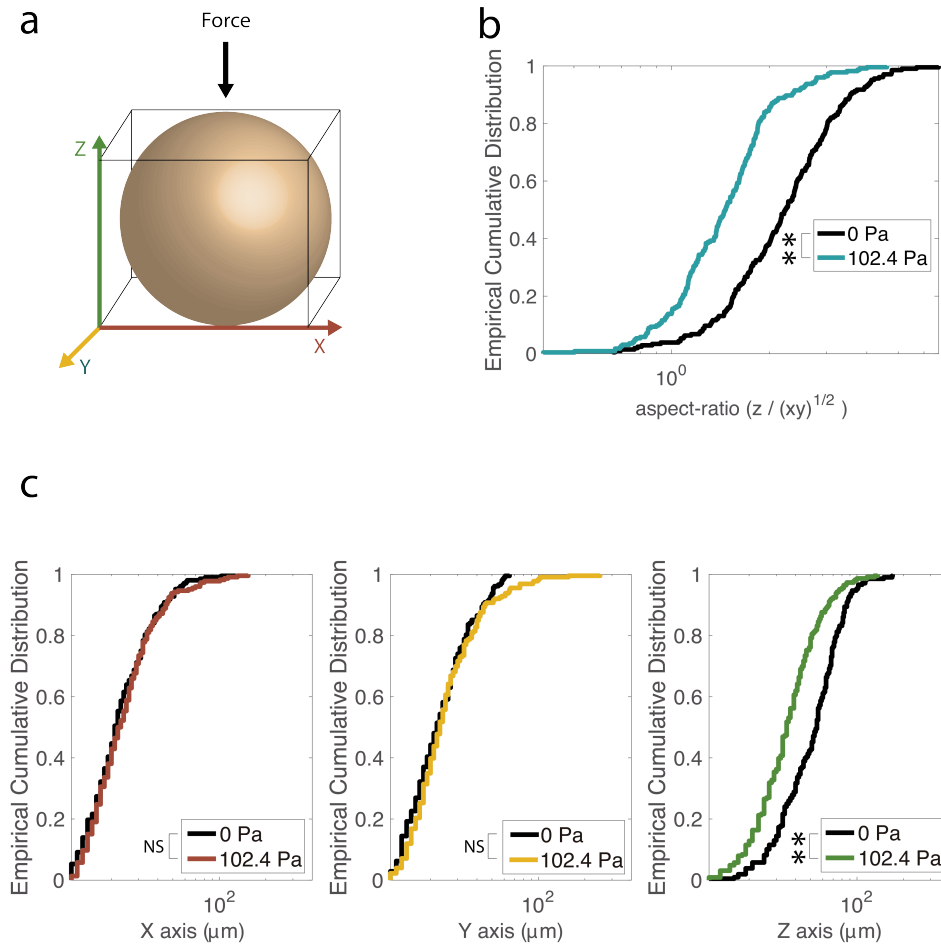


Figure 2.10: **Cell deformation in response to static compression.** (a) A minimal boundary box was calculated for each cell using Velocity Software (see details in methods section). The lengths of the  $x$ ,  $y$  and  $z$  sides of the boxes were stored for each cell, in control and compressed populations. (b) Empirical cumulative distribution of the  $z/\sqrt{xy}$  aspect-ratio for both populations. Compressed samples presented smaller aspect-ratio (two-sample Kolmogorov-Smirnov test,  $p < 0.005$ ). (c) Empirical cumulative distributions of the  $x$ ,  $y$  and  $z$  dimensions of the boundary box for both populations. Only the  $z$  dimension was significantly affected by the static load (two-sample Kolmogorov-Smirnov test,  $p < 0.005$ ). Horizontal axis of the plots is presented in log scale. Data consists of one experimental replicate composed by 4 technical replicates, number of cells used:  $N_{non-loaded} = 206$  and  $N_{loaded} = 224$ .

### 2.3.3 Cell viability in response to static load

We examine whether the cell viability was compromised due to the static compression. We first looked at possible cell death either by necrosis or apoptosis. To study necrosis, we performed two cell viability assays, the LDH release and the LIVE/DEAD viability/cytotoxicity assay. For apoptosis, we measured the protein levels of cleaved caspase-3, a critical executor of this pathway.

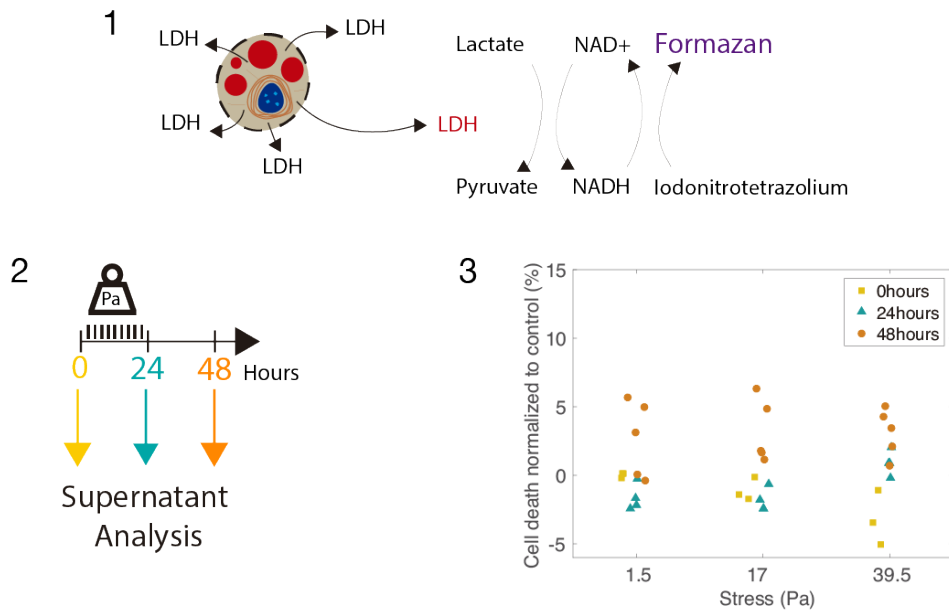
LDH assay, is a colorimetric assay that detects LDH present in the media as consequence of the cell membrane rupture (**Fig. 2.11 a<sub>1</sub>**). We investigate the LDH release at different time-points: before adding the weight, which corresponds to the basal LDH level; immediately after removing the weight, which accounts for the cell death during the 24 hours of compression; and lastly, one day after of removing the weight, to measure late cell death (**Fig. 2.11 a<sub>2</sub>**). On **Fig. 2.11 a<sub>3</sub>**, we observed a small but in some cases significant increase in cell death compared to the control (e.g. under the 39.5 Pa stress, we observed 3% cell death one day after removing the load). Because these percentages remained very small, we can conclude that most cells are alive.

To complement this result, we measured the percentage for live, dead and injured cells immediately after removing the load. After liberating the cells from the collagen hydrogel, cells were stained and analysed by flow cytometry. This allowed us to detect the live, dead and injured populations in the flow cytometry scatter plot (e.g, **Fig. 2.11 b<sub>1</sub>**). Live cells were stained by calcein-AM which was detected at a wavelength of 530 nm. Dead cells were stained with ethidium homodimer-1, which was detected at 610 nm. Finally injured cells, with compromised membranes, could be detected at both wavelengths. **Figure 2.11 b<sub>2</sub>** shows the percentage of dead, injured and live cells within the total population. In accordance with the LDH release result, the percentage of dead cells in samples under high stress was increased. This difference was significant but remain small (percentage of cell death of 1.4%, 1.5%, 1.4%, 2.2% and 3.3% under 0 Pa, 1.5 Pa, 17 Pa, 39.5 Pa and 102.4 Pa, respectively).



The percentages of cells injured were not significantly different in all samples (6.7%, 7.4%, 6.8%, 7.1% and 7.8%, in the same order as reported before). These results confirm that most cells are alive after applying compression.

a



b

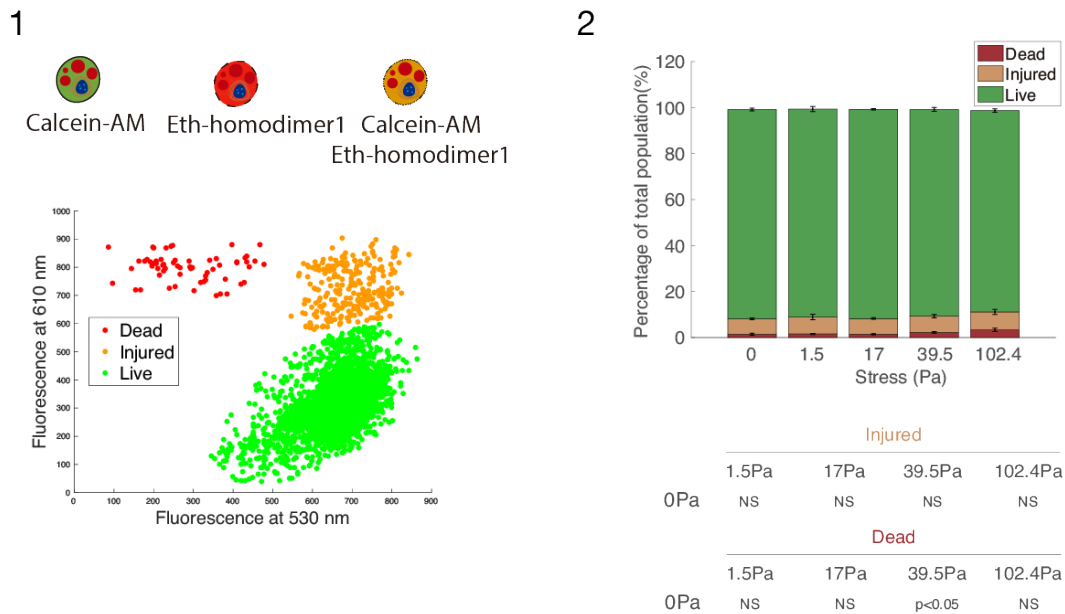


Figure 2.11: **Cell viability in response to the static compression.** (a<sub>1</sub>) LDH assay mechanism, see methods. (a<sub>2</sub>) Experimental timeline (a<sub>3</sub>) Percentage of cell death at the different time-points under 1.5 Pa, 17 Pa and 39.5 Pa stress. (b<sub>1</sub>) Schematic representation of the live and dead assay (top), and an example of the acquisition by flow cytometry (bottom). (b<sub>2</sub>) Percentage of live, injured and dead cells after 24 hours of compression (n=4). Error bars denote one standard deviation.(Kruskal-Wallis test, p<0.05)

Furthermore, we tested whether the load could trigger cellular apoptosis. Therefore, we looked at the protein expression of cleaved caspase-3. Cleaved caspase-3 is an indicator of apoptosis activation as it is either partially or totally responsible for the proteolytic cleavage of many key proteins. We measured the amount of protein expression in the entire cellular lysates that were either treated with an apoptotic inducer etoposide (a topoisomerase II inhibitor), loaded (102.4 Pa) for 24 hours, or non-treated and non-loaded (**Fig.2.12a**). It was possible to observe a clear band on cleaved caspase-3 in the positive control, as well as a slight increase in total caspase-3. We did not observe any changes between the control and the loaded sample, suggesting that experimental samples are not apoptotic.

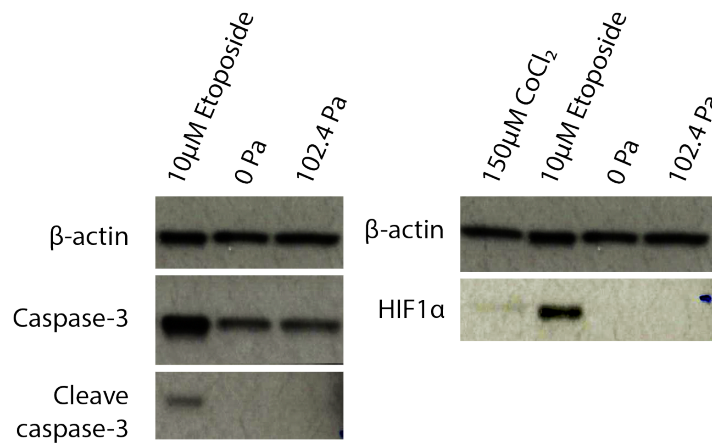


Figure 2.12: **Apoptosis and hypoxia markers.** (a) Protein expression blots of caspase-3 and cleaved caspase-3. (b) Protein expression blots of HIF-1 $\alpha$ .  $\beta$ -actin was used as loading control.

Our last step was to investigate whether the cells may be in hypoxia due to the physical barrier of the weight when placed on top of the hydrogel. Hypoxic conditions are known to trigger a cascade of events that alter adipose tissue functions [Trayhurn, 2013]. Therefore, it is crucial to dissect this effect from the mechanical stimulation. To test for hypoxia, we measured protein levels of HIF-1 $\alpha$ . As mentioned in the introduction chapter, in the presence of oxygen, HIF-1 $\alpha$  is ubiquitinated. On the other hand, in hypoxic conditions it translocates to the nucleus where it acts as a transcription factor. Therefore, high protein levels of HIF-1 $\alpha$  in hypoxic samples are expected. In the samples treated with cobalt chloride (CoCl<sub>2</sub>), which

prevents the ubiquitination of HIF-1 $\alpha$  in normoxia, it is possible to see a shaded band. An intenser band was expected, however this could be a consequence of a decay in activity at 24 hours [Lan et al., 2011]. On another hand, we found an unexpected band in the sample treated with etoposide. Importantly, the control sample (0 Pa) and loaded sample (102.4 Pa), did not show any presence of HIF-1 $\alpha$  (**Fig. 2.12**).

Taken together, these results show that compressing samples with static loads does not trigger higher levels of cell death, apoptosis nor hypoxia.

## 2.4 Discussion

In this chapter our main goal was to create a three-dimensional hydrogel to accommodate pre-adipocytes and adipocytes while statically compressing them for certain periods of time. In order to achieve this we used two well known systems, the 3T3-L1 pre-adipocytes and collagen type I hydrogels, in combination with static loads.

3T3-L1 is a well-established pre-adipose cell line developed from Swiss 3T3 cells, that display a fibroblast-like morphology. Similarly to primary pre-adipocytes, which are also fibroblast-shaped cells, under appropriate conditions they can acquire an adipocyte-like phenotype. Since this differentiation process is similar to the primary cell cultures, we choose to use 3T3-L1 to study the mechanobiological aspects of the adipocytes.

AT is rich in collagen and therefore we opted to use collagen type I hydrogels to create a three-dimensional *in vitro* microenvironment for our cultures. Mechanical properties of collagen hydrogels can easily be tuned by varying the collagen concentration, allowing us to reproduce mechanical features similar the ECM of AT. In this work, Young's modulus was measured by rheometry performing a strain sweep with strains ranging from 0.2% to 25% at a frequency of 1 Hz (see appendix A for methodology and results). For 4 mg/ml collagen hydrogels the measured Youngs Modulus was 1.82kPa, which is close to values reported for adipose tissue in the literature [Alkhouli et al., 2013; Geerligs et al., 2008].

Culturing the 3T3-L1 pre-adipocytes in collagen hydrogels resulted in fully differentiated adipocytes. The rate of differentiation was similar to the 2D cultures. At day 8, the majority of the adipocytes showed a spherical shape with the cytoplasm rich in lipid droplets. Associated with this result was the expression of the master regulators of adipogenesis PPAR $\gamma$  and C/EBP $\alpha$ , as well as the presence of adipocyte functional proteins, such as perilipin-1, vimentin and caveolin-1. Vimentin is the only intermediate filament present in adipocytes, which also undergoes changes in configuration during adipogenesis [Lieber and Evans, 1996]. An extended fibrillar array of vimentin is found in preadipocytes which turns into a regular intrafilament monolayer surrounding the forming lipid globules in adipocytes [Franke et al., 1987]. It plays an important role in stabilising small and medium lipid droplets in adipocytes as well as in the regulation of lipolysis, since it is a functional partner of hormone sensitive lipase (HSL) [Heid et al., 2014; Suzuki et al., 2011]. Caveolin-1 is involved in numerous functions such as fatty acid flux, triglycerol synthesis, lipid droplet targeting, pathways signalling and lipolysis synthesis [Pilch and Liu, 2011]. Lastly, perilipin-1 is a lipid droplet associated protein involved in the regulation of lipogenesis and lipolysis.

These results are in accordance with the literature, where successful cultures of 3T3-L1 in collagen type I hydrogels have been reported [Gentleman et al., 2006; Louis et al., 2017]. Moreover, collagen hydrogels have also been used in combination with primary cell lines [Emont et al., 2015]. Other systems, consisting of stem cells seeded in various types of materials such as electrospun polycaprolactone or poly-L-lactic acid fibers, porous bacterial nanocellulose scaffolds or in collagenous microbeads, have also been used to produce 3D cultures of adipocytes [Brännmark et al., 2014; Kang et al., 2007; Krontiras et al., 2015; Rubin et al., 2007; Shanti et al., 2008].

Since we are interested in compression, we designed cylindrical loads to compress the cell-seeded hydrogels. The loads were made of glass ceramic, a bio-compatible material. Our loads corresponded to pressures in the range of 0-1 mmHg, which corresponds to measured values of intra-abdominal pressure in healthy individuals.

We found that 1 mg/ml collagen hydrogels were too weak because they were almost maximally deformed at the lowest load imposed by the coverslip, and increasing the load had a negligible effect on strain. In contrast, 4mg/ml collagen hydrogels were stronger and exhibited a clear change in strain with increasing load. Therefore, we used the 4 mg/ml hydrogel in our following experiments.

The central region of the hydrogel was compressed, and we selected an ROI within this region as a target for our analysis. A preliminary finite element analysis showed that stress and strain distributions within the ROI were uniform (see Appendix A). This suggests that the whole cell population in ROI experienced similar mechanical stimuli. We also investigated the deformation of adipocytes caused by the imposed stress. The results showed approximately 20% of strain predominantly along the vertical axis ( $\epsilon_{zz}$ ), in agreement with the finite element analysis. This comprises almost three times less than the measured deformation of the hydrogels. A possible explanation for this result could be the fibre re-arrangement and loss of water content within the hydrogel in response to the load while accompanied the cell cytoskeleton rearrangement. These results show that not only the hydrogels are affected, but importantly also individual cells are strained.

Lastly, we evaluated whether this deformation could cause cellular damage as well as create unfavourable conditions such as hypoxia. We found neither of the two effects, ensuring that our future readouts will be a consequence of the mechanical stimulus and not of cell death or hypoxia. However, the hypoxia assay should be further investigated since the positive control showed a low signal. The cell viability assays were only performed in 1 mg/ml collagen hydrogels. Because they provide a poor support that results in high deformations, we believe that similar results apply to the 4 mg/ml collagen hydrogels.

To conclude, we described a tissue engineered 3D model composed of adipocytes seeded in collagen hydrogels. We showed that 3T3-L1 cells can differentiate into mature adipocytes. When we load the hydrogel, these adipocytes can undergo strains without compromising

the cell viability. This model will be used for the *in vitro* studies, investigating the effect of compression on adipocyte fate and function.





## **Chapter 3**

# **Effect of static compression on the lipid accumulation in adipocytes: 3D *in vitro* model**

### 3.1 Introduction

Obesity is a worldwide epidemic characterised by an excessive increase of white adipose tissue (WAT). Increased adiposity in visceral adipose tissue (VAT) has been implicated in the development of metabolic syndrome. This includes type-2 diabetes, cardiovascular diseases, dyslipidemia and abnormal production of adipokines. However, the cellular mechanisms behind these dysfunctions are incompletely understood. An interesting aspect associated with increased visceral adiposity is its positive correlation with intra-abdominal pressure, which increases from 5 mmHg in lean to 14 mmHg in obese individuals [De Keulenaer et al., 2012]. Given that VAT is confined in the abdominal space, we hypothesised that upon increased adiposity, visceral adipocytes experience compressive stress within this space. Understanding how adipocytes respond to compressive stress may allow us to understand the mechanisms involved in the obesity-related conditions.

Adipocytes are mechanosensitive cells with the ability to sense their size and microenvironment via autonomous mechanisms by triggering intracellular signals for functional adaptation [Pope et al., 2016]. An example of this is the mechano-sensitive ion channel - Swell1. This channel is implicated in the sensing of adipocyte volume during physiological and pathophysiological adipocyte expansion, which in turn mediates insulin-PI3K-AKT signalling [Zhang et al., 2017]. The  $\beta$ 1-integrin/ERK signalling pathway has also been proposed as a mechanism of endogenous volume sensing that modulates transcriptional programmes [Farnier et al., 2003]. Furthermore, an increase in lipid droplet size influences cell stiffness which consequently leads to the regulation of insulin sensitivity [Li et al., 2009; Shoham et al., 2014]. Interestingly, Shoham et al. [2012] showed that exposing 3T3-L1 pre-adipocytes to static mechanical stretching during differentiation accelerates lipid production, a mechanism proposed to be mediated by MEK signalling. While these studies uncover the role of mechanical forces in regulating adipocyte functions, it is not clear how mechanical stimulation, in particular compression, affects lipid metabolism in mature adipocytes.

The dynamics of lipid metabolism involve the formation (lipogenesis), expansion and break down of lipid droplets (lipolysis). Lipid droplets are made of triacylglycerols (TAG) and sterol esters shielded by a phospholipid monolayer that contains proteins such as perilipin-1, which are involved in their storage and mobilisation. The central players of lipolysis are the cytosolic lipases, such as adipose triglyceride lipase (ATGL) and hormone-sensitive lipase (HSL), that upon lipolytic stimuli ensure the break down of the stored lipids [Thiam and Beller, 2017]. The best known catalyst of lipolysis is the action of catecholamines via protein kinase A (PKA) cAMP-dependent pathway. However, other factors such as hormonal regulation, cytokines, endocannabinoids also regulate this process [Frühbeck et al., 2014].

Since adipocytes are mechanosensitive and increased adiposity may result in compressive stress between the adipocytes, in this chapter we studied the effect of these forces on the lipid metabolism. More precisely, we investigate the hypothesis that compressive stress provides a feedback mechanism to restrain further increase in lipid accumulation. To test this hypothesis we used the previously described three-dimensional engineered adipose tissue model composed by a collagen type I matrix and 3T3-L1 mature adipocytes. After statically compressing the adipocyte 3D cultures, we found that the mechanical stimulus triggers lipolysis via an increase of HSL activity and overexpression of ATGL. We also found that this response is primarily mediated by the ERK pathway upon stimulation. These results also suggest altered metabolic profile of the 3T3-L1 adipocytes in response to mechanical compression.

## 3.2 Materials and Methods

### 3.2.1 Experimental design and timeline

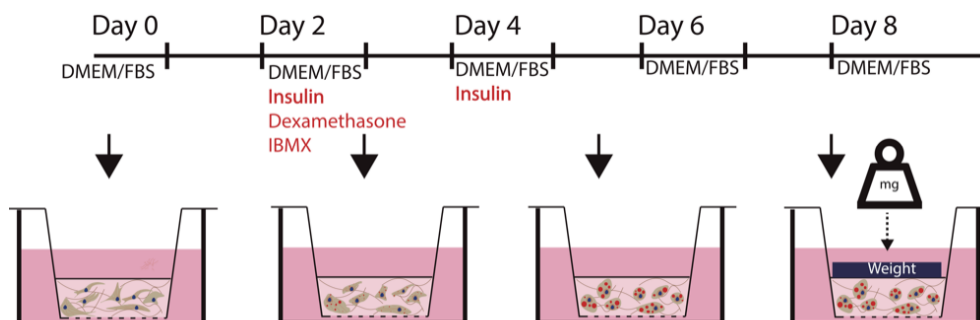


Figure 3.1: **Protocol timeline.** Schematic representation of the experimental procedure. After differentiating 3T3-L1 pre-adipocytes within the hydrogel, compression was applied (day 8).

3T3 L1 pre-adipocytes were cultured following the protocol mentioned in Chapter 2 (section 2.2.2.1) and encapsulated in 4 mg/ml collagen type I hydrogels. After encapsulation, the gels were casted in 0.4  $\mu\text{m}$  polyethylene terephthalate (PET) membrane transwells and let to polymerise for 30 mins at 37°C. Adipogenesis was induced after 2 days of normal culture by a standard adipogenic cocktail, in Chapter 2 (section 2.2.2.2). At day 8 cells were loaded with three different glass ceramic loads (corresponding to a stress of 17, 39.5 and 102.4 Pa) (**Fig. 3.2**). In order to control for transport limitations, a glass coverslip (corresponding to a stress of 1.5 Pa) with the same dimensions as the glass ceramic loads was placed on the top of the hydrogel. On the same day, two positive controls for lipolysis were used: isoproterenol (Iso), a potent  $\beta$ -adrenoreceptor agonist, at a concentration of 10 mM; and a combination of 10 mM of ISO and 10 mM of IBMX in order to reach sustainable high levels of lipolysis. Lipid accumulation and protein expression were evaluated at different time points, ranging from before compression up to after 24 hours of compression.

### 3.2.2 Lipid quantification by flow cytometry

After compression, the cells in the ROI were liberated from the collagen hydrogels by collagenase digestion and stained for neutral lipids. Samples were stained with DAPI (Sigma-Aldrich) at 1µg/ml and 0.1% v/v of AdipoRed™. Quantification in the flow cytometer (BD Fortessa) was performed after 30 minutes of cell staining. Compensation controls (unstained, and single staining for DAPI and AdipoRed™) were used in each experiment. Undifferentiated cells were used as control, the AdipoRed™ negative population. Each condition was always comprised of three technical replicates. Flow cytometry normalised data was used to combine different experiments in the same analysis.

### 3.2.3 Quantification of the surface area of adipocytes

The ROI cell suspensions were pipetted into glass bottom petri dishes. Solutions were allowed to stabilise in the Widefield Microscope for 30 mins. Images were acquired at 20x magnification. Surface area was measured by ImageJ. For cell volume calculations, we assumed spherical shape and calculated the volume by the following equation.

$$V_{adipocytes} = \frac{4}{3} \cdot \pi \cdot r^3 \quad (3.1)$$

where,  $V$  is the volume and  $r$  the cell radius.

### 3.2.4 Protein expression

Protein expression was measured by the western-blot technique (see Chapter 2, section 2.2.7). All blots were analysed by Image Studio™ Lite (LI-COR Biosciences). Primary antibodies used: Anti-Adipose Triglyceride Lipase antibody (1:500, EPR3444(2)) from Abcam; Polymerase I and transcript release factor (PTRF) (1:1000, sc-517589), PPARγ (1:1000, E-8) from Santa Cruz Biotechnology; Caveolin-1 (1:1000, D46G3), Perilipin1 (1:1000, D1D8),

HSL (1:1000, 4107), Phospho-HSL Ser563 (1:1000, 4139), Phospho-HSL Ser565 (1:1000, 4137), Phospho-HSL Ser660 (1:1000, 4126) from Cell Signalling; Vinculin (1:5000, V9131) from Sigma-Aldrich. Anti-mouse and anti-rabbit horseradish peroxidase secondary antibodies were from Santa Cruz Biotechnology.

### 3.2.5 Pathway Inhibitors

To determine which pathways are involved in the mechanical stimulation of lipolysis, samples were treated with three different inhibitors. Under the treatments, cells were stimulated with the mechanical load or with isoproterenol. U0126, H89 and Dorsomorphin from Abcam, were used to inhibit MAPK/Erk, PKA and AMPK pathways, at a concentration of 10uM, 50uM and 10uM, respectively. Samples were treated with the inhibitors for 3 hours for lipases studies, and for 24 hours for lipid content quantification.

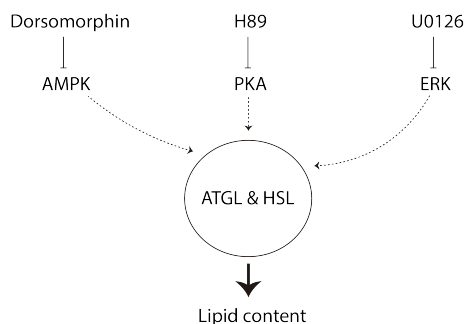


Figure 3.2: **Schematic representation of the pathway inhibitors.** Three inhibitors were used to test the involvement of AMPK, PKA and ERK on the mechano stimulated lipolysis.

### 3.2.6 Methyl- $\beta$ -cyclodextrin treatment

Methyl- $\beta$ -cyclodextrin was used to deplete the plasma membranes of cholesterol at a concentration of 5mM and 10mM. Cells were treated for 3 hours for lipases studies, and for 24 hours for lipid content quantification.

### **3.2.7 Immunofluorescence**

Immunostaining of Caveolin-1, Polymerase I and transcript release factor (PTRF) and lipid droplets was performed by standard procedures (see Chapter 2.2.6). The concentration used for primary antibodies was 1:1000 for LipidTox and 1:100 for anti-mouse IgG1 PTRF and anti-rabbit IgG Caveolin-1. Samples were then washed 3 times for 1 hour, and incubated with the corresponding secondary antibodies (Goat anti-mouse IgG1 Cross-Adsorbed Secondary Antibody, Alexa Fluor 488 and goat anti-rabbit Secondary Antibody, Alexa Fluor 633) for 2 hours at room temperature, in continuous agitation in the dark. Samples were then rinsed three times with PBS 1x for 10 minutes each and stained with DAPI (1:1000) diluted in PBS 1x for 20 minutes in the dark. Finally two washes of 15 minutes with PBS 1x was performed and samples were kept in PBS 1x until they were imaged by confocal microscopy (Leica SP8 inverted confocal microscope).

## **3.3 Results**

### **3.3.1 Lipolysis is load-dependent under static compression**

To test the hypothesis that lipolysis is affected by compression, we subjected differentiated 3T3-L1 adipocytes in 3D hydrogels to increased static stress for a maximum period of 24 hours. After mechanical stimulation, the loaded region (ROI) was isolated with a biopsy punch and placed into a digestion buffer. Liberated cells were then fixed and stained for neutral lipids. Lipid content was assessed by AdipoRed<sup>TM</sup> fluorescence signal measured by flow cytometry (**Fig. 3.3a**).

Four controls were added to the experiment. A non-loaded sample (0 Pa) was used as negative control. An isoproterenol-treated sample (Iso) was used as positive control for lipolysis, since it stimulates lipolysis via the cAMP-dependent pathway. Another sample treated with a combination of isoproterenol and IBMX was also used as positive control. IBMX, a

phosphodiesterase inhibitor, increases sustainable levels of cAMP and therefore ensures an increase of lipolysis. Lastly, we used a control for transport limitations (e.g. lack of oxygen and nutrients), which corresponded to a stress of 1.5 Pa. This load does not provide any significant strains to the sample and it is comprised of the same area (see previous Chapter).

We first investigated whether compression could affect lipolysis. For this, we compressed mature adipocytes with a stress of 102.4 Pa and compared to the negative control (0 Pa). To understand the timescale involved, lipid content was measured after 3, 6 and 24 hours of compression, immediately after removing the load. We found that 6 hours of compression, the lipid content in samples stimulated with a stress of 102.4 Pa presented significantly lower values in comparison to the non-loaded control sample. An even higher reduction of lipid content was observed when samples were compressed for 24 hours ( $p < 0.005$ ) (**Fig. 3.3b**).

We then investigated whether the amount of lipid reduction was stress-dependent. Therefore, we compressed the samples with 17 Pa, 39.5 Pa and 102.4 Pa at the timepoint that showed the largest effect, 24 hours. The positive controls were also treated for 24 hours. For all samples, we calculated the empirical cumulative distribution as well as the median fluorescence level. We found that for 17 Pa, 39.5 Pa and 102.4 Pa, a significant reduction in median fluorescence of respectively 14%, 19% and 33% was found compared to the 0 Pa control ( $p < 0.005$ ). Samples treated with isoproterenol and samples treated with the combination of Iso/IBMX showed a 38% and 41% decrease in median fluorescence in comparison to the control respectively ( $p < 0.005$ ) (**Fig. 3.3c and d**). This indicates that adipocytes stimulated with 102.4 Pa reached similar levels of lipid reduction as the positive controls.

Finally, we evaluated whether the reduction of lipid content resulted in changes in the cell diameter. To address this question, we measured the diameter of non-loaded and 102.4 Pa loaded samples after release from the hydrogels. For this, we used ImageJ software on images acquired by widefield microscopy (**Fig. 3.4a**). In line with the decrease in lipid content, we found a reduction in cell diameter in the loaded samples ( $p < 0.005$ ) (**Fig. 3.4b**). Assuming



spherical shape, we calculated the volumes for each cell. The ratio between median cell volume for loaded compared to control samples was 0.77. This value is in the same range as the ratio between median fluorescence of the 102.4 Pa loaded sample and control (0.86 for 24hr data from figure 3.3b and 0.67 for 102.4 Pa data from 3.3d).

Taken together, these results suggest that a gradual increase of compression leads to a decrease of lipid droplet size.

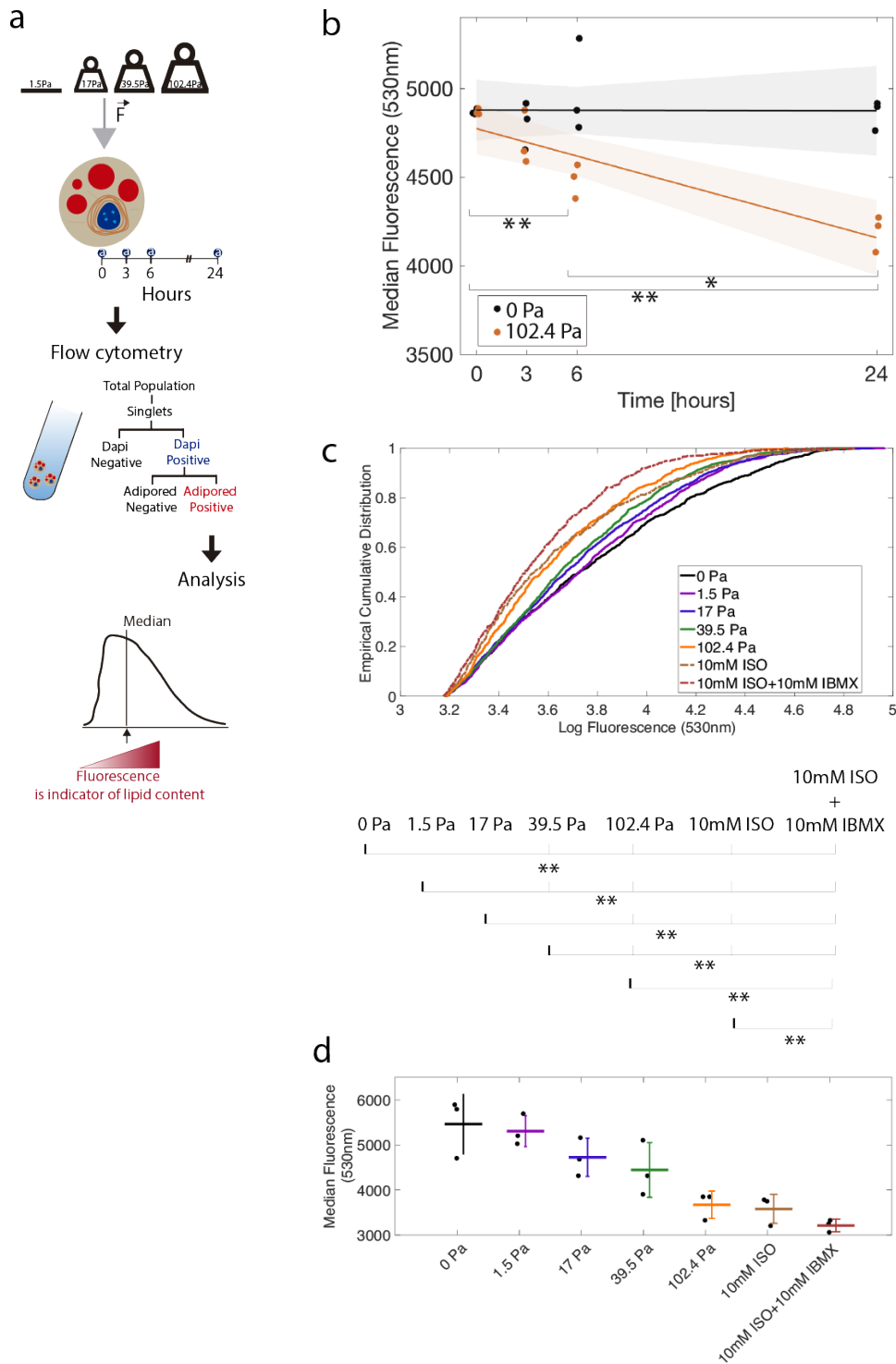


**Figure 3.3: Lipid accumulation is affected by static mechanical compression.** (a) Schematic representation of the experimental protocol. A glass coverslip (1.5 Pa) was placed on top of the hydrogel to control for transport limitations, whereas the three different glass ceramic weights were used to mechanically stimulate the 3T3 L1 adipocytes (top). Samples were analysed by flow cytometry at four time points (0, 3, 6 and 24 hours) (middle). Three technical replicates were used per condition and two experimental repeats were performed (see supplementary information). Full fluorescence distributions as well as median values were used for statistical analysis (bottom). (Figure legend continues in the next page.)

Figure 3.3: (Continued from previous page.) **(b)** Decrease in fluorescence starts after 3 hours of static compression. At 6 hours, lipid content is significantly different from the control and at 24 hours an even larger reduction is measured (Two sample t-test:  $**p < 0.01$ ,  $*p < 0.05$ ). **(c)** Empirical cumulative distributions of the AdipoRed<sup>TM</sup> positive populations at 24 hours. Both mechanically and chemically (isoproterenol and IBMX) stimulated populations are shifted towards lower fluorescence. A Kruskal-Wallis test was used to analyse significant differences ( $p < 0.005$ ). **(d)** Decrease in median fluorescence for all conditions at 24 hours. Experimental replicates are shown in supplementary figure S5. Horizontal lines are mean of medians, error bars denote one standard deviation.

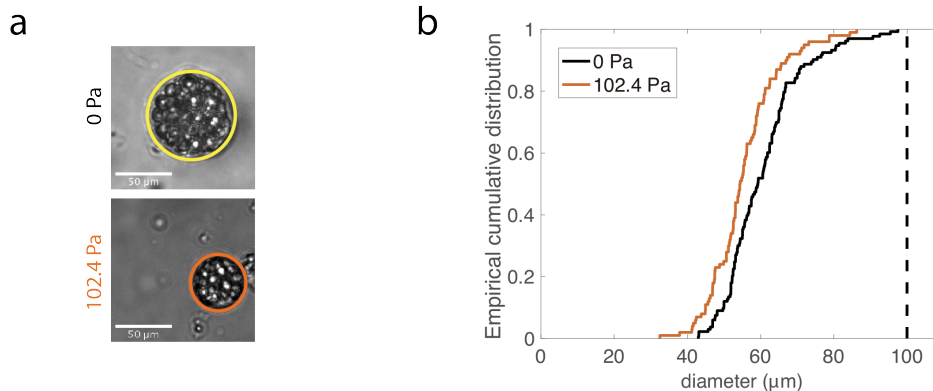
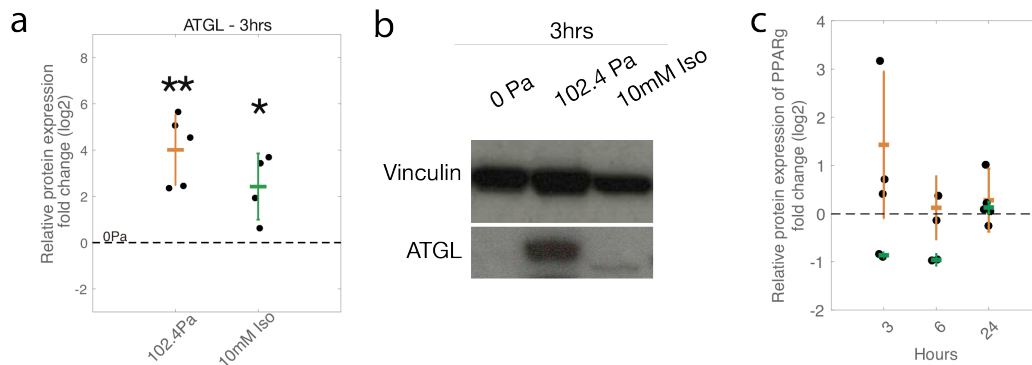


Figure 3.4: **Static mechanical compression decreases cell diameter.** **(a)** Representation of diameter analysis in ImageJ for non-loaded and 102.4 Pa stimulated samples. **(b)** Empirical cumulative distribution of cell area of compressed and non-compressed samples. Dashed line corresponds to the filter cut-off (pore size of  $100\mu\text{m}$ ). The empirical distributions are significantly different (two-sample Kolmogorov-Smirnov test,  $p < 0.05$ ,  $n_{\text{load}} = 100$  cells,  $n_{\text{ctrl}} = 133$  cells from one experimental set).

### 3.3.2 Compression activates lipolytic players

In order to understand how static compression promotes lipolysis, we analysed the lipolytic process in more detail. Lipolysis is mediated by multiple lipases, which convert triglycerides into diglycerides, monoglycerides and finally glycerol. As an end product of each step, free fatty acids are released and used to fulfil cellular metabolic needs or to be transported to other tissues. Central players of this process are adipose triglyceride lipase (ATGL), hormone sensitive lipase (HSL) and monoglyceride lipase (MGL). HSL and ATGL comprise of the main mechanism regulating the lipolysis [Nielsen et al., 2014; Schweiger et al., 2006]. Our initial focus was to evaluate the total protein expression of these two enzymes. We then also

investigated HSL activity by quantifying its phosphorylations. Because at 6 hours the lipid content was significantly different from the control, we chose to analyse the protein levels of the cells exposed to the maximum load at an earlier time, namely at 3 hours. For the HSL activity studies we extended the time points to 3, 6 and 24 hours. All measurements of lipid content were performed at 24 hours.



**Figure 3.5: Enhanced expression of ATGL in response to the load.** (a) Protein expression of total levels of ATGL after 3 hours of mechanical stimulation (102.4 Pa) and 10mM isoproterenol treatment. Levels of total ATGL are increased in relation to the control. One-sample t-test was used to measure significant differences (\*\* $p < 0.01$ , \* $p < 0.05$ ). (b) Protein quantification was normalised to vinculin as loading control. (c) Protein expression of total levels of PPAR $\gamma$  after 3 hours of mechanical stimulation (orange) and 10mM isoproterenol (green) treatment. Error bars denote one standard deviation.

### 3.3.2.1 First step of lipolysis - ATGL

ATGL is responsible for the first step of lipolysis mediating the conversion of triglycerides to diglycerides and it corresponds to the first rate limiting step. At 3 hours of compression, we found a significant increase of approximately 16-fold in protein expression of ATGL in relation to the control ( $p < 0.005$ ) (Fig. 3.5a and b). This suggests that this enzyme is promoting lipolysis, since overexpression of ATGL has been implicated in the reduction of TAG storage as well as the decrease of lipid droplet size [Duncan et al., 2007; Miyoshi et al., 2008].

Increased mRNA and protein levels of ATGL are linked to an increased expression of the master regulator of adipogenesis, PPAR $\gamma$ . We therefore tested whether the mechanical load was promoting the expression of PPAR $\gamma$ . To this end, we measured the protein expression of PPAR $\gamma$  over time (3, 6 and 24 hours). We found no significant changes between the highest load and the control at 3 and 24 hours suggesting that the load-mediated increase of ATGL was not mediated by PPAR $\gamma$  (**Fig. 3.5c**).

### 3.3.2.2 Second step of lipolysis - HSL

HSL is mainly responsible for the second step of lipolysis converting diglycerides to monoglycerides, but is also capable of hydrolysing ester bonds from other forms of lipids at lower rates. HSL activity is highly regulated posttranslationally through its phosphorylation at different sites. We therefore not only investigated total levels of HSL, but also the amount of phosphorylation in response to the mechanical stimulus. Regarding the total levels of HSL, we did not observe an effect in loaded samples compared to the non-loaded control (**Fig. 3.6a and b**).

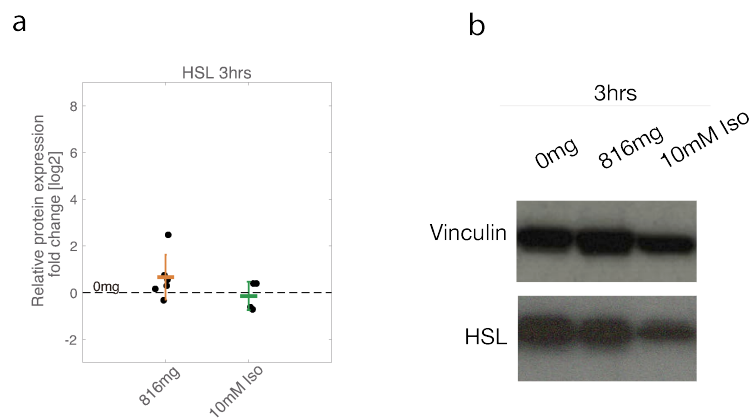
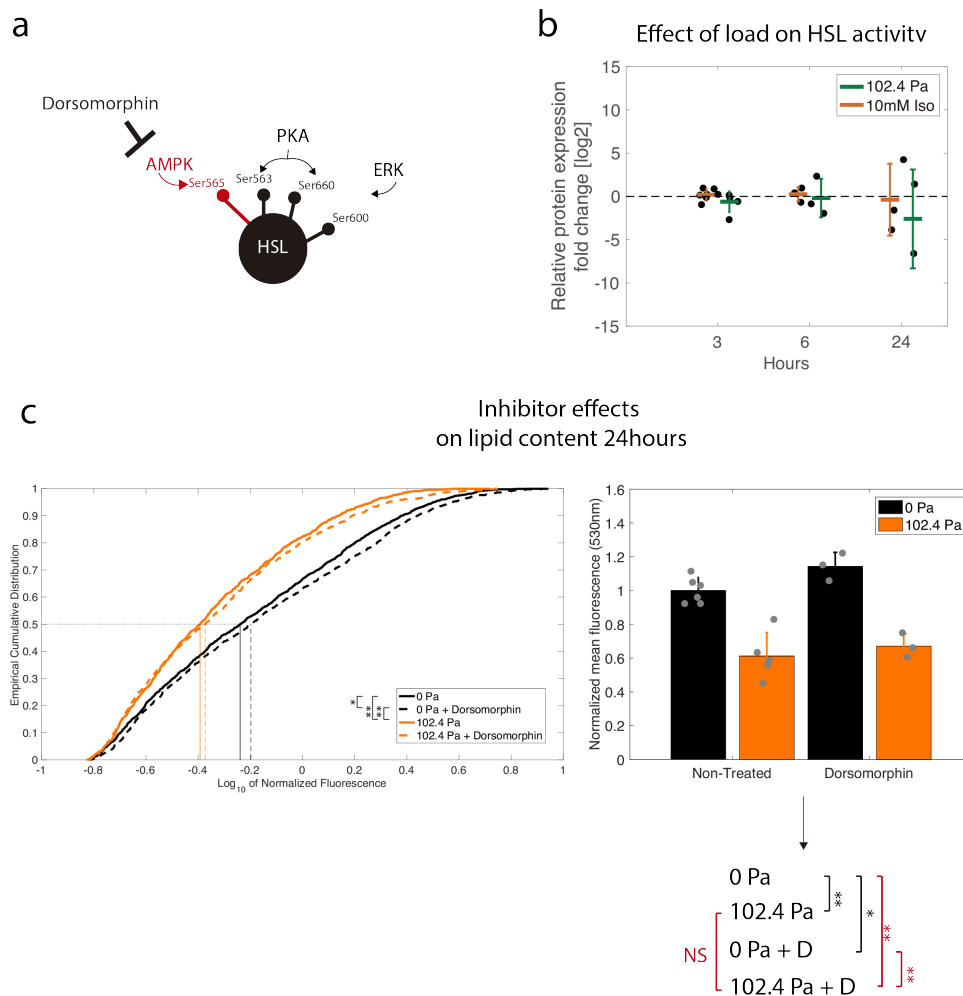


Figure 3.6: **Expression of total HSL in response to the load.** (a) Protein quantification of total HSL after 3 hours of mechanical stimulation and 10mM isoproterenol treatment. (b) Protein expression of total levels of HSL after 3 hours of mechanical stimulation. Levels of total HSL did not significantly increase in relation to the control. One-sample t-test was used to measure significant differences. Error bars denote one standard deviation.

We next studied the effect of the static compression on three phosphorylation sites of HSL, Ser565 (AMPK mediated) as well as Ser660 and Ser563 (which are mediated by PKA) (**Fig. 3.7a**). In addition, extracellular signal-regulated kinases (ERK) can phosphorylate HSL at Ser600, but there are no commercially available antibodies to measure Ser600. We therefore analysed the putative role of the ERK pathway by measuring phosphorylation levels of ERK1/2. For all pathways, we evaluated the effect of pathway-specific inhibitors (AMPK, PKA and ERK are inhibited by dorsomorphin, H89 and U0126, respectively). In contrast with total protein expression of HSL, we found a remarkable change in phosphorylation in response to the load indicating changes in the activity of the enzyme.

### **Effect of AMPK on HSL phosphorylation**

The phosphorylation levels of Ser565 at 3, 6 and 24 hours of loaded and isoproterenol treated samples were not significantly different from the control (**Fig. 3.7b**). This suggests that phosphorylation of Ser565 by AMPK is not involved in increased lipolysis. To further examine this outcome, we used dorsomorphin, a potent AMPK inhibitor. In line with the previous result, when simultaneously treating loaded samples with 10  $\mu$ M of dorsomorphin, no detectable changes in lipolysis were found (**Fig. 3.7c**). This supports the conclusion that AMPK is not involved in compression-mediated lipolysis.



**Figure 3.7: Activity of HSL mediated by the AMPK phosphorylation site.** (a) HSL has several phosphorylation sites, in this figure we are interested in activation of HSL via AMPK, at Ser565. (b) HSL phosphorylation at Ser565 after 3, 6 and 24 hours of compression. The AMPK phosphorylation site was not affected on any of these timepoints. One-sample t-test was used to measure significant differences between control and loaded samples ( $p < 0.01$ ,  $p < 0.05$ ). (c) Left: Empirical cumulative distribution of lipid content after 24 hours of mechanical stimulation with and without Dorsomorphin (D) treatment. Dorsomorphin failed to abolish the mechanically induced lipolysis. (Two sample Kolmogorov-Smirnov test was used to measure significant differences ( $**p < 0.01$ ,  $*p < 0.05$ ). Right: Mean lipid content of technical replicates from two experimental sets. Bars denote the mean of these means. Error bars denote one standard deviation. ( $**p < 0.01$ ,  $*p < 0.05$ ).

### **Effect of PKA on HSL phosphorylation**

In contrast to Ser565, phosphorylation at Ser660 and Ser563 were sensitive to mechanical loading. At 3 hours, mechanically stimulated samples had increased levels of phosphorylation by approximately 5-fold on Ser660 and by 22-fold on Ser563 compared to the non-loaded control ( $p < 0.05$ ). All values were normalised to corresponding total HSL levels. Samples treated with isoproterenol showed similar results. At 6 and 24 hours phosphorylation levels were back to the basal level (**Fig. 3.8b**).

We subsequently treated 120.4 Pa stimulated samples with a PKA inhibitor, H89. H89 is a competitive antagonist of the ATP sites on the catalytic subunits of PKA. The catalytic subunits are responsible for the phosphorylation of the target proteins upon ATP binding. Therefore, H89 inhibits the action of PKA. Despite of its primary target being PKA, H89 can also inhibit the ROCKII and S6K1 pathways at lower rates.

When treating the loaded samples with 50  $\mu\text{M}$  of H89, the effect of mechanical stimulation on lipid content at 24 hours was not abolished (**Fig. 3.8d**). Although, the phosphorylation levels of both serines were decreased upon treatment with H89 at 3 hours, the mean lipid content at 24 hours was not significantly different from loaded samples without H89 (**Fig. 3.8c**). However, the full distributions were significantly different, but presented only a small decrease in mechanically stimulated lipolysis (**Fig. 3.8c**). More data is therefore needed to assess the involvement of PKA. In isoproterenol-treated samples, H89 led to a partial decrease of the phosphorylation at Ser563 and had no effect on Ser660, even though the concentrations used in both isoproterenol and H89 were higher than the  $\text{IC}_{50}$  for both compounds.



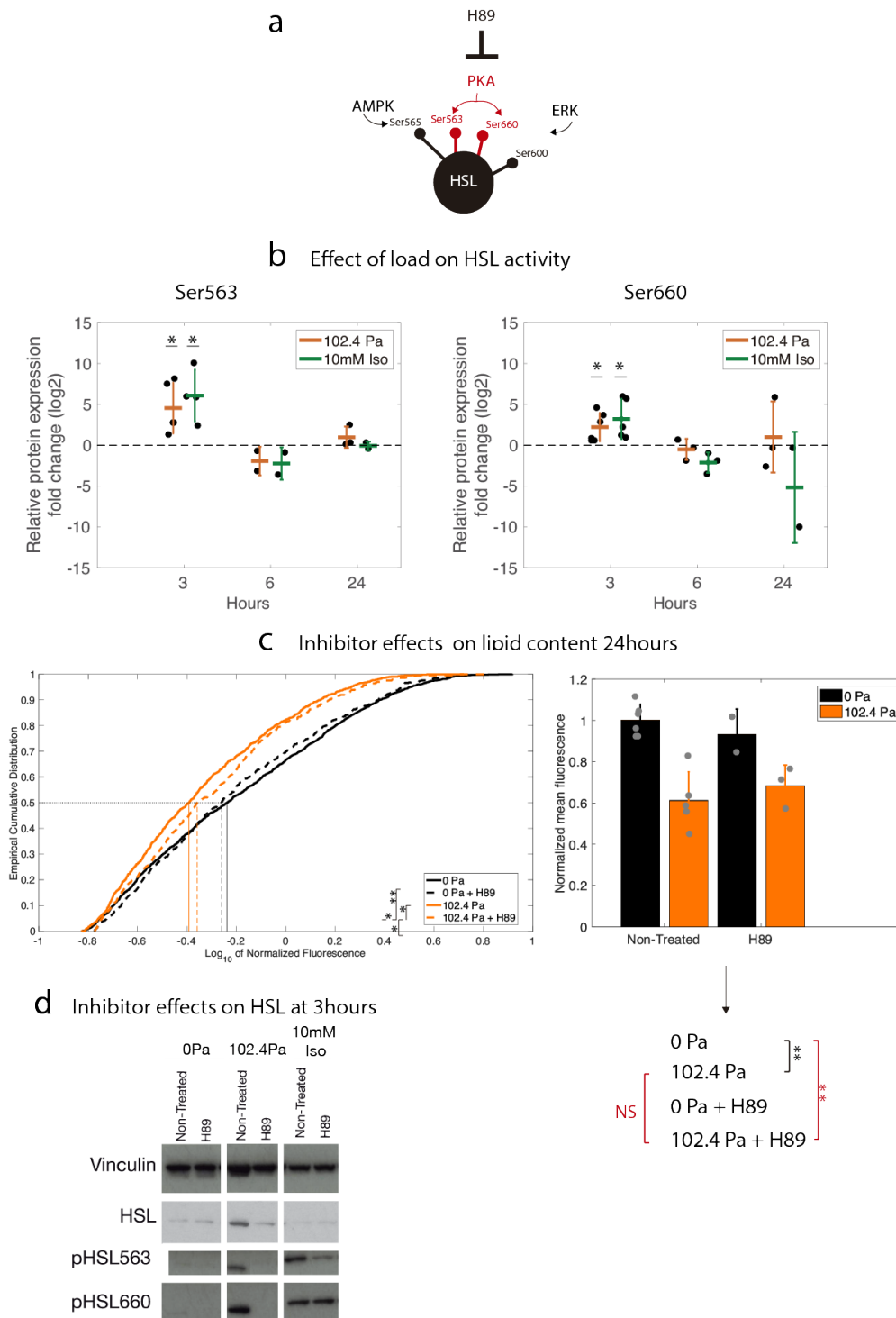


**Figure 3.8: Activity of HSL mediated by PKA phosphorylation sites.** (a) HSL has several phosphorylation sites, in this figure we are interested in activation of HSL via PKA, on Ser563 and Ser660. (b) HSL phosphorylation at Ser563 and Ser660 after 3, 6 and 24 hours of compression. PKA mediated phosphorylation was significantly increased in mechanically stimulated as well as in 10mM isoproterenol treated samples. Each point is one experimental replicate. One-sample t-tests was used to measure significant differences. (Continued from previous page).

Figure 3.8: (Continued from previous page.) (c) Left: Empirical cumulative distribution of lipid content after 24 hours of mechanical stimulation with and without H89 treatment. H89 led to a small decrease in mechanically induced lipolysis. Two sample Kolmogorov-Smirnov test was used to measure significant differences (\*\* $p < 0.01$ , \* $p < 0.05$ ). Mean lipid content of technical replicates from two experimental sets. Bars denote the mean of these means. Error bars denote one standard deviation. (\*\* $p < 0.01$ , \* $p < 0.05$ ). (d) Protein expression blots of total HSL and its phosphorylation at Ser563 and Ser565 at 3 hours after mechanical stimulation and isoproterenol treatment, under H89 effect. For these blots, we only have one dataset.

### Effect of ERK on HSL phosphorylation

Finally, we investigated the involvement of the ERK pathway in mechanically stimulated lipolysis. Activation of the ERK pathway can lead to HSL phosphorylation at Ser600 (**Fig. 3.9a**). Because of the inexistence of a commercial available antibody for this phosphorylation site, we evaluated the phosphorylation levels of a surrogate measure, ERK1/2. Loaded samples showed a clear increase in phosphorylation levels of ERK1/2, indicating that mechanical stimulation activates this pathway and may potentially activate HSL (**Fig. 3.9b**).

We subsequently used U0126 to treat both loaded samples and isoproterenol controls. The U0126 compound is a highly selective inhibitor of both MEK1 and MEK2, which are kinases that phosphorylate ERK1/2. We first confirmed that ERK1/2 phosphorylation was inhibited by U0126 (**Fig. 3.9c**).

When measuring the lipid content under U0126, mechanically stimulated lipolysis presented a significant difference from the 102.4 Pa non-treated sample ( $p < 0.005$ ). The normalised mean fluorescence of 102.4 Pa stimulated samples under U0126 reached almost similar values as non-loaded and non-treated controls. However, for larger adipocytes (in higher fluorescence), U0126 introduced a leftward-shift in the cumulative distribution (**Fig. 3.9e**). This suggests a potential lower effect of HSL activity mediated by the ERK-pathway on larger adipocytes.

In addition, the phosphorylation levels of ERK1/2 showed to be sensitive to H89 treatment (decrease to 69% in relation to loaded non-treated sample) (**Fig. 3.8c**). This observation suggests a possible role for ERK in the result obtained in the previous section, where we showed that H89 treatment reduced lipolysis. In line with this, phosphorylation levels of PKA-mediated serines 660 and 563 were also sensitive to the presence of the ERK inhibitor (**Fig. 3.8c**).

Taken together, these results uncovered the pivotal role of ERK in mediating mechanical-stimulated lipolysis.

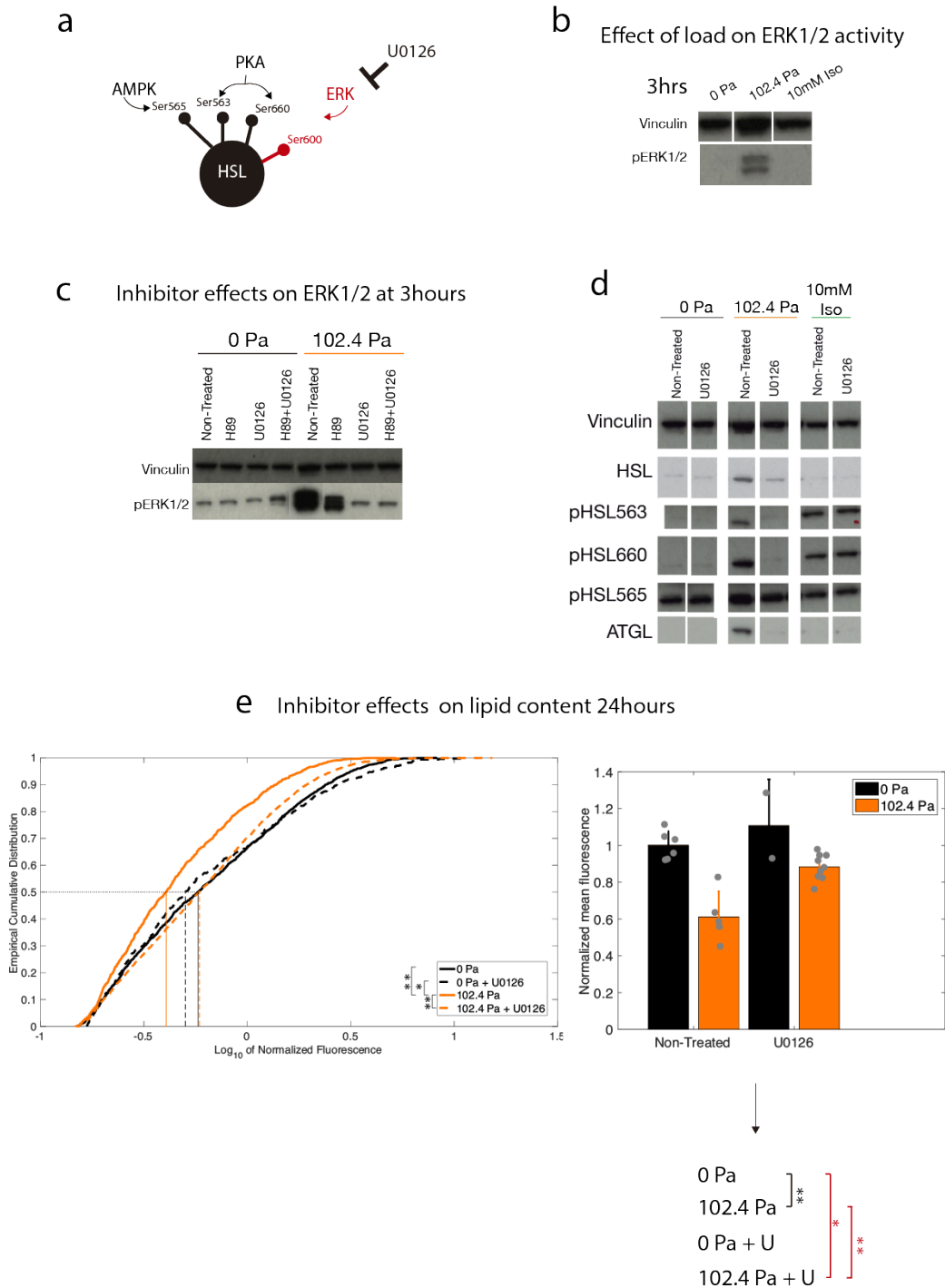


**Figure 3.9: Activity of HSL mediated by ERK phosphorylation sites.** (a) HSL has several phosphorylation sites, in this figure we are interested in activation of HSL via ERK, at Ser660. (b) Protein expression blots of phospho-ERK1/2 demonstrated a strong activation in response to the load. (c) ERK inhibitor U0126 (U) brought ERK1/2 phosphorylation to the baseline values in 3hours loaded samples. (d) Protein expression blots of total HSL and its phosphorylation sites at Ser563, Ser660 and Ser565 as well as ATGL at 3 hours of mechanical stimulation and isoproterenol treatment, under U0126. (Figure caption continued on next page)

Figure 3.9: (Continued from previous page.) (e) Left: Empirical cumulative distribution of lipid content after 24 hours of mechanical stimulation with and without U0126 treatment. U0126 successfully abolished the load effect. Two-sample Kolmogorov-Smirnov test was used to measure significant differences (\*\* $p < 0.01$ , \* $p < 0.05$ ). Right: Mean lipid content of technical replicates from two experimental sets. Bars denote the mean of these means. Error bars denote one standard deviation. (\*\* $p < 0.01$ , \* $p < 0.05$ )

### 3.3.2.3 Effect of H89 and U0126 on ATGL protein expression.

Because our results show an overexpression of ATGL in response to the mechanical stimulation, we wondered whether PKA and ERK signalling pathways could also be involved in this response. We therefore investigated the ATGL expression under simultaneous mechanical stimulation and PKA and ERK inhibitors. We found that treating loaded samples with these inhibitors nearly abolishes the ATGL overexpression found at 3 hours (**Fig. 3.10**). We therefore conclude that, under mechanical compression, ATGL protein expression is sensitive to the PKA and ERK pathway activation.

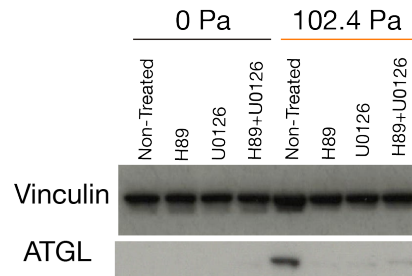
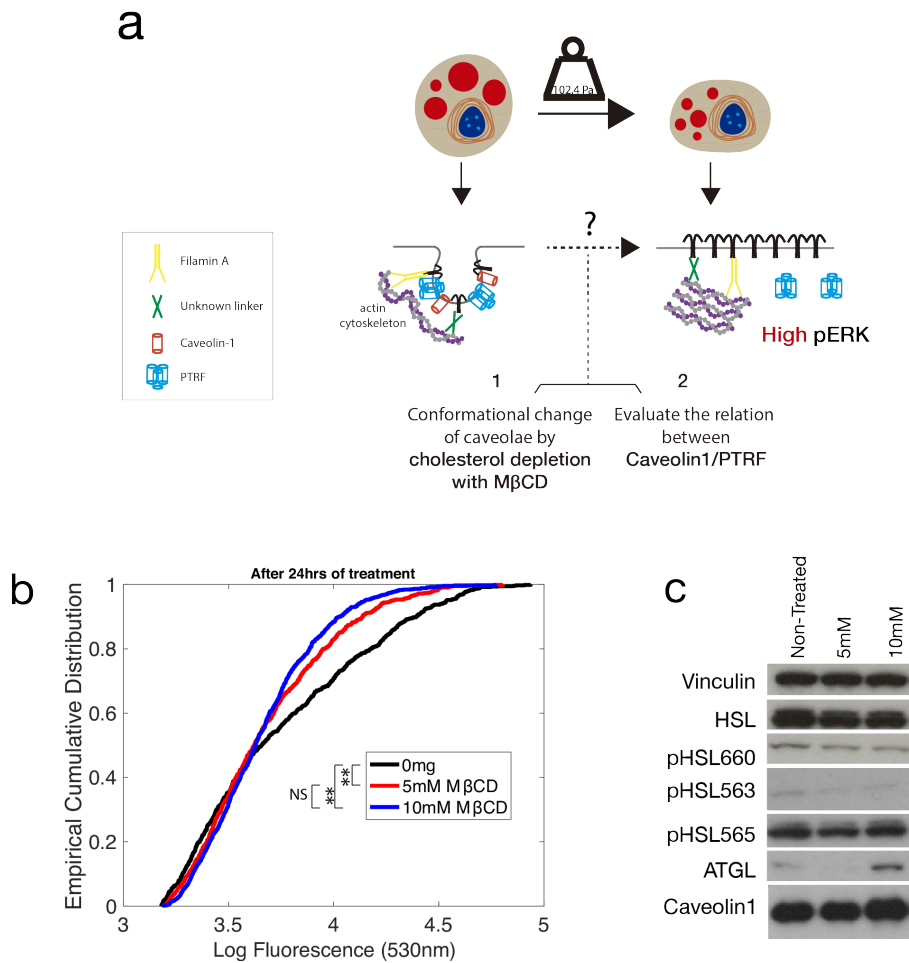


Figure 3.10: **Effect of PKA and ERK inhibitors on load-mediated ATGL overexpression.** PKA and ERK inhibitors abolish the ATGL activity after 3 hours of mechanical compression.

### 3.3.3 Caveolae as sensors of compression

Our results from this chapter suggest that the ERK pathway is a key player in the regulation of lipolysis in response to static loads. We also described in Chapter 1 how cells are strained under such loads. We therefore wondered whether the cell deformation is a trigger for the

activation of the ERK pathway. Such a deformation acts on the plasma membrane, where several types of receptors and proteins are located which are known to modulate ERK activity [Gortazar et al., 2013; Gudermann, 2001; Tanimura and Takeda, 2017]. In particular, we are interested in specialised structures called caveolae. Caveolae are flask-shaped invaginations that cover 30% to 50% of adipocytes plasma membrane, and contribute to membrane mechanics [Briand et al., 2014; Mayor, 2011]. Under tension, caveolae rapidly disassemble by flattening the membrane and activating several pathways, among which also ERK [Echarri and Del Pozo, 2015]. To test the involvement of caveolae on mechanically mediated lipolysis, we designed two approaches (**Fig. 3.11a**).



**Figure 3.11: Decreased lipid content upon  $M\beta CD$  treatment.** (a) Representation of the approach to test the involvement of caveolae on mechanically mediated lipolysis. We test the effect of changing caveolae shape (1), as well as the co-localisation of caveolin-1 and PTRF (2). (b) Empirical cumulative distribution of lipid content after 24 hours of  $M\beta CD$  treatment. Two-sample Kolmogorov-Smirnov test was used to measure significant differences (\*\* $p < 0.005$ ). (c) Protein expression blots of total HSL and its phosphorylation at Ser660, Ser563 and Ser565, total ATGL and caveolin-1. Total ATGL and caveolin-1 showed 3.42-fold and 1.21-fold increase in relation to the control non-treated, respectively. HSL phosphorylation showed a small decrease of expression in treated samples.

In the first approach, we chemically treated the mature adipocytes with methyl- $\beta$ -cyclodextrin ( $M\beta CD$ ) for 24 hours (Fig. 3.11a).  $M\beta CD$  acutely depletes the plasma membrane of cholesterol, which is known to play a fundamental role in the formation and maintenance of the caveolae [Hissa et al., 2017]. Upon depletion, the cell undergoes a profound cytoskeleton remodelling accompanied by caveolae disassembly [Biswas et al., 2019].

Upon 24 hours treatment of 3T3-L1 adipocytes with 5mM and 10mM of  $M\beta CD$ , we observed a decrease in lipid content and a different shape of the cumulative distribution of treated samples ( $p < 0.005$ ) (**Fig. 3.11b**). The decrease was most prominent in cells with high lipid content, while cells with low lipid content did not change in response to the  $M\beta CD$ . This suggests that the effect of  $M\beta CD$  seems to be stronger in larger adipocytes.

When analysing the lipases expression and HSL activity at 3 hours, we found that the expression of ATGL was higher in 10mM of  $M\beta CD$  treated samples (3.42-fold) (**Fig. 3.11c**). Surprisingly, at 5mM we did not observe such an increase, even though a significant reduction in lipid content was present. It is therefore likely that ATGL is not the only mediator of the effect of  $M\beta CD$  on lipolysis. Regarding HSL protein expression, unexpectedly, we did not observe increased activity, neither in total HSL nor in its corresponding phosphorylations (**Fig. 3.11c**). Furthermore, we did not observe significant changes in the phosphorylation of ERK1/2 under  $M\beta CD$  treatment, suggesting that caveolae disassembly may be triggering ATGL overexpression, independently of ERK pathway.

The second approach consisted in analysing the expression and location of two important proteins involved in the formation and the curvature of the caveolae, caveolin-1 and Polymerase I and transcript release factor (PTRF, also known as cavin-1) (**Fig. 3.12a**). We found that static compressive stress does not change the protein expression levels of caveolin-1 but increases the expression of PTRF nearly seven-fold (**Fig. 3.12a** and **b**). Overexpression of PTRF in 3T3-L1 adipocytes is implicated in the decrease of intracellular lipids, and therefore is involved in lipolysis [Perez-Diaz et al., 2014]. The appearance of a slower migrating PTRF band as seen in **Fig. 3.12b** has been postulated to be a result of PTRF phosphorylation. Furthermore, PTRF phosphorylation results in PTRF interaction with HSL at its serines 563 and 660 [Aboulaich et al., 2006]. Interestingly, we found that PKA inhibitor could partially rescue PTRF phosphorylation levels (from 7-fold to 3-fold). The ERK inhibitor, U0126, almost completely rescued the PTRF expression (from 7-fold to 1.8-fold). To our knowledge, the interaction between the ERK pathway and the expression of PTRF has never been described



before, and it would be interesting to study this further.

In order to understand whether the load influences the location of caveolin-1 and PTRF, we stained both control and the 102.4 Pa stimulated sample for both proteins (**Fig. 3.12c**). We observed that caveolin-1 did not present qualitative changes in response to the load, which is in agreement with the caveolin-1 quantification by western blot. Instead, PTRF showed a clear increase in fluorescence in the nucleus zone (not stained) (**Fig. 3.12c and d**). When calculating the correlation coefficient between the fluorescence intensities of the two stainings (caveolin-1 and PTRF) we observed a decrease from 0.12 in control to 0.04 in loaded samples. This indicates that intensities are less co-localised in loaded samples, that suggests less caveolae structures. However, more cells should be analysed in the future as well as to perform DAPI staining.

PTRF at the nucleus has a caveolae-independent transcriptional role. Nuclear PTRF is an indicator of metabolic challenges because it plays a crucial physiological role in maintaining adipocyte allostasis [Liu and Pilch, 2016]. PTRF is involved in the production of ribosomal RNA, enabling the cells to produce more proteins in situations of metabolic needs. A loss of PTRF causes dysregulation of ribosomal transcription in adipocytes, a process found in the pathogenesis of lipodystrophy. In order to understand whether compression resulted in an increased production of ribosomes, we therefore measured ribosomal protein S6 phosphorylation (**Supp. Fig. S6**). Phosphorylation of ribosomal protein S6 results from the activation of mammalian target of rapamycin complex 1, mTORC1 [Carnevalli et al., 2010]. mTORC1 kinase tunes ribosome biogenesis, cell volume and autophagy in the cell [Delarue et al., 2018]. We found a two-fold increase of this phosphorylation at 3 hours of compression, suggesting that mechanically stimulation of adipocytes trigger a change in the metabolic status. We also measured expression of phospho-AMPK, an indicator of metabolic stress and a inhibitor of mTOR. Unchanged expression of phospho-AMPK combined with the viability assays performed in Chapter 1, re-ensures that the activation of lipolysis rather than from metabolic stress (**Supp. Fig. S7**).

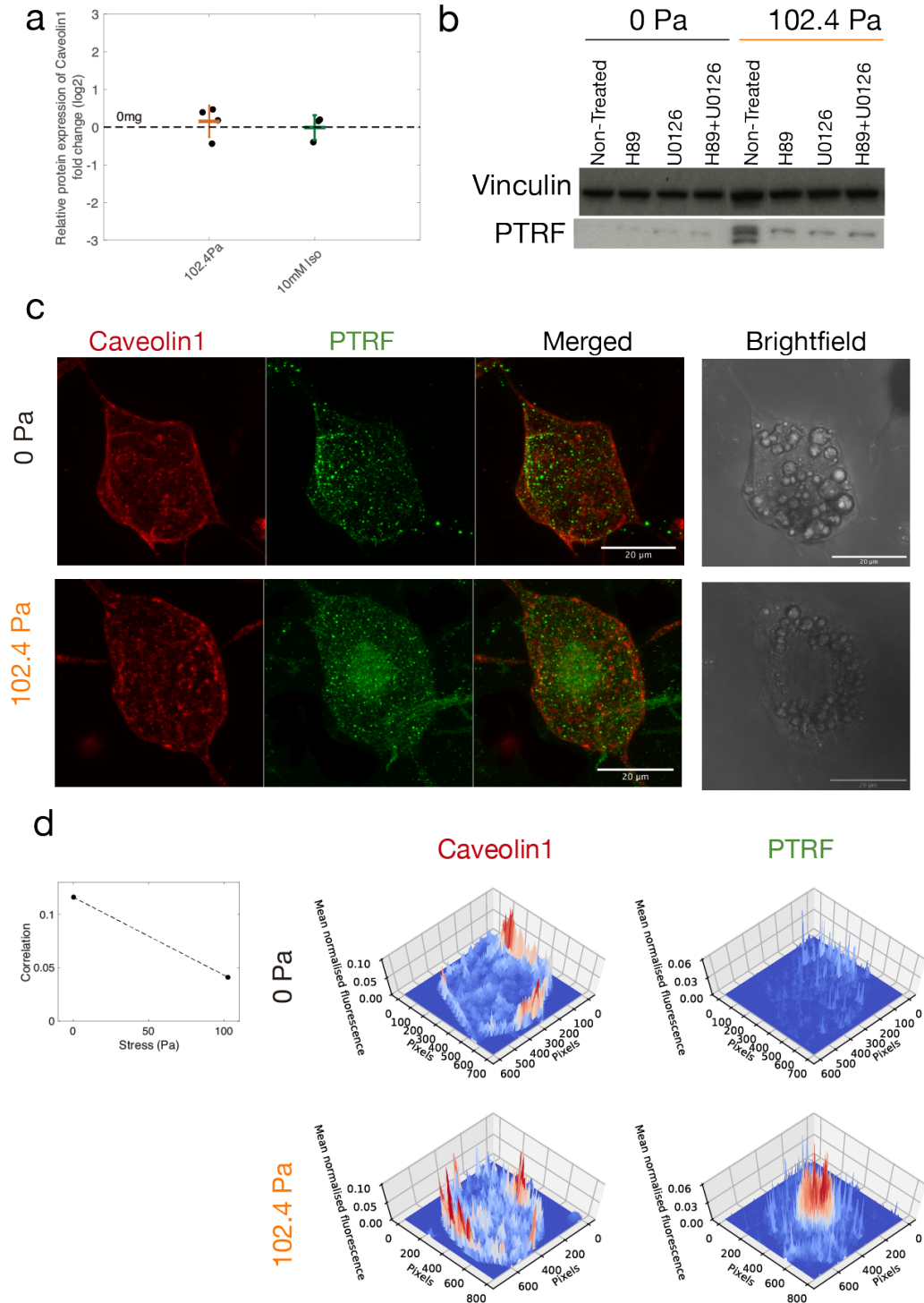


Figure 3.12: **Increased PTRF protein expression and its nuclear translocation upon mechanical stimulation.** (a) Caveolin-1 expression after 3 hours of compression. No significant changes were observed in loaded and isoproterenol treated samples in relation to the control. Error bars denote one standard deviation. (b) Protein expression blots of PTRF of control and loaded samples with and without PKA and ERK inhibitors at 3 hours. (c) Immunofluorescence of caveolin-1 (red) and PTRF (green) in loaded samples 6 hours after compression (figure scale bar is 20 $\mu$ m). Caption continues on the next page.

Figure 3.12: (Continued from previous page.) **(d)** Left: correlation coefficient between the pixels intensities of the two fluorescence channels of z-stack images. The correlation between the channels reduces by a factor in the compressed samples. Right: Mean of normalised fluorescence along the z-stack. In compressed samples, the mean values of PTRF are elevated in the central region of the cell.

### 3.4 Discussion

Lipid metabolism involves a tight regulation of many pathways and proteins. Identifying which factors mediate lipid mobilisation is an important step toward understand obesity-related conditions. Here, we studied how compressive stress affects lipolysis in mature adipocytes. We found that upon the mechanical stimulation, levels of lipid accumulation significantly decrease and this is accompanied by a strong activation of the lipolytic machinery. Upon 3 hours of static compression we observed overexpression of ATGL and increased activity of HSL. Finally, this seems to be mediated by ERK, since treating samples with ERK inhibitors nearly abolished this response and brought lipid content close to control (non-loaded) levels. Contrarily, AMPK and PKA inhibition did not affect the decrease in intracellular lipid content when adipocytes were mechanically stimulated, suggesting that these pathways are not primarily involved in mechanoregulation of lipolysis.

ATGL is responsible for the first step of the lipolytic response and its overexpression results in elevated basal and stimulated lipolysis in both mouse models and humans [Ahmadian et al., 2009]. Furthermore, ATGL-deficient mice exhibit massive ectopic lipid accumulation and become obese under low-fat diet [Haemmerle et al., 2006]. Similarly, ATGL-null mice shows a 70% reduction in lipolysis in response to  $\beta$ -adrenergic stimulation, [Nielsen et al., 2014], which consequently leads to expanded adipose tissue mass and obesity [Haemmerle et al., 2006; Schoiswohl et al., 2015]. ATGL is known to be primarily mediated by PKA (either by PKA-phosphorylation of its co-activator CGI-58 or by its own phosphorylation sites Ser406 and Ser430) [Duncan et al., 2007; Pagnon et al., 2012]. In 2007, an ATGL proteomics study noted that the Ser406 residue site could also be phosphorylated by ERK [Bartz

et al., 2007]. More recently, Hong S et al. showed that an increase in ERK phosphorylation due to proinflammatory cytokine-mediated signalling led to an increase in lipolysis [Hong et al., 2018]. This resulted from a phosphorylation of the  $\beta$ -3 adrenergic receptor at Ser247 by ERK MAP kinase. Finally, they observed that suppressing ERK phosphorylation with PD0325901, resulted in attenuated lipolysis and thermogenesis.

Contrary to ATGL, which only has affinity to one type of the lipid substrates (triglycerides), HSL can hydrolyse several types of substrates. The HSL maximal hydrolytic rate occurs from diglycerides to monoglycerides. HSL can be phosphorylated on several serines that consequently activate this enzyme. PKA is found to phosphorylate HSL at serines 563 and 660. Ser563 is thought to promote the translocation of HSL from the cytosol to the lipid droplets while Ser660 is critical for the activation of the enzyme [Anthonson et al., 1998; Daval et al., 2005; Nielsen et al., 2014]. However, the *in vitro* PKA-mediated HSL activation is only responsible for a twofold increase of HSL activity, suggesting that HSL activity is extensively mediated by other kinases [Kimmel and Sztalryd, 2016]. The ERK and AMPK pathways are other kinases involved on HSL enzymatic regulation [Drira et al., 2016; Farnier et al., 2003; Jeong et al., 2015].

In this work we found an overexpression of ATGL as well as a strong activation of the two serines Ser563 and Ser660 on HSL after 3 hours of compression. These responses were abolished by both the ERK and PKA inhibitors. However, when analysing the functional readout, the lipid content, we observed that only the ERK inhibitor had a substantial effect on suppressing the compression-mediated lipolysis. We observed that this effect was greater on adipocytes with lower intracellular lipid content, suggesting that larger adipocytes are less sensitive to ERK. We also found a subtle effect of H89 on lipid content, which could be caused by the inhibitory effect of H89 on the phosphorylation of ERK1/2. This interaction has been reported before [Yamashita et al., 2009]. Additionally, it was shown that ERK can phosphorylate  $\beta$ -3 adrenergic receptor at Ser247 and therefore increasing cAMP levels [Hong et al., 2018]. This pathway could explain the activation of PKA upon compression on

the serine sites.

Taken together, our data suggests that mechanical compression acts via the ERK pathway on ATGL and HSL, and subsequently affects lipolysis. Potentially, PKA is also affected by ERK, leading to a small contribution in stimulated lipolysis, but further investigation of this interaction is needed (**Fig. 3.13**). We also excluded the role of AMPK on the compression mediated lipolysis. Besides our identification of these lipolytic players in response to compressive stress, it would be important to further study the involvement of other players such as perilipin-1 and fatty acid transporters.

The ERK signalling pathway is a prototypic mitogen-activated protein kinase (MAPK) signalling cascade. It is well known that activation of ERK signalling results from the activation of membrane receptors by the extracellular matrix (ECM) or growth factors [Tanimura and Takeda, 2017]. As result of this activation, ERK can either be translocated to the nucleus where it assumes a transcription factor function, or it can interact with cytoplasmatic proteins for structural and functional regulation of the cell. Integrin-mediated adhesion and caveolae structures are known to modulate ERK pathway to promote different cellular functions.

Since we are promoting cell deformation by compressive stresses, we wondered whether this could lead to an alteration of the caveolae structures. Caveolae represent a big fraction of the adipocyte membrane and play an important role in the sensing of the extracellular environment and subsequently activating intracellular pathways [Parton and Del Pozo, 2013]. Disruption of their shape either by gene mutations affecting their structural proteins (caveolin-1 and PTRF) or by mechanical forces, culminates in several functional changes in different cell lines [Diz-Muñoz et al., 2013]. Animal models lacking in caveolin-1 and PTRF present severe lipodystrophy and insulin resistance [Briand et al., 2014].

We indirectly evaluated the possible role of caveolae disassembly in mediating lipolysis, by treating samples with  $M\beta CD$ .  $M\beta CD$  promotes caveolae disassembly by cholesterol depletion. Here we found that treating samples with  $M\beta CD$  stimulated lipolysis, a process

accompanied by ATGL overexpression, but without changes in HSL activity. This response predominantly occurred in adipocytes with higher intracellular lipids suggesting a major role for ATGL in this lipolytic process.

Loss of caveolae shape due to mechanical stimulation is known to stimulate ERK phosphorylation [Gortazar et al., 2013]. However, we did not find any significant difference in levels of phosphorylated ERK1/2 in response to the M $\beta$ CD (data not shown). This suggests that caveolae disassembly affects ATGL via a mechanism not involving ERK. Other sensors such as integrins may be responsible in increasing phosphorylated ERK upon compression. Therefore, the role of such membrane receptors in regulating compression-mediated lipolysis should be further investigated.

Liu et al. showed that caveolae disassembly on 3T3-L1 adipocytes treated M $\beta$ CD caused PTRF and caveolin-1 redistribution out of the lipid raft fractions. We investigated whether compressive stress could cause a similar redistribution. By analysing PTRF staining upon mechanical stimulation, we found that PTRF was more predominant around the nuclear area. We also found PTRF overexpression, which is associated with increased basal lipolysis due to its ability to phosphorylate HSL [Aboulaich et al., 2011]. Even though we did not directly assess the PTRF translocation to the nucleus, this pattern has been described as an indicator of metabolic changes [Liu and Pilch, 2016]. We did not find any changes on the location of caveolin-1 and neither in its protein expression.

In summary, we showed how compressive stresses affect lipolysis via ERK in a three dimensional system. The increased phosphorylation levels of ERK subsequently act on the expression of ATGL and the activation of HSL. We also suggest a possible role of ERK mediating an increase of PKA and PTRF levels. To our knowledge, our work is the first uncover the link between mechanical stimulation and cellular lipolytic activity in a three-dimensional environment. Our results are consistent with the observations of Li et al. [2013] and Hossain et al. [2010], who performed compression studies in two dimensions to study

the effect of mechanical stimulation in adipogenesis. The authors found a decreased lipid content in loaded-differentiated adipocytes, however they did not investigate the mechanisms behind those effects. Furthermore, our results indicate that caveolae could play a role in sensing static compression, potentially leading to PTRF overexpression and the translocation of PTRF to the cytosol and nucleus (**Fig. 3.13**).

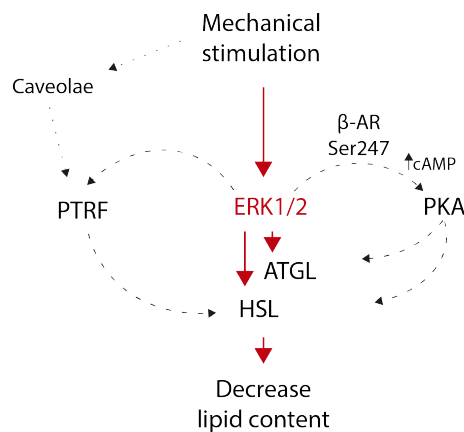


**Figure 3.13: Proposed interactions between mechanical stimulation and decreased lipid content.** Upon mechanical compression, levels of ERK1/2 are elevated activating ATGL and HSL, which consequently leads to a decrease of lipid content. Sub-pathways that may be altered are PKA via ERK1/2 phosphorylation on the  $\beta$ -adrenergic receptor, and release of PTRF from the plasma membrane for the cytosol where it interacts with HSL.

Our work uncovers a possible feedback mechanism of mechanical stimulation in regulating the accumulation of intracellular lipids. Since visceral adiposity positively correlates with intra-abdominal pressure, increased adiposity results in increase compressive stress, in turn inhibiting further lipid accumulation. Our findings therefore open new ways of understanding the lipid metabolism in visceral adipose tissue and could enable novel opportunities for treatments of obesity. Indeed, these mechanical forces may be contributing to the increased basal lipolysis found in visceral obesity. Finally, to further elucidate the role of compressive forces on lipolysis, we also performed *in vivo* studies (Chapter 4).





## **Chapter 4**

# **Effect of compression on lipolysis in adipocytes treated with fatty acids and in overweight animals**

## 4.1 Introduction

A hallmark of obesity is high levels of fatty acids in the circulation. This seems to be a consequence of increased levels of basal lipolysis in both visceral and subcutaneous adipose depots [Berndt et al., 2007; Gaidhu et al., 2010; Jocken and Blaak, 2008; Langin et al., 2005]. However, when lipolysis is stimulated, these high levels do not further increase [Gaidhu et al., 2010].

Obesity is characterised by an initial phase where adipocytes become hypertrophic (increased adipocyte size due to increased lipid content). Some studies have linked this hypertrophic growth with altered adipocyte function. For example, in a study on adult humans, levels of TAG in the circulation (hypertriglyceridemia) were shown to be highly correlated with fat cell size in VAT, independently of the body mass [Veilleux et al., 2011]. Another study showed that mice on a high fat diet presented decreased HSL phosphorylation levels after multiple days and simultaneously an increased adipocyte size [Gaidhu et al., 2010]. Additionally, studies on adipocyte hypertrophy have shown that an increase of adipocyte volume is itself sufficient to drive insulin resistance, independently of inflammatory responses. This was caused by impaired GLUT4 translocation to the plasma membranes in 3T3-L1 adipocytes that were challenged with saturated fatty acids [Kim et al., 2015]. Furthermore, the authors linked this effect to the deregulation of actin remodelling caused by the FA treatment [Kim et al., 2015].

Since these results show how cell size can alter adipocyte function, we wondered whether the cell size influences how mechanical stimuli are sensed. In the previous chapter, we showed that compression of normal 3T3-L1 adipocytes enhances the lipolytic pathway. This leads to decreased lipid accumulation. In this chapter we hypothesise that the lipolytic response to compression is impaired in hypertrophic adipocytes. To test this, we first treated 3T3-L1 adipocytes with a cocktail of fatty acids. We then mechanically stimulated treated adipocytes with the same setup as in the previous chapter. Finally, we tested the effect of compression

*in vivo* on the visceral fat of overweight mice.

This chapter describes the first set of preliminary data to test this hypothesis. We found that upon fatty acid treatment of 3T3-L1 adipocytes, the basal levels of HSL phosphorylation were elevated. Compressing these cells substantially reduced lipolysis. Qualitatively similar results were found in the *in vivo* model.

## 4.2 Materials and Methods

To understand how hypertrophic growth could impact lipolysis, our first aim was to develop a hypertrophic model of 3T3-L1 adipocytes. We treated 3T3-L1 adipocytes previously embedded in 4mg/ml collagen hydrogels with a fatty acid cocktail for two days. Analysis of the lipid content was performed by flow cytometry after the treatment. Our next aim was to assess how compression impacts the lipolytic process of FA-treated 3T3-L1 adipocytes. To achieve that, we applied a compressive stress of 102.4 Pa to the non-FA treated and treated cells for three hours. We then investigated the HSL activity by analysing the phosphorylation sites of this enzyme (Ser660 and Ser563). Our last aim was to translate this approach into an *in vivo* model. We first developed a compression device to allow compression of visceral fat, specifically the gonadal fat pad, for 2.5 hours in overweight mice. After harvesting the tissues, we analysed the HSL activity, as done *in vitro*.

### 4.2.1 Cell culture

3T3-L1 pre-adipocytes were cultured, encapsulated and differentiated following the protocol described before (see Chapter 2). We used 4mg/ml collagen type I hydrogels. At day 6 of the culture, cells were treated with fatty acids (Lipid Mixture 1, Sigma-Aldrich, see next section). At day 8, they were mechanically stimulated with a 102.4 Pa for 3 hours (**Fig. 4.1**). Samples treated with isoproterenol were used as positive control for lipolysis in non FA-treated samples.

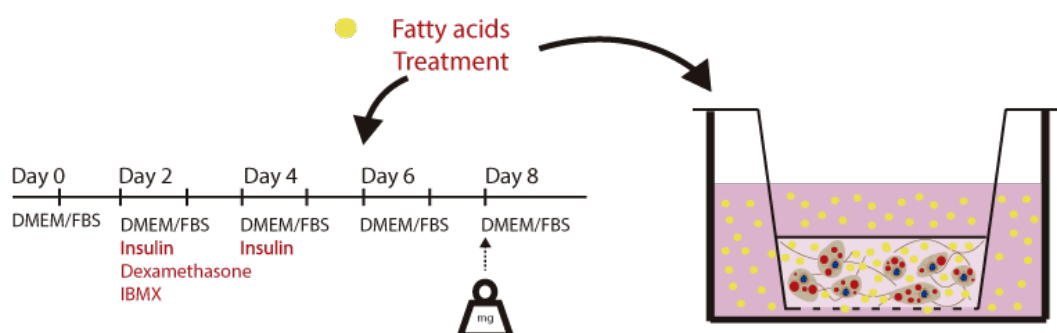


Figure 4.1: **Schematic representation of the *in vitro* protocol.** Timeline of the 3T3-L1 pre-adipocytes cell culture and differentiation. On the day 6, a cocktail of fatty acids was added to the media. On the day 8 the cell-seeded hydrogels were compressed with 102.4 Pa.

## 4.2.2 Fatty acid treatment

Cells were challenged with a fatty acid treatment to promote lipid accumulation. At day 6, growth media was switched to DMEM low glucose supplemented 1% pen-strep, 3% of bovine-serum albumin, and 2% of non-animal derived fatty acids (composed by 2  $\mu\text{g/ml}$  arachidonic and 10  $\mu\text{g/ml}$  each linoleic, linolenic, myristic, oleic, palmitic and stearic, 0.22 mg/ml cholesterol). Control cells were treated with the normal culture medium (high glucose DMEM, supplemented 1% pen-strep and 10% of FBS).

## 4.2.3 Lipid quantification

In order to ensure that the fatty acids treatment resulted in an increase of intracellular lipids, we measured the lipid content of the treated and non-treated samples. The quantification methods used were identical to the methods described in the previous chapter (see Chapter 2). The quantification of AdipoRed<sup>TM</sup> was performed on day 8.

## 4.2.4 Design of the compression device

The compression device was designed in Autodesk Inventor (see **Fig. 4.2** and supplementary information). The compression device was 3D printed using acrylonitrile butadiene styrene

(ABS). The sacrificial mold was removed, following a wash in 1N NaOH for 15 minutes. Finally, the compression unit was firstly rinsed with deionized water and then with 70% ethanol under the laminar flow cabinet. The devices were stored in sterile petri-dishes until the day of the surgery. On the day of the surgery, the perigonadal fat of the mice (**Fig. 4.2c**) was clamped between the upper part and the bottom part of the compression device (**Fig. 4.2a**). Three spacers were designed to provide three different levels of compression (supplementary information). However, only one spacer corresponding to a final space of 2mm was used.

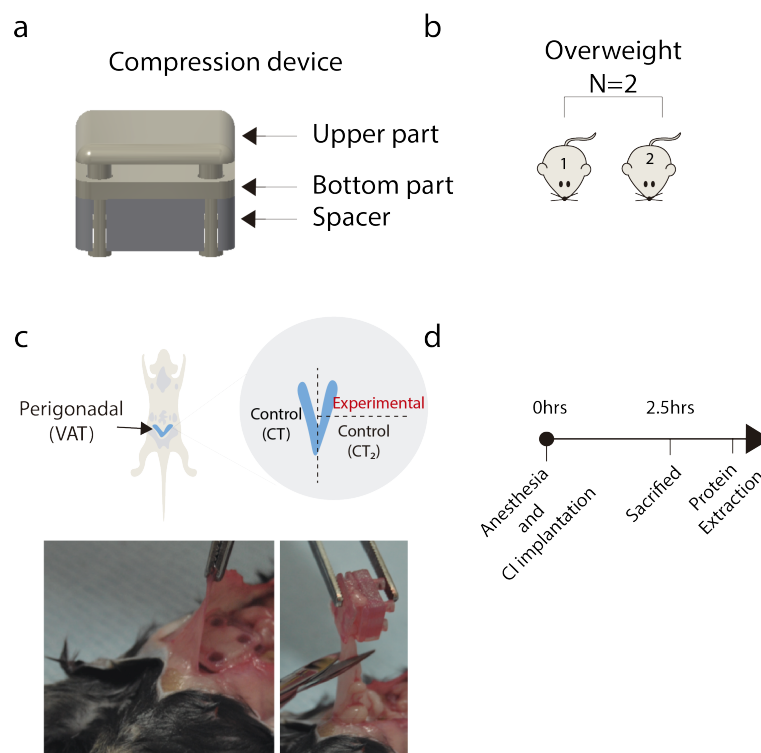


Figure 4.2: **Schematic representation of the *in vivo* protocol.** (a) Compression device was composed by three parts. The upper and bottom part ensure a proper compression area, and the spacer fixes the specific strain. (b) Two overweight mice were used for compression experiments. (c) The perigonadal fat which corresponds to visceral adipose tissue was exposed and one of the sides were compressed with the compression device. A image demonstrating the *in vivo* compression. (d) Timeline of the experiment.

#### 4.2.4.1 Animal Work

All procedures were carried out under the Animals (Scientific Procedure) Act, 1986 and Amendment Regulations, 2012.

**Animals.** All mice used in these studies were C57BL16 wild type males from the transgenic unit at Imperial College London. Mice were kept in standard laboratory cages (<5 per cage) with ad libitum access to water and standard laboratory RM1 chow in a temperate, humidity-controlled environment (21-23°C) with constant 12-hr light/dark cycle. Mice were monitored daily in accordance to Imperial's CBS regulations. Animals with age between 16 to 30 weeks, healthy and overweight were used for the studies. However, the healthy mice were not used for the compression study due to technical problems encountered during the experiment. This therefore did not allow us to analyse the effect of compression on a 'healthy' system and compared it to the *in vitro* results from the previous chapter.

#### Surgery

Before the starting of the surgery, mice were quickly induced in a gas anaesthetic chamber (short exposure to isoflurane 5%), followed by an intraperitoneal injection of 100 mg/kg ketamine and 10mg/kg xylazine to induce stable, surgical plane anaesthesia as a terminal procedure. All *in vivo* experiments were performed by Dr. Salem and her team. Briefly, an incision in the mouse abdomen was performed exposing the gonadal fat pad, (**Fig. 4.2a**). The compression device was placed in one of the sides of the fat pad (**Fig. 4.2c**). This corresponded to the experimental sample (named, Exp). The non-compressed zone on the same side of the fat pad was used as an internal control (named, CT2). On the other side of the pad, the tissue was exposed to the compression device but without compression, corresponding to our control (named CT). The experiments took place over 2.5hrs for both overweight mice. Animals were sacrificed by cervical displacement in the end of the experiment, without recovering from anesthesia. Tissues in both mice did not show visible changes on the blood supply at the end of the experiment. The tissues were collected and kept in 1x PBS on ice

until the protein extraction.

## 4.2.5 Protein expression

Protein expression was measured by western-blot technique (see Chapter 2). All blots were analysed by Image StudioTMLite (LI-COR Biosciences). Primary antibodies used: Anti-Adipose Triglyceride Lipase antibody (1:500, EPR3444(2)) from Abcam; Total HSL (1:1000, 4107), Phospho-HSL Ser563 (1:1000, 4139), Phospho-HSL Ser565 (1:1000, 4137), Phospho-HSL Ser660 (1:1000, 4126) from Cell Signalling; Vinculin (1:5000, V9131) from Sigma-Aldrich. Anti-mouse and anti-rabbit horse radish peroxidase secondary antibodies were from Santa Cruz Biotechnology.

### 4.2.5.1 Statistical analysis

This chapter contains preliminary data, and therefore the amount of replicates were not sufficient to perform formal statistical analysis. For the *in vitro* results we just had one replicate and for the *in vivo* work we used two mice for the compression experiment.

## 4.3 Results

### 4.3.1 Fatty acids treatment

To characterise whether the fatty acids lead to hypertrophic growth, we measured the 3T3-L1 adipocytes lipid content by flow cytometry after two days of treatment. On day 8, FA-treated and non-treated cells were released from the hydrogels and stained with AdipoRed<sup>TM</sup>. The empirical cumulative distributions of both populations are shown in **Fig. 4.3b**. FA-treated samples show a shift towards higher values of fluorescence in comparison to the non-treated controls. While this shift was statistically significant when analysing both distributions (two-sample Kolmogorov-Smirnov test,  $p < 0.005$ ), the differences remained small. Moreover, analysing the mean values of fluorescence units confirmed the small change between samples

(mean for non-treated: 757 fluorescence units, mean for FA-treated: 778 fluorescence units (no significant differences were found)) (**Fig. 4.3c**). Therefore, we cannot conclude that the cells are hypertrophic.

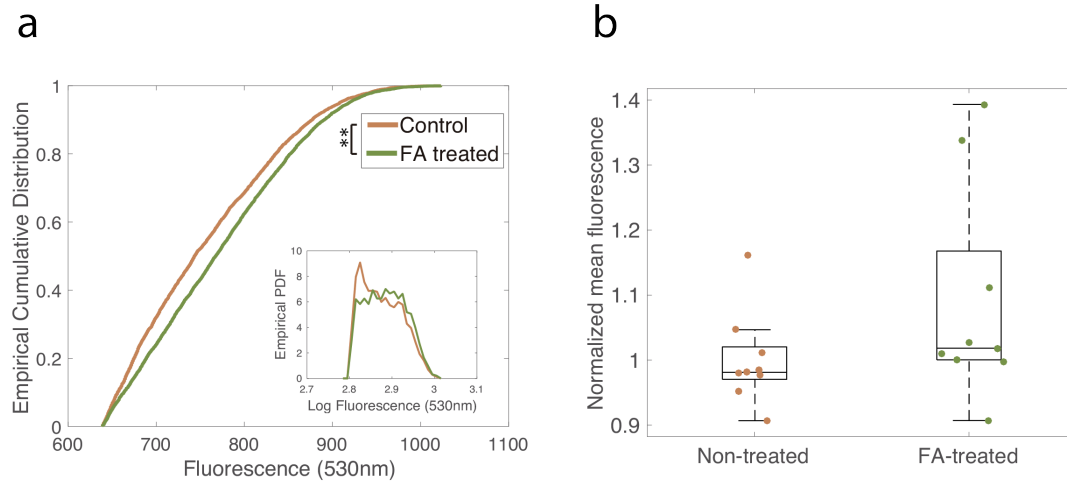


**Figure 4.3: Effects of FA treatment on lipid content.** Quantification of lipid content in treated and non-treated samples by flow cytometry (data is comprised of two experimental repeats). **(a)** Empirical cumulative distribution and the empirical probability density function. FA-treatment leads to a statistically significant increase (two-sample Kolmogorov-Smirnov test,  $p < 0.005$ ). **(b)** Means of fluorescence of each replicate. The distribution of means are not significantly different between the two conditions (two-sample t-test).

### 4.3.2 Attenuation of load-stimulated HSL activity

We first tested the effect of FA-treatment on the HSL expression and phosphorylation levels on Ser660 and Ser563 for both controls (non-treated and FA-treated). We observed that after FA-treatment, total HSL expression decreases. However, HSL phosphorylation was higher in FA-treated versus non-treated samples, presenting a 51-fold increase and 47-fold increase relative to the control for Ser660 and 563, respectively (**Fig. 4.5a and b**).

We next applied compression to the FA-treated adipocytes for 3 hours and measured levels of total HSL and HSL phosphorylation on the sites Ser660 and Ser563. For non-FA treated samples, the levels of phosphorylation of Ser563 and Ser660 were increased in loaded samples relatively to non-loaded samples (16-fold and 26-fold increase, respectively) (**Fig. 4.5c**).



This is in line with the results observed in the previous chapter. Interestingly, the pattern was altered in the FA-treated samples. In this case, we found a decrease of nearly 100% for both serines in relation to the non-loaded samples (**Fig. 4.5c and d**).

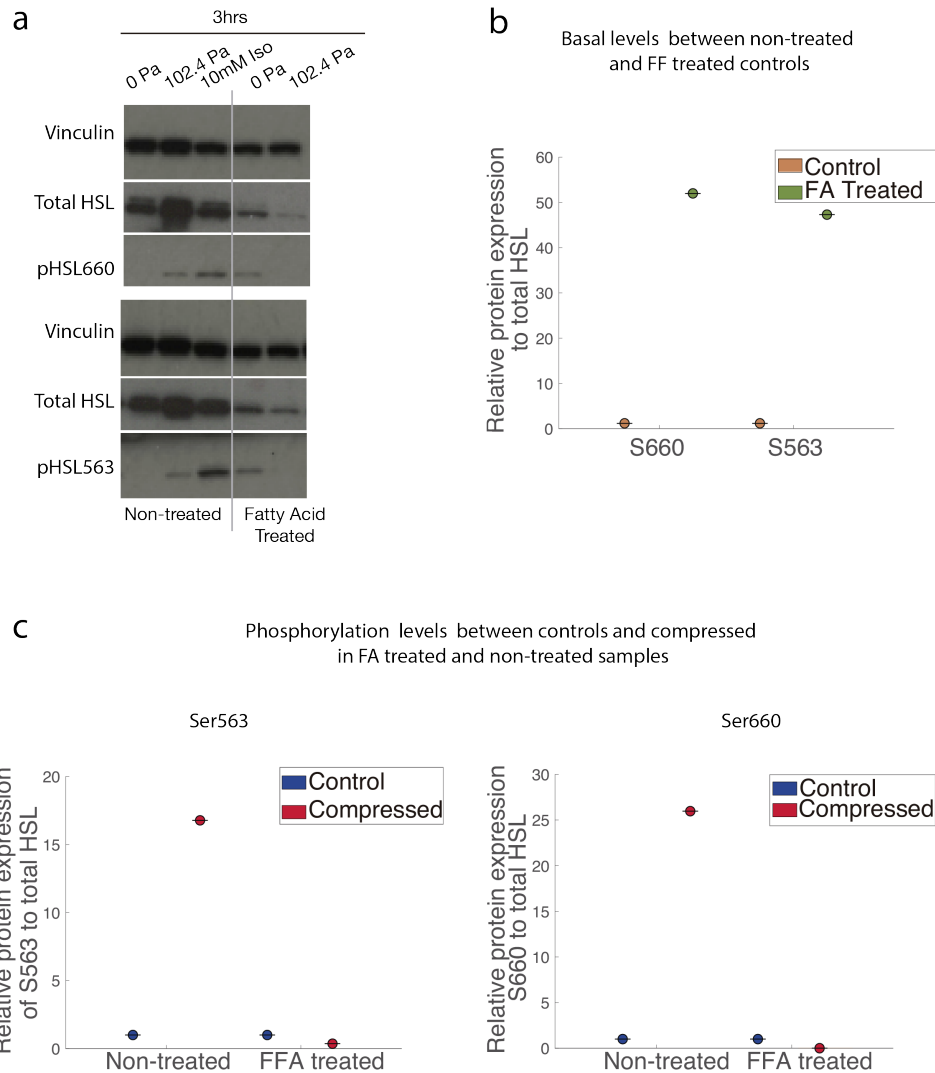


**Figure 4.4: Effects of FA treatment on HSL activity.** (a) Protein expression blots of HSL phosphorylation on Ser660 and Ser563 for FA non-treated samples (0 Pa, left), FA non-treated but mechanically stimulated (102.4 Pa, left), FA non-treated but isoproterenol stimulated (10mM Iso), FA-treated (0 Pa, right) and FA-treated and mechanically stimulated (102.4 Pa, right). (b) Relative protein expression of HSL phosphorylation at Ser660 and S563 for FA non-treated and treated samples. (c) Relative protein expression of HSL phosphorylation at Ser660 and S563 for FA-treated and non-treated samples with simultaneous compression.

We next examined whether the same effect of the compression seen in FA-treated samples

could be found in overweight animals. To achieve this, we developed a compression device enabling us to compress the gonadal tissue. Two phenotypes were used, normal weight animals and overweight animals. However, no compression was performed on normal animals, due to impaired blood supply (consequence of a technical problem) during the experiments.

We first analysed the differences in phosphorylation of HSL between these two phenotypes without compression. We found that in overweight mice, the basal HSL phosphorylation levels were higher than in normal animals. We found an increase in HSL phosphorylations (5-fold and 18-fold for Ser660 and 563, respectively) (**Fig. 4.5a** and **b**). Compressing the gonadal fat of overweight mice for 2.5 hours resulted in a decrease in phosphorylation at both sites, nearly abolishing their expression (**Fig. 4.5a** and **c**).

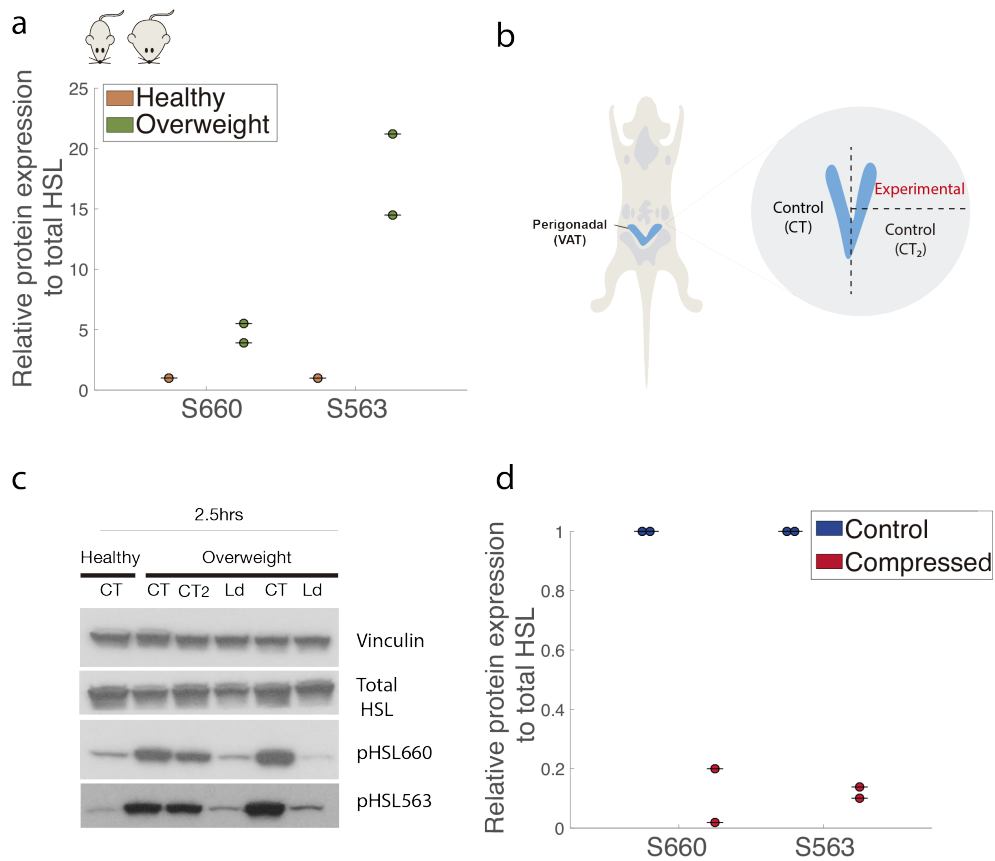


**Figure 4.5: Compression of gonadal fat leads to a decrease of HSL activity.** (a) Relative protein expression of HSL phosphorylation in normal and overweight mice (top). (b) Schematic of the different conditions used. Experimental (Ld) refers to the loaded samples. Control (CT) refers to unloaded samples on the opposite side of the fat pad from the loaded samples. Control 2 (CT<sub>2</sub>) refers to unloaded samples on the same side of the fat pad as the loaded samples. (c) Protein expression blots of total HSL and HSL phosphorylation on Ser660 and Ser563 for the normal mouse and overweight mice (bottom). (d) Relative protein expression of HSL phosphorylations in overweight mice, with and without compression.

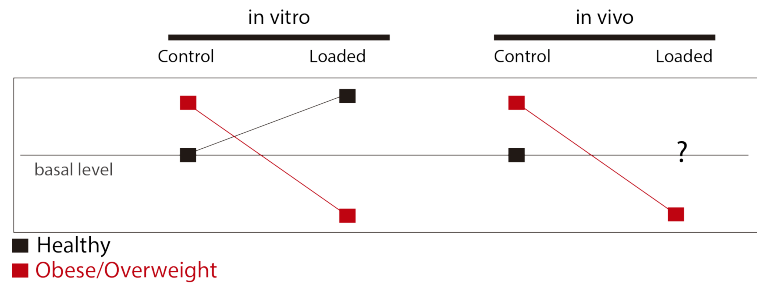


Figure 4.6: **Results summary.** In a healthy system *in vitro*, compression stimulates HSL activity. When the system shifts towards an obese phenotype, the compression acts in the opposite way by suppressing the activity of HSL. The *in vivo* experiments in overweight mice are in line with these findings.

### 4.3.3 Viability markers

Lastly, in order to ensure that the cell response was due to mechanical compression and not due to cellular damage, we measured the protein expression of the apoptotic marker, cleaved caspase-3. We found a decrease in expression of caspase-3 for the control samples (CT<sub>2</sub>) and loaded samples (Ld) (**Fig. 4.7**). We did not find any expression for cleaved caspase-3. However these results show no activation of apoptosis, a positive control should be included in the future.

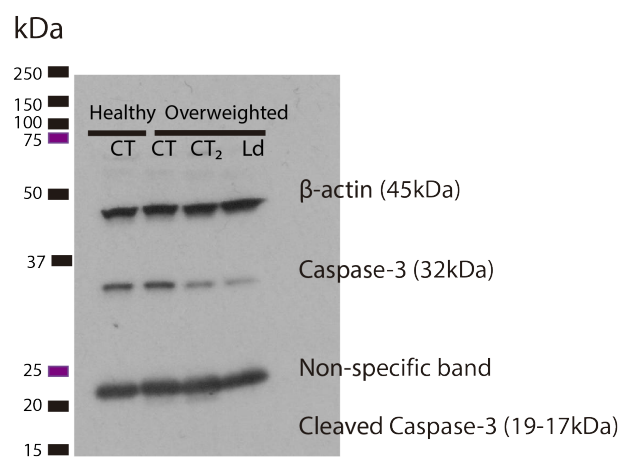


Figure 4.7: **Cell apoptosis markers.** Protein expression blots for caspase-3 and cleaved caspase-3.  $\beta$ -actin was used as loading control.

## 4.4 Discussion

This chapter consists of a preliminary study to test the hypothesis that enlarged adipocytes respond differently to mechanical stimulation, specifically compression. To achieve this, we first aimed to develop a hypertrophic *in vitro* model for compression of the adipocytes. We then used overweight mice to validate the effects observed in the *in vitro* system.

In obesity, adipocytes are characterised by an increased accumulation of triglycerides as a result of chronic positive energy balance. Therefore, to promote hypertrophic growth, we treated 3T3-L1 adipocytes with a cocktail of saturated, monounsaturated, polyunsaturated fatty acids and cholesterol for 2 days. We observed that the FA treatment generated a shift towards higher lipid content. However, because this shift was small and we did not investigate other parameters such as cell size, we could not conclude that FA-treated cells became hypertrophic. Similar treatments to promote hypertrophy have been used in previous work of Kim et al. [2015]. They reported that treating 3T3-L1 with a FA cocktail for 6 days resulted in larger lipid droplets ( $>500\mu\text{m}^3$ ) compared to non treated cells ( $<500\mu\text{m}^3$ ) [Kim et al., 2015]. Therefore, it would be interesting to increase the period of treatment in our samples.

Despite the fact that FA treatment on 3T3-L1 adipocytes did not result in hypertrophy, these cells presented different basal expression of HSL and HSL phosphorylations levels in relation to non-treated samples. As discussed previously, HSL together with ATGL are responsible for 98% of the TG hydrolase activity [Schweiger et al., 2006]. Changes in HSL activity result in alterations of the lipolytic process. Therefore, the increased levels of HSL phosphorylation at Ser660 and Ser563 in FA-treated adipocytes suggested a shift in the basal lipolytic process. Previous studies showed that treating cells with exogenous saturated fatty acids led to a reduction of the plasma membrane stiffness and elasticity [Sunshine and Iruela-Arispe, 2017; Weijers, 2015]. This observation allows us to hypothesise that also our FA treatment could mediate changes in the mechanical properties of the adipocytes, and therefore lead to a different HSL expression. Moreover, the presence of cholesterol in the FA cocktail could

have promoted high levels of cAMP in the cells and consequently promote lipolysis. This is because cholesterol acts as a positive regulator for certain G-protein coupled receptors (GPCRs) [Guixà-González et al., 2017].

A similar pattern as in our *in vitro* results was found in healthy and overweight mice. HSL phosphorylation on Ser660 and Ser563 was elevated in overweight mice compared to the healthy animals. Increased protein expression of HSL at Ser563 has been reported in obese individuals [Kinney et al., 2010]. It would therefore be interesting to dissect the mechanobiology behind the hypertrophic growth and increased basal levels of this enzyme, and consequently increased lipolysis.

When applying compression to the FA-treated 3T3-L1 adipocytes and to the gonadal fat of overweight mice, HSL phosphorylation decreased substantially compared to the controls. This result was opposite to our findings in the previous chapter, where mechanical compression of normal cells *in vitro* increased HSL phosphorylation. This indicates that the stimulation of lipolysis by compression is altered in FA-treated adipocytes. Hence, this could be linked to the earlier mentioned cellular membrane changes due to the FA treatment. In the *in vivo* model, we did not have data on the effect of compression in healthy mice, and thus we can not conclude that this response is only seen in overweight animals. It would be interesting to investigate the response to compression in healthy mice. Nonetheless, the qualitative agreement of the effect of compression in overweight mice and in FA-treated samples is striking. Related to this, Kinney et al. [2010] showed that catecholamine-stimulated lipolysis is reduced in obese mice under fasting conditions, and that this is associated with a decreased phosphorylation of Ser660. This suggests once again dysfunctional lipolysis in obese adipocytes.

In the previous chapter, we suggested the role of caveolae structures in triggering the mechanically mediated lipolysis as response to compression. It is known that caveolin-1 expression is correlated with increased lipid accumulation [Briand et al., 2014]. This overexpression of

caveolin-1 is accompanied by increased density of caveolae. It would be interesting to investigate the role of this increased density on the mechanical sensing and plasma membrane properties. Plasma membrane is crucial for interaction of the adipocyte with its microenvironment. For example, ion channels on the plasma membrane allow the cells to sense their volume, which consequently regulates insulin signalling and glucose homeostasis [Zhang et al., 2017]. Another study showed how cell size influences insulin signalling independently of inflammation [Kim et al., 2015]. These results uncover some aspects of how cell size can affect cell function. It would be interesting to further investigate the effect of cell size in our work.

Important next steps in this work are firstly to characterise in more detail the effects of FA treatment on the 3T3-L1 adipocytes and possible changes on the plasma membrane properties. Secondly, evaluation of adipocyte sizes and circulating FA levels in normal and overweight mice. Thirdly, increasing the n numbers and thus the reliability of the results. Fourthly, investigation of the response of healthy animals to compression. Fifthly, quantifying the compression applied by our devices would allow us to compare with physiological conditions. Lastly, it would be interesting to analyse post-compression catecholamine-stimulated lipolysis, since this would allow us to understand whether hypertrophy leads to dysfunctional stimulated lipolysis.

In summary, we have presented preliminary results on how FA-treated adipocytes respond to compression. We showed how these act differently compared to normal adipocytes. Moreover, the *in vitro* and *in vivo* results are in qualitative agreement. In light of our results, we hypothesise a possible homeostatic feedback mechanism, which involves the regulation of lipolysis by hypertrophy and the resulting changes in intra-abdominal pressure. In obesity, increased pressure caused by hypertrophy fails to stimulate lipolysis, dysregulating the homeostatic cycle.





## **Chapter 5**

### **Conclusions and Future Work**

## 5.1 Conclusions

We hypothesised that intra-abdominal pressure acts as a homeostatic mechanism to further inhibit increase in visceral fat. Because this pressure would manifest itself as a compressive stress on cells, we decided to investigate the effects of mechanical compression at the cellular level. In this thesis, we investigated the effect of static compression on the adipocyte lipid metabolism, in particular lipolysis. Our work uncovers a link between compression and increased lipolysis. More specifically, we showed that static compression activates lipolysis. Moreover, preliminary results suggested that the interaction between compression and lipolysis is disrupted in FA-treated cells as well as in overweight animals. Further understanding why the mechanical sensing is altered in these cells may lead to new approaches in treating obesity-related conditions.

In chapter 2, we established a 3D model enabling us to apply different levels of compression to mature adipocytes. We successfully differentiated and grew 3T3-L1 pre-adipocytes in type I collagen hydrogels. We then showed that this engineered tissues could be loaded with different levels of stress leading to cell deformation. We estimate that the stress applied in this system was between 0 and 1 mmHg, which is within the physiological range. We then used this system to further investigate the effect of compression on adipocyte lipolysis.

In chapter 3, we found that stimulating adipocytes with static compression for 24 hours resulted in a decrease of intracellular lipid content. The level of reduction was similar to that observed in response to isoproterenol stimulated lipolysis. In line with this decrease was the fact that loaded samples had a reduced cell volume. When investigating the mechanisms related to the diminished intracellular lipids, we found that at 3 hours of compression, the lipolytic players HSL and ATGL were enhanced. We showed increased activity of HSL in response to the load in the first 3 hours of compression. We then studied the role of three pathways potentially activating HSL, the AMPK, PKA and ERK pathways. We found that the ERK pathway played a pivotal role in the mechanically stimulated lipolysis. Lastly, we

showed that varying the plasma membrane configuration, by depleting cholesterol, led to a reduction of intracellular lipids. This suggests that mechanical compression could enhance lipolysis through changes in the membrane properties. We then analysed the expression and location of caveolin-1 and PTRF proteins, which play important roles in caveolae structures in the membrane. We found an overexpression of PTRF, which seemed to be localised around the nuclear area in loaded samples. Similar observations have been reported as indicators of metabolic changes [Liu and Pilch, 2016].

In chapter 4, we investigated whether increased adipocyte size, as seen in obesity, could result in a different response to compression. To study this we used two models of obesity, an *in vitro* model where adipocytes were treated with fatty acids, and *in vivo* model using overweight mice. Our preliminary data revealed that compressing samples treated with fatty acids and samples from overweight mice leads to inhibition of lipolysis, an opposite response of our observations in normal cells. Furthermore, we found that the basal levels of HSL phosphorylations were increased in non-loaded samples. This data points towards a disruption of the normal sensing of mechanical stimuli under FA-treatment and in overweight mice.

By studying the effects of compression at the cellular level, we have set the first step towards understanding whether stresses within the abdominal cavity can influence the intracellular lipid content. Based on our findings, we propose that compression can act as a homeostatic mechanism, inhibiting further increases in adiposity in normal cells. Furthermore, based on preliminary results we hypothesise that in obesity both the increased stress as well as the increased adipocyte size disrupt the promotion of lipolysis under compression (**Fig. 5.1**).

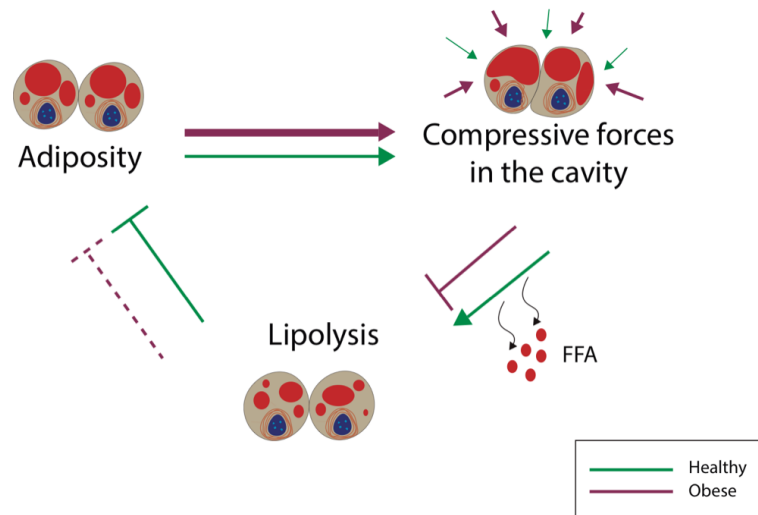


Figure 5.1: **Hypothesis.** We hypothesise a homeostatic feedback mechanism, where hypertrophy results in increased compressive stress, in turn stimulating lipolysis releasing free fatty acids (FFA). In obesity, the compressive stress fails to stimulate lipolysis, disrupting the homeostatic cycle.

## 5.2 Future Work

Our work showed the involvement of compressive stress in modulating the lipid homeostasis. Despite uncovering a link between compression and the lipolytic process, several questions remain to be addressed in future work. Furthermore, this work presents several limitations: (1) the use of clonal cell lines instead of primary cell lines of visceral adipose tissue limits the answer of whether this mechanical response is only in the visceral cavity or general for all adipocytes; (2) the collagenous nature of the scaffold that upon mechanical stimulation may increase the collagen concentration around the cells in the ROI. This may contribute to the response observed; (3) the system only allows for uniaxial and static compression and it is not immediately clear how much of the stress is experienced by the cells since the collagen may absorb it partially.

In the next future work section we will first discuss questions directly related to the results reported in this thesis, focused on reproducing, expanding and better understanding our findings. A second section is dedicated to more broad open questions that could prove interesting

avenues for follow-up studies and future research.

## **Next experiments**

Regarding the **in vitro** model, we predominantly used a compressive stress of 102.4 Pa, which corresponds to approximately 1 mmHg. This is indeed in the range of healthy individuals (0-7mmHg), but lower than in obese individuals (7-17mmHg). However, we currently do not know what stress the cells feel within the hydrogel itself. This should be **further investigated with detailed simulations using viscoelastic models**, better approximating the hydrogel properties. With this information, we plan to adapt our compression to mimic stresses both in the range of healthy individuals as well as in obese individuals.

We found a significant decrease of intracellular lipids in mechanically stimulated samples. Further **characterisation of the structure of the lipid droplets during compression** could be studied to support our data. For example, it would be interesting to study whether the mechanical stimulus enables the fusion of lipid droplets and influences the activity of lipid-droplet associated proteins such as cell death-inducing DFF45-like effector (CIDE) family proteins and FABP.

It would also be important to perform functional assays, such as glycerol and fatty acid measurements, in response to stimulated-catecholamines lipolysis. This would allow us **to assess whether stimulated lipolysis is impaired by mechanical compression**.

We found an overexpression of ATGL in adipocytes from compressed samples. We plan **to evaluate the ATGL activity** by either evaluating its phosphorylation sites or the phosphorylation of its co-activators. Furthermore, the development of 3T3-L1 cell lines with knock-downs for HSL and ATGL would allow us to understand **which is the principal lipase mediating mechanically-stimulated lipolysis**, and whether other players are involved. Alternatively, inhibitors of HSL and ATGL could be used.

Our results showed how ERK1/2 plays a major role in the mechanically stimulated lipolysis.

We plan to further investigate what mechanism leads to the phosphorylation of ERK1/2. We hypothesise that changes in membrane tension could lead to such activation. It would therefore be interesting **to measure such tensions in response to the load**, using fluorescent membrane tension probes [Colom et al., 2018]. Since integrins have been shown to regulate the ERK pathway, it would also be interesting **to further investigate the role of integrins in mediating the mechanical lipolysis**. Finally, it would be interesting to identify which mechanism impairs this pathway in FA-treated adipocytes.

We specifically focused on investigating the potential involvement of caveolae in the mechanical transduction. Since we observed an altered PTRF expression and location, our results suggest that the caveolae structure may be modified by compression. It remains to be investigated how these structures are affected, for example by **investigating whether mechanical stimuli flatten caveolae**, for example using transmission electron microscopy.

Regarding our animal work, we plan to **analyse the effect of gonadal fat compression in normal mice as well in better characterised obese mice** and confirm whether there is a different response to mechanical stimulation between these phenotypes. Moreover, we aim to better characterise the cell size and lipid content of adipocytes from both healthy and overweight mice, before and after compression. Since we observed a similar effect on HSL phosphorylation after fatty acid treatment, it would also be interesting to measure values of fatty acids in overweight mice. We then plan to disentangle whether adipocyte size or levels of FAs (or both) are determinant in tuning the lipolytic response to compression.

## **Follow-up research**

We used static compression in our work, but it would also be interesting **to develop a device providing dynamic compression to the cells**. This could more closely reflect the varying stresses under *in vivo* conditions.

The increased compressive stresses within the abdominal area arise from the correlation be-

tween IAP and BMI. However, it remains to be investigated what **magnitude of compressive stress the cells feel in the viscera of healthy and obese individuals**, and whether it is uniform in the whole cavity or varies between the different VAT depots. Therefore, it would be interesting to investigate such stresses in both physiological and pathophysiologic range, as well as quantifying these values during the evolution of obesity. Despite the fact that the AT in mouse models differs from humans, it would be interesting to use animal models for the development of pressure sensors that could be installed in the abdominal cavity. The compression in our work is directional, parallel to the axis of cylindrical symmetry. This approach could be adapted to better approximate the stresses measured by the sensors.

Furthermore, such abdominal pressure sensors could be used simultaneously with **an abdominal balloon that could deliver different compressive stress levels**. This would allow us to further dissect the role of the compression regulating visceral adiposity. A key experiment could be to implant the abdominal balloon in healthy mice and observe the evolution of the effect of compression under high fat diet.

It would be interesting to understand whether the observed effect of compression is not only restricted to VAT, or whether VAT and SAT exhibit different responses. If such differences are uncovered, it would be interesting to analyse whether they have a different gene signature responsible for mechanical sensing.

Finally, our work was only focused on lipolysis. However, we wonder whether lipogenesis and insulin signalling are also affected by compressive stress. Metabolomics studies could be considered in order to obtain a better picture of potential metabolic changes under static compression.





# Chapter 6

## Bibliography

- Abarca-Gómez, L. e. a. (2017). Worldwide trends in body-mass index, underweight, overweight, and obesity from 1975 to 2016: a pooled analysis of 2416 population-based measurement studies in 128·9 million children, adolescents, and adults. *The Lancet*, 390(10113):2627–2642.
- Aboulaich, N., Chui, P. C., Asara, J. M., Flier, J. S., and Maratos-Flier, E. (2011). Polymerase I and transcript release factor regulates lipolysis via a phosphorylation-dependent mechanism. *Diabetes*, 60(3):757–765.
- Aboulaich, N., Örtengren, U., Vener, A. V., and Strålfors, P. (2006). Association and insulin regulated translocation of hormone-sensitive lipase with PTRF. *Biochemical and Biophysical Research Communications*, 350(3):657–661.
- Aggarwal, A., Costa, M. J., Rivero-Gutiérrez, B., Ji, L., Morgan, S. L., and Feldman, B. J. (2017). The Circadian Clock Regulates Adipogenesis by a Per3 Crosstalk Pathway to Klf15. *Cell Reports*, 21(9):2367–2375.
- Ahmadian, M., Duncan, R. E., Varady, K. A., Frasson, D., Hellerstein, M. K., Birkenfeld, A. L., Samuel, V. T., Shulman, G. I., Wang, Y., Kang, C., and Sul, H. S. (2009). Adipose Overexpression of Desnutrin Promotes Fatty Acid Use and Attenuates Diet-Induced Obesity. *Diabetes*, 58(4):855–866.
- Ali, A. T., Hochfeld, W. E., Myburgh, R., and Pepper, M. S. (2013). Adipocyte and adipogenesis. *European Journal of Cell Biology*, 92(6-7):229–236.
- Alkhouli, N., Bell, J., Tham, J. C., Winlove, C. P., Liversedge, N., Welbourn, R., Green, E., Knight, B., Mansfield, J., Kos, K., and Shore, A. C. (2013). The mechanical properties of human adipose tissues and their relationships to the structure and composition of the extracellular matrix. *American Journal of Physiology-Endocrinology and Metabolism*, 305(12):E1427–E1435.
- Anthonsen, M. W., Rönstrand, L., Wernstedt, C., Degerman, E., and Holm, C. (1998). Identification of novel phosphorylation sites in hormone-sensitive lipase that are phosphorylated in response to isoproterenol and govern activation properties in vitro. *Journal of Biological Chemistry*, 273(1):215–221.

- Argolo, D. F., Hudis, C. A., and Iyengar, N. M. (2018). The Impact of Obesity on Breast Cancer. *Current Oncology Reports*, 20(6):47.
- Arner, P., Andersson, D. P., Bäckdahl, J., Dahlman, I., and Rydén, M. (2018). Weight Gain and Impaired Glucose Metabolism in Women Are Predicted by Inefficient Subcutaneous Fat Cell Lipolysis. *Cell Metabolism*, 28(1):45–54.
- Arner, P. and Rydén, M. (2015). Fatty acids, obesity and insulin resistance. *Obesity Facts*, 8(2):147–155.
- Barber, J. R. (2010). *Elasticity*, volume 172 of *Solid Mechanics and Its Applications*. Springer Netherlands, Dordrecht.
- Bartz, R., Zehmer, J. K., Zhu, M., Chen, Y., Serrero, G., Zhao, Y., and Liu, P. (2007). Dynamic activity of lipid droplets: Protein phosphorylation and GTP-mediated protein translocation. *Journal of Proteome Research*, 6(8):3256–3265.
- Berndt, J., Kralisch, S., Klötting, N., Ruschke, K., Kern, M., Fasshauer, M., Schön, M., Stumvoll, M., and Blüher, M. (2007). Adipose Triglyceride Lipase Gene Expression in Human Visceral Obesity. *Experimental and Clinical Endocrinology & Diabetes*, 116(04):203–210.
- Biswas, A., Kashyap, P., Datta, S., Sengupta, T., and Sinha, B. (2019). Cholesterol Depletion by M $\beta$ CD Enhances Cell Membrane Tension and Its Variations-Reducing Integrity. *Biophysical Journal*, 116(8):1456–1468.
- Blüher, M., Michael, M. D., Peroni, O. D., Ueki, K., Carter, N., Kahn, B. B., and Kahn, C. R. (2002). Adipose tissue selective insulin receptor knockout protects against obesity and obesity-related glucose intolerance. *Developmental Cell*, 3(1):25–38.
- Boudreau, N. and Weaver, V. (2006). Forcing the Third Dimension. *Cell*, 125(3):429–431.
- Brännmark, C., Paul, A., Ribeiro, D., Magnusson, B., Brolén, G., Enejder, A., and Forslöw, A. (2014). Increased adipogenesis of human adipose-derived stem cells on polycaprolactone fiber matrices. *PLoS ONE*, 9(11).
- Briand, N., Prado, C., Mabileau, G., Lasnier, F., Le Lièpvre, X., Covington, J. D., Ravussin, E., Le Lay, S., and Dugail, I. (2014). Caveolin-1 expression and cavin stability regulate caveolae dynamics in adipocyte lipid store fluctuation. *Diabetes*, 63(12):4032–4044.
- Carnevalli, L. S., Masuda, K., Frigerio, F., Le Bacquer, O., Um, S. H., Gandin, V., Topisirovic, I., Sonenberg, N., Thomas, G., and Kozma, S. C. (2010). S6K1 Plays a Critical Role in Early Adipocyte Differentiation. *Developmental Cell*, 18(5):763–774.
- Cassandri, M., Smirnov, A., Novelli, F., Pitolli, C., Agostini, M., Malewicz, M., Melino, G., and Raschellà, G. (2017). Zinc-finger proteins in health and disease. *Cell Death Discovery*, 3:17071.
- Castro, A. P. G., Laity, P., Shariatzadeh, M., Wittkowske, C., Holland, C., and Lacroix, D. (2016). Combined numerical and experimental biomechanical characterization of soft collagen hydrogel substrate. *Journal of Materials Science: Materials in Medicine*, 27(4):1–9.

- Castro, A. P. G., Yao, J., Battisti, T., and Lacroix, D. (2018). Poroelastic Modeling of Highly Hydrated Collagen Hydrogels: Experimental Results vs. Numerical Simulation With Custom and Commercial Finite Element Solvers. *Frontiers in Bioengineering and Biotechnology*, 6.
- Chan, D. C., Barrett, H. P. R., and Watts, G. F. (2004). Dyslipidemia in Visceral Obesity. *American Journal of Cardiovascular Drugs*, 4(4):227–246.
- Chapman, A. B., Knight, D. M., and Ringold, G. M. (1985). Glucocorticoid regulation of adipocyte differentiation: Hormonal triggering of the developmental program and induction of a differentiation-dependent gene. *Journal of Cell Biology*, 101(4):1227–1235.
- Chau, Y. Y., Bandiera, R., Serrels, A., Martínez-Estrada, O. M., Qing, W., Lee, M., Slight, J., Thornburn, A., Berry, R., Mchaffie, S., Stimson, R. H., Walker, B. R., Chapuli, R. M., Schedl, A., and Hastie, N. (2014). Visceral and subcutaneous fat have different origins and evidence supports a mesothelial source. *Nature Cell Biology*, 16(4):367–375.
- Chawla, A. and Lazar, M. A. (1994). Peroxisome proliferator and retinoid signaling pathways co-regulate preadipocyte phenotype and survival. *Proceedings of the National Academy of Sciences*, 91(5):1786–1790.
- Choe, S. S., Huh, J. Y., Hwang, I. J., Kim, J. I., and Kim, J. B. (2016). Adipose Tissue Remodeling: Its Role in Energy Metabolism and Metabolic Disorders. *Frontiers in Endocrinology*, 7(April).
- Chouchani, E. T. and Kajimura, S. (2019). Metabolic adaptation and maladaptation in adipose tissue. *Nature Metabolism*, 1(2):189–200.
- Christodoulides, C., Lagathu, C., Sethi, J. K., and Vidal-Puig, A. (2009). Adipogenesis and WNT signalling. *Trends in Endocrinology & Metabolism*, 20(1):16–24.
- Cinti, S., Mitchell, G., Barbatelli, G., Murano, I., Ceresi, E., Faloia, E., Wang, S., Fortier, M., Greenberg, A. S., and Obin, M. S. (2005). Adipocyte death defines macrophage localization and function in adipose tissue of obese mice and humans. *Journal of Lipid Research*, 46(11):2347–2355.
- Colom, A., Derivery, E., Soleimanpour, S., Tomba, C., Molin, M. D., Sakai, N., González-Gaitán, M., Matile, S., and Roux, A. (2018). A fluorescent membrane tension probe. *Nature Chemistry*, 10(11):1118–1125.
- Comley, K. and Fleck, N. A. (2010). A micromechanical model for the Young's modulus of adipose tissue. *International Journal of Solids and Structures*, 47(21):2982–2990.
- Cristancho, A. G. and Lazar, M. A. (2011). Forming functional fat: a growing understanding of adipocyte differentiation. *Nature Reviews Molecular Cell Biology*, 12(11):722–734.
- Dalmas, E., Toubal, A., Alzaid, F., Blazek, K., Eames, H. L., Lebozec, K., Pini, M., Hainault, I., Montastier, E., Denis, R. G. P., Ancel, P., Lacombe, A., Ling, Y., Allatif, O., Cruciani-Guglielmacci, C., André, S., Viguerie, N., Poitou, C., Stich, V., Torcivia, A., Foufelle, F., Luquet, S., Aron-Wisnewsky, J., Langin, D., Clément, K., Udalova, I. A., and Venteclef,

- N. (2015). Irf5 deficiency in macrophages promotes beneficial adipose tissue expansion and insulin sensitivity during obesity. *Nature Medicine*, 21(6):610–618.
- Darlington, G. J., Ross, S. E., and MacDougald, O. A. (1998). The Role of C/EBP Genes in Adipocyte Differentiation. *Journal of Biological Chemistry*, 273(46):30057–30060.
- Daval, M., Diot-Dupuy, F., Bazin, R., Hainault, I., Viollet, B., Vaulont, S., Hajduch, E., Ferré, P., and Foufelle, F. (2005). Anti-lipolytic action of AMP-activated protein kinase in rodent adipocytes. *Journal of Biological Chemistry*, 280(26):25250–25257.
- De Keulenaer, B. L., De Waele, J. J., Powell, B., and Malbrain, M. L. N. G. (2012). What is normal intra-abdominal pressure and how is it affected by positioning, body mass and positive end-expiratory pressure? In *Applied Physiology in Intensive Care Medicine 2*, pages 219–226. Springer Berlin Heidelberg, Berlin, Heidelberg.
- de Mello, A. H., Costa, A. B., Engel, J. D. G., and Rezin, G. T. (2018). Mitochondrial dysfunction in obesity. *Life Sciences*, 192:26–32.
- Delarue, M., Brittingham, G. P., Pfeffer, S., Surovtsev, I. V., Pinglay, S., Kennedy, K. J., Schaffer, M., Gutierrez, J. I., Sang, D., Poterewicz, G., Chung, J. K., Plitzko, J. M., Groves, J. T., Jacobs-Wagner, C., Engel, B. D., and Holt, L. J. (2018). mTORC1 Controls Phase Separation and the Biophysical Properties of the Cytoplasm by Tuning Crowding. *Cell*, 174(2):338–349.
- Diz-Muñoz, A., Fletcher, D. A., and Weiner, O. D. (2013). Use the force: membrane tension as an organizer of cell shape and motility. *Trends in Cell Biology*, 23(2):47–53.
- Drira, R., Matsumoto, T., Agawa, M., and Sakamoto, K. (2016). Ice Plant ( *Mesembryanthemum crystallinum* ) Extract Promotes Lipolysis in Mouse 3T3-L1 Adipocytes Through Extracellular Signal-Regulated Kinase Activation. *Journal of Medicinal Food*, 19(3):274–280.
- Duncan, R. E., Ahmadian, M., Jaworski, K., Sarkadi-Nagy, E., and Sul, H. S. (2007). Regulation of Lipolysis in Adipocytes. *Annual Review of Nutrition*, 27(1):79–101.
- Echarri, A. and Del Pozo, M. A. (2015). Caveolae - mechanosensitive membrane invaginations linked to actin filaments. *Journal of Cell Science*, 128(15):2747–2758.
- Emont, M. P., Yu, H., Jun, H., Hong, X., Maganti, N., Stegemann, J. P., and Wu, J. (2015). Using a 3D Culture System to Differentiate Visceral Adipocytes In Vitro. *Endocrinology*, 156(12):4761–4768.
- Escobedo, N. and Oliver, G. (2017). The Lymphatic Vasculature: Its Role in Adipose Metabolism and Obesity. *Cell Metabolism*, 26(4):598–609.
- Farnier, C., Krief, S., Blache, M., Diot-Dupuy, F., Mory, G., Ferre, P., and Bazin, R. (2003). Adipocyte functions are modulated by cell size change: Potential involvement of an integrin/ERK signalling pathway. *International Journal of Obesity*, 27(10):1178–1186.
- Flynn, L. and Woodhouse, K. A. (2008). Adipose tissue engineering with cells in engineered matrices. *Organogenesis*, 4(4):228–235.

- Franke, W. W., Hergt, M., and Grund, C. (1987). Rearrangement of the vimentin cytoskeleton during adipose conversion: Formation of an intermediate filament cage around lipid globules. *Cell*, 49(1):131–141.
- Frayn, K. N., Karpe, F., Fielding, B. A., Macdonald, I. A., and Coppack, S. W. (2003). Integrative physiology of human adipose tissue. *International Journal of Obesity*, 27(8):875–888.
- Frühbeck, G., Méndez-Giménez, L., Fernández-Formoso, J.-A., Fernández, S., and Rodríguez, A. (2014). Regulation of adipocyte lipolysis. *Nutrition Research Reviews*, 27(1):63–93.
- Gaidhu, M. P., Anthony, N. M., Patel, P., Hawke, T. J., and Ceddia, R. B. (2010). Dysregulation of lipolysis and lipid metabolism in visceral and subcutaneous adipocytes by high-fat diet: role of ATGL, HSL, and AMPK. *American Journal of Physiology-Cell Physiology*, 298(4):C961–C971.
- Geerligs, M., Peters, G. W. M., Ackermans, P. A. J., Oomens, C. W. J., and Baaijens, F. P. T. (2008). Linear viscoelastic behavior of subcutaneous adipose tissue. *Biorheology*, 45(6):677–688.
- Gentleman, E., Nauman, E. A., Livesay, G. A., and Dee, K. C. (2006). Collagen Composite Biomaterials Resist Contraction While Allowing Development of Adipocytic Soft Tissue In Vitro. *Tissue Engineering*, 12(6):1639–1649.
- Gesta, S., Tseng, Y.-H., and Kahn, C. R. (2007). Developmental Origin of Fat: Tracking Obesity to Its Source. *Cell*, 131(2):242–256.
- Ghaben, A. L. and Scherer, P. E. (2019). Adipogenesis and metabolic health. *Nature Reviews Molecular Cell Biology*, 20(4):242–258.
- Gomillion, C. T. and Burg, K. J. L. (2006). Stem cells and adipose tissue engineering. *Biomaterials*, 27(36):6052–63.
- Gong, J., Sun, Z., Wu, L., Xu, W., Schieber, N., Xu, D., Shui, G., Yang, H., Parton, R. G., and Li, P. (2011). Fsp27 promotes lipid droplet growth by lipid exchange and transfer at lipid droplet contact sites. *Journal of Cell Biology*, 195(6):953–963.
- González-Muniesa, P., Martínez-González, M.-A., Hu, F. B., Després, J.-P., Matsuzawa, Y., Loos, R. J. F., Moreno, L. A., Bray, G. A., and Martínez, J. A. (2017). Obesity. *Nature Reviews Disease Primers*, 3:17034.
- Gortazar, A. R., Martin-Millan, M., Bravo, B., Plotkin, L. I., and Bellido, T. (2013). Crosstalk between caveolin-1/extracellular signal-regulated kinase (ERK) and  $\beta$ -catenin survival pathways in osteocyte mechanotransduction. *Journal of Biological Chemistry*, 288(12):8168–8175.
- Green, H. and Kehinde, O. (1974). Sublines of mouse 3T3 cells that accumulate lipid. *Cell*, 1(3):113–116.

- Green, H. and Kehinde, O. (1975). An established preadipose cell line and its differentiation in culture II. Factors affecting the adipose conversion. *Cell*, 5(1):19–27.
- Green, H. and Kehinde, O. (1976). Spontaneous heritable changes leading to increased adipose conversion in 3T3 cells. *Cell*, 7(1):105–113.
- Green, H. and Meuth, M. (1974). An established pre-adipose cell line and its differentiation in culture. *Cell*, 3(2):127–133.
- Greenberg, A. S., Shen, W. J., Muliro, K., Patel, S., Souza, S. C., Roth, R. A., and Kraemer, F. B. (2001). Stimulation of Lipolysis and Hormone-sensitive Lipase via the Extracellular Signal-regulated Kinase Pathway. *Journal of Biological Chemistry*, 276(48):45456–45461.
- Gudermann, T. (2001). Multiple pathways of ERK activation by G protein-coupled receptors. *Novartis Foundation symposium*, 239:68–79.
- Guixà-González, R., Albasanz, J. L., Rodríguez-Espigares, I., Pastor, M., Sanz, F., Martí-Solano, M., Manna, M., Martínez-Seara, H., Hildebrand, P. W., Martín, M., and Selent, J. (2017). Membrane cholesterol access into a G-protein-coupled receptor. *Nature Communications*, 8(1):14505.
- Haemmerle, G., Lass, A., Zimmermann, R., Gorkiewicz, G., Meyer, C., Rozman, J., Heldmaier, G., Maier, R., Theussl, C., Eder, S., Kratky, D., Wagner, E. F., Klingenspor, M., Hoefler, G., and Zechner, R. (2006). Defective lipolysis and altered energy metabolism in mice lacking adipose triglyceride lipase. *Science*, 312(5774):734–737.
- Haeusler, R. A., McGraw, T. E., and Accili, D. (2017). Biochemical and cellular properties of insulin receptor signalling. *Nature Reviews Molecular Cell Biology*, 19(1):31–44.
- Han, T. S. and Lean, M. E. (2016). A clinical perspective of obesity, metabolic syndrome and cardiovascular disease. *JRSM Cardiovascular Disease*, 5:204800401663337.
- Harms, M. and Seale, P. (2013). Brown and beige fat: Development, function and therapeutic potential. *Nature Medicine*, 19(10):1252–1263.
- Hauner, H., Schmid, P., and Pfeiffer, E. F. (1987). Glucocorticoids and insulin promote the differentiation of human adipocyte precursor cells into fat cells. *Journal of Clinical Endocrinology and Metabolism*, 64(4):832–835.
- Heckmann, B. L., Zhang, X., Saarinen, A. M., and Liu, J. (2016). Regulation of G0/G1 Switch Gene 2 (G0S2) Protein Ubiquitination and Stability by Triglyceride Accumulation and ATGL Interaction. *PLOS ONE*, 11(6):e0156742.
- Heid, H., Rickelt, S., Zimbelmann, R., Winter, S., Schumacher, H., Dörflinger, Y., Kuhn, C., and Franke, W. W. (2014). On the formation of lipid droplets in human adipocytes: The organization of the perilipin-vimentin cortex. *PLoS ONE*, 9(2).
- Hissa, B., Oakes, P. W., Pontes, B., Ramírez-San Juan, G., and Gardel, M. L. (2017). Cholesterol depletion impairs contractile machinery in neonatal rat cardiomyocytes. *Scientific Reports*, 7(1):43764.

- Hong, S., Song, W., Zushin, P. J. H., Liu, B., Jedrychowski, M. P., Mina, A. I., Deng, Z., Cabarkapa, D., Hall, J. A., Palmer, C. J., Aliakbarian, H., Szpyt, J., Gygi, S. P., Tavakkoli, A., Lynch, L., Perrimon, N., and Banks, A. S. (2018). Phosphorylation of Beta-3 adrenergic receptor at serine 247 by ERK MAP kinase drives lipolysis in obese adipocytes. *Molecular Metabolism*, 12:25–38.
- Hossain, M. G., Iwata, T., Mizusawa, N., Shima, S. W. N., Okutsu, T., Ishimoto, K., and Yoshimoto, K. (2010). Compressive force inhibits adipogenesis through COX-2-mediated down-regulation of PPAR $\gamma$ 2 and C/EBP $\alpha$ . *Journal of Bioscience and Bioengineering*, 109(3):297–303.
- Jansson, J.-O., Palsdottir, V., Hägg, D. A., Schéle, E., Dickson, S. L., Anesten, F., Bake, T., Montelius, M., Bellman, J., Johansson, M. E., Cone, R. D., Drucker, D. J., Wu, J., Aleksic, B., Törnqvist, A. E., Sjögren, K., Gustafsson, J.-Å., Windahl, S. H., and Ohlsson, C. (2017). Body weight homeostat that regulates fat mass independently of leptin in rats and mice. *Proceedings of the National Academy of Sciences*, 115(2):427–432.
- Jeffery, E., Wing, A., Holtrup, B., Sebo, Z., Kaplan, J. L., Saavedra-Peña, R., Church, C. D., Colman, L., Berry, R., and Rodeheffer, M. S. (2016). The Adipose Tissue Microenvironment Regulates Depot-Specific Adipogenesis in Obesity. *Cell Metabolism*, 24(1):142–150.
- Jeong, H. Y., Yun, H. J., Kim, B. W., Lee, E. W., and Kwon, H. J. (2015). Widdrol-induced lipolysis is mediated by PKC and MEK/ERK in 3T3-L1 adipocytes. *Molecular and Cellular Biochemistry*, 410(1-2):247–254.
- Jocken, J. W. and Blaak, E. E. (2008). Catecholamine-induced lipolysis in adipose tissue and skeletal muscle in obesity. *Physiology and Behavior*, 94(2):219–230.
- Kang, X., Xie, Y., Powell, H. M., James Lee, L., Belury, M. A., Lannutti, J. J., and Kniss, D. A. (2007). Adipogenesis of murine embryonic stem cells in a three-dimensional culture system using electrospun polymer scaffolds. *Biomaterials*, 28(3):450–458.
- Karpe, F. and Pinnick, K. E. (2015). Biology of upper-body and lower-body adipose tissue - Link to whole-body phenotypes. *Nature Reviews Endocrinology*, 11(2):90–100.
- Katzengold, R., Shoham, N., Benayahu, D., and Gefen, A. (2015). Simulating single cell experiments in mechanical testing of adipocytes. *Biomechanics and Modeling in Mechanobiology*, 14(3):537–547.
- Kim, J. I., Huh, J. Y., Sohn, J. H., Choe, S. S., Lee, Y. S., Lim, C. Y., Jo, A., Park, S. B., Han, W., and Kim, J. B. (2015). Lipid-Overloaded Enlarged Adipocytes Provoke Insulin Resistance Independent of Inflammation. *Molecular and Cellular Biology*, 35(10):1686–1699.
- Kim, J. Y., Van De Wall, E., Laplante, M., Azzara, A., Trujillo, M. E., Hofmann, S. M., Schraw, T., Durand, J. L., Li, H., Li, G., Jelicks, L. A., Mehler, M. F., Hui, D. Y., Deshaies, Y., Shulman, G. I., Schwartz, G. J., and Scherer, P. E. (2007). Obesity-associated improvements in metabolic profile through expansion of adipose tissue. *Journal of Clinical Investigation*, 117(9):2621–2637.

- Kimmel, A. R. and Sztalryd, C. (2016). The Perilipins: Major Cytosolic Lipid Droplet-Associated Proteins and Their Roles in Cellular Lipid Storage, Mobilization, and Systemic Homeostasis. *Annual Review of Nutrition*, 36(1):471–509.
- Kinney, B. P., Qiao, L., LeVaugh, J. M., and Shao, J. (2010). B56 $\alpha$ /Protein Phosphatase 2A Inhibits Adipose Lipolysis in High-Fat Diet-Induced Obese Mice. *Endocrinology*, 151(8):3624–3632.
- Knapp, D. M., Barocas, V. H., Moon, A. G., Yoo, K., Petzold, L. R., and Tranquillo, R. T. (2002). Rheology of reconstituted type I collagen gel in confined compression. *Journal of Rheology*, 41(5):971–993.
- Kobayashi, K., Inoguchi, T., Maeda, Y., Nakashima, N., Kuwano, A., Eto, E., Ueno, N., Sasaki, S., Sawada, F., Fujii, M., Matoba, Y., Sumiyoshi, S., Kawate, H., and Takayanagi, R. (2008). The Lack of the C-Terminal Domain of Adipose Triglyceride Lipase Causes Neutral Lipid Storage Disease through Impaired Interactions with Lipid Droplets. *The Journal of Clinical Endocrinology & Metabolism*, 93(7):2877–2884.
- Krontiras, P., Gatenholm, P., and Hagg, D. A. (2015). Adipogenic differentiation of stem cells in three-dimensional porous bacterial nanocellulose scaffolds. *Journal of Biomedical Materials Research - Part B Applied Biomaterials*, 103(1):195–203.
- Kwon, H., Kim, D., and Kim, J. S. (2017). Body Fat Distribution and the Risk of Incident Metabolic Syndrome: A Longitudinal Cohort Study. *Scientific Reports*, 7(1).
- Lackey, D. E., Burk, D. H., Ali, M. R., Mostaedi, R., Smith, W. H., Park, J., Scherer, P. E., Seay, S. A., McCoin, C. S., Bonaldo, P., and Adams, S. H. (2014). Contributions of adipose tissue architectural and tensile properties toward defining healthy and unhealthy obesity. *American journal of physiology. Endocrinology and metabolism*, 306(3):233–46.
- Lan, A., Liao, X., Mo, L., Yang, C., Yang, Z., Wang, X., Hu, F., Chen, P., Feng, J., Zheng, D., and Xiao, L. (2011). Hydrogen Sulfide Protects against Chemical Hypoxia-Induced Injury by Inhibiting ROS-Activated ERK1/2 and p38MAPK Signaling Pathways in PC12 Cells. *PLoS ONE*, 6(10):e25921.
- Langin, D., Dicker, A., Tavernier, G., Hoffstedt, J., Mairal, A., Ryden, M., Arner, E., Sicard, A., Jenkins, C. M., Viguerie, N., van Harmelen, V., Gross, R. W., Holm, C., and Arner, P. (2005). Adipocyte Lipases and Defect of Lipolysis in Human Obesity. *Diabetes*, 54(11):3190–3197.
- Lawler, H. M., Underkofler, C. M., Kern, P. A., Erickson, C., Bredbeck, B., and Rasouli, N. (2016). Adipose tissue hypoxia, inflammation, and fibrosis in obese insulin-sensitive and obese insulin-resistant subjects. *Journal of Clinical Endocrinology and Metabolism*, 101(4):1422–1428.
- Lecoultre, V. and Ravussin, E. (2011). Brown adipose tissue and aging. *Current Opinion in Clinical Nutrition and Metabolic Care*, 14(1):1–6.



- Lee, B., Zhou, X., Riching, K., Eliceiri, K. W., Keely, P. J., Guelcher, S. A., Weaver, A. M., and Jiang, Y. (2014). A three-dimensional computational model of collagen network mechanics. *PLoS ONE*, 9(11):1–12.
- Leitner, B. P., Huang, S., Brychta, R. J., Duckworth, C. J., Baskin, A. S., McGehee, S., Tal, I., Dieckmann, W., Gupta, G., Kolodny, G. M., Pacak, K., Herscovitch, P., Cypess, A. M., and Chen, K. Y. (2017). Mapping of human brown adipose tissue in lean and obese young men. *Proceedings of the National Academy of Sciences*, 114(32):8649–8654.
- Levy, A., Enzer, S., Shoham, N., Zaretsky, U., and Gefen, A. (2012). Large, but not small sustained tensile strains stimulate adipogenesis in culture. *Annals of Biomedical Engineering*, 40(5):1052–1060.
- Li, G., Fu, N., Yang, X., Li, M., Ba, K., Wei, X., Fu, Y., Yao, Y., Cai, X., and Lin, Y. (2013). Mechanical compressive force inhibits adipogenesis of adipose stem cells. *Cell Proliferation*, 46(5):586–594.
- Li, Q., Hosaka, T., Jambaldorj, B., Nakaya, Y., and Funaki, M. (2009). Extracellular matrix with the rigidity of adipose tissue helps 3T3-L1 adipocytes maintain insulin responsiveness. *The Journal of Medical Investigation: JMI*, 56(3-4):142–149.
- Lidell, M. E. and Enerbäck, S. (2010). Brown adipose tissue—a new role in humans? *Nature Reviews Endocrinology*, 6(6):319–325.
- Lieber, J. G. and Evans, R. M. (1996). Disruption of the vimentin intermediate filament system during adipose conversion of 3T3-L1 cells inhibits lipid droplet accumulation. *Journal of Cell Science*, 109(13):3047–3058.
- Lijnen, H. R., Maquoi, E., Hansen, L. B., Van Hoef, B., Frederix, L., and Collen, D. (2002). Matrix metalloproteinase inhibition impairs adipose tissue development in mice. *Arteriosclerosis, Thrombosis, and Vascular Biology*, 22(3):374–379.
- Liu, L. and Pilch, P. F. (2016). PTRF/Cavin-1 promotes efficient ribosomal RNA transcription in response to metabolic challenges. *eLife*, 5(August).
- Louis, F., Kitano, S., Mano, J. F., and Matsusaki, M. (2019). 3D collagen microfibers stimulate the functionality of preadipocytes and maintain the phenotype of mature adipocytes for long term cultures. *Acta Biomaterialia*, 84:194–207.
- Louis, F., Pannetier, P., Souguir, Z., Le Cerf, D., Valet, P., Vannier, J. P., Vidal, G., and Demange, E. (2017). A biomimetic hydrogel functionalized with adipose ECM components as a microenvironment for the 3D culture of human and murine adipocytes. *Biotechnology and Bioengineering*, 114(8):1813–1824.
- Lowe, C. E., O’Rahilly, S., and Rochford, J. J. (2011). Adipogenesis at a glance. *Journal of Cell Science*, 124(16):2681–2686.
- Luong, Q., Huang, J., and Lee, K. Y. (2019). Deciphering White Adipose Tissue Heterogeneity. *Biology*, 8(2):23.

- Lustig, M., Gefen, A., and Benayahu, D. (2018). Adipogenesis and lipid production in adipocytes subjected to sustained tensile deformations and elevated glucose concentration: a living cell-scale model system of diabetes. *Biomechanics and Modeling in Mechanobiology*, 17(3):903–913.
- Madsen, M. S., Siersbaek, R., Boergesen, M., Nielsen, R., and Mandrup, S. (2013). Peroxisome Proliferator-Activated Receptor  $\alpha$  and C/EBP $\alpha$  Synergistically Activate Key Metabolic Adipocyte Genes by Assisted Loading. *Molecular and Cellular Biology*, 34(6):939–954.
- Malbrain, M. L. N. G. (2004). Different techniques to measure intra-abdominal pressure (IAP): time for a critical re-appraisal. *Intensive Care Medicine*, 30(3):357–371.
- Mariman, E. C. M. and Wang, P. (2010). Adipocyte extracellular matrix composition, dynamics and role in obesity. *Cellular and Molecular Life Sciences*, 67(8):1277–1292.
- Mayor, S. (2011). Need Tension Relief Fast? Try Caveolae. *Cell*, 144(3):323–324.
- McBeath, R., Pirone, D. M., Nelson, C. M., Bhadriraju, K., and Chen, C. S. (2004). Cell shape, cytoskeletal tension, and RhoA regulate stem cell lineage commitment. *Developmental cell*, 6(4):483–95.
- Meyers, A., Weiskittel, T. M., and Dalhaimer, P. (2017). Lipid Droplets: Formation to Breakdown. *Lipids*, 52(6):465–475.
- Milanesi, R. and Caregnato, R. C. A. (2016). Intra-abdominal pressure: an integrative review. *Einstein (São Paulo)*, 14(3):423–430.
- Miyoshi, H., Perfield, J. W., Obin, M. S., and Greenberg, A. S. (2008). Adipose triglyceride lipase regulates basal lipolysis and lipid droplet size in adipocytes. *Journal of Cellular Biochemistry*, 105(6):1430–1436.
- Miyoshi, H., Perfield, J. W., Souza, S. C., Shen, W. J., Zhang, H. H., Stancheva, Z. S., Kraemer, F. B., Obin, M. S., and Greenberg, A. S. (2007). Control of adipose triglyceride lipase action by serine 517 of perilipin A globally regulates protein kinase  $\alpha$ -stimulated lipolysis in adipocytes. *Journal of Biological Chemistry*, 282(2):996–1002.
- Morrison, S. and McGee, S. L. (2015). 3T3-L1 adipocytes display phenotypic characteristics of multiple adipocyte lineages. *Adipocyte*, 4(4):295–302.
- Musi, N. and Guardado-Mendoza, R. (2014). Adipose Tissue as an Endocrine Organ. In *Cellular Endocrinology in Health and Disease*, pages 229–237. Elsevier.
- Nascimento, E. B., Sparks, L. M., Divoux, A., van Gisbergen, M. W., Broeders, E. P., Jörgensen, J. A., Schaart, G., Bouvy, N. D., van Marken Lichtenbelt, W. D., and Schrauwen, P. (2018). Genetic Markers of Brown Adipose Tissue Identity and In Vitro Brown Adipose Tissue Activity in Humans. *Obesity*, 26(1):135–140.
- Niederauer, S., de Gennaro, J., Nygaard, I., Petelenz, T., and Hitchcock, R. (2017). Development of a novel intra-abdominal pressure transducer for large scale clinical studies. *Biomedical Microdevices*, 19(4).

- Nielsen, T. S., Jessen, N., Jørgensen, J. O. L., Møller, N., and Lund, S. (2014). Dissecting adipose tissue lipolysis: molecular regulation and implications for metabolic disease. *Journal of Molecular Endocrinology*, 52(3).
- Nobusue, H., Onishi, N., Shimizu, T., Sugihara, E., Oki, Y., Sumikawa, Y., Chiyoda, T., Akashi, K., Saya, H., and Kano, K. (2014). Regulation of MKL1 via actin cytoskeleton dynamics drives adipocyte differentiation. *Nature Communications*, 5:3368.
- Ogus, S., Ke, Y., Qiu, J., Wang, B., and Chehab, F. F. (2003). Hyperleptinemia precipitates diet-induced obesity in transgenic mice overexpressing leptin. *Endocrinology*, 144(7):2865–2869.
- Olzmann, J. A. and Carvalho, P. (2019). Dynamics and functions of lipid droplets. *Nature Reviews Molecular Cell Biology*, 20(3):137–155.
- Otabe, S., Yuan, X., Fukutani, T., Wada, N., Hashinaga, T., Nakayama, H., Hirota, N., Kojima, M., and Yamada, K. (2007). Overexpression of human adiponectin in transgenic mice results in suppression of fat accumulation and prevention of premature death by high-calorie diet. *American Journal of Physiology-Endocrinology and Metabolism*, 293(1):E210–E218.
- Pagnon, J., Matzaris, M., Stark, R., Meex, R. C. R., Macaulay, S. L., Brown, W., O'Brien, P. E., Tiganis, T., and Watt, M. J. (2012). Identification and functional characterization of protein kinase A phosphorylation sites in the major lipolytic protein, adipose triglyceride lipase. *Endocrinology*, 153(9):4278–4289.
- Parimisetty, A., Dorsemans, A.-C., Awada, R., Ravanan, P., Diotel, N., and Lefebvre d'Herle, C. (2016). Secret talk between adipose tissue and central nervous system via secreted factors—An emerging frontier in the neurodegenerative research. *Journal of Neuroinflammation*, 13(1):67.
- Park, H.-Y., Kwon, H. M., Lim, H. J., Hong, B. K., Lee, J. Y., Park, B. E., Jang, Y. S., Cho, S. Y., and Kim, H.-S. (2013). Potential role of leptin in angiogenesis: leptin induces endothelial cell proliferation and expression of matrix metalloproteinases in vivo and in vitro. *Experimental & Molecular Medicine*, 33(2):95–102.
- Parlee, S. D., Lentz, S. I., Mori, H., and MacDougald, O. A. (2014). Quantifying Size and Number of Adipocytes in Adipose Tissue. In *Methods in Enzymology*, volume 537, pages 93–122.
- Parton, R. G. and Del Pozo, M. A. (2013). Caveolae as plasma membrane sensors, protectors and organizers. *Nature Reviews Molecular Cell Biology*, 14(2):98–112.
- Peirce, V., Carobbio, S., and Vidal-Puig, A. (2014). The different shades of fat. *Nature*, 510(7503):76–83.
- Pellegrinelli, V., Carobbio, S., and Vidal-Puig, A. (2016). Adipose tissue plasticity: how fat depots respond differently to pathophysiological cues. *Diabetologia*, 59(6):1075–1088.

- Pellegrinelli, V., Heuvingh, J., Du Roure, O., Rouault, C., Devulder, A., Klein, C., Lacasa, M., Clément, E., Lacasa, D., and Clément, K. (2014). Human adipocyte function is impacted by mechanical cues. *Journal of Pathology*, 233(2):183–195.
- Perez-Diaz, S., Johnson, L. A., DeKroon, R. M., Moreno-Navarrete, J. M., Alzate, O., Fernandez-Real, J. M., Maeda, N., and Arbones-Mainar, J. M. (2014). Polymerase I and transcript release factor (PTRF) regulates adipocyte differentiation and determines adipose tissue expandability. *FASEB Journal*, 28(8):3769–3779.
- Peter, T., Erding, H., and Spiegelman, B. M. (1994). Stimulation of Adipogenesis by PPAR $\gamma$ 2, a Lipid-Activated in Fibroblasts Transcription Factor. *Cell*, 79:1147–1156.
- Pilch, P. F. and Liu, L. (2011). Fat caves: caveolae, lipid trafficking and lipid metabolism in adipocytes. *Trends in Endocrinology & Metabolism*, 22(8):318–324.
- Pope, B. D., Warren, C. R., Parker, K. K., and Cowan, C. A. (2016). Microenvironmental Control of Adipocyte Fate and Function. *Trends in Cell Biology*, 26(10):745–755.
- Rajan, N., Habermehl, J., Coté, M. F., Doillon, C. J., and Mantovani, D. (2007). Preparation of ready-to-use, storable and reconstituted type I collagen from rat tail tendon for tissue engineering applications. *Nature Protocols*, 1(6):2753–2758.
- Rosen, E. D., Sarraf, P., Troy, A. E., Bradwin, G., Moore, K., Milstone, D. S., Spiegelman, B. M., and Mortensen, R. M. (1999). PPAR $\gamma$  is required for the differentiation of adipose tissue in vivo and in vitro. *Molecular Cell*, 4(4):611–617.
- Rosen, E. D. and Spiegelman, B. M. (2014). What We Talk About When We Talk About Fat. *Cell*, 156(1-2):20–44.
- Rubin, J. P., Bennett, J. M., Doctor, J. S., Tebbets, B. M., and Marra, K. G. (2007). Collagenous microbeads as a scaffold for tissue engineering with adipose-derived stem cells. *Plastic and Reconstructive Surgery*, 120(2):414–424.
- Ruiz-Ojeda, F., Rupérez, A., Gomez-Llorente, C., Gil, A., and Aguilera, C. (2016). Cell Models and Their Application for Studying Adipogenic Differentiation in Relation to Obesity: A Review. *International Journal of Molecular Sciences*, 17(7):1040.
- Rutkowski, J. M., Stern, J. H., and Scherer, P. E. (2015). The cell biology of fat expansion. *The Journal of Cell Biology*, 208(5):501–512.
- Salazar-Olivo, L. A., Castro-Muñozledo, F., and Kuri-Harcuch, W. (1995). A preadipose 3T3 cell variant highly sensitive to adipogenic factors and to human growth hormone. *Journal of Cell Science*, 108 (Pt 5):2101–2107.
- Schoiswohl, G., Stefanovic-Racic, M., Menke, M. N., Wills, R. C., Surlow, B. A., Basantani, M. K., Sitnick, M. T., Cai, L., Yazbeck, C. F., Stolz, D. B., Pulinilkunnil, T., O’Doherty, R. M., and Kershaw, E. E. (2015). Impact of reduced ATGL-mediated adipocyte lipolysis on obesity-associated insulin resistance and inflammation in male mice. *Endocrinology*, 156(10):3610–3624.

- Schweiger, M., Schoiswohl, G., Lass, A., Radner, F. P. W., Haemmerle, G., Malli, R., Graier, W., Cornaciu, I., Oberer, M., Salvayre, R., Fischer, J., Zechner, R., and Zimmermann, R. (2008). The C-terminal region of human adipose triglyceride lipase affects enzyme activity and lipid droplet binding. *Journal of Biological Chemistry*, 283(25):17211–17220.
- Schweiger, M., Schreiber, R., Haemmerle, G., Lass, A., Fledelius, C., Jacobsen, P., Tornqvist, H., Zechner, R., and Zimmermann, R. (2006). Adipose triglyceride lipase and hormone-sensitive lipase are the major enzymes in adipose tissue triacylglycerol catabolism. *Journal of Biological Chemistry*, 281(52):40236–40241.
- Sen, B., Xie, Z., Case, N., Ma, M., Rubin, C., and Rubin, J. (2008). Mechanical strain inhibits adipogenesis in mesenchymal stem cells by stimulating a durable  $\beta$ -catenin signal. *Endocrinology*, 149(12):6065–6075.
- Shan, T., Zhang, P., Jiang, Q., Xiong, Y., Wang, Y., and Kuang, S. (2016). Adipocyte-specific deletion of mTOR inhibits adipose tissue development and causes insulin resistance in mice. *Diabetologia*, 59(9):1995–2004.
- Shanti, R. M., Janjanin, S., Li, W. J., Nesti, L. J., Mueller, M. B., Tzeng, M. B., and Tuan, R. S. (2008). In vitro adipose tissue engineering using an electrospun nanofibrous scaffold. *Annals of Plastic Surgery*, 61(5):566–571.
- Shen, W. J., Patel, S., Eriksson, J. E., and Kraemer, F. B. (2010). Vimentin is a functional partner of hormone sensitive lipase and facilitates lipolysis. *Journal of Proteome Research*, 9(4):1786–1794.
- Shoham, N., Girshovitz, P., Katzungold, R., Shaked, N. T., Benayahu, D., and Gefen, A. (2014). Adipocyte stiffness increases with accumulation of lipid droplets. *Biophysical Journal*, 106(6):1421–1431.
- Shoham, N., Gottlieb, R., Sharabani-Yosef, O., Zaretsky, U., Benayahu, D., and Gefen, A. (2012). Static mechanical stretching accelerates lipid production in 3T3-L1 adipocytes by activating the MEK signaling pathway. *AJP: Cell Physiology*, 302(2):C429–C441.
- Shoham, N., Mor-Yossef Moldovan, L., Benayahu, D., and Gefen, A. (2015). Multiscale Modeling of Tissue-Engineered Fat: Is There a Deformation-Driven Positive Feedback Loop in Adipogenesis? *Tissue Engineering Part A*, 21(7-8):1354–1363.
- Silvestri, C., Martella, A., Poloso, N. J., Piscitelli, F., Capasso, R., Izzo, A., Woodward, D. F., and Di Marzo, V. (2013). Anandamide-derived Prostaglandin F<sub>2</sub> $\alpha$  Negatively Regulates Adipogenesis. *Journal of Biological Chemistry*, 288(32):23307–23321.
- Sinha, B., Köster, D., Ruez, R., Gonnord, P., Bastiani, M., Abankwa, D., Stan, R. V., Butler-Browne, G., Védie, B., Johannes, L., Morone, N., Parton, R. G., Raposo, G., Sens, P., Lamaze, C., and Nassoy, P. (2011). Cells respond to mechanical stress by rapid disassembly of caveolae. *Cell*, 144(3):402–413.
- Smit, M., Werner, M. J. M., Lansink-Hartgring, A. O., Dieperink, W., Zijlstra, J. G., and van Meurs, M. (2016). How central obesity influences intra-abdominal pressure: a prospective, observational study in cardiothoracic surgical patients. *Annals of Intensive Care*, 6(1):99.

- Song, Z., Xiaoli, A., and Yang, F. (2018). Regulation and Metabolic Significance of De Novo Lipogenesis in Adipose Tissues. *Nutrients*, 10(10):1383.
- Sordella, R., Jiang, W., Chen, G. C., Curto, M., and Settleman, J. (2003). Modulation of rho GTPase signaling regulates a switch between adipogenesis and myogenesis.
- Spalding, K. L., Arner, E., Westermark, P. O., Bernard, S., Buchholz, B. A., Bergmann, O., Blomqvist, L., Hoffstedt, J., Näslund, E., Britton, T., Concha, H., Hassan, M., Rydén, M., Frisén, J., and Arner, P. (2008). Dynamics of fat cell turnover in humans. *Nature*, 453(7196):783–787.
- Su, S., Guntur, A. R., Nguyen, D. C., Fakory, S. S., Doucette, C. C., Leech, C., Lotana, H., Kelley, M., Kohli, J., Martino, J., Sims-Lucas, S., Liaw, L., Vary, C., Rosen, C. J., and Brown, A. C. (2018). A Renewable Source of Human Beige Adipocytes for Development of Therapies to Treat Metabolic Syndrome. *Cell Reports*, 25(11):3215–3228.
- Sugrue, M., De Waele, J. J., De Keulenaer, B. L., Roberts, D. J., and Malbrain, M. L. (2015). A user's guide to intra-abdominal pressure measurement. *Anestezjologia Intensywna Terapia*, 47(3):241–251.
- Suh, J. M., Gao, X., McKay, J., McKay, R., Salo, Z., and Graff, J. M. (2006). Hedgehog signaling plays a conserved role in inhibiting fat formation. *Cell Metabolism*, 3(1):25–34.
- Sun, Z., Gong, J., Wu, H., Xu, W., Wu, L., Xu, D., Gao, J., Wu, J.-w., Yang, H., Yang, M., and Li, P. (2013). Perilipin1 promotes unilocular lipid droplet formation through the activation of Fsp27 in adipocytes. *Nature Communications*, 4(1):1594.
- Sunshine, H. and Iruela-Arispe, M. L. (2017). Membrane lipids and cell signaling. *Current Opinion in Lipidology*, 28(5):408–413.
- Suzuki, M., Shinohara, Y., Ohsaki, Y., and Fujimoto, T. (2011). Lipid droplets: Size matters. *Journal of Electron Microscopy*, 60(SUPPL. 1):101–116.
- Sztalryd, C. and Brasaemle, D. L. (2017). The perilipin family of lipid droplet proteins: Gatekeepers of intracellular lipolysis. *Biochimica et Biophysica Acta (BBA) - Molecular and Cell Biology of Lipids*, 1862(10):1221–1232.
- Tanabe, Y. (2004). Inhibition of adipocyte differentiation by mechanical stretching through ERK-mediated downregulation of PPAR 2. *Journal of Cell Science*, 117(16):3605–3614.
- Tanabe, Y., Matsunaga, Y., Saito, M., and Nakayama, K. (2008). Involvement of Cyclooxygenase-2 in Synergistic Effect of Cyclic Stretching and Eicosapentaenoic Acid on Adipocyte Differentiation. *Journal of Pharmacological Sciences*, 106(3):478–484.
- Tanabe, Y. and Nakayama, K. (2004). Mechanical stretching inhibits adipocyte differentiation of 3T3-L1 cells: the molecular mechanism and pharmacological regulation. *Folia Pharmacologica Japonica*, 124(5):337–344.
- Tanimura, S. and Takeda, K. (2017). ERK signalling as a regulator of cell motility. *The Journal of Biochemistry*, 162(3):145–154.

- Teichert-Kuliszewska, K., Hamilton, B. S., Roncari, D. A., Kirkland, J. L., Gillon, W. S., Deitel, M., and Hollenberg, C. H. (1996). Increasing vimentin expression associated with differentiation of human and rat preadipocytes. *International journal of obesity and related metabolic disorders : journal of the International Association for the Study of Obesity*, 20 Suppl 3:108–13.
- Thiam, A. R. and Beller, M. (2017). The why, when and how of lipid droplet diversity. *Journal of Cell Science*, 130(2):315–324.
- Thompson, B. R., Lobo, S., and Bernlohr, D. A. (2010). Fatty acid flux in adipocytes: The in's and out's of fat cell lipid trafficking. *Molecular and Cellular Endocrinology*, 318(1-2):24–33.
- Tontonoz, P., Hu, E., Graves, R. A., Budavari, A. I., and Spiegelman, B. M. (1994). mPPAR $\gamma$ 2: Tissue-specific regulator of an adipocyte enhancer. *Genes and Development*, 8(10):1224–1234.
- Tordjman, J. (2013). Histology of Adipose Tissue. In *Physiology and Physiopathology of Adipose Tissue*, volume 9782817803, pages 67–75. Springer Paris, Paris.
- Trayhurn, P. (2013). Hypoxia and adipose tissue function and dysfunction in obesity. *Physiological Reviews*, 93(1):1–21.
- Trayhurn, P. and Beattie, J. H. (2008). Physiological role of adipose tissue: white adipose tissue as an endocrine and secretory organ. *Proceedings of the Nutrition Society*, 60(03):329–339.
- Trayhurn, P., Wang, B., and Wood, I. S. (2008). Hypoxia in adipose tissue: A basis for the dysregulation of tissue function in obesity? *British Journal of Nutrition*, 100(2):227–235.
- Uhler, C. and Shivashankar, G. V. (2017). Regulation of genome organization and gene expression by nuclear mechanotransduction. *Nature Reviews Molecular Cell Biology*, 18(12):717–727.
- Veilleux, A., Caron-Jobin, M., Noël, S., Laberge, P. Y., and Tchernof, A. (2011). Visceral adipocyte hypertrophy is associated with dyslipidemia independent of body composition and fat distribution in women. *Diabetes*, 60(5):1504–1511.
- Villena, J. A., Roy, S., Sarkadi-Nagy, E., Kim, K.-H. H., Hei, S. S., and Sul, H. S. (2004). Desnutrin, an adipocyte gene encoding a novel patatin domain-containing protein, is induced by fasting and glucocorticoids: Ectopic expression of desnutrin increases triglyceride hydrolysis. *Journal of Biological Chemistry*, 279(45):47066–47075.
- Vining, K. H. and Mooney, D. J. (2017). Mechanical forces direct stem cell behaviour in development and regeneration. *Nature Reviews Molecular Cell Biology*, 18(12):728–742.
- Wang, S., Idrissi, F. Z., Hermansson, M., Grippa, A., Ejsing, C. S., and Carvalho, P. (2018). Seipin and the membrane-shaping protein Pex30 cooperate in organelle budding from the endoplasmic reticulum. *Nature Communications*, 9(1).

- Wei, S., Zhang, L., Zhou, X., Du, M., Jiang, Z., Hausman, G. J., Bergen, W. G., Zan, L., and Dodson, M. V. (2013). Emerging roles of zinc finger proteins in regulating adipogenesis. *Cellular and Molecular Life Sciences*, 70(23):4569–4584.
- Weijers, R. N. M. (2015). Membrane flexibility, free fatty acids, and the onset of vascular and neurological lesions in type 2 diabetes. *Journal of Diabetes & Metabolic Disorders*, 15(1):13.
- Yamashita, Y., Hishinuma, M., and Shimada, M. (2009). Activation of PKA, p38 MAPK and ERK1/2 by gonadotropins in cumulus cells is critical for induction of EGF-like factor and TACE/ADAM17 gene expression during in vitro maturation of porcine COCs. *Journal of Ovarian Research*, 2(1):20.
- Yang, X., Lu, X., Lombès, M., Rha, G. B., Chi, Y. I., Guerin, T. M., Smart, E. J., and Liu, J. (2010). The G0/G1 Switch Gene 2 Regulates Adipose Lipolysis through Association with Adipose Triglyceride Lipase. *Cell Metabolism*, 11(3):194–205.
- Yeganeh, A., Stelmack, G. L., Fandrich, R. R., Halayko, A. J., Kardami, E., and Zahradka, P. (2012). Connexin 43 phosphorylation and degradation are required for adipogenesis. *Biochimica et Biophysica Acta (BBA) - Molecular Cell Research*, 1823(10):1731–1744.
- Young, D. A., Ibrahim, D. O., Hu, D., and Christman, K. L. (2011). Injectable hydrogel scaffold from decellularized human lipoaspirate. *Acta Biomaterialia*, 7(3):1040–1049.
- Zamora-Mendoza, R., Rosas-Vargas, H., Ramos-Cervantes, M. T., Garcia-Zuniga, P., Perez-Lorenzana, H., Mendoza-Lorenzo, P., Perez-Ortiz, A. C., Estrada-Mena, F. J., Miliar-Garcia, A., Lara-Padilla, E., Ceballos, G., Rodriguez, A., Villarreal, F., and Ramirez-Sanchez, I. (2018). Dysregulation of mitochondrial function and biogenesis modulators in adipose tissue of obese children. *International Journal of Obesity*, 42(4):618–624.
- Zechner, R., Zimmermann, R., Eichmann, T. O., Kohlwein, S. D., Haemmerle, G., Lass, A., and Madeo, F. (2012). FAT SIGNALS - Lipases and Lipolysis in Lipid Metabolism and Signaling. *Cell Metabolism*, 15(3):279–291.
- Zhang, Y., Xie, L., Gunasekar, S. K., Tong, D., Mishra, A., Gibson, W. J., Wang, C., Fidler, T., Marthaler, B., Klingelhutz, A., Abel, E. D., Samuel, I., Smith, J. K., Cao, L., and Sah, R. (2017). SWELL1 is a regulator of adipocyte size, insulin signalling and glucose homeostasis. *Nature Cell Biology*, 19(5):504–517.
- Zimmermann, R. (2004). Fat Mobilization in Adipose Tissue Is Promoted by Adipose Triglyceride Lipase. *Science*, 306(5700):1383–1386.

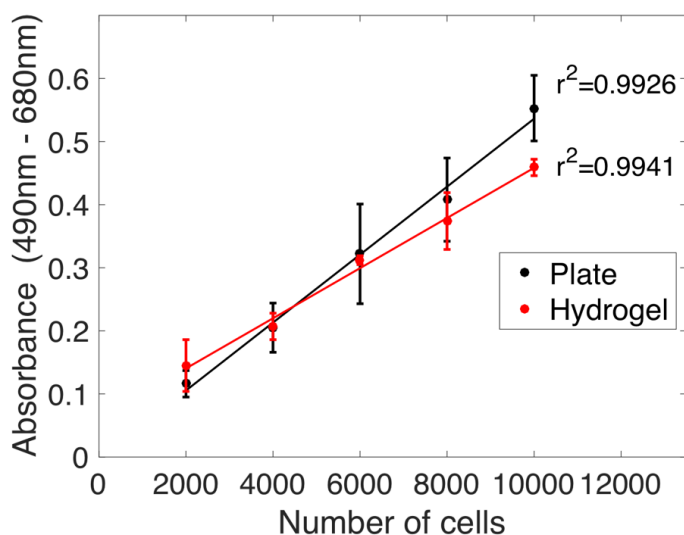


## **Chapter 7**

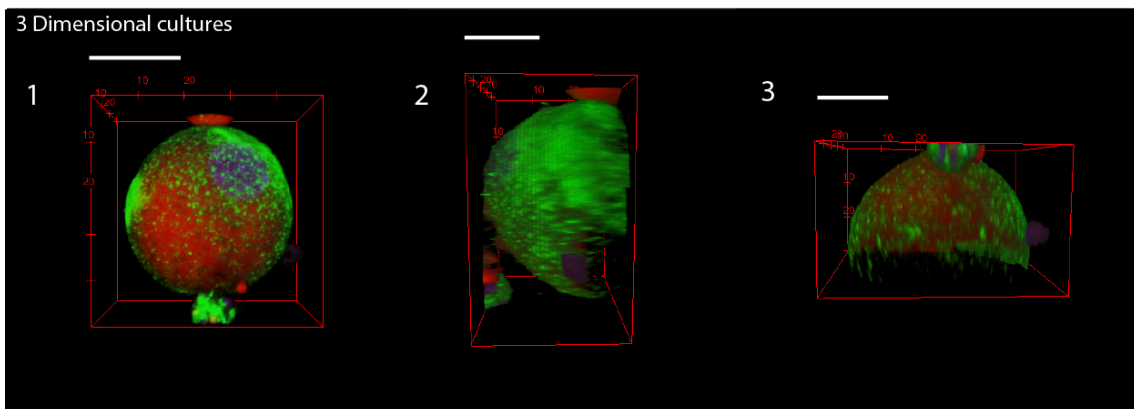
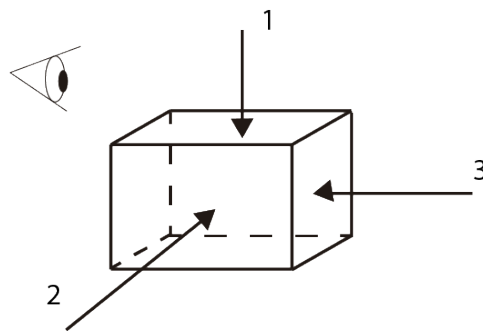
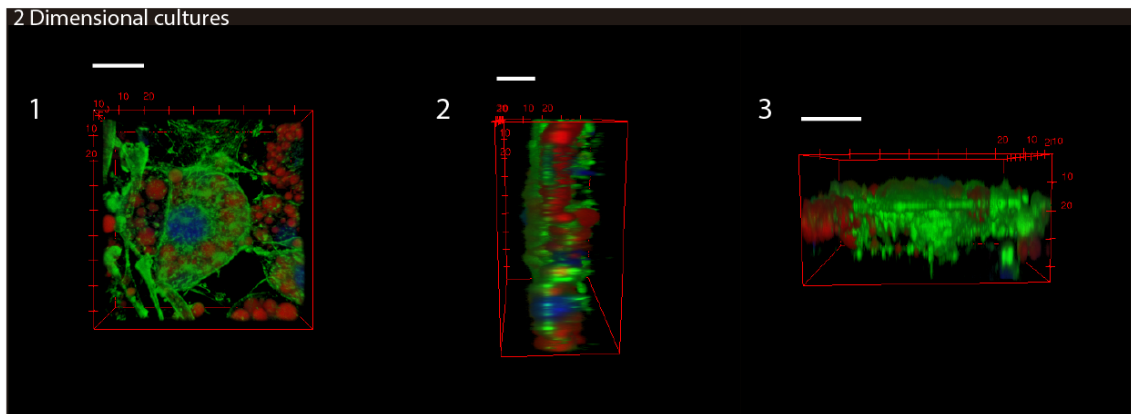
### **Supplementary Information**

## 7.1 Supplementary Information Chapter 2

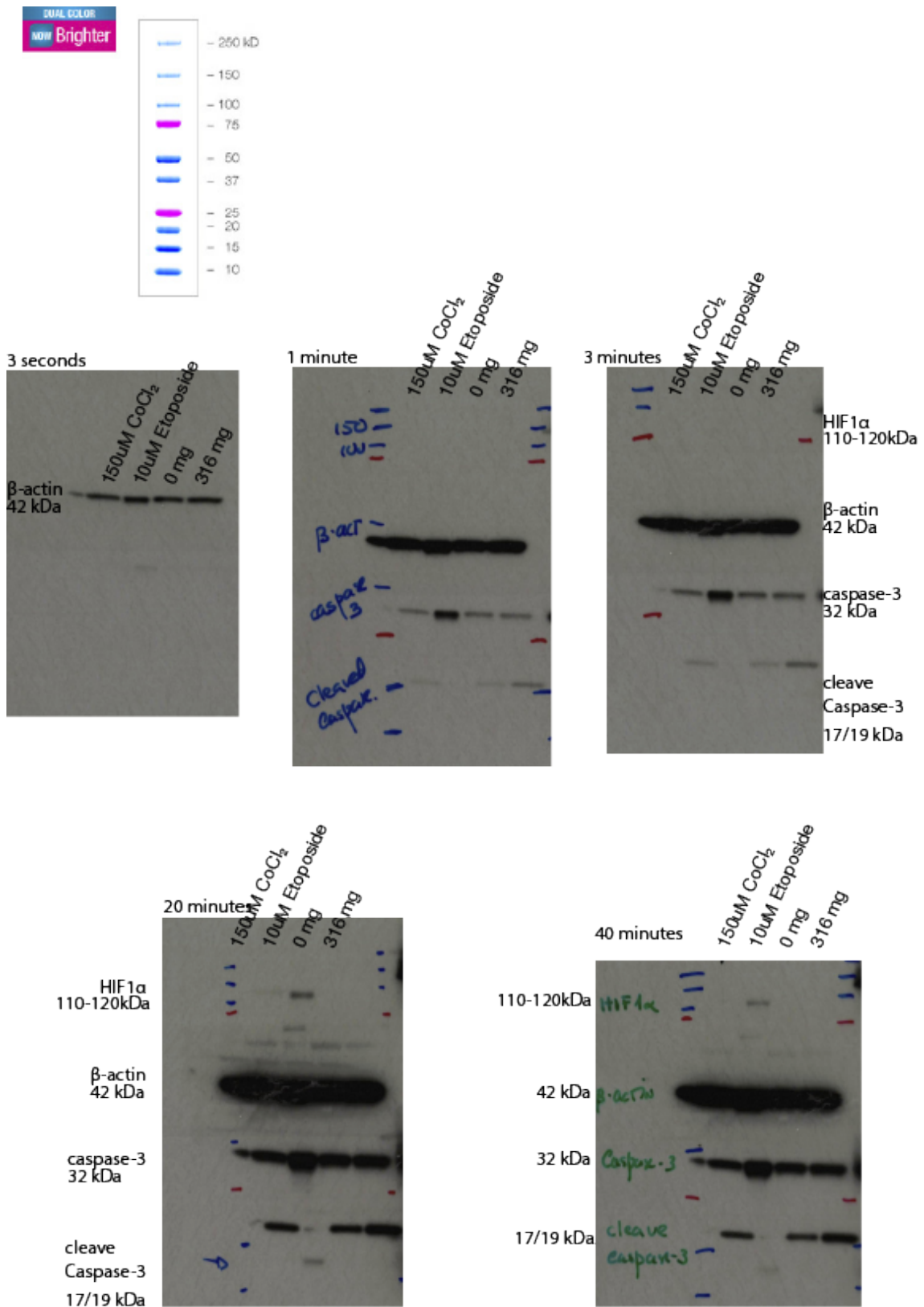
We obtained the standard curves for cells cultures in plate and cells cultures within the hydrogel. In hydrogel, the media volume is higher than in the two dimensional cultures. Therefore, the protocol described in the chapter 2 had to be validated in both conditions. For both cultures were seeded with six different cell concentrations (corresponding to 2000, 4000, 6000, 8000, 10000 and 12000 cells per plate and hydrogel) and left overnight for cell attachment. For each concentration either in plate or in hydrogel six technical replicates were performed. Next day, for each concentration in both cultures, three replicates received pure water (controls) whereas the other three replicates received the lysis buffer (corresponding to the maximum release of LDH). **Figure S1** shows the standard curves for the corresponding cultures.



Supplementary Figure S1: **LDH standard curve for 2D and 3D cultures.** For each concentration, three technical replicates were performed.

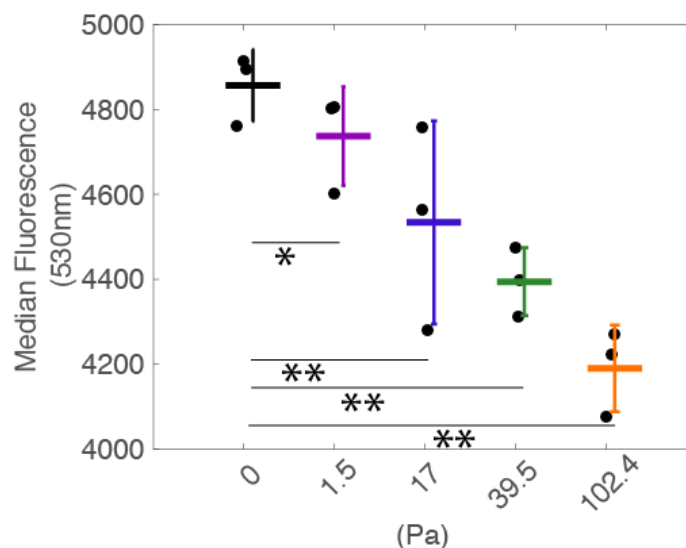


Supplementary Figure S2: **3D projections of adipocytes at day 8 in both 2D and 3D cultures.** At this resolution, it was not possible to acquire the entire cell in the 3D culture. Scale bar correspond to  $20\mu\text{m}$ .

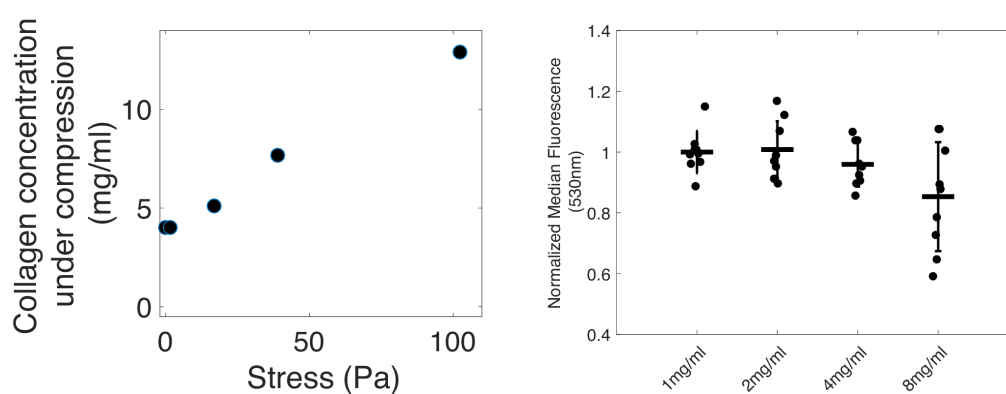


Supplementary Figure S3: Full-length Western blot figures.

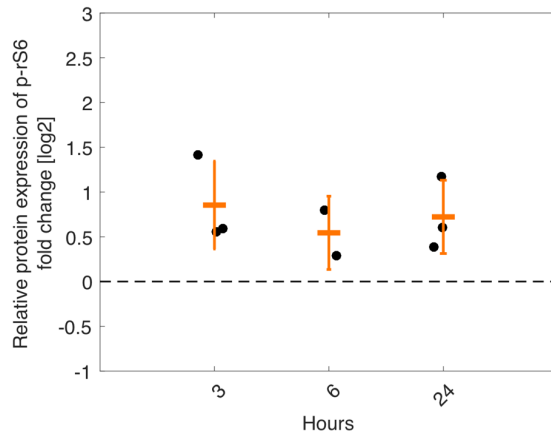
## 7.2 Supplementary Information Chapter 3



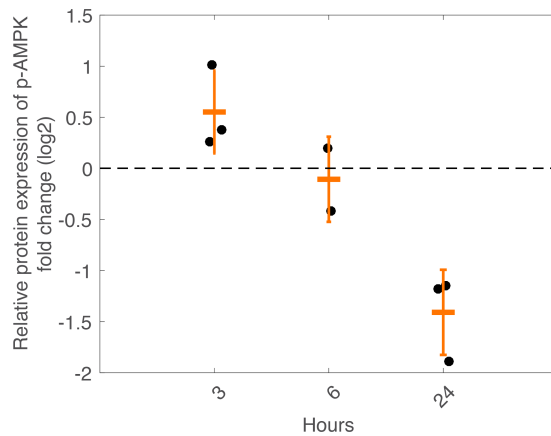
Supplementary Figure S4: **Lipid accumulation is affected by static mechanical compression - 2nd data set.** A two sample Kolmogorov-Smirnov test was used to analyse significant differences: \* $p < 0.01$  and \*\* $p < 0.001$ .



Supplementary Figure S5: **Effects of collagen concentration on lipid accumulation.** (Left) Predicted collagen concentration in the ROI after compression. (Right) 3T3-L1 pre-adipocytes were cultured in the different collagen concentrations hydrogels for 12 days. Lipid content was measured by flow cytometry.



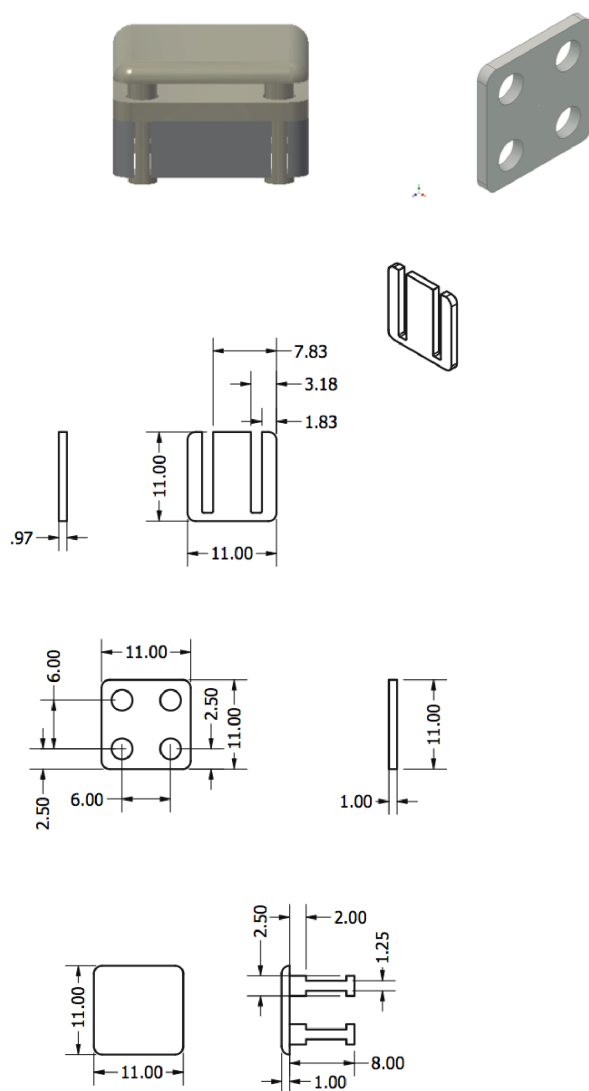
Supplementary Figure S6: **Overtime protein expression of phosphorylated ribosomal S6 in loaded samples.** Phospho-rS6 protein levels were normalised to vinculin.



Supplementary Figure S7: **Overtime protein expression of phospho-AMPK in loaded samples.** phospho-AMPK protein levels were normalised to vinculin.

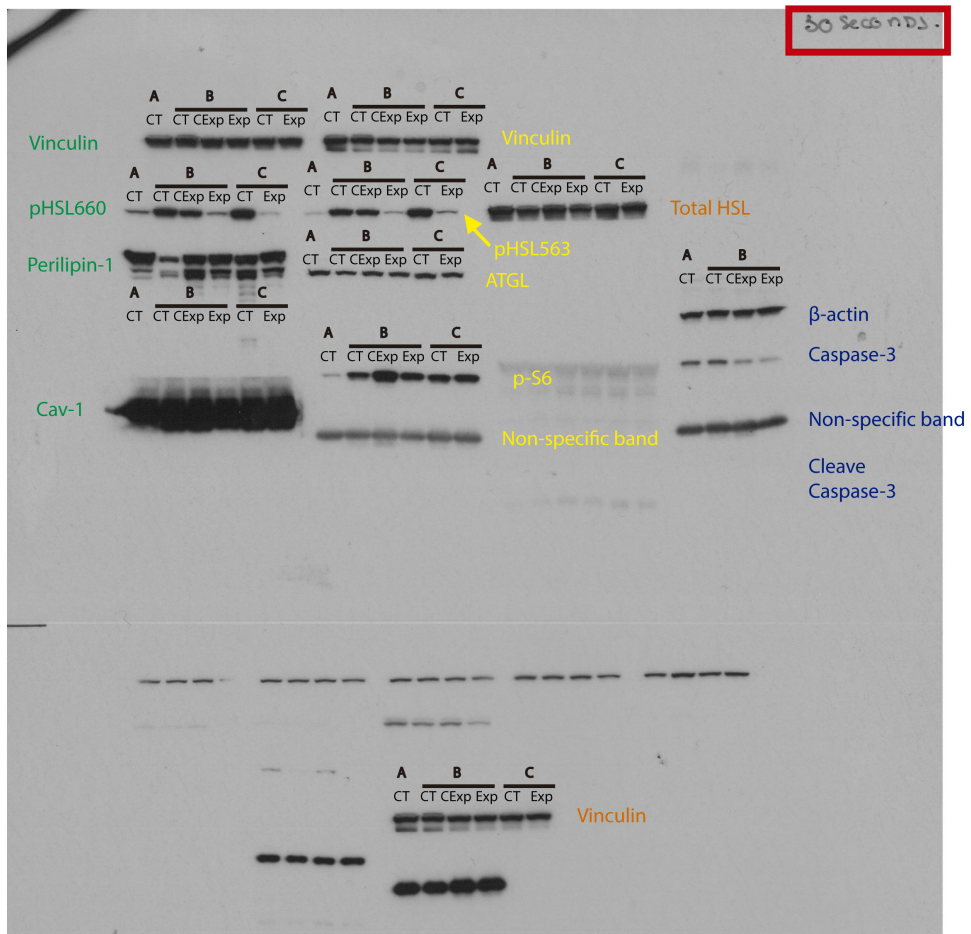
For all western blots see appendix B.

## 7.3 Supplementary Information Chapter 4



Supplementary Figure S8: **Compression device drawings.**

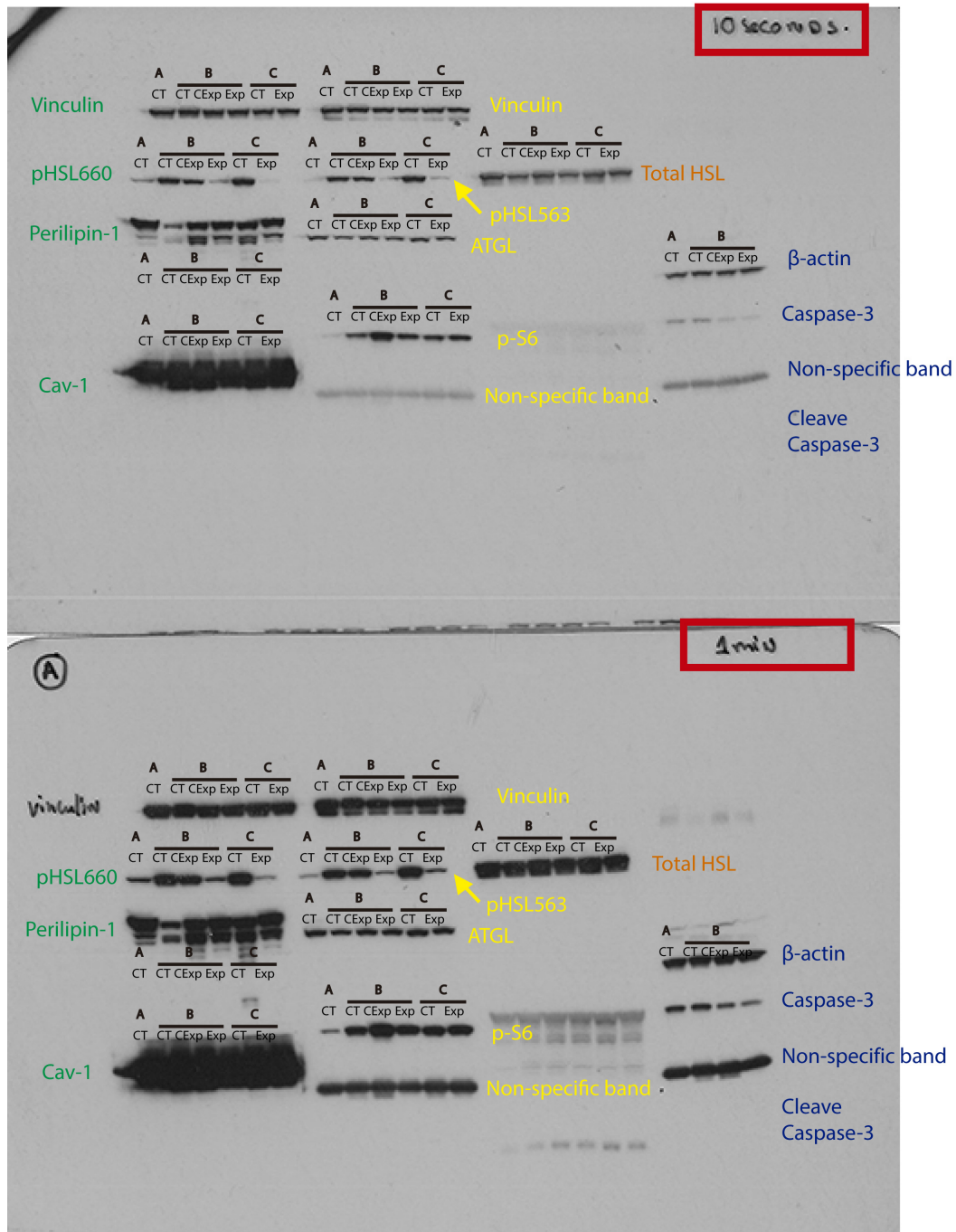
Each colour corresponds to the same panel/lane.  
This means that each protein has its corresponding loading control.



Supplementary Figure S9: **Full-length Western blot figures, 30 seconds.**

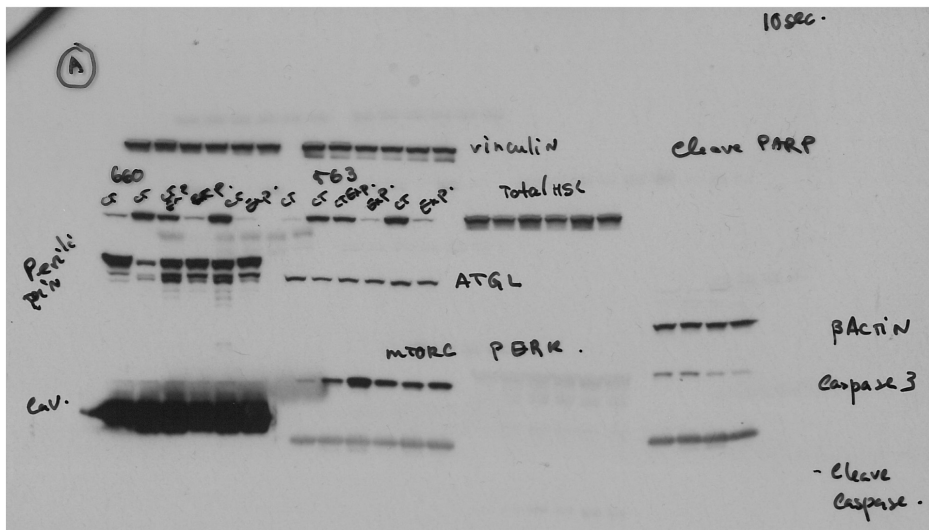
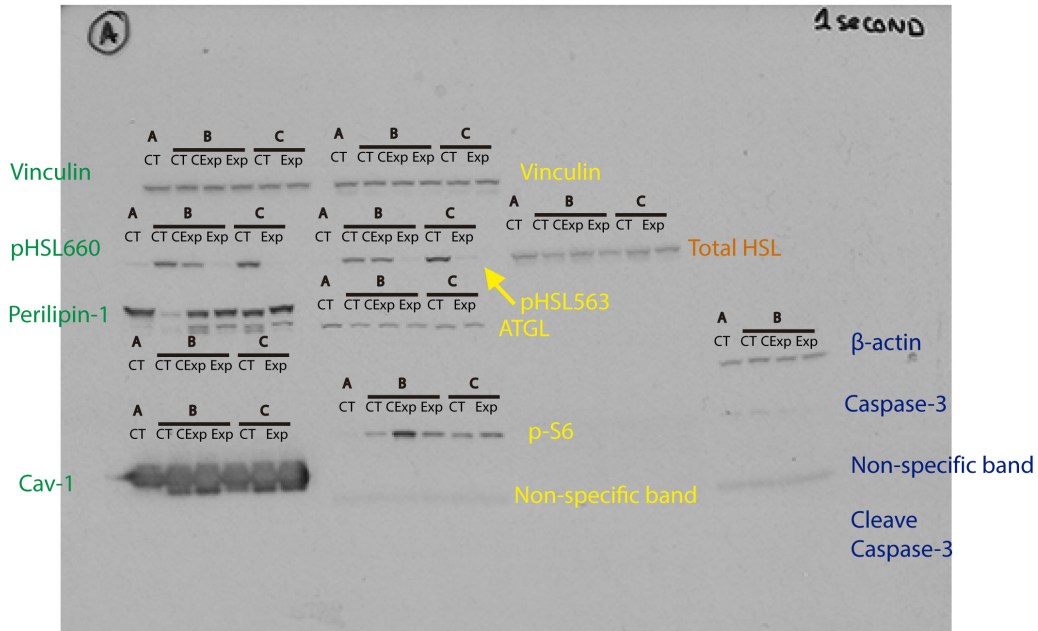


Each colour corresponds to the same panel/lane.  
 This means that each protein has its corresponding loading control.



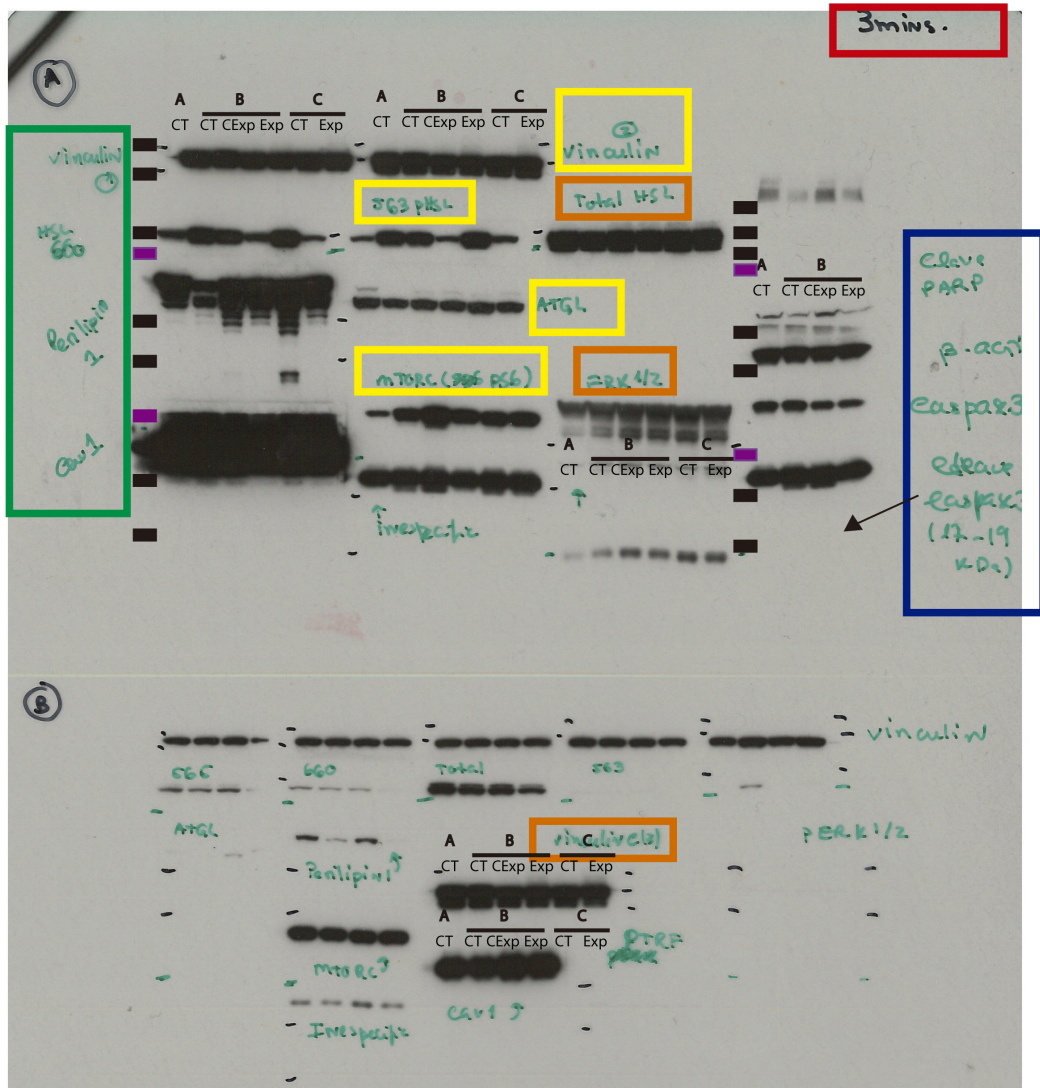
Supplementary Figure S10: Full-length Western blot figures, 10 seconds and 1 minute.

Each colour corresponds to the same panel/lane.  
 This means that each protein has its corresponding loading control.



Supplementary Figure S11: Full-length Western blot figures, 1 and 10 seconds.

Each colour corresponds to the same panel/lane.  
 This means that each protein has its corresponding loading control.



Supplementary Figure S12: Full-length Western blot figures, 3 minutes.



# **Appendix A**

## **Finite Element Model**

## Introduction

In this appendix, we present a computational model which we developed to understand the stress and strain distributions underneath the load. Our aim was to evaluate whether the cells located in the region of interest (ROI) were experiencing approximately similar stress/strain. To achieve this aim, a finite element analysis was performed.

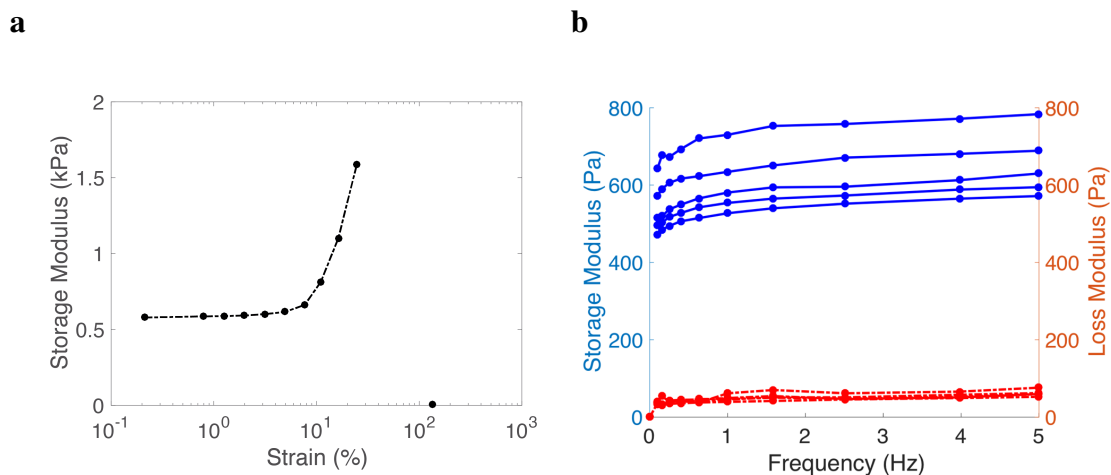
Computational modelling of collagen hydrogels is a field in current development. Characterisation of collagen hydrogels is challenging because of their complex viscoelastic properties [Castro et al., 2016, 2018]. These properties depend on many experimental parameters such as collagen concentration, crosslinking properties, fiber orientation and magnitude of mechanical stimulation [Castro et al., 2016, 2018].

In this appendix, we first performed rheological experiments on the collagen hydrogels at different concentrations to get an insight about their mechanical properties. We then used these results to perform a finite element analysis. A linear-elastic model was used to get an approximation of the stresses and strains present in our compression experiments. Because this preliminary analysis assumes a linearly elastic material, which is not appropriate for collagen gels, the results obtained from this analysis are incomplete. For this reason this section was placed in appendix. For more accurate predictions, more complex models are necessary, however such models are beyond the scope of this work.

### A.1 Rheological experiments

Mechanical measurements of collagen gels were performed in the hydrated state. Shear viscoelastic properties of the 1,2 and 4 mg/ml collagen type I hydrogels were analysed using a rheometer (AR 2000; TA Instruments) comprised of cone-plate geometry with a 40mm diameter and 2° cone angle and Rheology Advantage software (TA Instruments). Fresh collagen hydrogels were polymerised *in situ* to avoid contact problems between the hydrogel and

the cone. Briefly, 1 ml of cold neutralised collagen solution was placed on the pre-cooled bottom plate at 5°C and subsequently the cone was moved down to contact the solution. Polymerisation was induced by bringing up the temperature to 37°C for 20 minutes. Measurements were then performed at 25°C, and a few drops of 1x phosphate buffered saline solution (PBS) were used on the sides of the cone plate to hydrate the gels. A trap jacket was also used to prevent dehydration during the measurements. We performed a strain sweep with strains ranging from 0.2 to 25% at a frequency of 1 Hz. This showed that 1% strain is located in the linear elastic region (**Fig.A.1a**). We measured the storage and loss modulus ( $G'$  and  $G''$ , respectively) using a frequency sweep from 0.5 to 5 Hz at 1% strain. The  $G'$  was measured at 1 Hz for each sample. The Young's modulus can be calculated as  $E=3G'$  (see below), assuming incompressibility. The final Young's modulus value is a mean of the 3 to 5 samples measured for each concentration in two different batches of extracted collagen type I. The Young's modulus of 4mg/ml collagen hydrogels was used for the finite element simulations.



Supplementary Figure A.1: **Strain and frequency sweep for the collagen type I hydrogel.** (a) Viscoelastic storage modulus for 4mg/ml hydrogel in function of strain at a frequency of 1 Hz. (b) Viscoelastic storage and loss modulus for 4mg/ml hydrogel in function of frequency at a strain of 1%.

From **Fig.A.1b**, we observed that the storage modulus ( $G'$ ) is larger than the loss modulus ( $G''$ ). This implies that the elastic component of the material is more prominent than the

viscous component. To a first approximation, we therefore considered the hydrogel as a linear elastic material. In such a material, the stiffness is characterised by the Young's modulus ( $E$ ), which is given by the relation of stress ( $\sigma$ ) to strain ( $\epsilon$ ) for a deformation along one axis:

$$E = \frac{\sigma}{\epsilon} \quad (\text{A.1})$$

The shear modulus ( $G$ ) is defined by the relation of shear stress to shear strain, and the bulk modulus ( $K$ ) by the relation between pressure and volume change. The Young's modulus can also be expressed in function of shear and bulk modulus:

$$E = \frac{9G}{3 + \frac{G}{K}} \quad (\text{A.2})$$

For incompressible materials the bulk modulus becomes much larger than the shear modulus,  $K \gg G$ . In this case, we can approximate  $\frac{G}{K} \approx 0$ . Hydrogels are mainly composed by water and therefore we can assume incompressibility as a first approximation. In this case equation A.2 becomes:

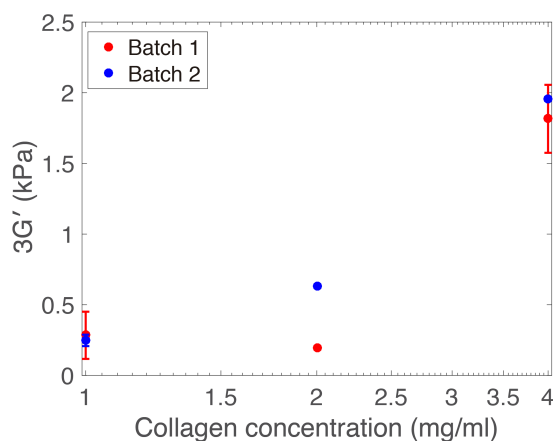
$$E = 3G \quad (\text{A.3})$$

The storage modulus ( $G'$ ) from our rheology experiment (**Fig.A.1**) is a dynamic modulus, which means it relates the stress to the strain under an oscillatory deformation. Therefore, it can be calculated by:

$$G' = \frac{\sigma_0}{\epsilon_0} \cos \delta \quad (\text{A.4})$$

Here,  $\sigma_0$  is the amplitude of the stress,  $\epsilon_0$  is the amplitude of the strain and  $\delta$  is the phase lag between the stress and the strain. For a perfectly elastic material  $\delta = 0$  and therefore  $G' = G$ . Using this approximation and equation A.3, we calculated the Young's modulus for the hydrogels with different collagen concentrations. As expected, we observed an increased Young's modulus with an increase of collagen concentration (**Fig.A.2**). The calculated Young's modulus for 4 mg/ml hydrogels was 1.8 kPa.





Supplementary Figure A.2: **Storage modulus in function of collagen concentration.** Three times the storage modulus (used to approximate the Young's modulus) for 1, 2 and 4mg/ml collagen hydrogels.

## A.2 Finite element analysis

The finite element method (FEM) is a numerical technique where a body is approximated as a collection of smaller components (the elements). In this way, a structure analysis is simplified by considering only forces propagating between the elements. The analysis becomes more accurate when the elements are smaller, but the computational cost becomes higher. The way in which the body is divided into the elements is called meshing, and a good mesh size is usually determined by reducing the size until the solution is converged. In this work, finite elements simulations were performed in Ansys Mechanical APDL version 17.0.

Hydrogels were casted into cylindrical wells and therefore, we used an axisymmetric analysis. As discussed in the previous section, the collagen type I hydrogel was modeled as linear elastic material. The parameters used were corresponding to 4mg/ml hydrogels at 1 Hz frequency of strain (see previous section), given by  $E = 1.82\text{kPa}$ . Following the literature, we used a Poisson ratio of 0.43, which corresponded to 4mg/ml randomly oriented collagen type I hydrogel [Lee et al., 2014].

The dimensions of the cylindrical culture insert were 6mm radius ( $r$ ) and we used a volume ( $V$ ) of 270 $\mu$ l. Following these details we found a height ( $h$ ) of 2.39mm using:

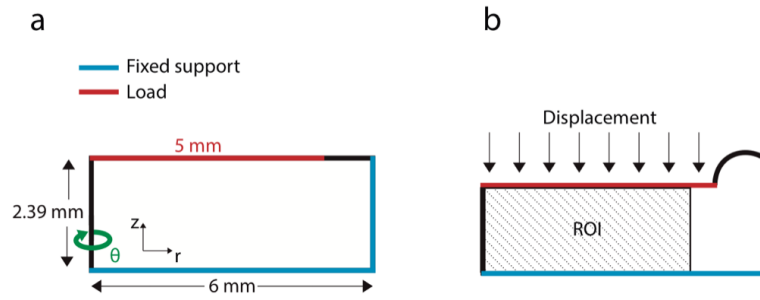
$$h = \frac{V}{\pi \cdot r^2} \quad (\text{A.5})$$

A circular loading area with radius of 5mm, corresponding to the weight, was defined on the top of the hydrogel (**Fig.A.3a**, red). The boundaries were simulated as fixed support (**Fig.A.3a**, blue). The load causes an indentation of the hydrogel (**Fig.A.3b**), therefore we simulate the effect of load as an indentation. We did not simulate the load as a force since analytical calculations showed a non-uniform stress distribution underneath the load. In short, following Barber [2010], we considered an indentation caused by a flat cylindrical punch. At the boundary of the punch, the solution of this problem can be written in terms of a potential function  $\phi$  and its derivative

$$\frac{\partial \phi}{\partial z} = -\frac{Eu_0}{\pi(1+\nu)(1-\nu)} \mathcal{I} [\ln(r^2 + (z+ia)^2 + z+ia)] \quad (\text{A.6})$$

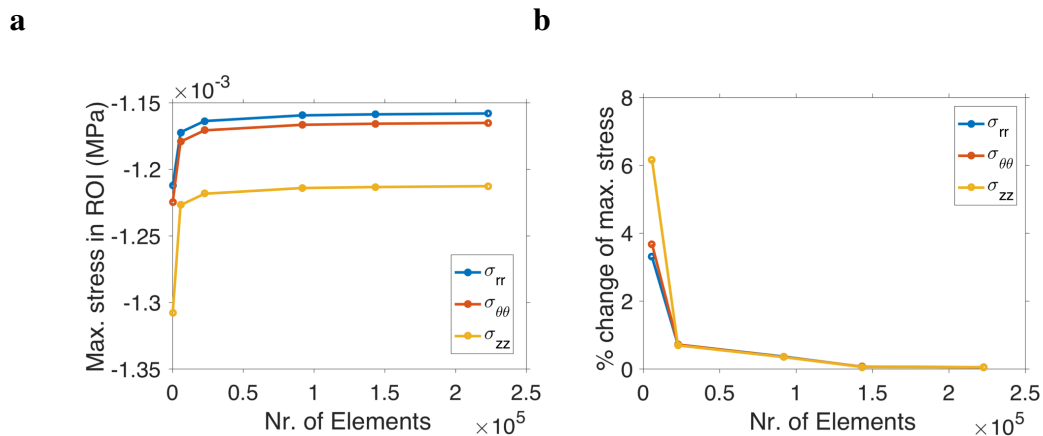
where  $E$  is the Young's modulus,  $\nu$  is the Poisson ratio,  $u_0$  is the displacement,  $\mathcal{I}$  denotes the imaginary part,  $a$  is the punch radius and  $i$  is the imaginary unit. The stress components were solved using the Mathematica software. For example, the normal stress component  $\sigma_{zz} = z\partial^3\phi/\partial z^3 - \partial^2\phi/\partial z^2$ , resulting in

$$\sigma_{zz}(0 \leq r < a, z = 0) = \frac{Eu_0}{\pi(1+\nu)(1-\nu)\sqrt{a^2 - r^2}} \quad (\text{A.7})$$



Supplementary Figure A.3: **Cross section of the simulated hydrogel.** (a) Due to cylindrical symmetry we performed an axisymmetric finite element simulation. The cross section of the hydrogel has dimensions 6mm x 2.39mm (black). The left edge corresponds to the axis of symmetry (green). The load has a radius of 5mm (red). The boundaries of the culture insert were simulated as fixed support (blue). (b) Simulation of the displacement. The region of the interest corresponds to the radius of 4mm (shaded).

We computed the mesh convergence of the finite element model using a displacement of 0.0238 mm (1%). To test the convergence, we used different grid sizes and plotted the maximum of all normal stress components in the region of interest (Fig.A.4a). We observed convergence for the smallest grid size (0.08mm, i.e. largest number of elements), which was confirmed by a percentage change in the maximum stresses approaching zero (Fig.A.4b).



Supplementary Figure A.4: **Mesh convergence.** (a) Maximum of normal stress components (zz, rr,  $\theta\theta$ ) in function of number of elements. (b) Percentage change of the maximum stress for increasing number of elements. The values are converged for the largest number of elements, corresponding to a grid size of 0.008mm.

In order to understand which displacements correspond to our loads, we calculated the force

( $F$ ) in relation to the displacement. To achieve this we integrated the stress components acting along the  $z$ -dimension underneath the load. This results in the following equation:

$$F = 2\pi \int_0^R (\sigma_{zz}(r) + \sigma_{rz}(r)) \cdot r \cdot dr \quad (\text{A.8})$$

where  $R = 5\text{mm}$ .

The contribution of the shear component  $\sigma_{rz}$  is negligible compared to the normal component  $\sigma_{zz}$  in our case (10 orders of magnitude smaller), and therefore  $F$  will be mainly dependent on the latter. To implement equation A.8, we discretised the integral according to the mesh nodes. The discrete version is given by:

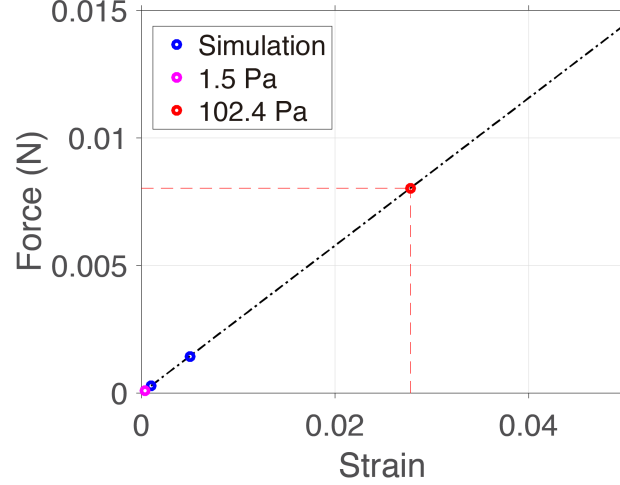
$$F = 2\pi \sum_i \sigma_{zz}^i \cdot r_i \cdot \Delta r \quad (\text{A.9})$$

Where the sum goes over all nodes under the load (corresponding to the red edge in **Fig.A.3a**),  $\sigma_{zz}^i$  denotes the stress on the  $i$ th node,  $r_i$  is the radius of the  $i$ th node and  $\Delta r$  is the radius step between two nodes. We validated this calculation by simulating a force instead of a displacement, and confirming that the calculated force was equal to the applied force.

In the case of a linear elastic material, the relationship between force and strain is linear. Therefore, we simulated two displacements and calculated this relation:

$$F = a \cdot \epsilon \quad (\text{A.10})$$

Where  $\epsilon$  is the strain and  $a$  is the slope of the linear relation. We found  $a = 0.289\text{ N}$ . We now calculate the displacements for the used loads corresponding to 1.5 Pa and 102.4 Pa stress, using the buoyancy forces calculated in **Fig. 2.3**. From equation A.10 we found a strain of 0.00034 for 1.5 Pa and 0.0278 for 102.4 Pa (**Fig.A.5**).



Supplementary Figure A.5: **Relation between force and displacement.** Blue dots correspond to the simulated displacements (0.001 and 0.005). The black line corresponds to the linear relation between the force and the displacement. The magenta and red dots correspond to the displacements caused by the 1.5 Pa and 102.4 Pa stress, respectively.

We can now use the calculated displacements to simulate the stress and strain distributions in the hydrogel. More precisely, we are interested in the mean and variance of the stress and strain in the ROI. To calculate the mean, we integrate the stress or the strain component over the whole volume corresponding to the ROI and subsequently divided by the volume:

$$\mu = \frac{2\pi \int_0^Z \int_0^R \xi(r, z) \cdot r \cdot dr \cdot dz}{\pi \cdot R^2 \cdot Z} \quad (\text{A.11})$$

where  $\xi(r, z)$  is either a component of the stress tensor or component of strain,  $R = 4\text{mm}$  (corresponding to ROI) and  $Z = 2.39\text{mm}$ . Similar to equation A.9, we discretised the integrals in equation A.11:

$$\mu = \frac{2\pi \sum_i \sum_j \xi_{ij} \cdot r_j \cdot \Delta r \cdot \Delta z}{\pi \cdot R^2 \cdot Z} \quad (\text{A.12})$$

Here, each node in the mesh is represented by two indices  $i$  and  $j$ , where  $i$  represents the  $z$ -dimension and  $j$  represents the  $r$ -dimension. Furthermore,  $\xi_{ij}$  corresponds to the stress or strain in that particular node,  $r_j$  the value of the radius of the node, and  $\Delta r$  and  $\Delta z$  corresponds to the step in  $r$  and  $z$  in the mesh.

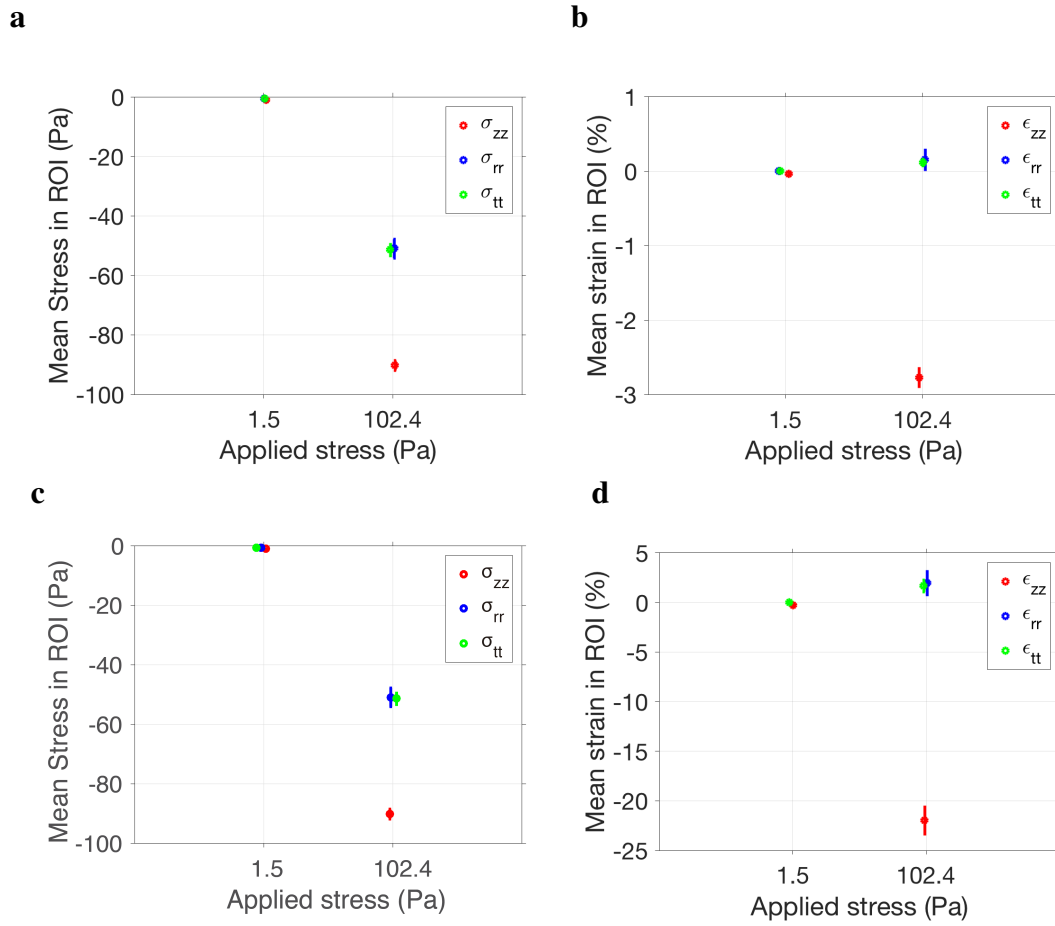
Similarly, we calculated the variance by:

$$V = \frac{\int_0^Z \int_0^R (\xi(r, z) - \mu)^2 2\pi \cdot r \cdot dr \cdot dz}{\pi \cdot R^2 \cdot Z} \quad (\text{A.13})$$

The corresponding discrete version of the previous equation is:

$$V = \frac{\sum_i \sum_j (\xi_{ij} - \mu)^2 2\pi \cdot r_j \cdot \Delta r \cdot \Delta z}{\pi \cdot R^2 \cdot Z} \quad (\text{A.14})$$

From equation A.12 and A.14, we could evaluate the stress and strain distributions in the whole region of interest as well as quantify the stress variance within the ROI (**Figs. A.6 and A.7**). As expected, from **Fig. A.6** it is possible to observe that the normal stress components increase with the load. For the load corresponding to 1.5 Pa stress, all the stresses and strains are nearly zero and very uniform in the ROI (**Fig. A.7a and b**). For the load corresponding to 102.4 Pa, the stress distributions of  $\sigma_{rr}$  and  $\sigma_{\theta\theta}$  are similar, whereas for  $\sigma_{zz}$  the values of stress are nearly double. For the strains,  $\epsilon_{rr}$  and  $\epsilon_{\theta\theta}$  are close to zero, while  $\epsilon_{zz}$  presents a higher strain. This is in qualitative agreement with our results for the cell deformations under compression.



Supplementary Figure A.6: **Mean stress and strain in the ROI for a Young's modulus 1.8 kPa (top) and 122.5 Pa (bottom).** (a,c) Mean stress for the different normal components of the stress tensor. (b,d) Mean strain along the three axes. The error bars denote one standard deviation. Standard deviations were calculated from the square root of the variance (equation A.14).

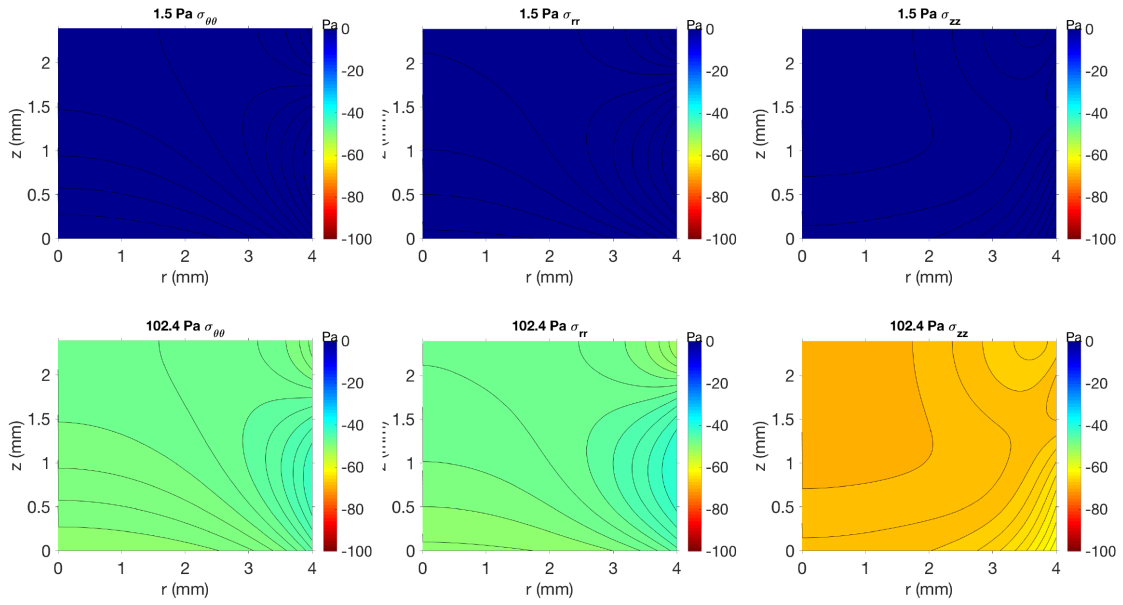
The obtained strains are much smaller (**Fig. A.6**) compared to our empirically measured strains of the hydrogel (**Fig. 2.9**). Since we compressed during 24 hours, we can observe from **Fig. A.1b** that our calculated value for the Young's modulus at 1Hz is likely an overestimation. We can consider 24 hours as a frequency of (1/86400) Hz. For such small values, our data from the frequency sweep suggests substantially lower values for the storage modulus. It has indeed been reported that short-time strains of collagen hydrogels can give rise to much higher moduli compared to long-time strains [Knapp et al., 2002]. We therefore made additional simulations, where we approximated the Young's modulus by calculating

the slope of the linear fit to our stress-strain data in **Fig. 2.9**. In this way, we find a Young's modulus of 122.5 Pa and the obtained strains are in the same order of magnitude as the experimentally measured strains. The resulting distributions for stress and strain remain close to uniform in the ROI (**Fig. A.6c and d**).

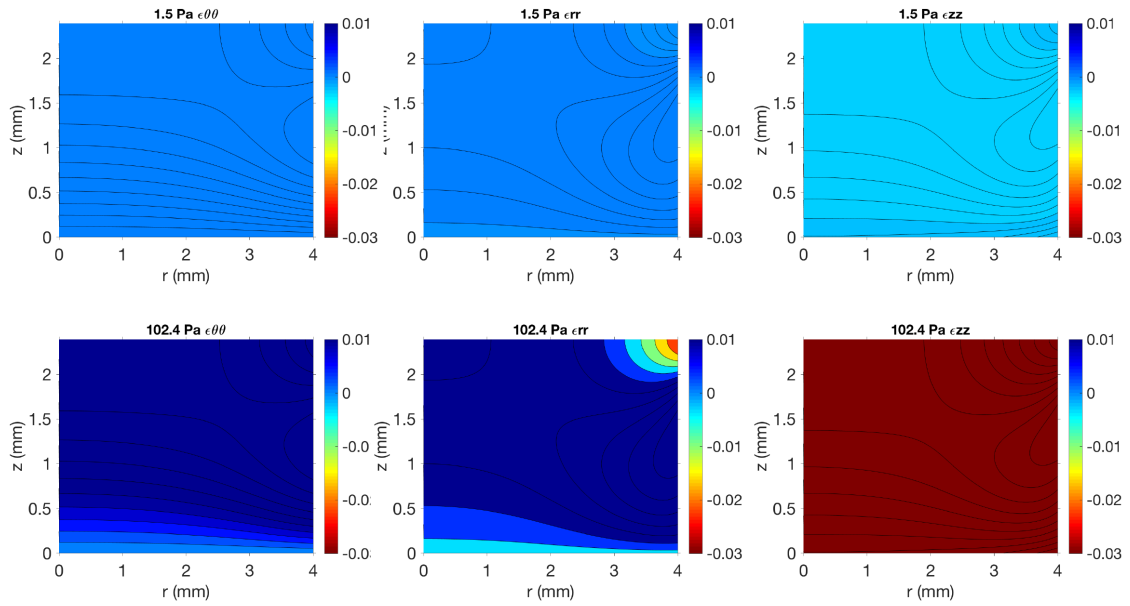
In summary, these results give us an insight that the cells in the ROI experience similar stresses and strains. Moreover, the strain results qualitatively agree with the results from the cell deformations measured by microscopy. However, this model has several limitations. We approximated the hydrogel as a linear elastic material, and used the parameters obtained at 1 Hz frequency of strain. Since we compress during 24 hours, these parameters result in much lower strains compared to our measurements (**Fig. 2.9**). Indeed, when approximating the Young's modulus from **Fig. 2.9**, we obtain strains closer to our measured values. It would be interesting future work to explore these distributions in more complex viscoelastic models.



a



b

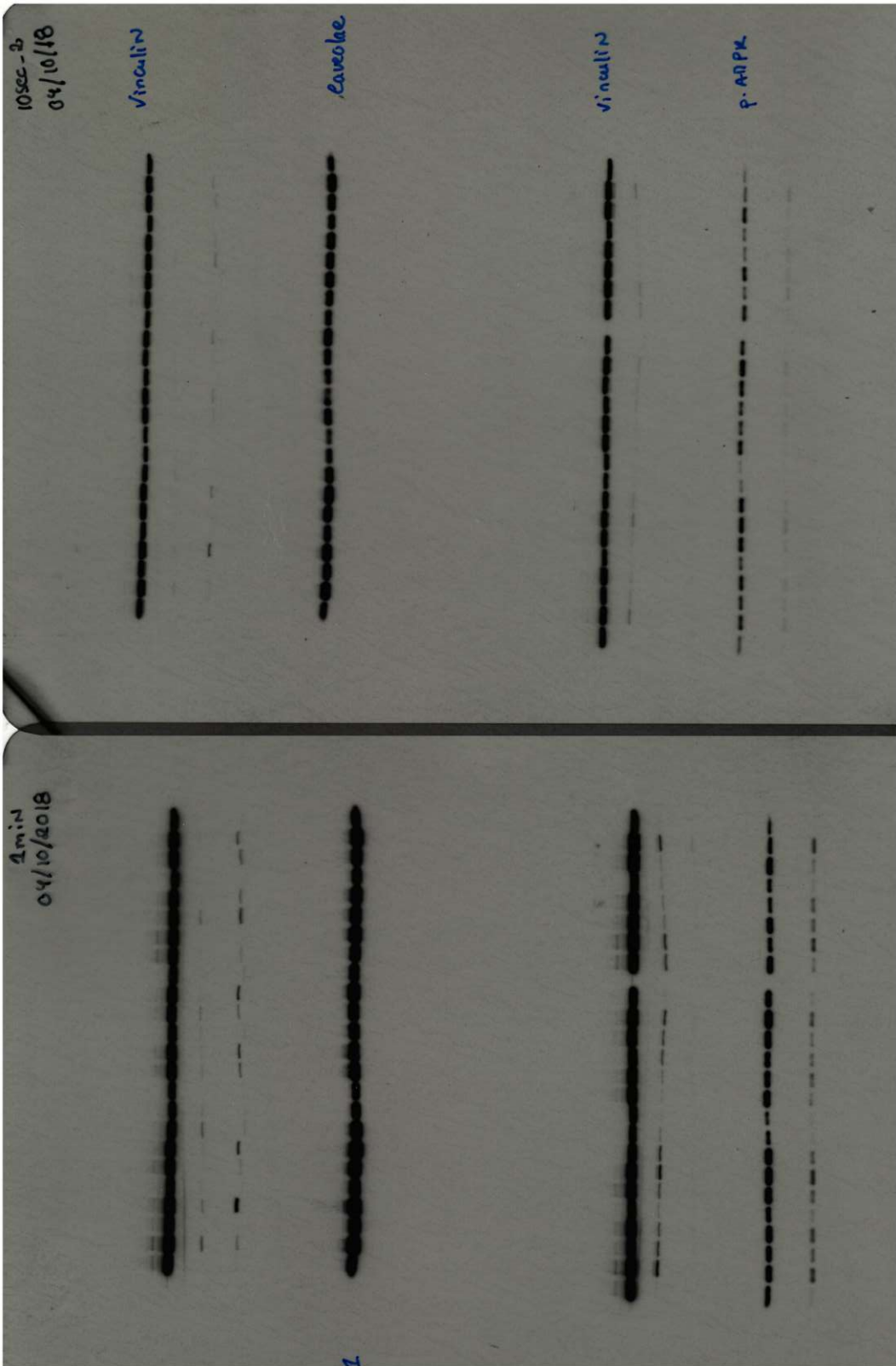


Supplementary Figure A.7: **Stress and strain distributions in the ROI for Young's modulus 1.8 kPa.** (a) Stress distributions under 1.5 Pa and 102.4 Pa compression. (b) Strain distributions under 1.5 Pa and 102.4 Pa compression.

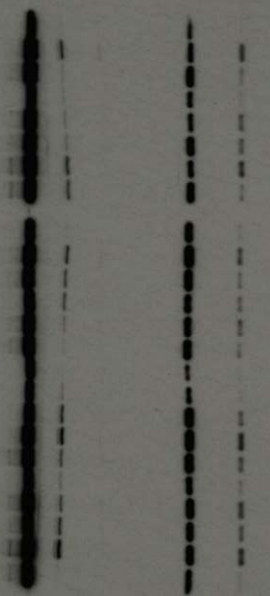
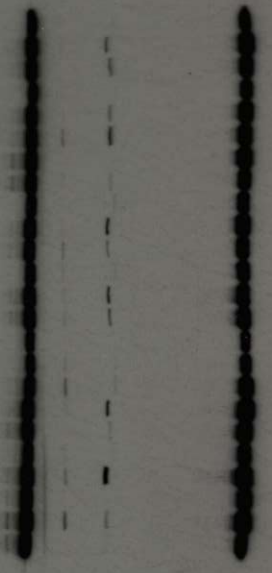


# **Appendix B**

## **Western-blot chapter 3**



4min  
04/10/2018

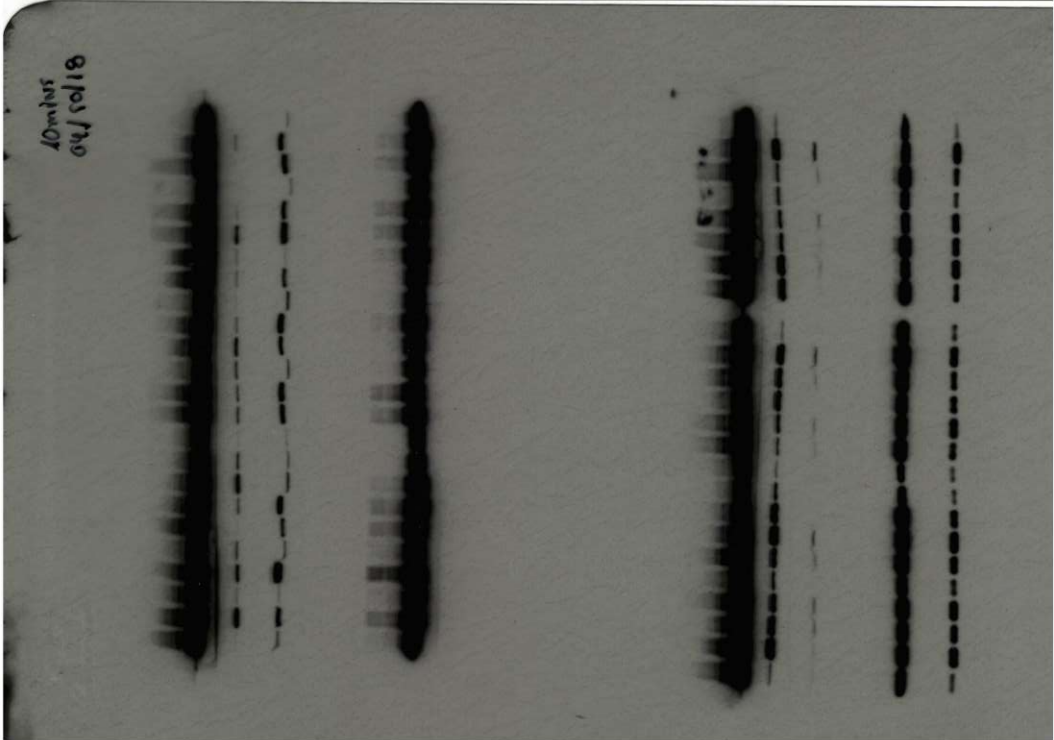
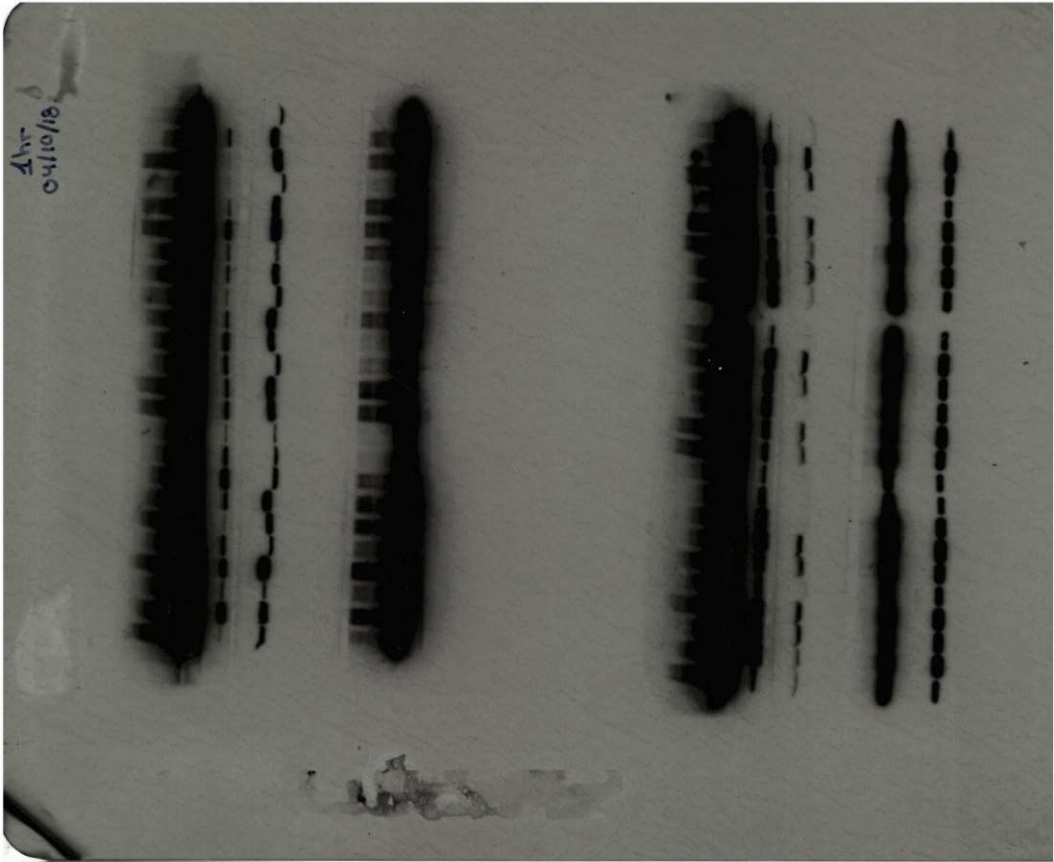


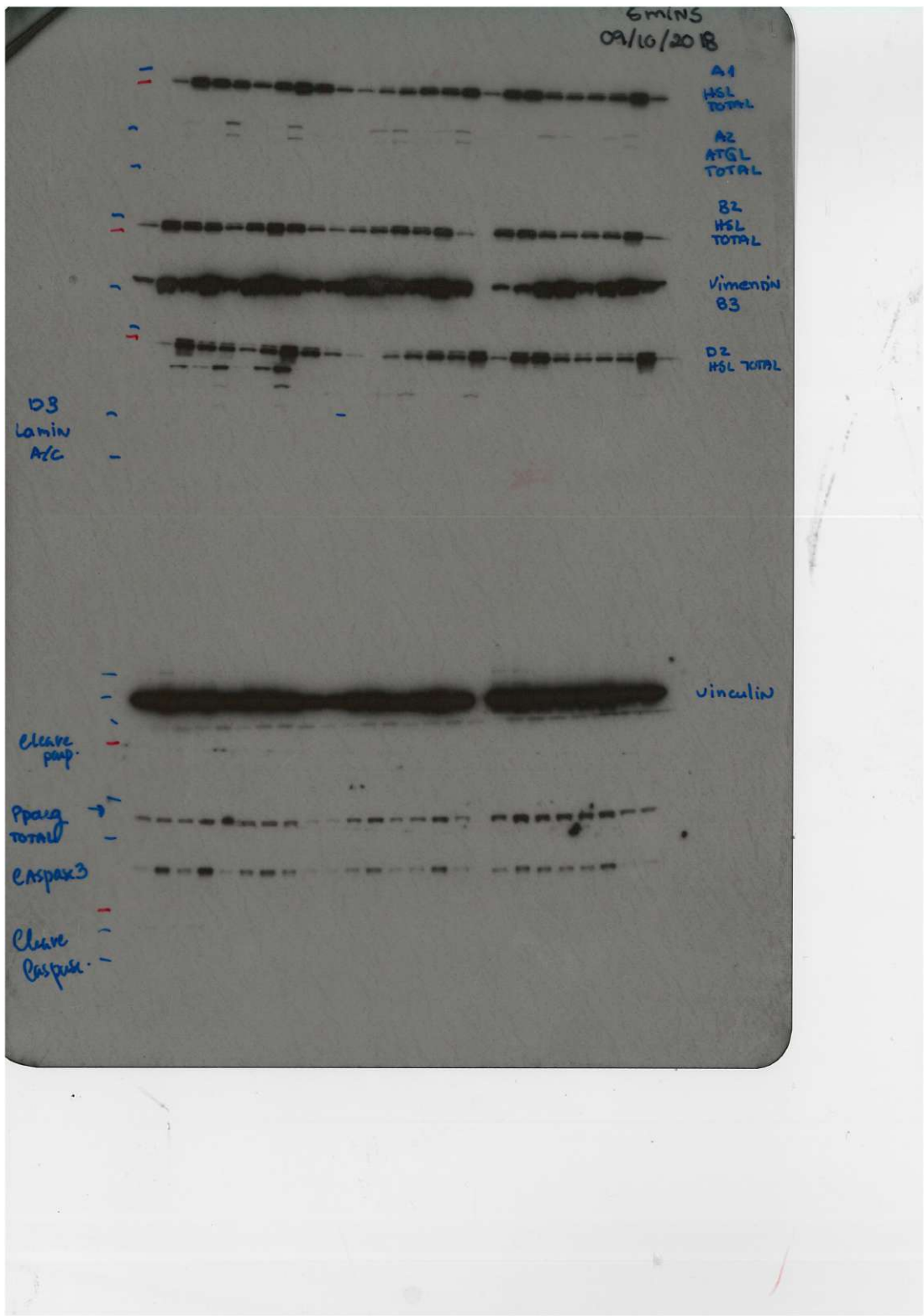
5min  
04/10/2018



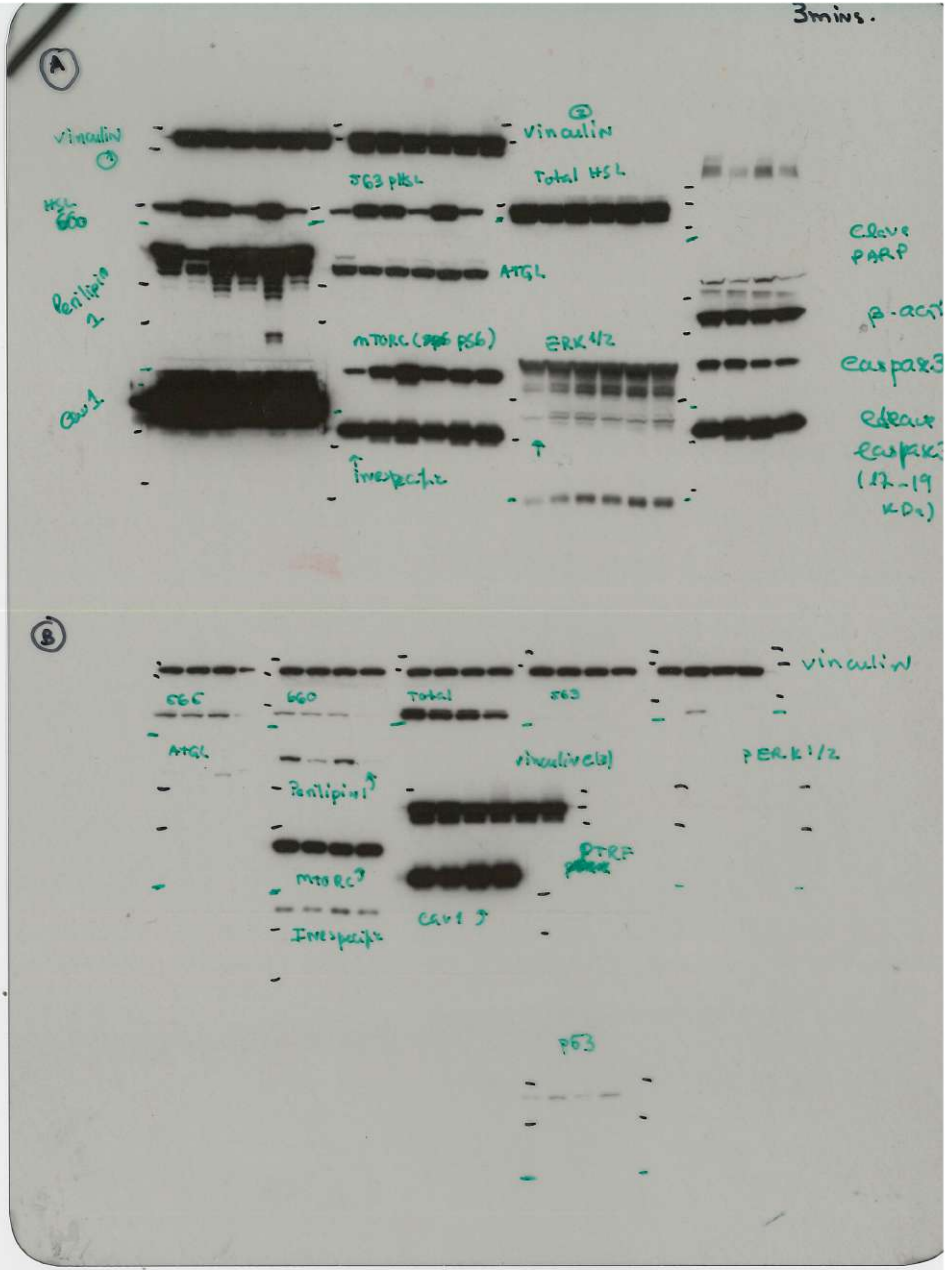
CR1-3h  
CR2-3h  
CR3-3h  
CR4-3h  
CR5-3h  
CR6-3h  
CR7-3h  
CR8-3h  
CR9-3h  
CR10-3h  
CR11-3h  
CR12-3h  
CR13-3h  
CR14-3h  
CR15-3h  
CR16-3h  
CR17-3h  
CR18-3h  
CR19-3h  
CR20-3h  
CR21-3h  
CR22-3h  
CR23-3h  
CR24-3h  
CR25-3h  
CR26-3h  
CR27-3h  
CR28-3h  
CR29-3h  
CR30-3h  
CR31-3h  
CR32-3h  
CR33-3h  
CR34-3h  
CR35-3h  
CR36-3h  
CR37-3h  
CR38-3h  
CR39-3h  
CR40-3h  
CR41-3h  
CR42-3h  
CR43-3h  
CR44-3h  
CR45-3h  
CR46-3h  
CR47-3h  
CR48-3h  
CR49-3h  
CR50-3h  
CR51-3h  
CR52-3h  
CR53-3h  
CR54-3h  
CR55-3h  
CR56-3h  
CR57-3h  
CR58-3h  
CR59-3h  
CR60-3h  
CR61-3h  
CR62-3h  
CR63-3h  
CR64-3h  
CR65-3h  
CR66-3h  
CR67-3h  
CR68-3h  
CR69-3h  
CR70-3h  
CR71-3h  
CR72-3h  
CR73-3h  
CR74-3h  
CR75-3h  
CR76-3h  
CR77-3h  
CR78-3h  
CR79-3h  
CR80-3h  
CR81-3h  
CR82-3h  
CR83-3h  
CR84-3h  
CR85-3h  
CR86-3h  
CR87-3h  
CR88-3h  
CR89-3h  
CR90-3h  
CR91-3h  
CR92-3h  
CR93-3h  
CR94-3h  
CR95-3h  
CR96-3h  
CR97-3h  
CR98-3h  
CR99-3h  
CR100-3h  
CR101-3h  
CR102-3h  
CR103-3h  
CR104-3h  
CR105-3h  
CR106-3h  
CR107-3h  
CR108-3h  
CR109-3h  
CR110-3h  
CR111-3h  
CR112-3h  
CR113-3h  
CR114-3h  
CR115-3h  
CR116-3h  
CR117-3h  
CR118-3h  
CR119-3h  
CR120-3h  
CR121-3h  
CR122-3h  
CR123-3h  
CR124-3h  
CR125-3h  
CR126-3h  
CR127-3h  
CR128-3h  
CR129-3h  
CR130-3h  
CR131-3h  
CR132-3h  
CR133-3h  
CR134-3h  
CR135-3h  
CR136-3h  
CR137-3h  
CR138-3h  
CR139-3h  
CR140-3h  
CR141-3h  
CR142-3h  
CR143-3h  
CR144-3h  
CR145-3h  
CR146-3h  
CR147-3h  
CR148-3h  
CR149-3h  
CR150-3h  
CR151-3h  
CR152-3h  
CR153-3h  
CR154-3h  
CR155-3h  
CR156-3h  
CR157-3h  
CR158-3h  
CR159-3h  
CR160-3h  
CR161-3h  
CR162-3h  
CR163-3h  
CR164-3h  
CR165-3h  
CR166-3h  
CR167-3h  
CR168-3h  
CR169-3h  
CR170-3h  
CR171-3h  
CR172-3h  
CR173-3h  
CR174-3h  
CR175-3h  
CR176-3h  
CR177-3h  
CR178-3h  
CR179-3h  
CR180-3h  
CR181-3h  
CR182-3h  
CR183-3h  
CR184-3h  
CR185-3h  
CR186-3h  
CR187-3h  
CR188-3h  
CR189-3h  
CR190-3h  
CR191-3h  
CR192-3h  
CR193-3h  
CR194-3h  
CR195-3h  
CR196-3h  
CR197-3h  
CR198-3h  
CR199-3h  
CR200-3h  
CR201-3h  
CR202-3h  
CR203-3h  
CR204-3h  
CR205-3h  
CR206-3h  
CR207-3h  
CR208-3h  
CR209-3h  
CR210-3h  
CR211-3h  
CR212-3h  
CR213-3h  
CR214-3h  
CR215-3h  
CR216-3h  
CR217-3h  
CR218-3h  
CR219-3h  
CR220-3h  
CR221-3h  
CR222-3h  
CR223-3h  
CR224-3h  
CR225-3h  
CR226-3h  
CR227-3h  
CR228-3h  
CR229-3h  
CR230-3h  
CR231-3h  
CR232-3h  
CR233-3h  
CR234-3h  
CR235-3h  
CR236-3h  
CR237-3h  
CR238-3h  
CR239-3h  
CR240-3h  
CR241-3h  
CR242-3h  
CR243-3h  
CR244-3h  
CR245-3h  
CR246-3h  
CR247-3h  
CR248-3h  
CR249-3h  
CR250-3h  
CR251-3h  
CR252-3h  
CR253-3h  
CR254-3h  
CR255-3h  
CR256-3h  
CR257-3h  
CR258-3h  
CR259-3h  
CR260-3h  
CR261-3h  
CR262-3h  
CR263-3h  
CR264-3h  
CR265-3h  
CR266-3h  
CR267-3h  
CR268-3h  
CR269-3h  
CR270-3h  
CR271-3h  
CR272-3h  
CR273-3h  
CR274-3h  
CR275-3h  
CR276-3h  
CR277-3h  
CR278-3h  
CR279-3h  
CR280-3h  
CR281-3h  
CR282-3h  
CR283-3h  
CR284-3h  
CR285-3h  
CR286-3h  
CR287-3h  
CR288-3h  
CR289-3h  
CR290-3h  
CR291-3h  
CR292-3h  
CR293-3h  
CR294-3h  
CR295-3h  
CR296-3h  
CR297-3h  
CR298-3h  
CR299-3h  
CR300-3h  
CR301-3h  
CR302-3h  
CR303-3h  
CR304-3h  
CR305-3h  
CR306-3h  
CR307-3h  
CR308-3h  
CR309-3h  
CR310-3h  
CR311-3h  
CR312-3h  
CR313-3h  
CR314-3h  
CR315-3h  
CR316-3h  
CR317-3h  
CR318-3h  
CR319-3h  
CR320-3h  
CR321-3h  
CR322-3h  
CR323-3h  
CR324-3h  
CR325-3h  
CR326-3h  
CR327-3h  
CR328-3h  
CR329-3h  
CR330-3h  
CR331-3h  
CR332-3h  
CR333-3h  
CR334-3h  
CR335-3h  
CR336-3h  
CR337-3h  
CR338-3h  
CR339-3h  
CR340-3h  
CR341-3h  
CR342-3h  
CR343-3h  
CR344-3h  
CR345-3h  
CR346-3h  
CR347-3h  
CR348-3h  
CR349-3h  
CR350-3h  
CR351-3h  
CR352-3h  
CR353-3h  
CR354-3h  
CR355-3h  
CR356-3h  
CR357-3h  
CR358-3h  
CR359-3h  
CR360-3h  
CR361-3h  
CR362-3h  
CR363-3h  
CR364-3h  
CR365-3h  
CR366-3h  
CR367-3h  
CR368-3h  
CR369-3h  
CR370-3h  
CR371-3h  
CR372-3h  
CR373-3h  
CR374-3h  
CR375-3h  
CR376-3h  
CR377-3h  
CR378-3h  
CR379-3h  
CR380-3h  
CR381-3h  
CR382-3h  
CR383-3h  
CR384-3h  
CR385-3h  
CR386-3h  
CR387-3h  
CR388-3h  
CR389-3h  
CR390-3h  
CR391-3h  
CR392-3h  
CR393-3h  
CR394-3h  
CR395-3h  
CR396-3h  
CR397-3h  
CR398-3h  
CR399-3h  
CR400-3h  
CR401-3h  
CR402-3h  
CR403-3h  
CR404-3h  
CR405-3h  
CR406-3h  
CR407-3h  
CR408-3h  
CR409-3h  
CR410-3h  
CR411-3h  
CR412-3h  
CR413-3h  
CR414-3h  
CR415-3h  
CR416-3h  
CR417-3h  
CR418-3h  
CR419-3h  
CR420-3h  
CR421-3h  
CR422-3h  
CR423-3h  
CR424-3h  
CR425-3h  
CR426-3h  
CR427-3h  
CR428-3h  
CR429-3h  
CR430-3h  
CR431-3h  
CR432-3h  
CR433-3h  
CR434-3h  
CR435-3h  
CR436-3h  
CR437-3h  
CR438-3h  
CR439-3h  
CR440-3h  
CR441-3h  
CR442-3h  
CR443-3h  
CR444-3h  
CR445-3h  
CR446-3h  
CR447-3h  
CR448-3h  
CR449-3h  
CR450-3h  
CR451-3h  
CR452-3h  
CR453-3h  
CR454-3h  
CR455-3h  
CR456-3h  
CR457-3h  
CR458-3h  
CR459-3h  
CR460-3h  
CR461-3h  
CR462-3h  
CR463-3h  
CR464-3h  
CR465-3h  
CR466-3h  
CR467-3h  
CR468-3h  
CR469-3h  
CR470-3h  
CR471-3h  
CR472-3h  
CR473-3h  
CR474-3h  
CR475-3h  
CR476-3h  
CR477-3h  
CR478-3h  
CR479-3h  
CR480-3h  
CR481-3h  
CR482-3h  
CR483-3h  
CR484-3h  
CR485-3h  
CR486-3h  
CR487-3h  
CR488-3h  
CR489-3h  
CR490-3h  
CR491-3h  
CR492-3h  
CR493-3h  
CR494-3h  
CR495-3h  
CR496-3h  
CR497-3h  
CR498-3h  
CR499-3h  
CR500-3h  
CR501-3h  
CR502-3h  
CR503-3h  
CR504-3h  
CR505-3h  
CR506-3h  
CR507-3h  
CR508-3h  
CR509-3h  
CR510-3h  
CR511-3h  
CR512-3h  
CR513-3h  
CR514-3h  
CR515-3h  
CR516-3h  
CR517-3h  
CR518-3h  
CR519-3h  
CR520-3h  
CR521-3h  
CR522-3h  
CR523-3h  
CR524-3h  
CR525-3h  
CR526-3h  
CR527-3h  
CR528-3h  
CR529-3h  
CR530-3h  
CR531-3h  
CR532-3h  
CR533-3h  
CR534-3h  
CR535-3h  
CR536-3h  
CR537-3h  
CR538-3h  
CR539-3h  
CR540-3h  
CR541-3h  
CR542-3h  
CR543-3h  
CR544-3h  
CR545-3h  
CR546-3h  
CR547-3h  
CR548-3h  
CR549-3h  
CR550-3h  
CR551-3h  
CR552-3h  
CR553-3h  
CR554-3h  
CR555-3h  
CR556-3h  
CR557-3h  
CR558-3h  
CR559-3h  
CR560-3h  
CR561-3h  
CR562-3h  
CR563-3h  
CR564-3h  
CR565-3h  
CR566-3h  
CR567-3h  
CR568-3h  
CR569-3h  
CR570-3h  
CR571-3h  
CR572-3h  
CR573-3h  
CR574-3h  
CR575-3h  
CR576-3h  
CR577-3h  
CR578-3h  
CR579-3h  
CR580-3h  
CR581-3h  
CR582-3h  
CR583-3h  
CR584-3h  
CR585-3h  
CR586-3h  
CR587-3h  
CR588-3h  
CR589-3h  
CR590-3h  
CR591-3h  
CR592-3h  
CR593-3h  
CR594-3h  
CR595-3h  
CR596-3h  
CR597-3h  
CR598-3h  
CR599-3h  
CR600-3h  
CR601-3h  
CR602-3h  
CR603-3h  
CR604-3h  
CR605-3h  
CR606-3h  
CR607-3h  
CR608-3h  
CR609-3h  
CR610-3h  
CR611-3h  
CR612-3h  
CR613-3h  
CR614-3h  
CR615-3h  
CR616-3h  
CR617-3h  
CR618-3h  
CR619-3h  
CR620-3h  
CR621-3h  
CR622-3h  
CR623-3h  
CR624-3h  
CR625-3h  
CR626-3h  
CR627-3h  
CR628-3h  
CR629-3h  
CR630-3h  
CR631-3h  
CR632-3h  
CR633-3h  
CR634-3h  
CR635-3h  
CR636-3h  
CR637-3h  
CR638-3h  
CR639-3h  
CR640-3h  
CR641-3h  
CR642-3h  
CR643-3h  
CR644-3h  
CR645-3h  
CR646-3h  
CR647-3h  
CR648-3h  
CR649-3h  
CR650-3h  
CR651-3h  
CR652-3h  
CR653-3h  
CR654-3h  
CR655-3h  
CR656-3h  
CR657-3h  
CR658-3h  
CR659-3h  
CR660-3h  
CR661-3h  
CR662-3h  
CR663-3h  
CR664-3h  
CR665-3h  
CR666-3h  
CR667-3h  
CR668-3h  
CR669-3h  
CR670-3h  
CR671-3h  
CR672-3h  
CR673-3h  
CR674-3h  
CR675-3h  
CR676-3h  
CR677-3h  
CR678-3h  
CR679-3h  
CR680-3h  
CR681-3h  
CR682-3h  
CR683-3h  
CR684-3h  
CR685-3h  
CR686-3h  
CR687-3h  
CR688-3h  
CR689-3h  
CR690-3h  
CR691-3h  
CR692-3h  
CR693-3h  
CR694-3h  
CR695-3h  
CR696-3h  
CR697-3h  
CR698-3h  
CR699-3h  
CR700-3h  
CR701-3h  
CR702-3h  
CR703-3h  
CR704-3h  
CR705-3h  
CR706-3h  
CR707-3h  
CR708-3h  
CR709-3h  
CR710-3h  
CR711-3h  
CR712-3h  
CR713-3h  
CR714-3h  
CR715-3h  
CR716-3h  
CR717-3h  
CR718-3h  
CR719-3h  
CR720-3h  
CR721-3h  
CR722-3h  
CR723-3h  
CR724-3h  
CR725-3h  
CR726-3h  
CR727-3h  
CR728-3h  
CR729-3h  
CR730-3h  
CR731-3h  
CR732-3h  
CR733-3h  
CR734-3h  
CR735-3h  
CR736-3h  
CR737-3h  
CR738-3h  
CR739-3h  
CR740-3h  
CR741-3h  
CR742-3h  
CR743-3h  
CR744-3h  
CR745-3h  
CR746-3h  
CR747-3h  
CR748-3h  
CR749-3h  
CR750-3h  
CR751-3h  
CR752-3h  
CR753-3h  
CR754-3h  
CR755-3h  
CR756-3h  
CR757-3h  
CR758-3h  
CR759-3h  
CR760-3h  
CR761-3h  
CR762-3h  
CR763-3h  
CR764-3h  
CR765-3h  
CR766-3h  
CR767-3h  
CR768-3h  
CR769-3h  
CR770-3h  
CR771-3h  
CR772-3h  
CR773-3h  
CR774-3h  
CR775-3h  
CR776-3h  
CR777-3h  
CR778-3h  
CR779-3h  
CR780-3h  
CR781-3h  
CR782-3h  
CR783-3h  
CR784-3h  
CR785-3h  
CR786-3h  
CR787-3h  
CR788-3h  
CR789-3h  
CR790-3h  
CR791-3h  
CR792-3h  
CR793-3h  
CR794-3h  
CR795-3h  
CR796-3h  
CR797-3h  
CR798-3h  
CR799-3h  
CR800-3h  
CR801-3h  
CR802-3h  
CR803-3h  
CR804-3h  
CR805-3h  
CR806-3h  
CR807-3h  
CR808-3h  
CR809-3h  
CR810-3h  
CR811-3h  
CR812-3h  
CR813-3h  
CR814-3h  
CR815-3h  
CR816-3h  
CR817-3h  
CR818-3h  
CR819-3h  
CR820-3h  
CR821-3h  
CR822-3h  
CR823-3h  
CR824-3h  
CR825-3h  
CR826-3h  
CR827-3h  
CR828-3h  
CR829-3h  
CR830-3h  
CR831-3h  
CR832-3h  
CR833-3h  
CR834-3h  
CR835-3h  
CR836-3h  
CR837-3h  
CR838-3h  
CR839-3h  
CR840-3h  
CR841-3h  
CR842-3h  
CR843-3h  
CR844-3h  
CR845-3h  
CR846-3h  
CR847-3h  
CR848-3h  
CR849-3h  
CR850-3h  
CR851-3h  
CR852-3h  
CR853-3h  
CR854-3h  
CR855-3h  
CR856-3h  
CR857-3h  
CR858-3h  
CR859-3h  
CR860-3h  
CR861-3h  
CR862-3h  
CR863-3h  
CR864-3h  
CR865-3h  
CR866-3h  
CR867-3h  
CR868-3h  
CR869-3h  
CR870-3h  
CR871-3h  
CR872-3h  
CR873-3h  
CR874-3h  
CR875-3h  
CR876-3h  
CR877-3h  
CR878-3h  
CR879-3h  
CR880-3h  
CR881-3h  
CR882-3h  
CR883-3h  
CR884-3h  
CR885-3h  
CR886-3h  
CR887-3h  
CR888-3h  
CR889-3h  
CR890-3h  
CR891-3h  
CR892-3h  
CR893-3h  
CR894-3h  
CR895-3h  
CR896-3h  
CR897-3h  
CR898-3h  
CR899-3h  
CR900-3h  
CR901-3h  
CR902-3h  
CR903-3h  
CR904-3h  
CR905-3h  
CR906-3h  
CR907-3h  
CR908-3h  
CR909-3h  
CR910-3h  
CR911-3h  
CR912-3h  
CR913-3h  
CR914-3h  
CR915-3h  
CR916-3h  
CR917-3h  
CR918-3h  
CR919-3h  
CR920-3h  
CR921-3h  
CR922-3h  
CR923-3h  
CR924-3h  
CR925-3h  
CR926-3h  
CR927-3h  
CR928-3h  
CR929-3h  
CR930-3h  
CR931-3h  
CR932-3h  
CR933-3h  
CR934-3h  
CR935-3h  
CR936-3h  
CR937-3h  
CR938-3h  
CR939-3h  
CR940-3h  
CR941-3h  
CR942-3h  
CR943-3h  
CR944-3h  
CR945-3h  
CR946-3h  
CR947-3h  
CR948-3h  
CR949-3h  
CR950-3h  
CR951-3h  
CR952-3h  
CR953-3h  
CR954-3h  
CR955-3h  
CR956-3h  
CR957-3h  
CR958-3h  
CR959-3h  
CR960-3h  
CR961-3h  
CR962-3h  
CR963-3h  
CR964-3h  
CR965-3h  
CR966-3h  
CR967-3h  
CR968-3h  
CR969-3h  
CR970-3h  
CR971-3h  
CR972-3h  
CR973-3h  
CR974-3h  
CR975-3h  
CR976-3h  
CR977-3h  
CR978-3h  
CR979-3h  
CR980-3h  
CR981-3h  
CR982-3h  
CR983-3h  
CR984-3h  
CR985-3h  
CR986-3h  
CR987-3h  
CR988-3h  
CR989-3h  
CR990-3h  
CR991-3h  
CR992-3h  
CR993-3h  
CR994-3h  
CR995-3h  
CR996-3h  
CR997-3h  
CR998-3h  
CR999-3h  
CR1000-3h

vinculin  
PHSL 563  
p150Cas1  
p150Cas1  
vinculin  
NSL 565  
ADPK  
pS6

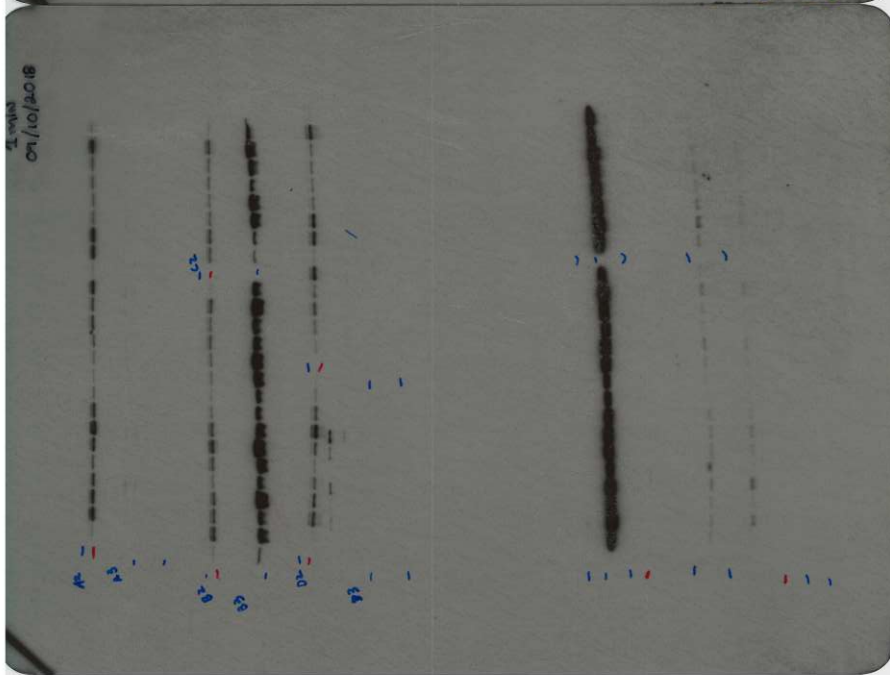
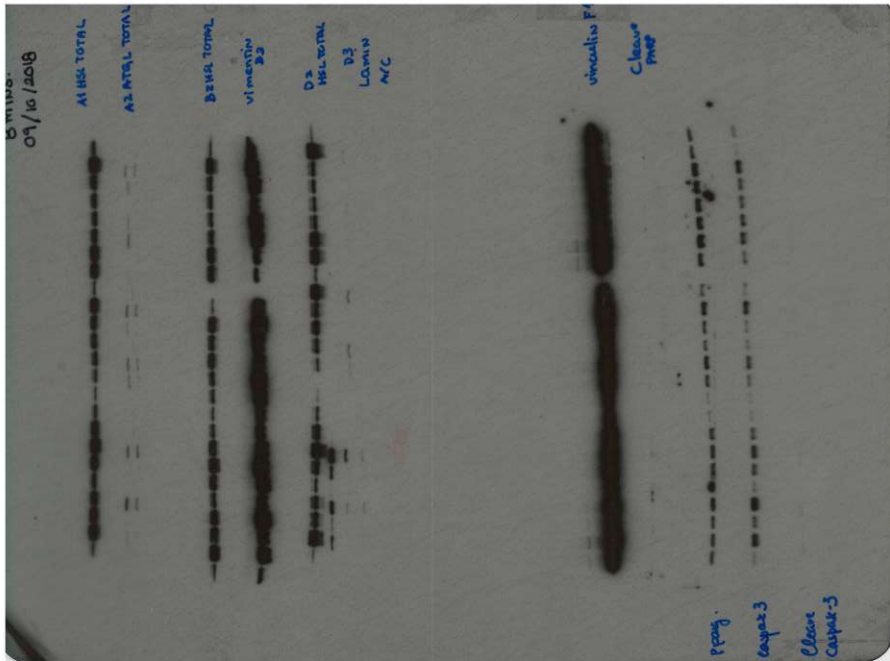


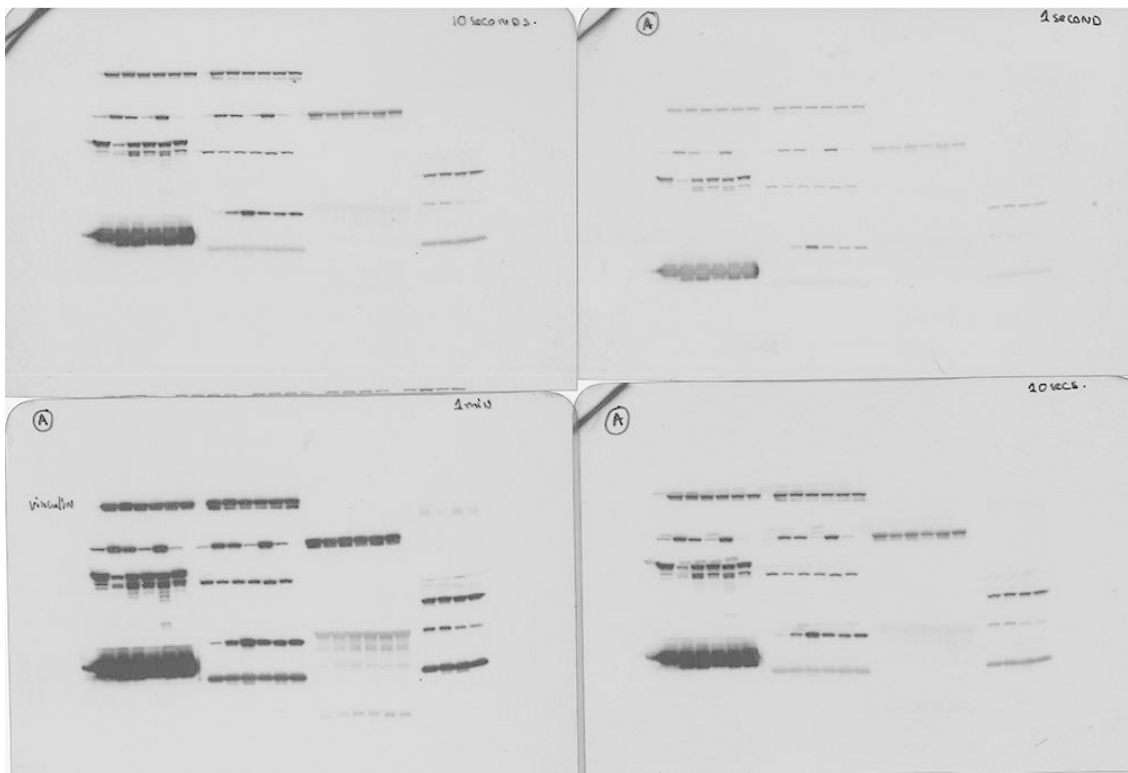


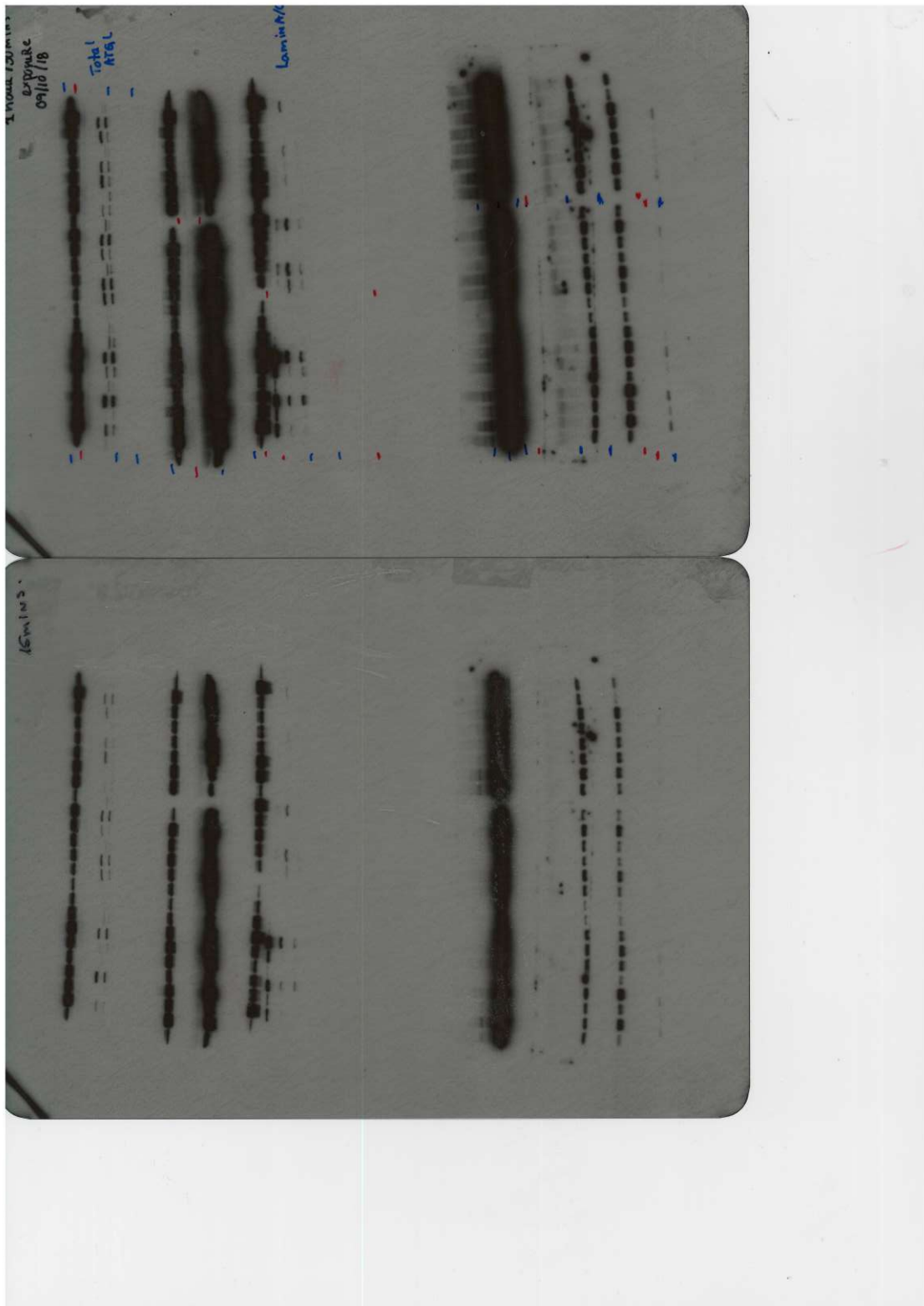
3mins.

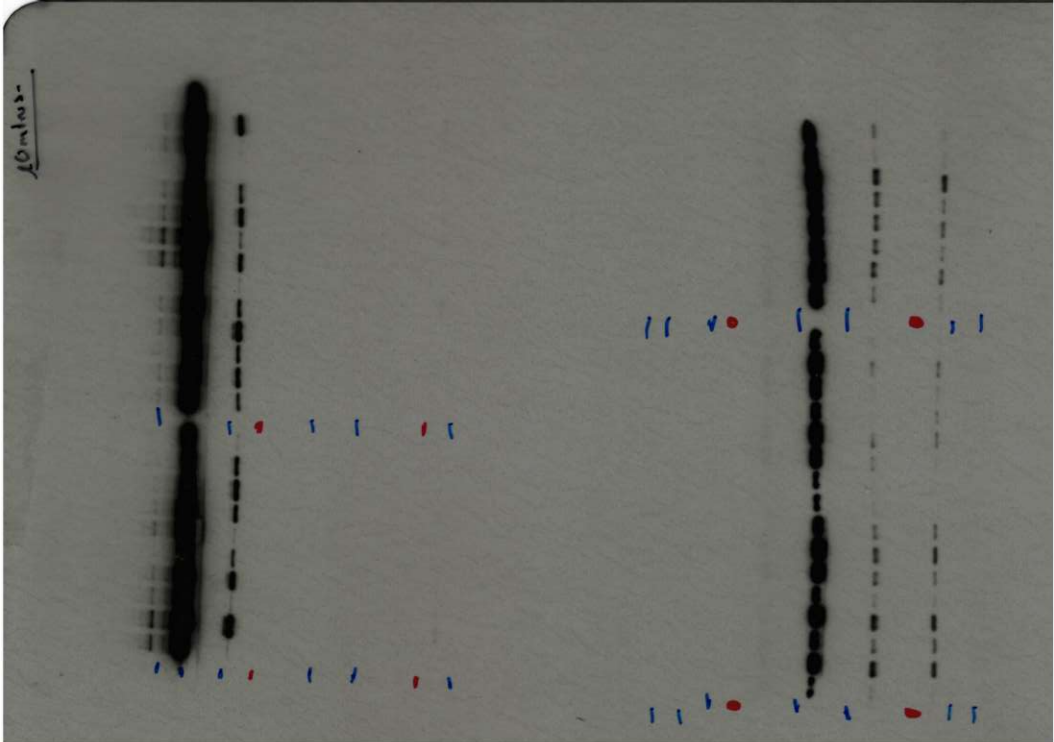
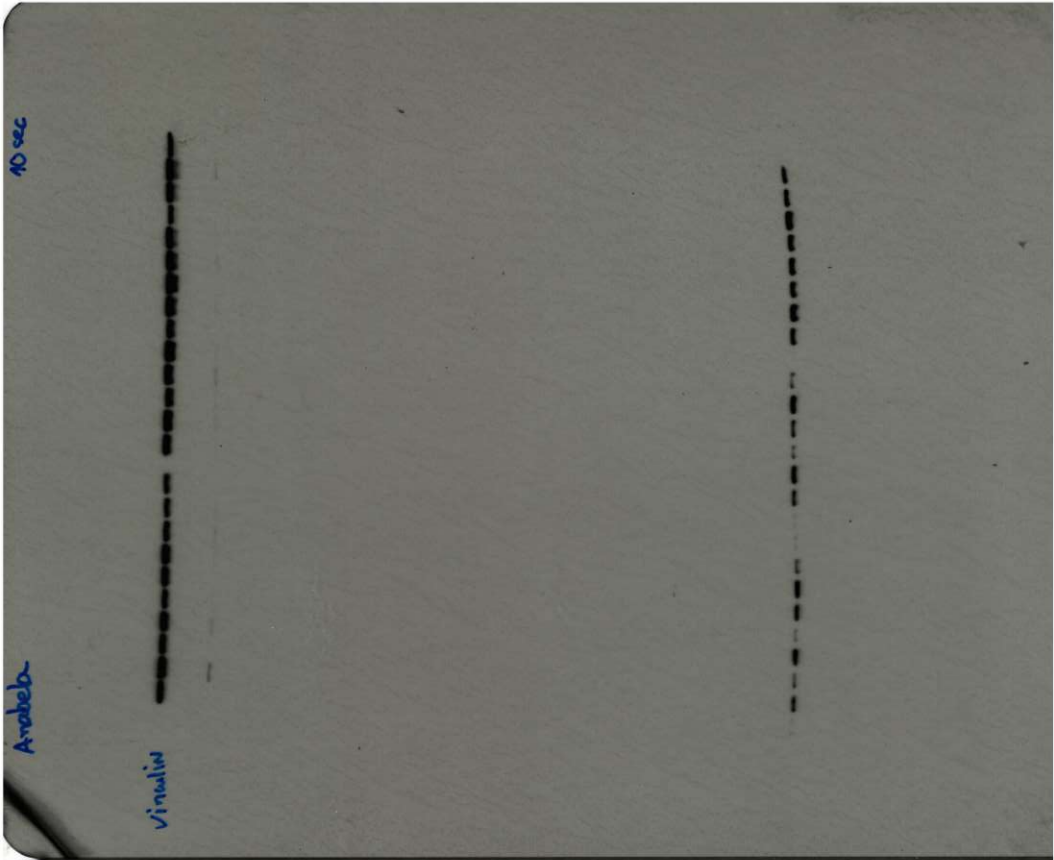


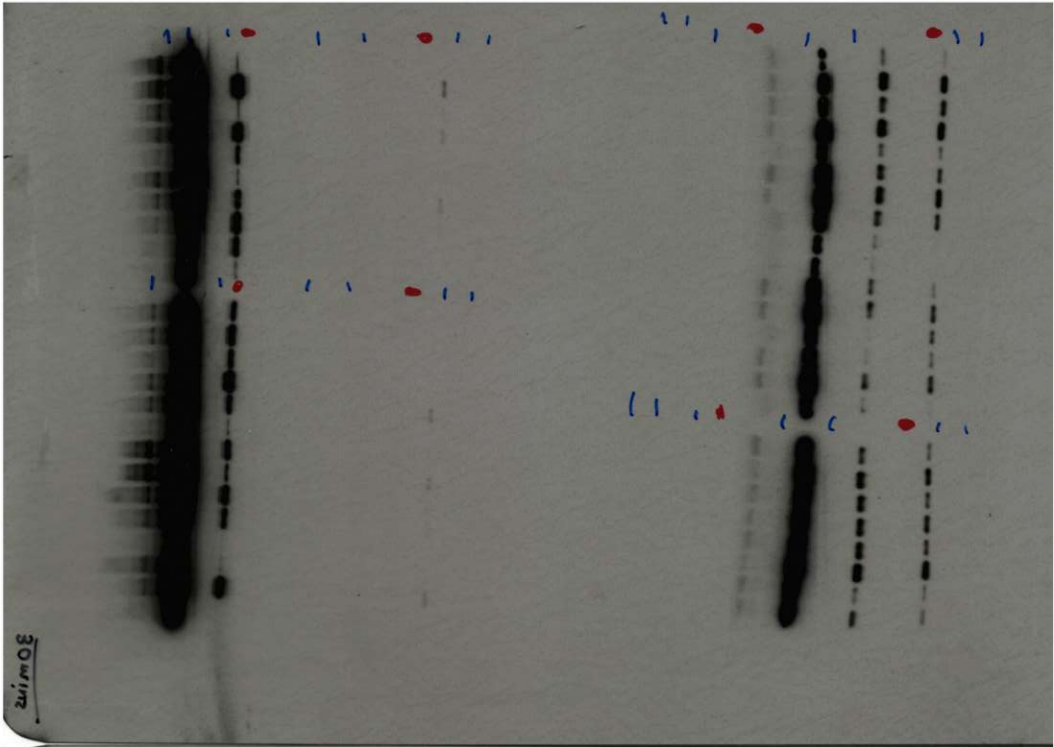
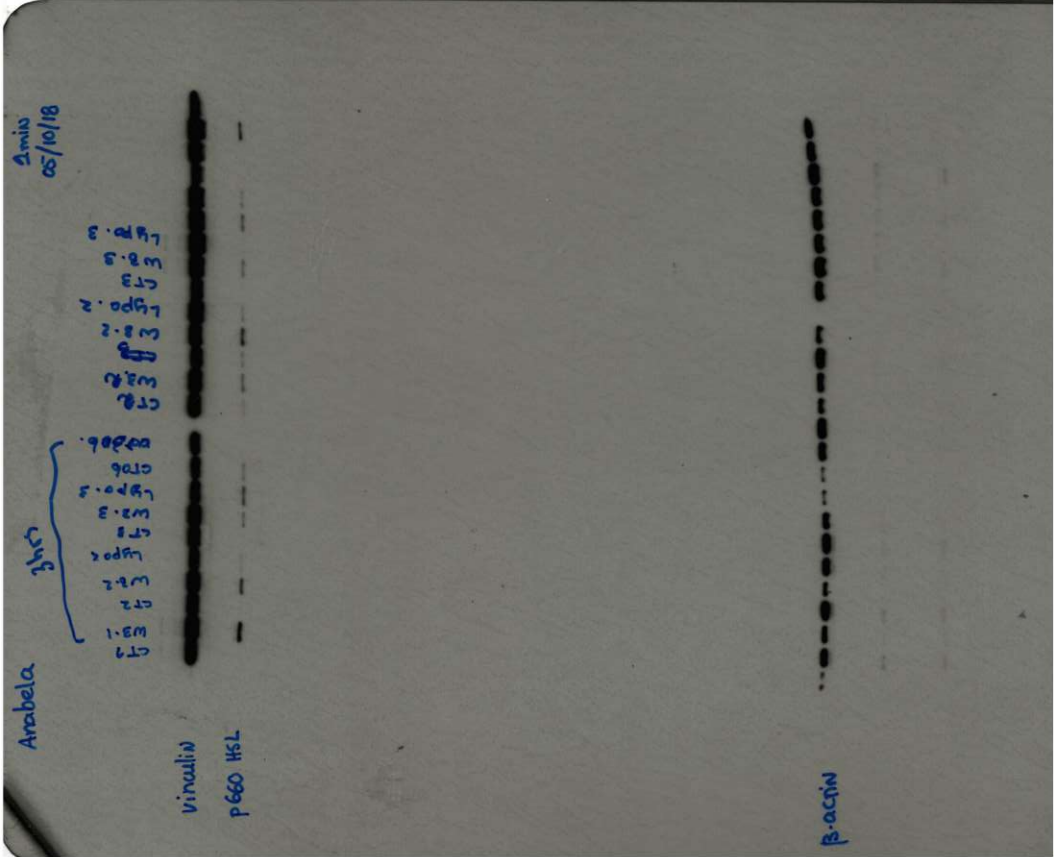


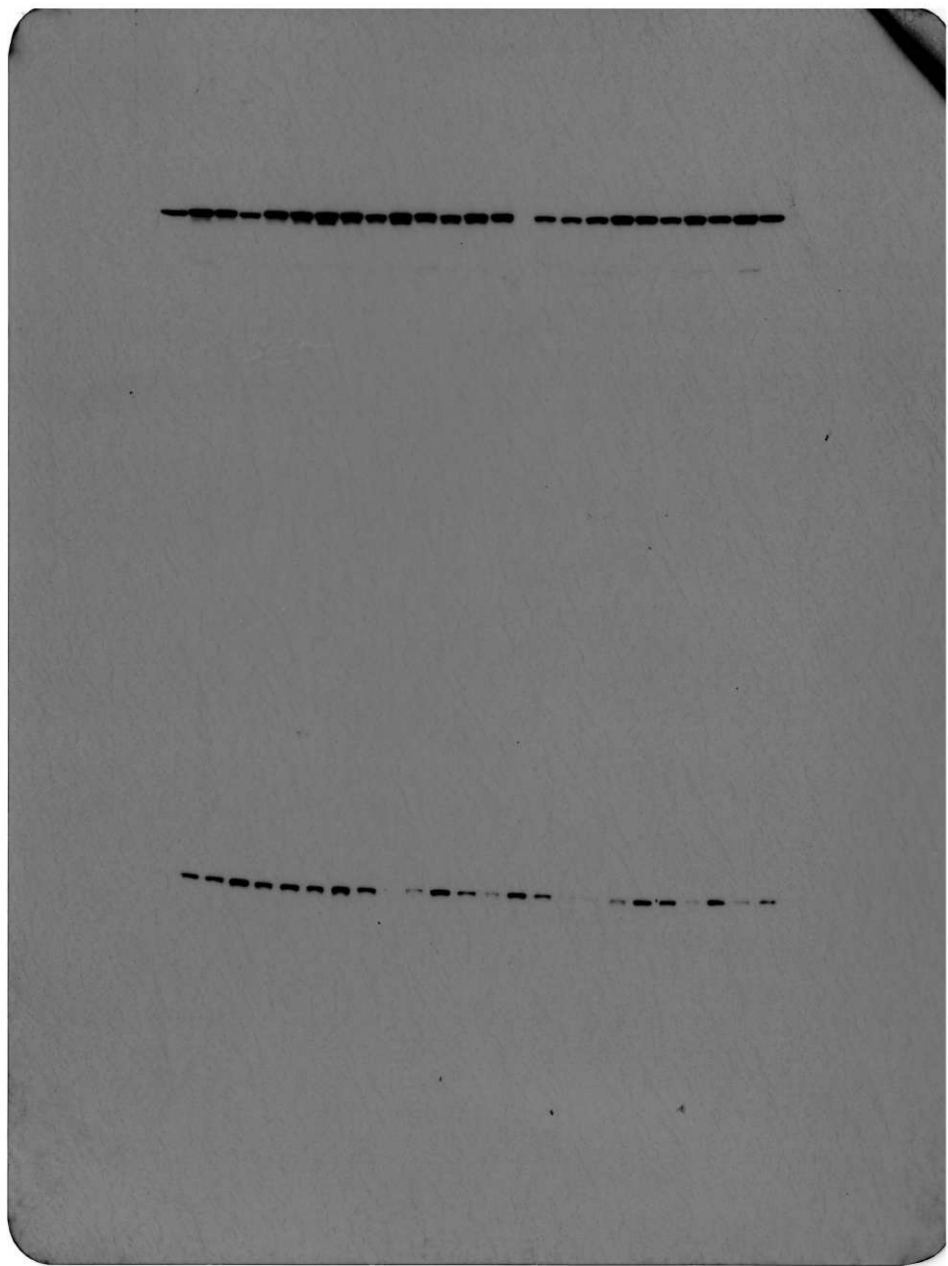


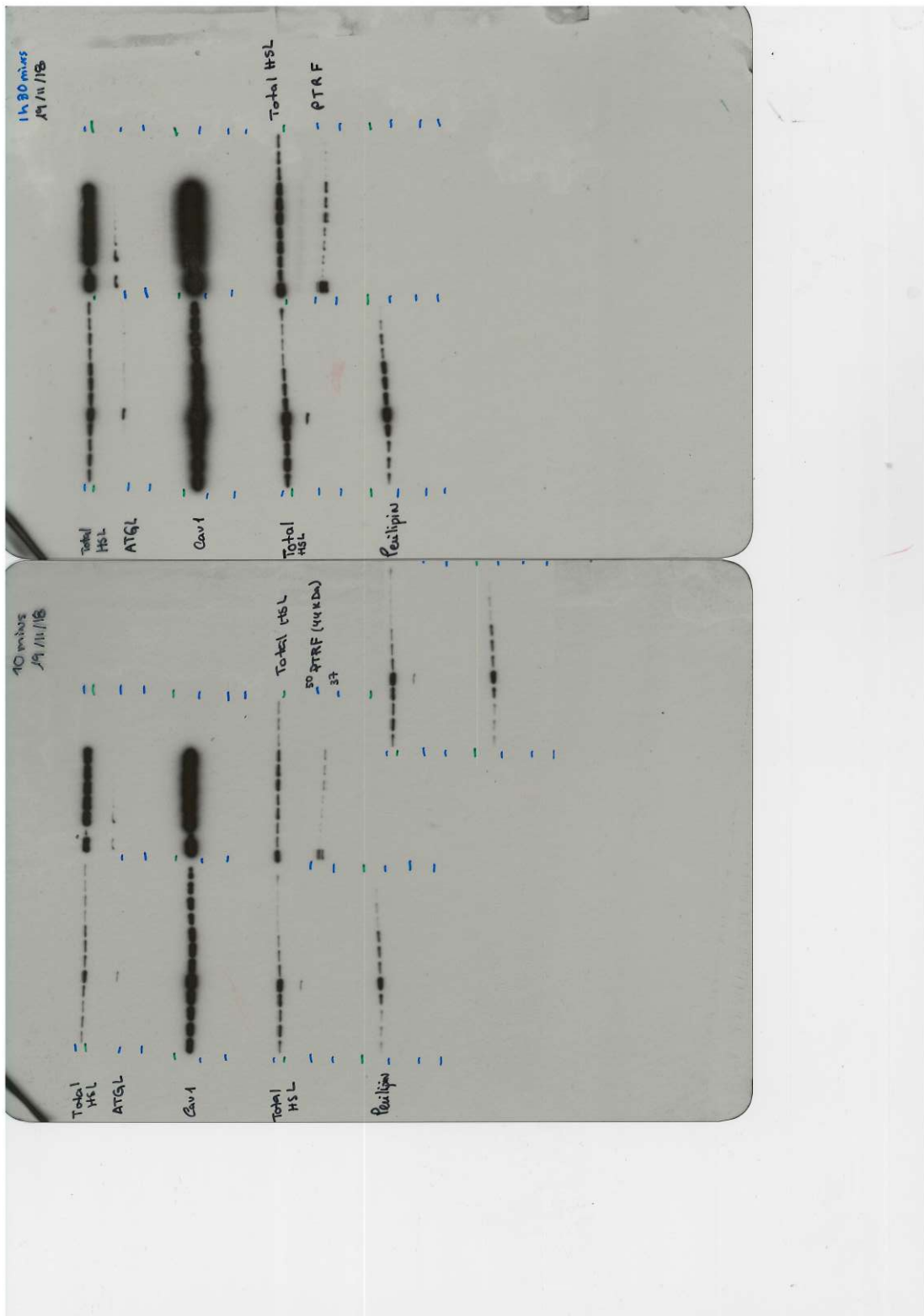


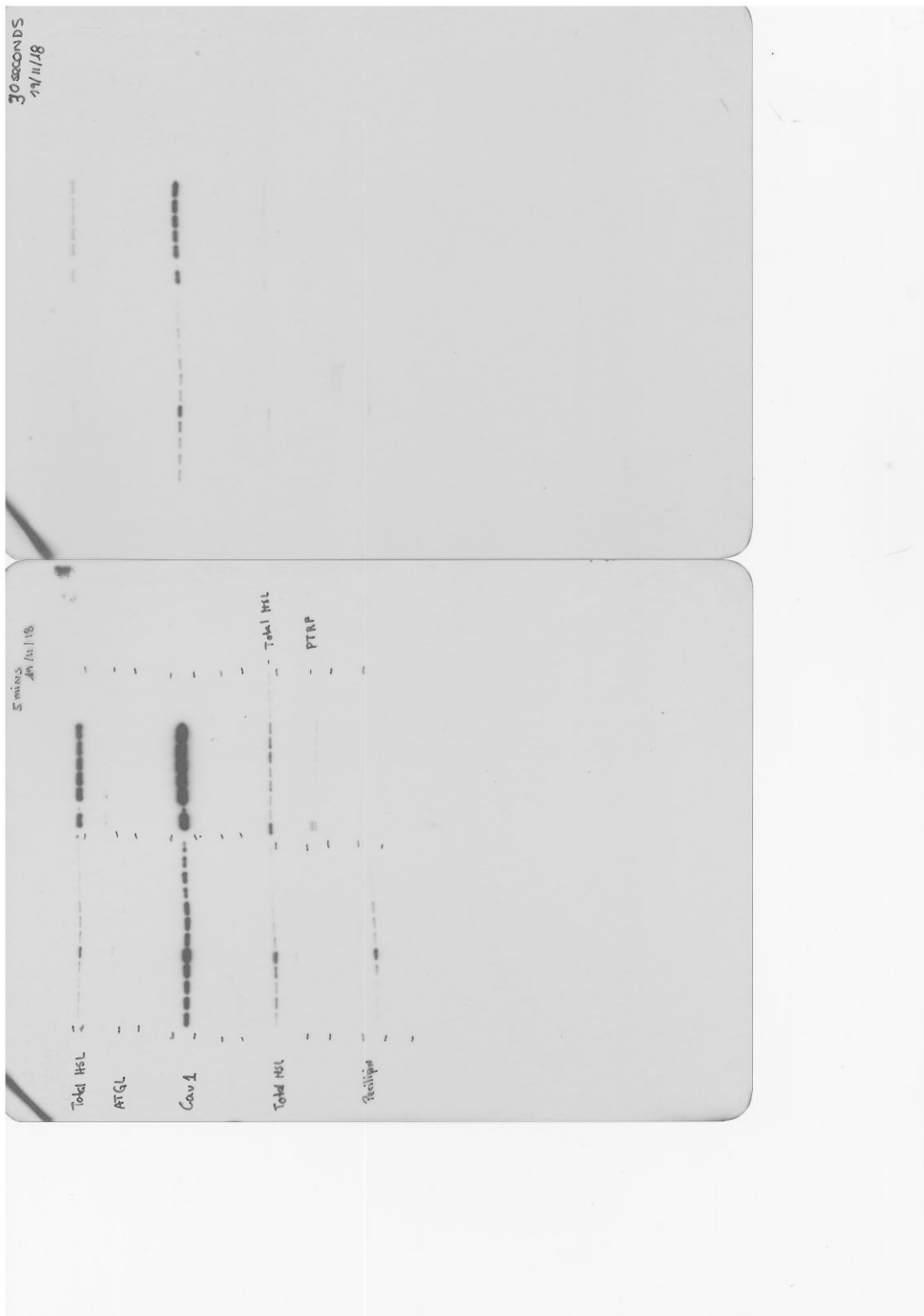




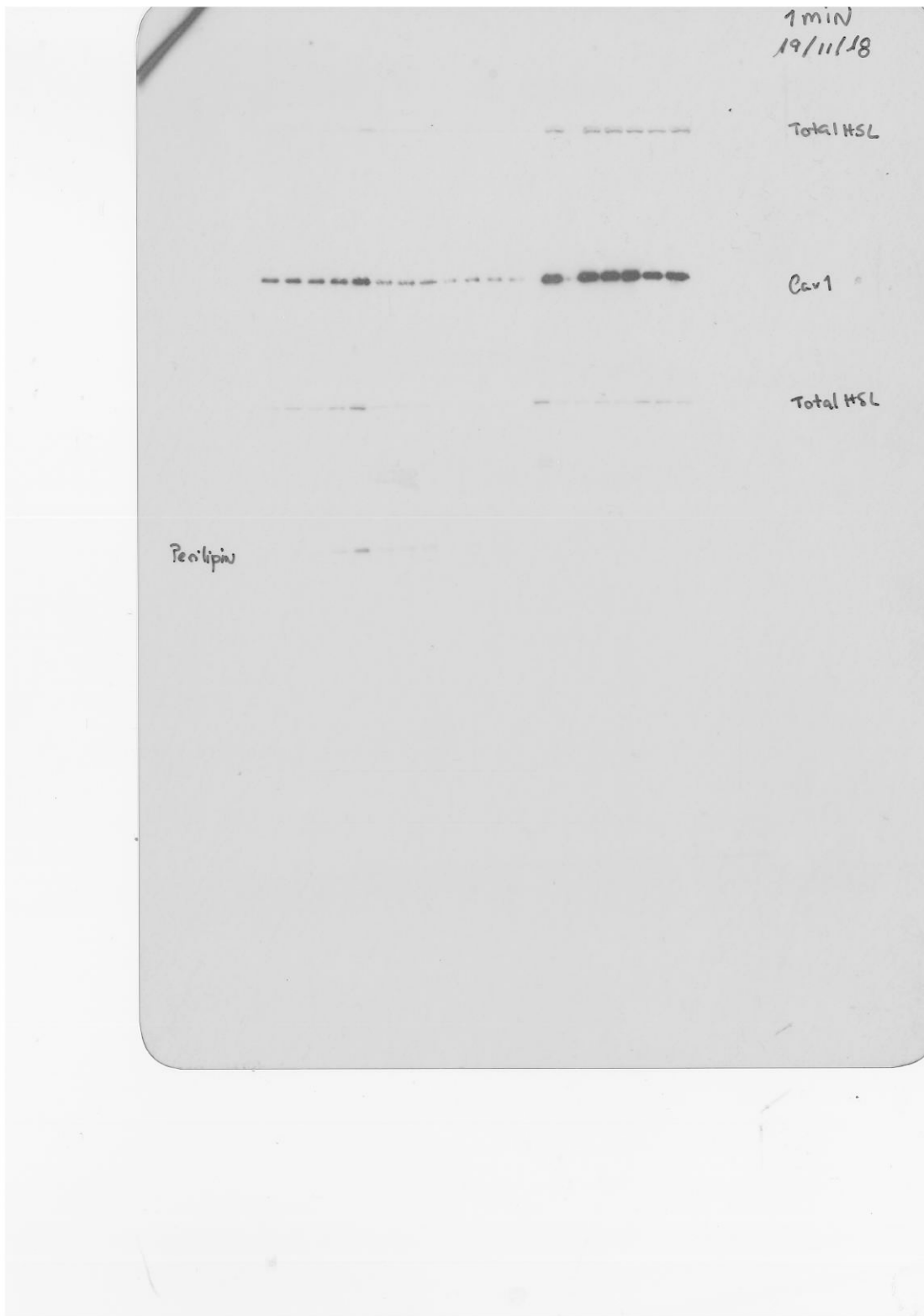


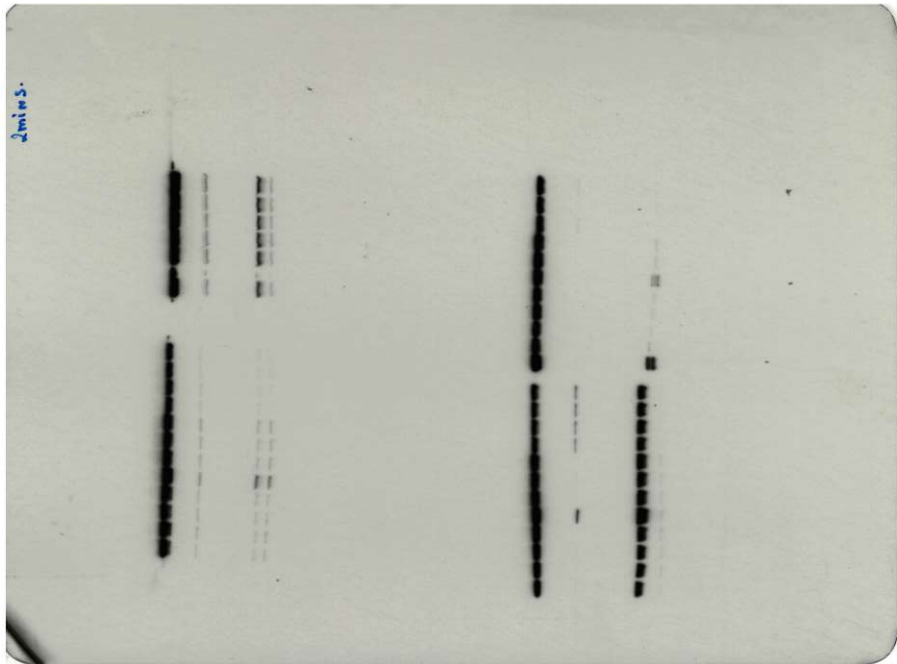


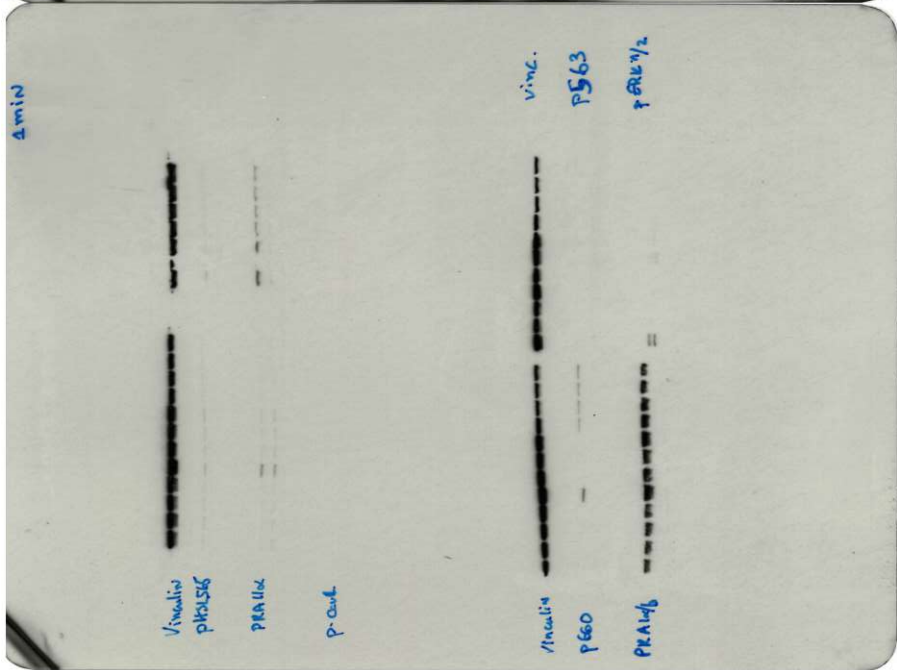
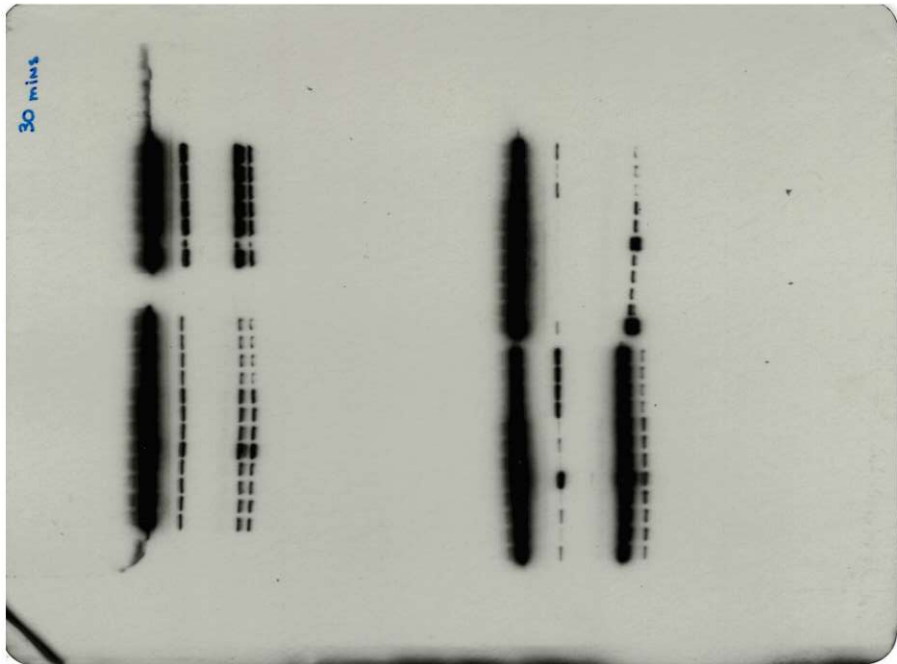


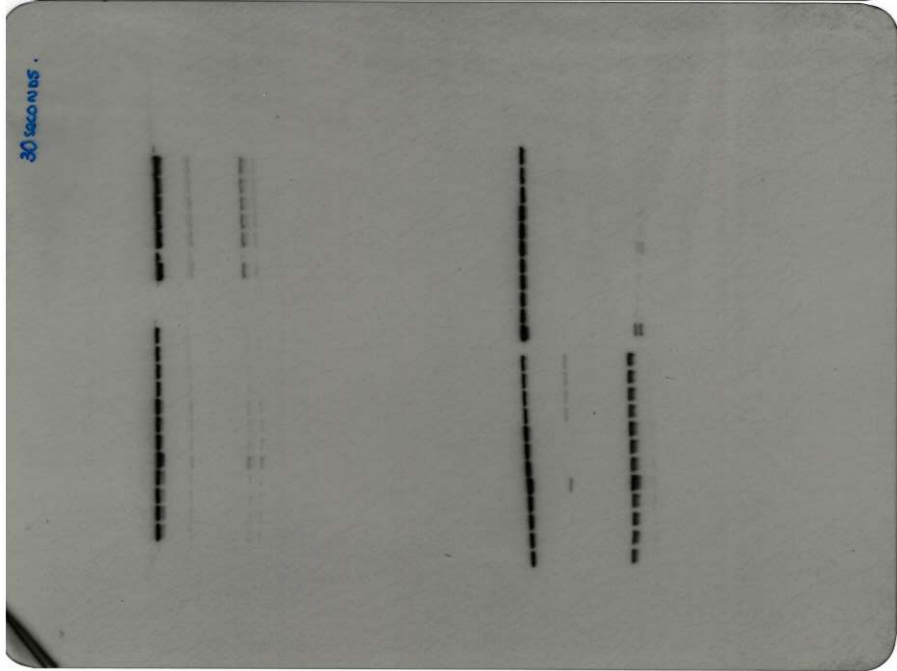
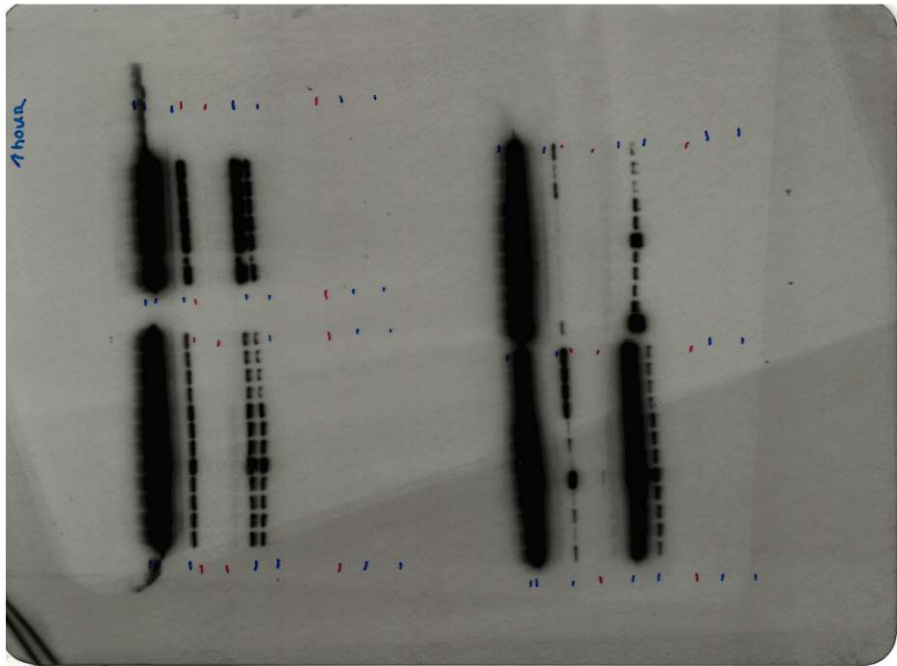


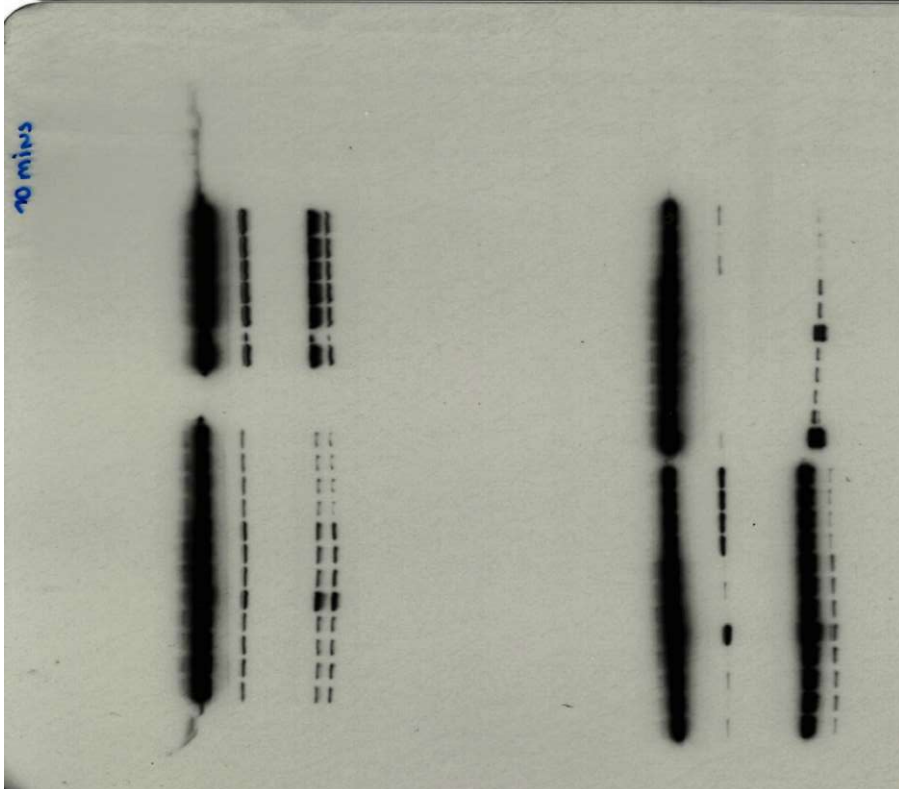
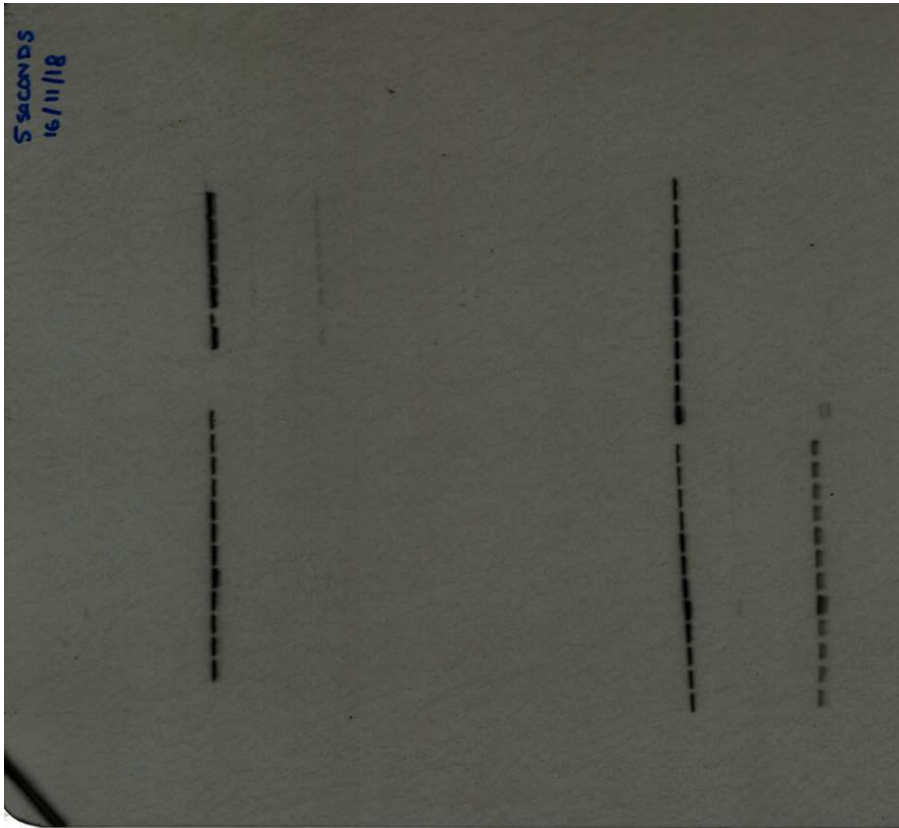


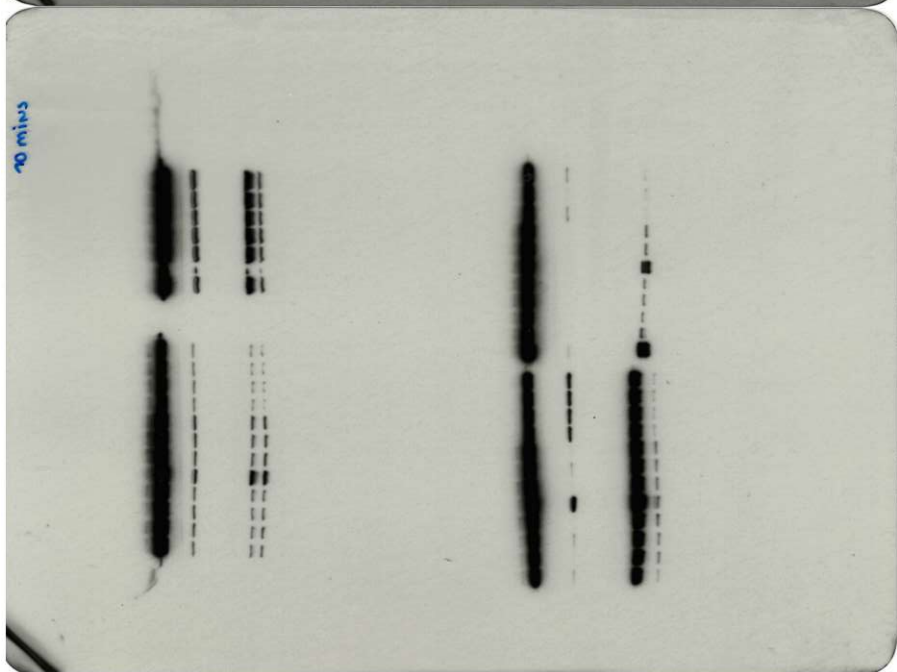
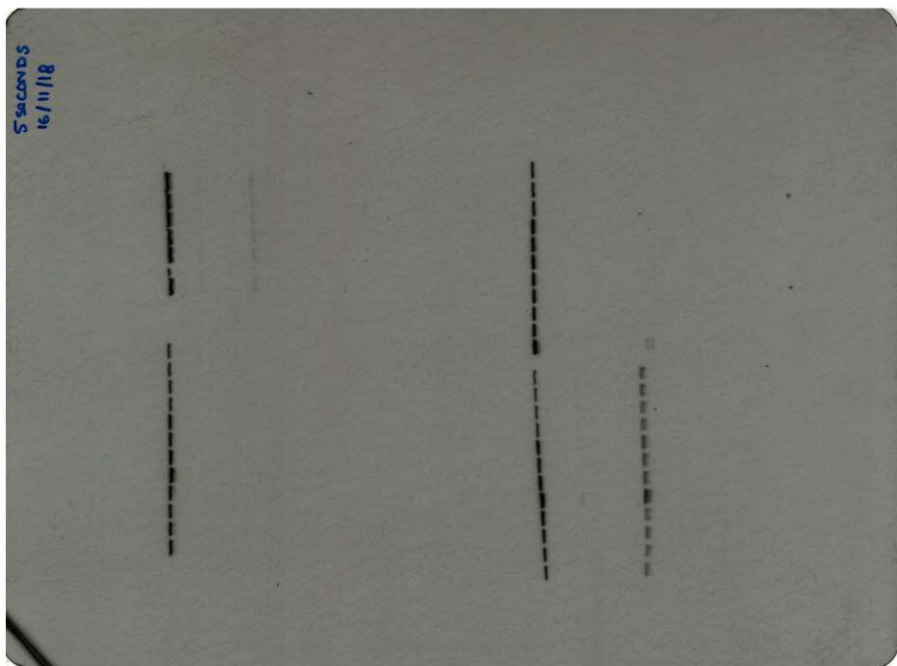


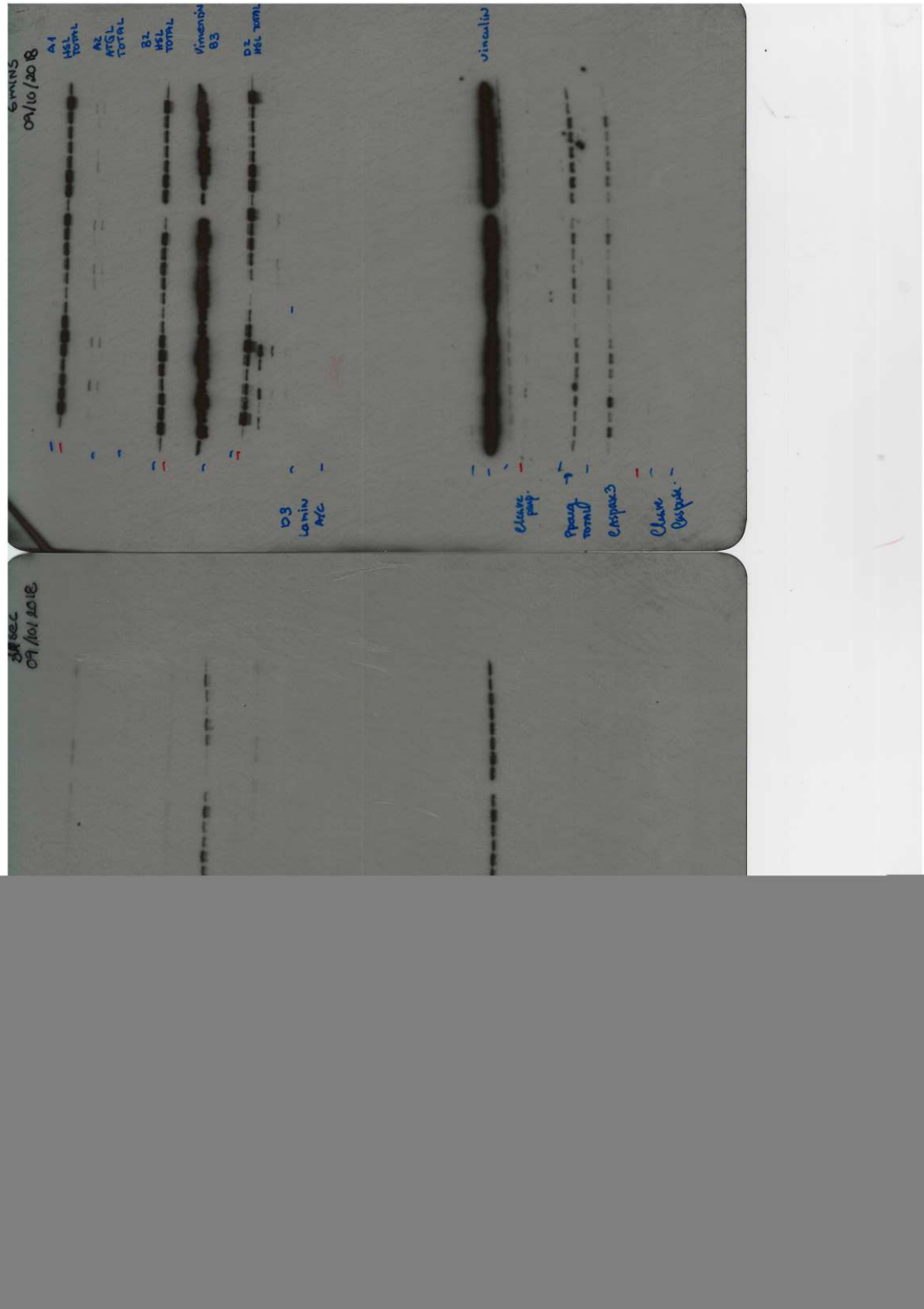


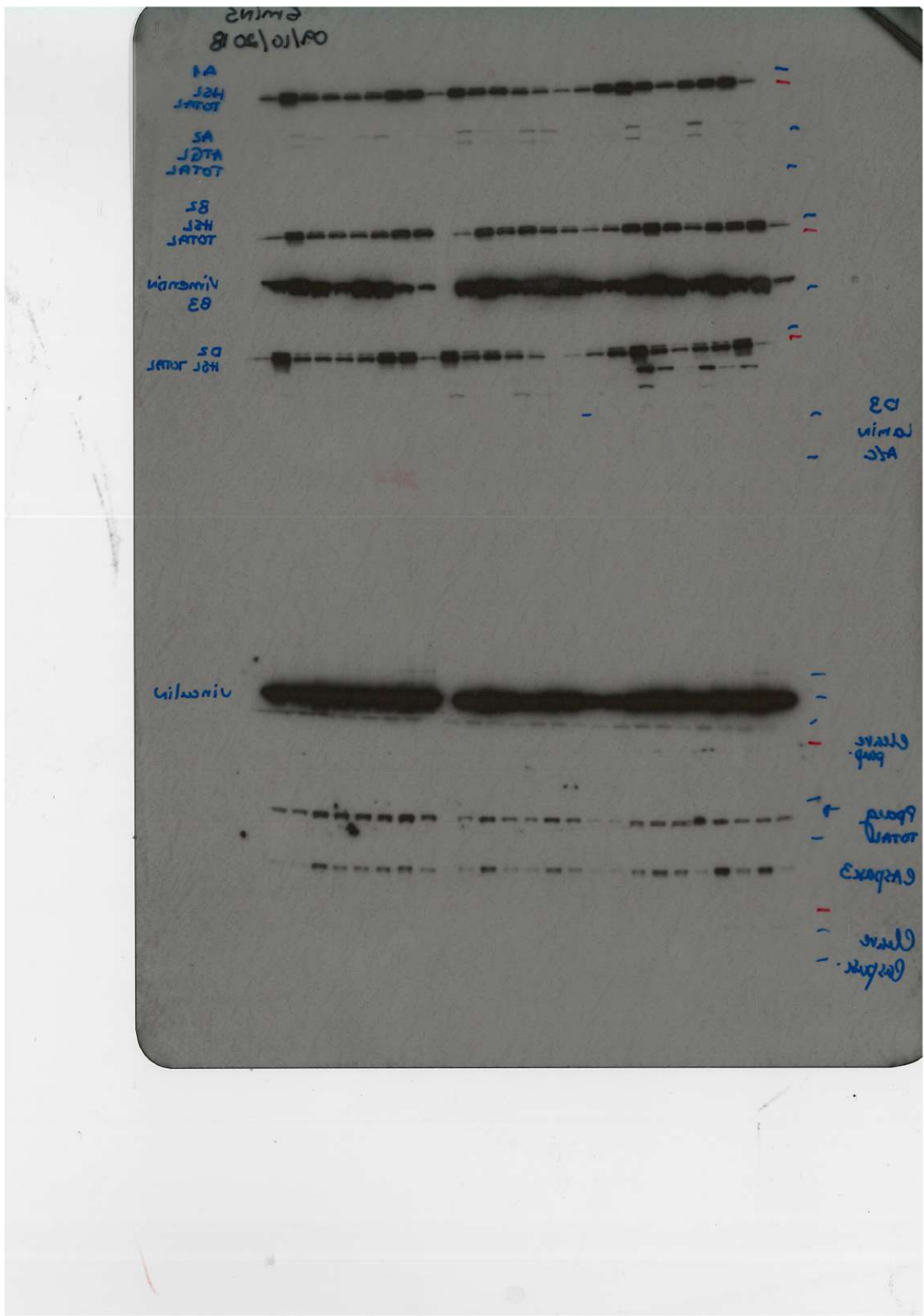




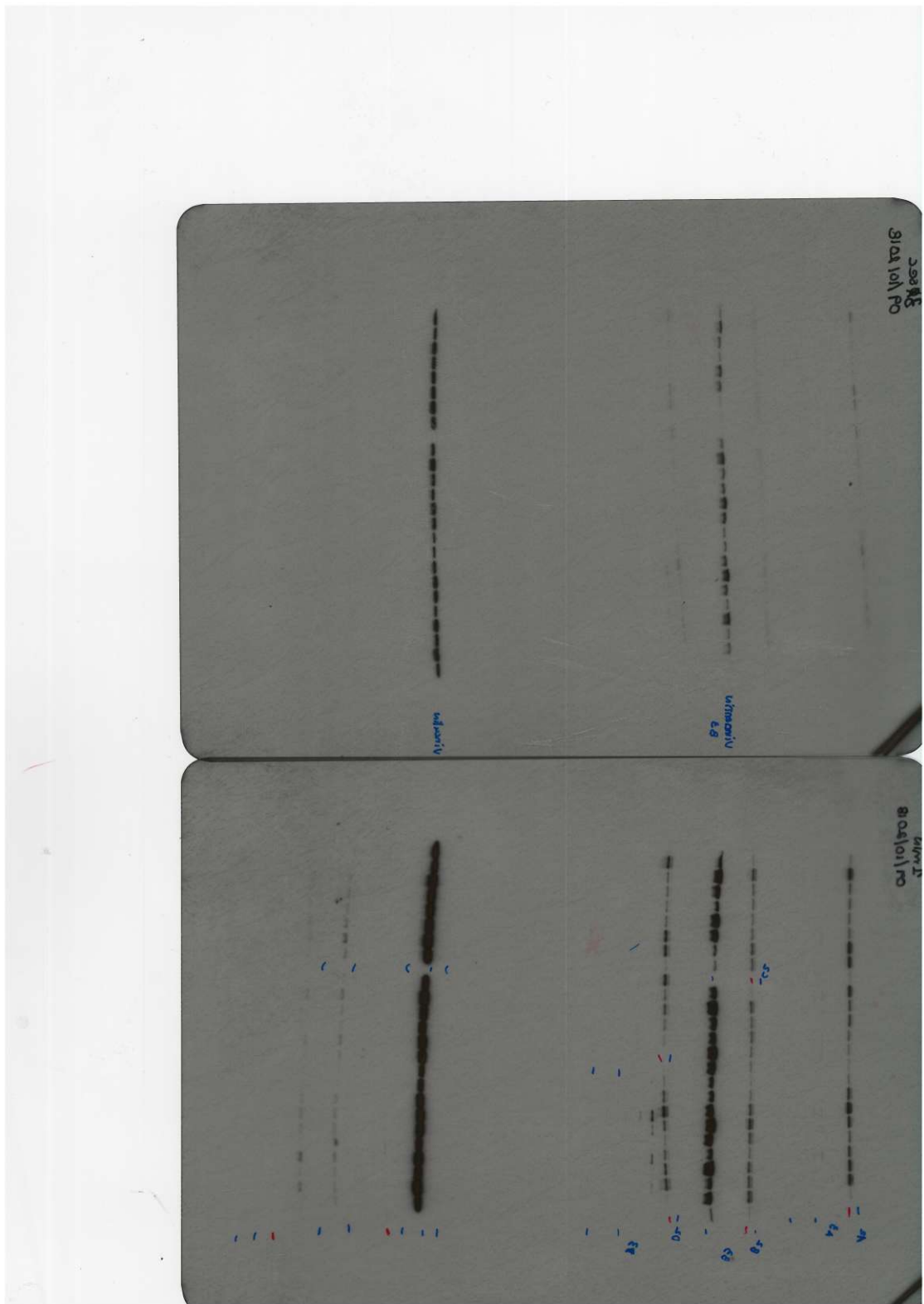


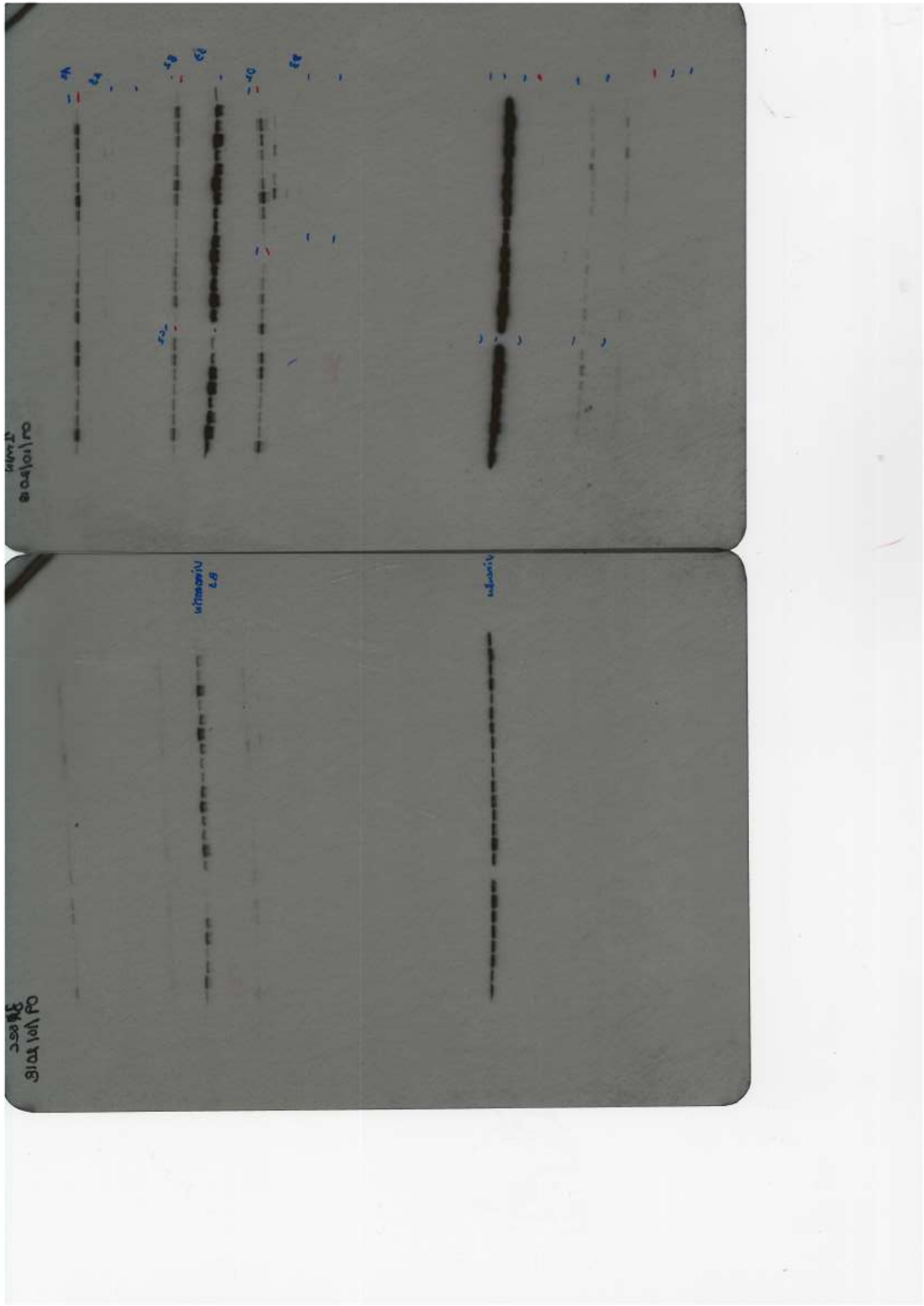


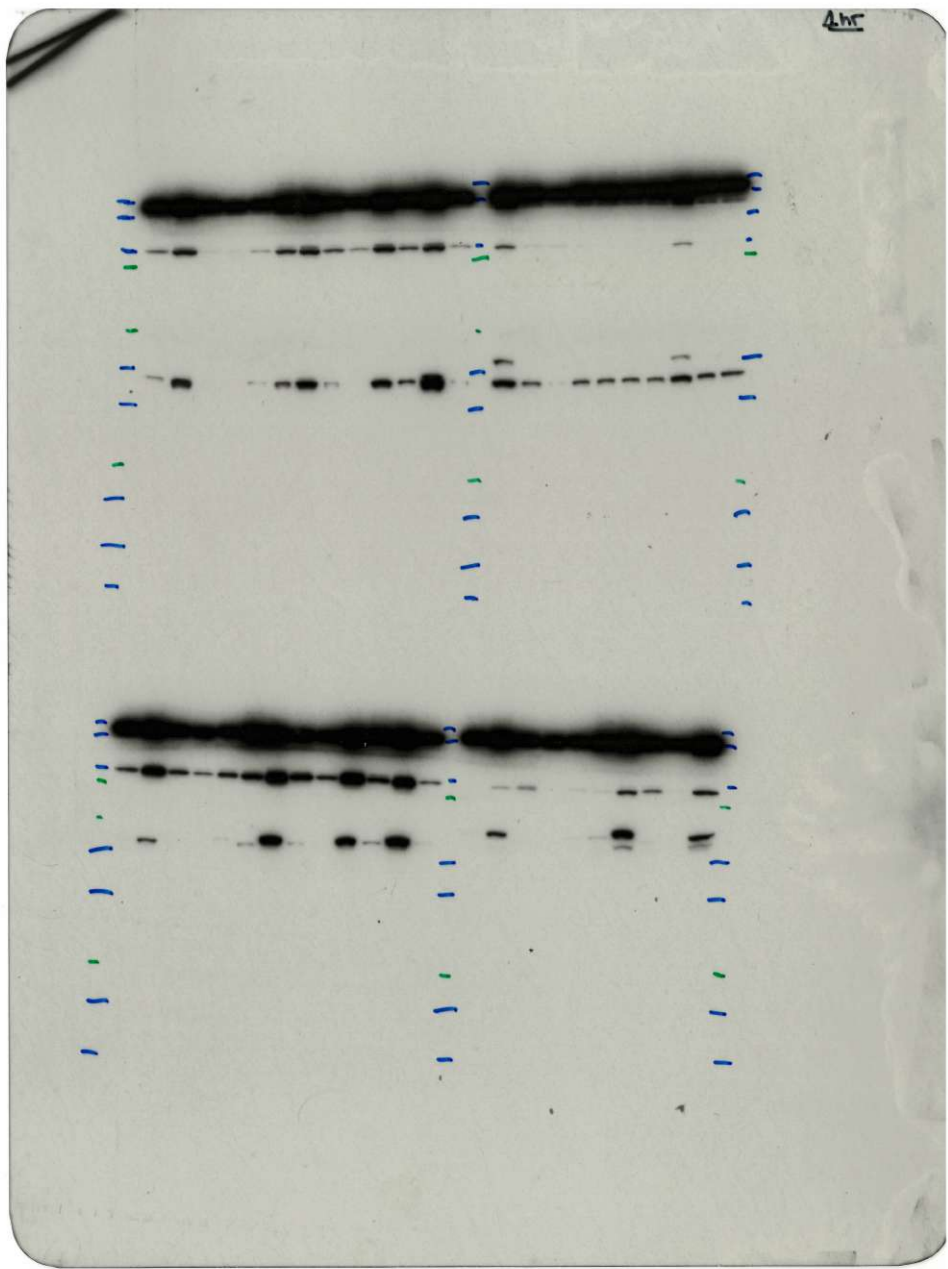


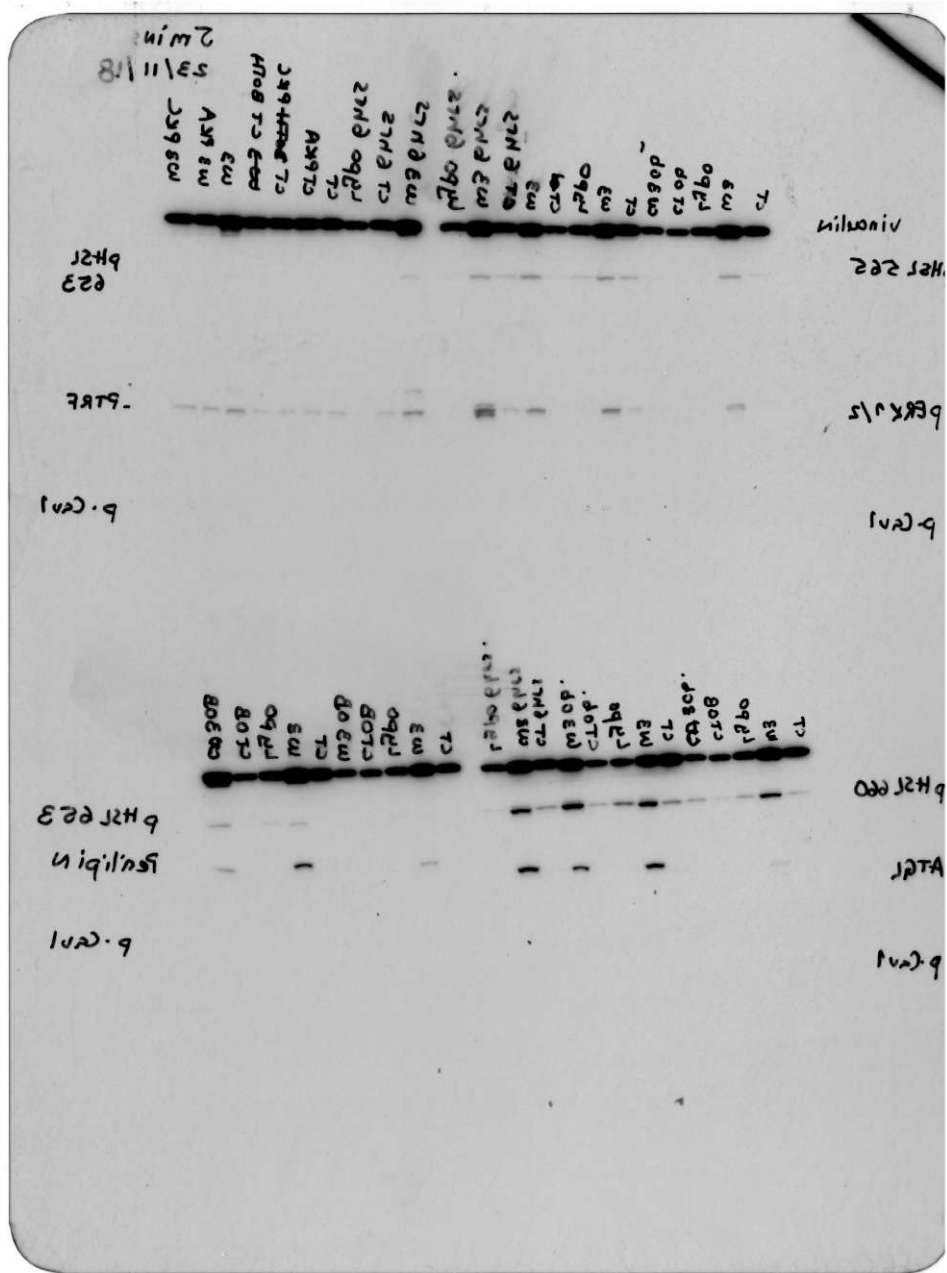






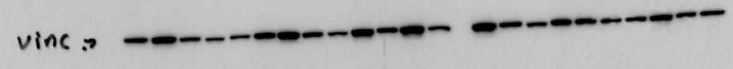






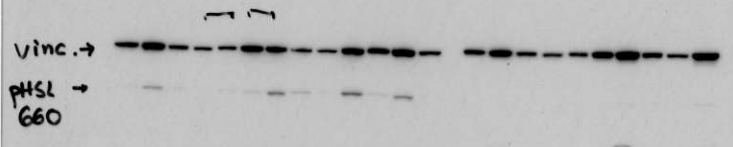
Imu  
23/11/18

vinc →



A Western blot image showing a single row of five dark bands. The bands are of similar intensity and are connected by a dashed line. The label 'vinc →' is positioned to the left of the first band.

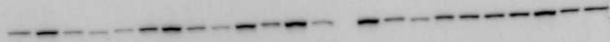
vinc →  
pHSL →  
G60



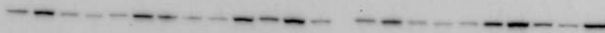
A Western blot image showing three rows of five bands each. The top row is labeled 'vinc →', the middle row 'pHSL →', and the bottom row 'G60'. The bands in the top row are the most prominent. The middle row has bands of moderate intensity, and the bottom row has the faintest bands. A dashed line connects the bands in each row. There are some small handwritten marks above the top row of bands.

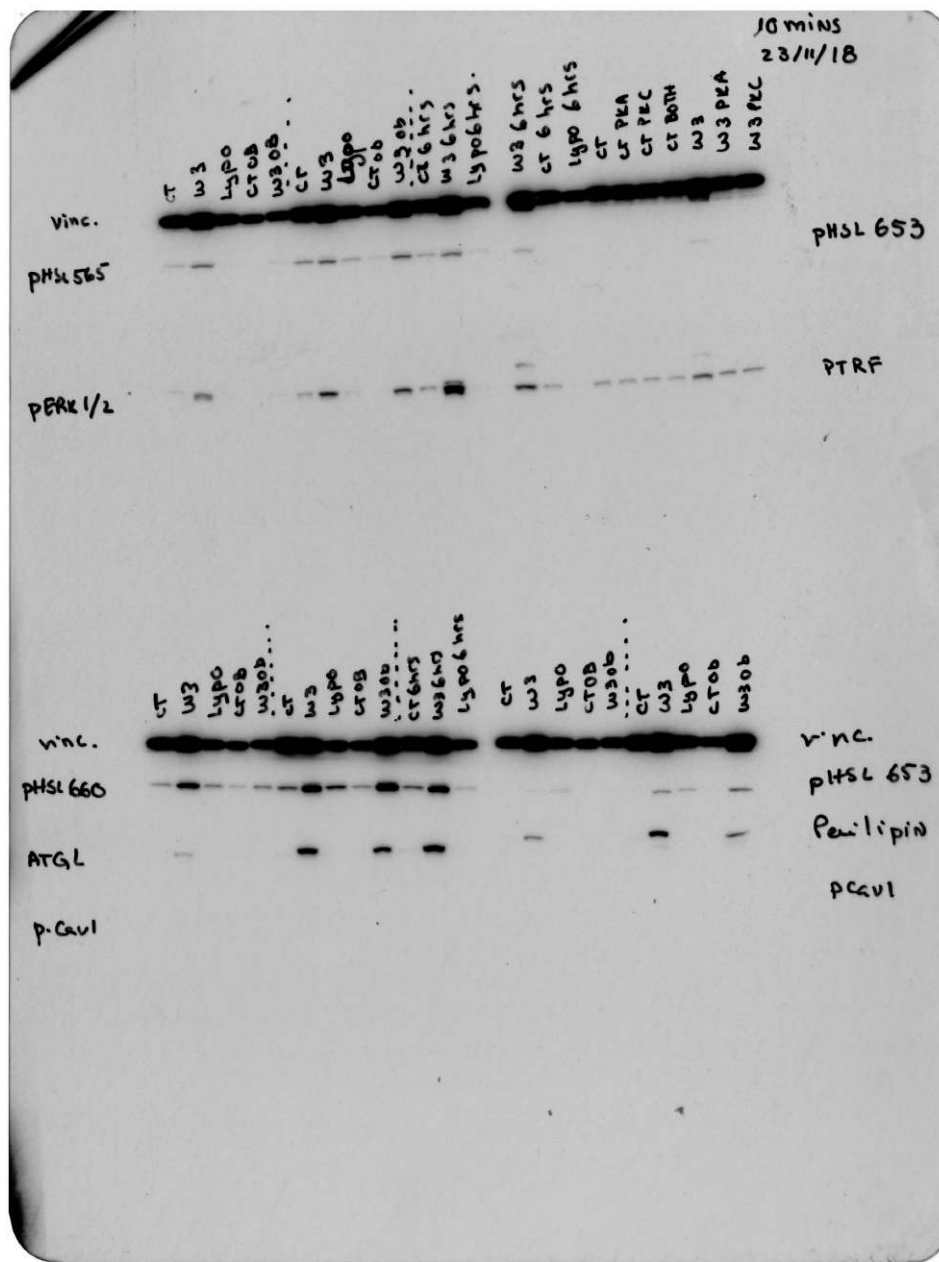
20 seconds  
23 / 11 / 2018

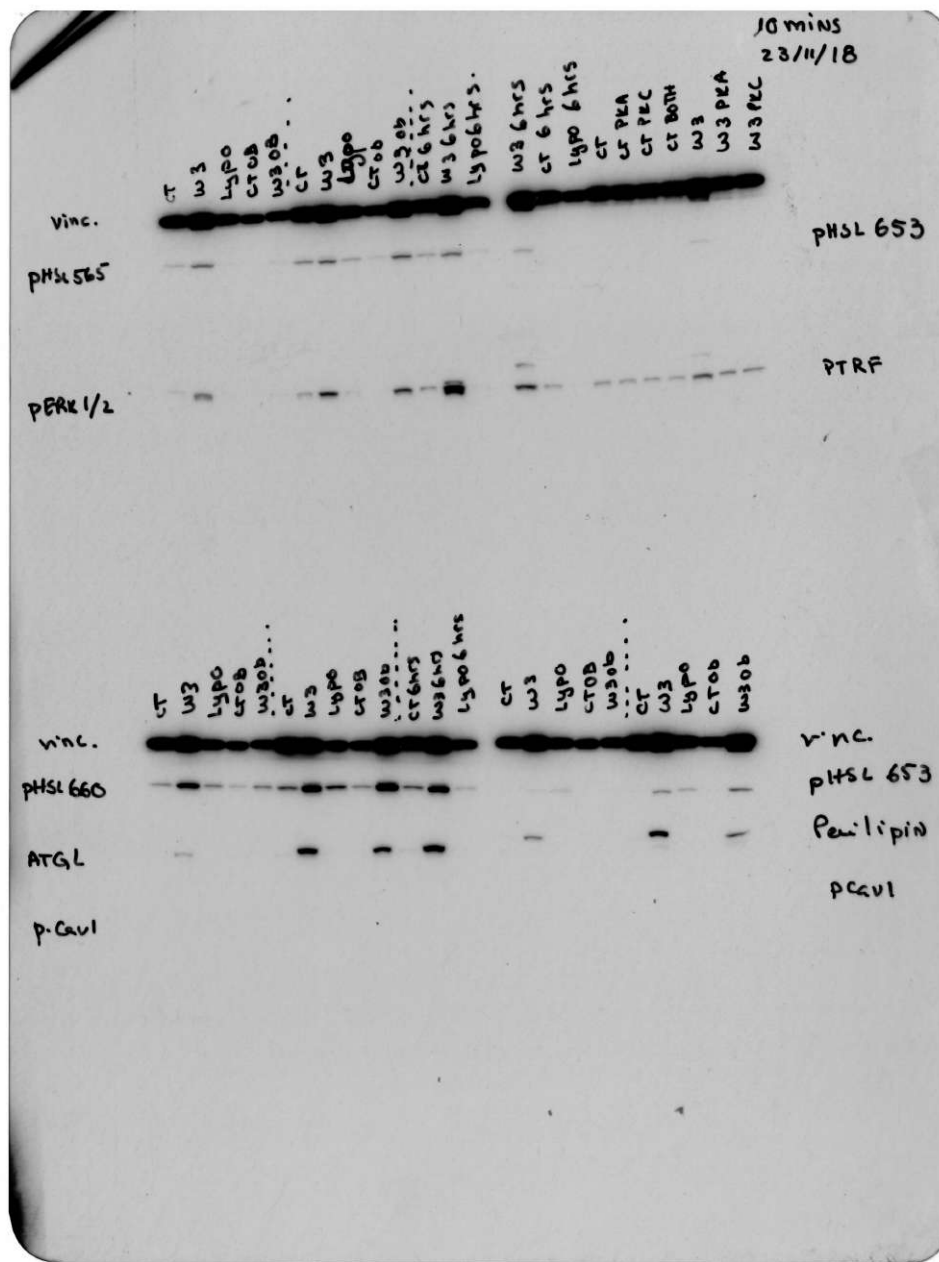
vinc.



vinc.

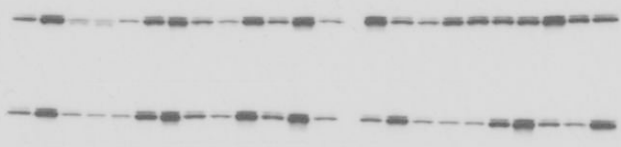
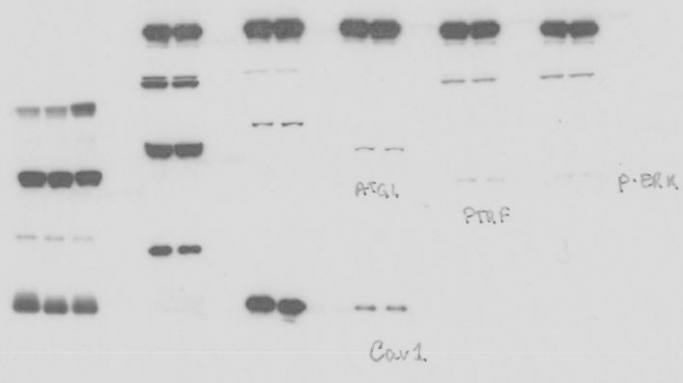








19-12-18  
Anabela  
Smirns





# **Appendix C**

## **Permissions**

<b>SPRINGER NATURE LICENSE TERMS AND CONDITIONS</b>	
Jun 29, 2019	
<p>This Agreement between Imperial College London -- Anabela Areias ("You") and Springer Nature ("Springer Nature") consists of your license details and the terms and conditions provided by Springer Nature and Copyright Clearance Center.</p>	
License Number	4617891309822
License date	Jun 28, 2019
Licensed Content Publisher	Springer Nature
Licensed Content Publication	Nature Reviews Disease Primers
Licensed Content Title	Obesity
Licensed Content Author	Pedro González-Muniesa, Miguel-Angel Martínez-González, Frank B. Hu, Jean-Pierre Després, Yuji Matsuzawa et al.
Licensed Content Date	Jun 15, 2017
Licensed Content Volume	3
Type of Use	Thesis/Dissertation
Requestor type	academic/university or research institute
Format	electronic
Portion	figures/tables/illustrations
Number of figures/tables/illustrations	1
High-res required	no
Will you be translating?	no
Circulation/distribution	<501
Author of this Springer Nature content	no
Title	Mechanobiology of adipocytes
Institution name	Imperial College London
Expected presentation date	Aug 2019
Portions	Figure 2
Requestor Location	Imperial College London South Kensington Campus Prince Consort Road  London, SW7 2AZ United Kingdom Attn: Anabela Areias
Total	0.00 GBP
Terms and Conditions	

## Springer Nature Customer Service Centre GmbH Terms and Conditions

This agreement sets out the terms and conditions of the licence (the **Licence**) between you and **Springer Nature Customer Service Centre GmbH** (the **Licensor**). By clicking 'accept' and completing the transaction for the material (**Licensed Material**), you also confirm your acceptance of these terms and conditions.

### 1. Grant of Licence

- 1. 1.** The Licensor grants you a personal, non-exclusive, non-transferable, world-wide licence to reproduce the Licensed Material for the purpose specified in your order only. Licences are granted for the specific use requested in the order and for no other use, subject to the conditions below.
- 1. 2.** The Licensor warrants that it has, to the best of its knowledge, the rights to license reuse of the Licensed Material. However, you should ensure that the material you are requesting is original to the Licensor and does not carry the copyright of another entity (as credited in the published version).
- 1. 3.** If the credit line on any part of the material you have requested indicates that it was reprinted or adapted with permission from another source, then you should also seek permission from that source to reuse the material.

### 2. Scope of Licence

- 2. 1.** You may only use the Licensed Content in the manner and to the extent permitted by these Ts&Cs and any applicable laws.
- 2. 2.** A separate licence may be required for any additional use of the Licensed Material, e.g. where a licence has been purchased for print only use, separate permission must be obtained for electronic re-use. Similarly, a licence is only valid in the language selected and does not apply for editions in other languages unless additional translation rights have been granted separately in the licence. Any content owned by third parties are expressly excluded from the licence.
- 2. 3.** Similarly, rights for additional components such as custom editions and derivatives require additional permission and may be subject to an additional fee. Please apply to [Journalpermissions@springernature.com](mailto:Journalpermissions@springernature.com) / [bookpermissions@springernature.com](mailto:bookpermissions@springernature.com) for these rights.
- 2. 4.** Where permission has been granted **free of charge** for material in print, permission may also be granted for any electronic version of that work, provided that the material is incidental to your work as a whole and that the electronic version is essentially equivalent to, or substitutes for, the print version.
- 2. 5.** An alternative scope of licence may apply to signatories of the [STM Permissions Guidelines](#), as amended from time to time.

### 3. Duration of Licence

- 3. 1.** A licence for is valid from the date of purchase ('Licence Date') at the end of the relevant period in the below table:

Scope of Licence	Duration of Licence
Post on a website	12 months
Presentations	12 months
Books and journals	Lifetime of the edition in the language purchased

#### 4. Acknowledgement

**4. 1.** The Licensor's permission must be acknowledged next to the Licenced Material in print. In electronic form, this acknowledgement must be visible at the same time as the figures/tables/illustrations or abstract, and must be hyperlinked to the journal/book's homepage. Our required acknowledgement format is in the Appendix below.

#### 5. Restrictions on use

**5. 1.** Use of the Licensed Material may be permitted for incidental promotional use and minor editing privileges e.g. minor adaptations of single figures, changes of format, colour and/or style where the adaptation is credited as set out in Appendix 1 below. Any other changes including but not limited to, cropping, adapting, omitting material that affect the meaning, intention or moral rights of the author are strictly prohibited.

**5. 2.** You must not use any Licensed Material as part of any design or trademark.

**5. 3.** Licensed Material may be used in Open Access Publications (OAP) before publication by Springer Nature, but any Licensed Material must be removed from OAP sites prior to final publication.

#### 6. Ownership of Rights

**6. 1.** Licensed Material remains the property of either Licensor or the relevant third party and any rights not explicitly granted herein are expressly reserved.

#### 7. Warranty

IN NO EVENT SHALL LICENSOR BE LIABLE TO YOU OR ANY OTHER PARTY OR ANY OTHER PERSON OR FOR ANY SPECIAL, CONSEQUENTIAL, INCIDENTAL OR INDIRECT DAMAGES, HOWEVER CAUSED, ARISING OUT OF OR IN CONNECTION WITH THE DOWNLOADING, VIEWING OR USE OF THE MATERIALS REGARDLESS OF THE FORM OF ACTION, WHETHER FOR BREACH OF CONTRACT, BREACH OF WARRANTY, TORT, NEGLIGENCE, INFRINGEMENT OR OTHERWISE (INCLUDING, WITHOUT LIMITATION, DAMAGES BASED ON LOSS OF PROFITS, DATA, FILES, USE, BUSINESS OPPORTUNITY OR CLAIMS OF THIRD PARTIES), AND WHETHER OR NOT THE PARTY HAS BEEN ADVISED OF THE POSSIBILITY OF SUCH DAMAGES. THIS LIMITATION SHALL APPLY NOTWITHSTANDING ANY FAILURE OF ESSENTIAL PURPOSE OF ANY LIMITED REMEDY PROVIDED HEREIN.

#### 8. Limitations

**8. 1. BOOKS ONLY:** Where '**reuse in a dissertation/thesis**' has been selected the following terms apply: Print rights of the final author's accepted manuscript (for clarity, NOT the published version) for up to 100 copies, electronic rights for use only on a personal website or institutional repository as defined by the Sherpa guideline ([www.sherpa.ac.uk/romeo/](http://www.sherpa.ac.uk/romeo/)).

**9. Termination and Cancellation**

- 9. 1.** Licences will expire after the period shown in Clause 3 (above).
- 9. 2.** Licensee reserves the right to terminate the Licence in the event that payment is not received in full or if there has been a breach of this agreement by you.

**Appendix 1 – Acknowledgements:****For Journal Content:**

Reprinted by permission from [the Licensor]: [Journal Publisher (e.g. Nature/Springer/Palgrave)] [JOURNAL NAME] [REFERENCE CITATION (Article name, Author(s) Name), [COPYRIGHT] (year of publication)

**For Advance Online Publication papers:**

Reprinted by permission from [the Licensor]: [Journal Publisher (e.g. Nature/Springer/Palgrave)] [JOURNAL NAME] [REFERENCE CITATION (Article name, Author(s) Name), [COPYRIGHT] (year of publication), advance online publication, day month year (doi: 10.1038/sj.[JOURNAL ACRONYM].)

**For Adaptations/Translations:**

Adapted/Translated by permission from [the Licensor]: [Journal Publisher (e.g. Nature/Springer/Palgrave)] [JOURNAL NAME] [REFERENCE CITATION (Article name, Author(s) Name), [COPYRIGHT] (year of publication)

**Note: For any republication from the British Journal of Cancer, the following credit line style applies:**

Reprinted/adapted/translated by permission from [the Licensor]: on behalf of Cancer Research UK: : [Journal Publisher (e.g. Nature/Springer/Palgrave)] [JOURNAL NAME] [REFERENCE CITATION (Article name, Author(s) Name), [COPYRIGHT] (year of publication)

**For Advance Online Publication papers:**

Reprinted by permission from The [the Licensor]: on behalf of Cancer Research UK: [Journal Publisher (e.g. Nature/Springer/Palgrave)] [JOURNAL NAME] [REFERENCE CITATION (Article name, Author(s) Name), [COPYRIGHT] (year of publication), advance online publication, day month year (doi: 10.1038/sj.[JOURNAL ACRONYM])

**For Book content:**

Reprinted/adapted by permission from [the Licensor]: [Book Publisher (e.g. Palgrave Macmillan, Springer etc) [Book Title] by [Book author(s)] [COPYRIGHT] (year of publication)

**Other Conditions:**

Version 1.2

Questions? [customer@copyright.com](mailto:customer@copyright.com) or +1-855-239-3415 (toll free in the US) or +1-978-646-2777.





**ELSEVIER LICENSE  
TERMS AND CONDITIONS**

Jun 29, 2019

---

This Agreement between Imperial College London -- Anabela Areias ("You") and Elsevier ("Elsevier") consists of your license details and the terms and conditions provided by Elsevier and Copyright Clearance Center.

License Number	4617490947335
License date	Jun 28, 2019
Licensed Content Publisher	Elsevier
Licensed Content Publication	International Journal of Solids and Structures
Licensed Content Title	A micromechanical model for the Young's modulus of adipose tissue
Licensed Content Author	Kerstyn Comley, Norman A. Fleck
Licensed Content Date	Oct 15, 2010
Licensed Content Volume	47
Licensed Content Issue	21
Licensed Content Pages	9
Start Page	2982
End Page	2990
Type of Use	reuse in a thesis/dissertation
Intended publisher of new work	other
Portion	figures/tables/illustrations
Number of figures/tables/illustrations	1
Format	electronic
Are you the author of this Elsevier article?	No
Will you be translating?	No
Original figure numbers	Figure 6
Title of your thesis/dissertation	Mechanobiology of adipocytes
Publisher of new work	Imperial College London
Expected completion date	Aug 2019
Estimated size (number of pages)	1
Requestor Location	Imperial College London South Kensington Campus Prince Consort Road  London, SW7 2AZ United Kingdom Attn: Anabela Areias
Publisher Tax ID	GB 494 6272 12

Total

0.00 GBP

[Terms and Conditions](#)

### INTRODUCTION

1. The publisher for this copyrighted material is Elsevier. By clicking "accept" in connection with completing this licensing transaction, you agree that the following terms and conditions apply to this transaction (along with the Billing and Payment terms and conditions established by Copyright Clearance Center, Inc. ("CCC"), at the time that you opened your Rightslink account and that are available at any time at <http://myaccount.copyright.com>).

### GENERAL TERMS

2. Elsevier hereby grants you permission to reproduce the aforementioned material subject to the terms and conditions indicated.

3. Acknowledgement: If any part of the material to be used (for example, figures) has appeared in our publication with credit or acknowledgement to another source, permission must also be sought from that source. If such permission is not obtained then that material may not be included in your publication/copies. Suitable acknowledgement to the source must be made, either as a footnote or in a reference list at the end of your publication, as follows:

"Reprinted from Publication title, Vol /edition number, Author(s), Title of article / title of chapter, Pages No., Copyright (Year), with permission from Elsevier [OR APPLICABLE SOCIETY COPYRIGHT OWNER]." Also Lancet special credit - "Reprinted from The Lancet, Vol. number, Author(s), Title of article, Pages No., Copyright (Year), with permission from Elsevier."

4. Reproduction of this material is confined to the purpose and/or media for which permission is hereby given.

5. Altering/Modifying Material: Not Permitted. However figures and illustrations may be altered/adapted minimally to serve your work. Any other abbreviations, additions, deletions and/or any other alterations shall be made only with prior written authorization of Elsevier Ltd. (Please contact Elsevier at [permissions@elsevier.com](mailto:permissions@elsevier.com)). No modifications can be made to any Lancet figures/tables and they must be reproduced in full.

6. If the permission fee for the requested use of our material is waived in this instance, please be advised that your future requests for Elsevier materials may attract a fee.

7. Reservation of Rights: Publisher reserves all rights not specifically granted in the combination of (i) the license details provided by you and accepted in the course of this licensing transaction, (ii) these terms and conditions and (iii) CCC's Billing and Payment terms and conditions.

8. License Contingent Upon Payment: While you may exercise the rights licensed immediately upon issuance of the license at the end of the licensing process for the transaction, provided that you have disclosed complete and accurate details of your proposed use, no license is finally effective unless and until full payment is received from you (either by publisher or by CCC) as provided in CCC's Billing and Payment terms and conditions. If full payment is not received on a timely basis, then any license preliminarily granted shall be deemed automatically revoked and shall be void as if never granted. Further, in the event that you breach any of these terms and conditions or any of CCC's Billing and Payment terms and conditions, the license is automatically revoked and shall be void as if never granted. Use of materials as described in a revoked license, as well as any use of the materials beyond the scope of an unrevoked license, may constitute copyright infringement and publisher reserves the right to take any and all action to protect its copyright in the materials.

9. Warranties: Publisher makes no representations or warranties with respect to the licensed material.

10. Indemnity: You hereby indemnify and agree to hold harmless publisher and CCC, and their respective officers, directors, employees and agents, from and against any and all

claims arising out of your use of the licensed material other than as specifically authorized pursuant to this license.

11. **No Transfer of License:** This license is personal to you and may not be sublicensed, assigned, or transferred by you to any other person without publisher's written permission.

12. **No Amendment Except in Writing:** This license may not be amended except in a writing signed by both parties (or, in the case of publisher, by CCC on publisher's behalf).

13. **Objection to Contrary Terms:** Publisher hereby objects to any terms contained in any purchase order, acknowledgment, check endorsement or other writing prepared by you, which terms are inconsistent with these terms and conditions or CCC's Billing and Payment terms and conditions. These terms and conditions, together with CCC's Billing and Payment terms and conditions (which are incorporated herein), comprise the entire agreement between you and publisher (and CCC) concerning this licensing transaction. In the event of any conflict between your obligations established by these terms and conditions and those established by CCC's Billing and Payment terms and conditions, these terms and conditions shall control.

14. **Revocation:** Elsevier or Copyright Clearance Center may deny the permissions described in this License at their sole discretion, for any reason or no reason, with a full refund payable to you. Notice of such denial will be made using the contact information provided by you. Failure to receive such notice will not alter or invalidate the denial. In no event will Elsevier or Copyright Clearance Center be responsible or liable for any costs, expenses or damage incurred by you as a result of a denial of your permission request, other than a refund of the amount(s) paid by you to Elsevier and/or Copyright Clearance Center for denied permissions.

#### LIMITED LICENSE

The following terms and conditions apply only to specific license types:

15. **Translation:** This permission is granted for non-exclusive world **English** rights only unless your license was granted for translation rights. If you licensed translation rights you may only translate this content into the languages you requested. A professional translator must perform all translations and reproduce the content word for word preserving the integrity of the article.

16. **Posting licensed content on any Website:** The following terms and conditions apply as follows: Licensing material from an Elsevier journal: All content posted to the web site must maintain the copyright information line on the bottom of each image; A hyper-text must be included to the Homepage of the journal from which you are licensing at <http://www.sciencedirect.com/science/journal/xxxx> or the Elsevier homepage for books at <http://www.elsevier.com>; Central Storage: This license does not include permission for a scanned version of the material to be stored in a central repository such as that provided by Heron/XanEdu.

Licensing material from an Elsevier book: A hyper-text link must be included to the Elsevier homepage at <http://www.elsevier.com>. All content posted to the web site must maintain the copyright information line on the bottom of each image.

**Posting licensed content on Electronic reserve:** In addition to the above the following clauses are applicable: The web site must be password-protected and made available only to bona fide students registered on a relevant course. This permission is granted for 1 year only. You may obtain a new license for future website posting.

17. **For journal authors:** the following clauses are applicable in addition to the above:

#### Preprints:

A preprint is an author's own write-up of research results and analysis, it has not been peer-reviewed, nor has it had any other value added to it by a publisher (such as formatting, copyright, technical enhancement etc.).

Authors can share their preprints anywhere at any time. Preprints should not be added to or enhanced in any way in order to appear more like, or to substitute for, the final versions of

articles however authors can update their preprints on arXiv or RePEc with their Accepted Author Manuscript (see below).

If accepted for publication, we encourage authors to link from the preprint to their formal publication via its DOI. Millions of researchers have access to the formal publications on ScienceDirect, and so links will help users to find, access, cite and use the best available version. Please note that Cell Press, The Lancet and some society-owned have different preprint policies. Information on these policies is available on the journal homepage.

**Accepted Author Manuscripts:** An accepted author manuscript is the manuscript of an article that has been accepted for publication and which typically includes author-incorporated changes suggested during submission, peer review and editor-author communications.

Authors can share their accepted author manuscript:

- immediately
  - via their non-commercial person homepage or blog
  - by updating a preprint in arXiv or RePEc with the accepted manuscript
  - via their research institute or institutional repository for internal institutional uses or as part of an invitation-only research collaboration work-group
  - directly by providing copies to their students or to research collaborators for their personal use
  - for private scholarly sharing as part of an invitation-only work group on commercial sites with which Elsevier has an agreement
- After the embargo period
  - via non-commercial hosting platforms such as their institutional repository
  - via commercial sites with which Elsevier has an agreement

In all cases accepted manuscripts should:

- link to the formal publication via its DOI
- bear a CC-BY-NC-ND license - this is easy to do
- if aggregated with other manuscripts, for example in a repository or other site, be shared in alignment with our hosting policy not be added to or enhanced in any way to appear more like, or to substitute for, the published journal article.

**Published journal article (JPA):** A published journal article (JPA) is the definitive final record of published research that appears or will appear in the journal and embodies all value-adding publishing activities including peer review co-ordination, copy-editing, formatting, (if relevant) pagination and online enrichment.

Policies for sharing publishing journal articles differ for subscription and gold open access articles:

**Subscription Articles:** If you are an author, please share a link to your article rather than the full-text. Millions of researchers have access to the formal publications on ScienceDirect, and so links will help your users to find, access, cite, and use the best available version.

Theses and dissertations which contain embedded PJAs as part of the formal submission can be posted publicly by the awarding institution with DOI links back to the formal publications on ScienceDirect.

If you are affiliated with a library that subscribes to ScienceDirect you have additional private sharing rights for others' research accessed under that agreement. This includes use for classroom teaching and internal training at the institution (including use in course packs and courseware programs), and inclusion of the article for grant funding purposes.

**Gold Open Access Articles:** May be shared according to the author-selected end-user license and should contain a [CrossMark logo](#), the end user license, and a DOI link to the formal publication on ScienceDirect.

Please refer to Elsevier's [posting policy](#) for further information.

18. **For book authors** the following clauses are applicable in addition to the above: Authors are permitted to place a brief summary of their work online only. You are not allowed to download and post the published electronic version of your chapter, nor may you scan the printed edition to create an electronic version. **Posting to a repository:** Authors are permitted to post a summary of their chapter only in their institution's repository.

19. **Thesis/Dissertation:** If your license is for use in a thesis/dissertation your thesis may be submitted to your institution in either print or electronic form. Should your thesis be published commercially, please reapply for permission. These requirements include permission for the Library and Archives of Canada to supply single copies, on demand, of the complete thesis and include permission for Proquest/UMI to supply single copies, on demand, of the complete thesis. Should your thesis be published commercially, please reapply for permission. Theses and dissertations which contain embedded PJAs as part of the formal submission can be posted publicly by the awarding institution with DOI links back to the formal publications on ScienceDirect.

#### **Elsevier Open Access Terms and Conditions**

You can publish open access with Elsevier in hundreds of open access journals or in nearly 2000 established subscription journals that support open access publishing. Permitted third party re-use of these open access articles is defined by the author's choice of Creative Commons user license. See our [open access license policy](#) for more information.

#### **Terms & Conditions applicable to all Open Access articles published with Elsevier:**

Any reuse of the article must not represent the author as endorsing the adaptation of the article nor should the article be modified in such a way as to damage the author's honour or reputation. If any changes have been made, such changes must be clearly indicated.

The author(s) must be appropriately credited and we ask that you include the end user license and a DOI link to the formal publication on ScienceDirect.

If any part of the material to be used (for example, figures) has appeared in our publication with credit or acknowledgement to another source it is the responsibility of the user to ensure their reuse complies with the terms and conditions determined by the rights holder.

#### **Additional Terms & Conditions applicable to each Creative Commons user license:**

**CC BY:** The CC-BY license allows users to copy, to create extracts, abstracts and new works from the Article, to alter and revise the Article and to make commercial use of the Article (including reuse and/or resale of the Article by commercial entities), provided the user gives appropriate credit (with a link to the formal publication through the relevant DOI), provides a link to the license, indicates if changes were made and the licensor is not represented as endorsing the use made of the work. The full details of the license are available at <http://creativecommons.org/licenses/by/4.0>.

**CC BY NC SA:** The CC BY-NC-SA license allows users to copy, to create extracts, abstracts and new works from the Article, to alter and revise the Article, provided this is not done for commercial purposes, and that the user gives appropriate credit (with a link to the formal publication through the relevant DOI), provides a link to the license, indicates if changes were made and the licensor is not represented as endorsing the use made of the work. Further, any new works must be made available on the same conditions. The full details of the license are available at <http://creativecommons.org/licenses/by-nc-sa/4.0>.

**CC BY NC ND:** The CC BY-NC-ND license allows users to copy and distribute the Article, provided this is not done for commercial purposes and further does not permit distribution of the Article if it is changed or edited in any way, and provided the user gives appropriate credit (with a link to the formal publication through the relevant DOI), provides a link to the license, and that the licensor is not represented as endorsing the use made of the work. The full details of the license are available at <http://creativecommons.org/licenses/by-nc-nd/4.0>.

Any commercial reuse of Open Access articles published with a CC BY NC SA or CC BY NC ND license requires permission from Elsevier and will be subject to a fee.

Commercial reuse includes:

- Associating advertising with the full text of the Article
- Charging fees for document delivery or access
- Article aggregation
- Systematic distribution via e-mail lists or share buttons

Posting or linking by commercial companies for use by customers of those companies.

**20. Other Conditions:**

v1.9

**Questions? [customer@copyright.com](mailto:customer@copyright.com) or +1-855-239-3415 (toll free in the US) or +1-978-646-2777.**



**ELSEVIER LICENSE  
TERMS AND CONDITIONS**

Jun 29, 2019

---

This Agreement between Imperial College London -- Anabela Areias ("You") and Elsevier ("Elsevier") consists of your license details and the terms and conditions provided by Elsevier and Copyright Clearance Center.

License Number	4616150921659
License date	Jun 25, 2019
Licensed Content Publisher	Elsevier
Licensed Content Publication	Trends in Cell Biology
Licensed Content Title	Microenvironmental Control of Adipocyte Fate and Function
Licensed Content Author	Benjamin D. Pope,Curtis R. Warren,Kevin Kit Parker,Chad A. Cowan
Licensed Content Date	Oct 1, 2016
Licensed Content Volume	26
Licensed Content Issue	10
Licensed Content Pages	11
Start Page	745
End Page	755
Type of Use	reuse in a thesis/dissertation
Intended publisher of new work	other
Portion	figures/tables/illustrations
Number of figures/tables/illustrations	1
Format	electronic
Are you the author of this Elsevier article?	No
Will you be translating?	No
Original figure numbers	table 1
Title of your thesis/dissertation	Mechanobiology of adipocytes
Publisher of new work	Imperial College London
Expected completion date	Aug 2019
Estimated size (number of pages)	1
Requestor Location	Imperial College London South Kensington Campus Prince Consort Road  London, SW7 2AZ United Kingdom Attn: Anabela Areias
Publisher Tax ID	GB 494 6272 12

Total 0.00 USD  
Terms and Conditions

### INTRODUCTION

1. The publisher for this copyrighted material is Elsevier. By clicking "accept" in connection with completing this licensing transaction, you agree that the following terms and conditions apply to this transaction (along with the Billing and Payment terms and conditions established by Copyright Clearance Center, Inc. ("CCC"), at the time that you opened your Rightslink account and that are available at any time at <http://myaccount.copyright.com>).

### GENERAL TERMS

2. Elsevier hereby grants you permission to reproduce the aforementioned material subject to the terms and conditions indicated.

3. Acknowledgement: If any part of the material to be used (for example, figures) has appeared in our publication with credit or acknowledgement to another source, permission must also be sought from that source. If such permission is not obtained then that material may not be included in your publication/copies. Suitable acknowledgement to the source must be made, either as a footnote or in a reference list at the end of your publication, as follows:

"Reprinted from Publication title, Vol /edition number, Author(s), Title of article / title of chapter, Pages No., Copyright (Year), with permission from Elsevier [OR APPLICABLE SOCIETY COPYRIGHT OWNER]." Also Lancet special credit - "Reprinted from The Lancet, Vol. number, Author(s), Title of article, Pages No., Copyright (Year), with permission from Elsevier."

4. Reproduction of this material is confined to the purpose and/or media for which permission is hereby given.

5. Altering/Modifying Material: Not Permitted. However figures and illustrations may be altered/adapted minimally to serve your work. Any other abbreviations, additions, deletions and/or any other alterations shall be made only with prior written authorization of Elsevier Ltd. (Please contact Elsevier at [permissions@elsevier.com](mailto:permissions@elsevier.com)). No modifications can be made to any Lancet figures/tables and they must be reproduced in full.

6. If the permission fee for the requested use of our material is waived in this instance, please be advised that your future requests for Elsevier materials may attract a fee.

7. Reservation of Rights: Publisher reserves all rights not specifically granted in the combination of (i) the license details provided by you and accepted in the course of this licensing transaction, (ii) these terms and conditions and (iii) CCC's Billing and Payment terms and conditions.

8. License Contingent Upon Payment: While you may exercise the rights licensed immediately upon issuance of the license at the end of the licensing process for the transaction, provided that you have disclosed complete and accurate details of your proposed use, no license is finally effective unless and until full payment is received from you (either by publisher or by CCC) as provided in CCC's Billing and Payment terms and conditions. If full payment is not received on a timely basis, then any license preliminarily granted shall be deemed automatically revoked and shall be void as if never granted. Further, in the event that you breach any of these terms and conditions or any of CCC's Billing and Payment terms and conditions, the license is automatically revoked and shall be void as if never granted. Use of materials as described in a revoked license, as well as any use of the materials beyond the scope of an unrevoked license, may constitute copyright infringement and publisher reserves the right to take any and all action to protect its copyright in the materials.

9. Warranties: Publisher makes no representations or warranties with respect to the licensed material.

10. Indemnity: You hereby indemnify and agree to hold harmless publisher and CCC, and their respective officers, directors, employees and agents, from and against any and all



claims arising out of your use of the licensed material other than as specifically authorized pursuant to this license.

11. **No Transfer of License:** This license is personal to you and may not be sublicensed, assigned, or transferred by you to any other person without publisher's written permission.

12. **No Amendment Except in Writing:** This license may not be amended except in a writing signed by both parties (or, in the case of publisher, by CCC on publisher's behalf).

13. **Objection to Contrary Terms:** Publisher hereby objects to any terms contained in any purchase order, acknowledgment, check endorsement or other writing prepared by you, which terms are inconsistent with these terms and conditions or CCC's Billing and Payment terms and conditions. These terms and conditions, together with CCC's Billing and Payment terms and conditions (which are incorporated herein), comprise the entire agreement between you and publisher (and CCC) concerning this licensing transaction. In the event of any conflict between your obligations established by these terms and conditions and those established by CCC's Billing and Payment terms and conditions, these terms and conditions shall control.

14. **Revocation:** Elsevier or Copyright Clearance Center may deny the permissions described in this License at their sole discretion, for any reason or no reason, with a full refund payable to you. Notice of such denial will be made using the contact information provided by you. Failure to receive such notice will not alter or invalidate the denial. In no event will Elsevier or Copyright Clearance Center be responsible or liable for any costs, expenses or damage incurred by you as a result of a denial of your permission request, other than a refund of the amount(s) paid by you to Elsevier and/or Copyright Clearance Center for denied permissions.

#### LIMITED LICENSE

The following terms and conditions apply only to specific license types:

15. **Translation:** This permission is granted for non-exclusive world **English** rights only unless your license was granted for translation rights. If you licensed translation rights you may only translate this content into the languages you requested. A professional translator must perform all translations and reproduce the content word for word preserving the integrity of the article.

16. **Posting licensed content on any Website:** The following terms and conditions apply as follows: Licensing material from an Elsevier journal: All content posted to the web site must maintain the copyright information line on the bottom of each image; A hyper-text must be included to the Homepage of the journal from which you are licensing at <http://www.sciencedirect.com/science/journal/xxxxx> or the Elsevier homepage for books at <http://www.elsevier.com>; Central Storage: This license does not include permission for a scanned version of the material to be stored in a central repository such as that provided by Heron/XanEdu.

Licensing material from an Elsevier book: A hyper-text link must be included to the Elsevier homepage at <http://www.elsevier.com>. All content posted to the web site must maintain the copyright information line on the bottom of each image.

**Posting licensed content on Electronic reserve:** In addition to the above the following clauses are applicable: The web site must be password-protected and made available only to bona fide students registered on a relevant course. This permission is granted for 1 year only. You may obtain a new license for future website posting.

17. **For journal authors:** the following clauses are applicable in addition to the above:

#### Preprints:

A preprint is an author's own write-up of research results and analysis, it has not been peer-reviewed, nor has it had any other value added to it by a publisher (such as formatting, copyright, technical enhancement etc.).

Authors can share their preprints anywhere at any time. Preprints should not be added to or enhanced in any way in order to appear more like, or to substitute for, the final versions of

articles however authors can update their preprints on arXiv or RePEc with their Accepted Author Manuscript (see below).

If accepted for publication, we encourage authors to link from the preprint to their formal publication via its DOI. Millions of researchers have access to the formal publications on ScienceDirect, and so links will help users to find, access, cite and use the best available version. Please note that Cell Press, The Lancet and some society-owned have different preprint policies. Information on these policies is available on the journal homepage.

**Accepted Author Manuscripts:** An accepted author manuscript is the manuscript of an article that has been accepted for publication and which typically includes author-incorporated changes suggested during submission, peer review and editor-author communications.

Authors can share their accepted author manuscript:

- immediately
  - via their non-commercial person homepage or blog
  - by updating a preprint in arXiv or RePEc with the accepted manuscript
  - via their research institute or institutional repository for internal institutional uses or as part of an invitation-only research collaboration work-group
  - directly by providing copies to their students or to research collaborators for their personal use
  - for private scholarly sharing as part of an invitation-only work group on commercial sites with which Elsevier has an agreement
- After the embargo period
  - via non-commercial hosting platforms such as their institutional repository
  - via commercial sites with which Elsevier has an agreement

In all cases accepted manuscripts should:

- link to the formal publication via its DOI
- bear a CC-BY-NC-ND license - this is easy to do
- if aggregated with other manuscripts, for example in a repository or other site, be shared in alignment with our hosting policy not be added to or enhanced in any way to appear more like, or to substitute for, the published journal article.

**Published journal article (JPA):** A published journal article (JPA) is the definitive final record of published research that appears or will appear in the journal and embodies all value-adding publishing activities including peer review co-ordination, copy-editing, formatting, (if relevant) pagination and online enrichment.

Policies for sharing publishing journal articles differ for subscription and gold open access articles:

**Subscription Articles:** If you are an author, please share a link to your article rather than the full-text. Millions of researchers have access to the formal publications on ScienceDirect, and so links will help your users to find, access, cite, and use the best available version.

Theses and dissertations which contain embedded PJAs as part of the formal submission can be posted publicly by the awarding institution with DOI links back to the formal publications on ScienceDirect.

If you are affiliated with a library that subscribes to ScienceDirect you have additional private sharing rights for others' research accessed under that agreement. This includes use for classroom teaching and internal training at the institution (including use in course packs and courseware programs), and inclusion of the article for grant funding purposes.

**Gold Open Access Articles:** May be shared according to the author-selected end-user license and should contain a [CrossMark logo](#), the end user license, and a DOI link to the formal publication on ScienceDirect.

Please refer to Elsevier's [posting policy](#) for further information.

18. **For book authors** the following clauses are applicable in addition to the above: Authors are permitted to place a brief summary of their work online only. You are not allowed to download and post the published electronic version of your chapter, nor may you scan the printed edition to create an electronic version. **Posting to a repository:** Authors are permitted to post a summary of their chapter only in their institution's repository.

19. **Thesis/Dissertation:** If your license is for use in a thesis/dissertation your thesis may be submitted to your institution in either print or electronic form. Should your thesis be published commercially, please reapply for permission. These requirements include permission for the Library and Archives of Canada to supply single copies, on demand, of the complete thesis and include permission for Proquest/UMI to supply single copies, on demand, of the complete thesis. Should your thesis be published commercially, please reapply for permission. Theses and dissertations which contain embedded PJAs as part of the formal submission can be posted publicly by the awarding institution with DOI links back to the formal publications on ScienceDirect.

#### **Elsevier Open Access Terms and Conditions**

You can publish open access with Elsevier in hundreds of open access journals or in nearly 2000 established subscription journals that support open access publishing. Permitted third party re-use of these open access articles is defined by the author's choice of Creative Commons user license. See our [open access license policy](#) for more information.

#### **Terms & Conditions applicable to all Open Access articles published with Elsevier:**

Any reuse of the article must not represent the author as endorsing the adaptation of the article nor should the article be modified in such a way as to damage the author's honour or reputation. If any changes have been made, such changes must be clearly indicated.

The author(s) must be appropriately credited and we ask that you include the end user license and a DOI link to the formal publication on ScienceDirect.

If any part of the material to be used (for example, figures) has appeared in our publication with credit or acknowledgement to another source it is the responsibility of the user to ensure their reuse complies with the terms and conditions determined by the rights holder.

#### **Additional Terms & Conditions applicable to each Creative Commons user license:**

**CC BY:** The CC-BY license allows users to copy, to create extracts, abstracts and new works from the Article, to alter and revise the Article and to make commercial use of the Article (including reuse and/or resale of the Article by commercial entities), provided the user gives appropriate credit (with a link to the formal publication through the relevant DOI), provides a link to the license, indicates if changes were made and the licensor is not represented as endorsing the use made of the work. The full details of the license are available at <http://creativecommons.org/licenses/by/4.0>.

**CC BY NC SA:** The CC BY-NC-SA license allows users to copy, to create extracts, abstracts and new works from the Article, to alter and revise the Article, provided this is not done for commercial purposes, and that the user gives appropriate credit (with a link to the formal publication through the relevant DOI), provides a link to the license, indicates if changes were made and the licensor is not represented as endorsing the use made of the work. Further, any new works must be made available on the same conditions. The full details of the license are available at <http://creativecommons.org/licenses/by-nc-sa/4.0>.

**CC BY NC ND:** The CC BY-NC-ND license allows users to copy and distribute the Article, provided this is not done for commercial purposes and further does not permit distribution of the Article if it is changed or edited in any way, and provided the user gives appropriate credit (with a link to the formal publication through the relevant DOI), provides a link to the license, and that the licensor is not represented as endorsing the use made of the work. The full details of the license are available at <http://creativecommons.org/licenses/by-nc-nd/4.0>.

Any commercial reuse of Open Access articles published with a CC BY NC SA or CC BY NC ND license requires permission from Elsevier and will be subject to a fee.

Commercial reuse includes:

- Associating advertising with the full text of the Article
- Charging fees for document delivery or access
- Article aggregation
- Systematic distribution via e-mail lists or share buttons

Posting or linking by commercial companies for use by customers of those companies.

**20. Other Conditions:**

v1.9

**Questions? [customer@copyright.com](mailto:customer@copyright.com) or +1-855-239-3415 (toll free in the US) or +1-978-646-2777.**



<b>SPRINGER NATURE LICENSE TERMS AND CONDITIONS</b>	
Jun 29, 2019	
This Agreement between Imperial College London -- Anabela Areias ("You") and Springer Nature ("Springer Nature") consists of your license details and the terms and conditions provided by Springer Nature and Copyright Clearance Center.	
License Number	4616160116373
License date	Jun 25, 2019
Licensed Content Publisher	Springer Nature
Licensed Content Publication	Intensive Care Medicine
Licensed Content Title	What is normal intra-abdominal pressure and how is it affected by positioning, body mass and positive end-expiratory pressure?
Licensed Content Author	B. L. De Keulenaer, J. J. De Waele, B. Powell et al
Licensed Content Date	Jan 1, 2009
Licensed Content Volume	35
Licensed Content Issue	6
Type of Use	Thesis/Dissertation
Requestor type	academic/university or research institute
Format	electronic
Portion	figures/tables/illustrations
Number of figures/tables/illustrations	1
Will you be translating?	no
Circulation/distribution	<501
Author of this Springer Nature content	no
Title	Mechanobiology of adipocytes
Institution name	Imperial College London
Expected presentation date	Aug 2019
Portions	Table 2
Requestor Location	Imperial College London South Kensington Campus Prince Consort Road  London, SW7 2AZ United Kingdom Attn: Anabela Areias
Total	0.00 GBP
Terms and Conditions	

### Springer Nature Customer Service Centre GmbH Terms and Conditions

This agreement sets out the terms and conditions of the licence (the **Licence**) between you and **Springer Nature Customer Service Centre GmbH** (the **Licensor**). By clicking 'accept' and completing the transaction for the material (**Licensed Material**), you also confirm your acceptance of these terms and conditions.

#### 1. Grant of Licence

- 1. 1.** The Licensor grants you a personal, non-exclusive, non-transferable, world-wide licence to reproduce the Licensed Material for the purpose specified in your order only. Licences are granted for the specific use requested in the order and for no other use, subject to the conditions below.
- 1. 2.** The Licensor warrants that it has, to the best of its knowledge, the rights to license reuse of the Licensed Material. However, you should ensure that the material you are requesting is original to the Licensor and does not carry the copyright of another entity (as credited in the published version).
- 1. 3.** If the credit line on any part of the material you have requested indicates that it was reprinted or adapted with permission from another source, then you should also seek permission from that source to reuse the material.

#### 2. Scope of Licence

- 2. 1.** You may only use the Licensed Content in the manner and to the extent permitted by these Ts&Cs and any applicable laws.
- 2. 2.** A separate licence may be required for any additional use of the Licensed Material, e.g. where a licence has been purchased for print only use, separate permission must be obtained for electronic re-use. Similarly, a licence is only valid in the language selected and does not apply for editions in other languages unless additional translation rights have been granted separately in the licence. Any content owned by third parties are expressly excluded from the licence.
- 2. 3.** Similarly, rights for additional components such as custom editions and derivatives require additional permission and may be subject to an additional fee. Please apply to [Journalpermissions@springernature.com](mailto:Journalpermissions@springernature.com) / [bookpermissions@springernature.com](mailto:bookpermissions@springernature.com) for these rights.
- 2. 4.** Where permission has been granted **free of charge** for material in print, permission may also be granted for any electronic version of that work, provided that the material is incidental to your work as a whole and that the electronic version is essentially equivalent to, or substitutes for, the print version.
- 2. 5.** An alternative scope of licence may apply to signatories of the [STM Permissions Guidelines](#), as amended from time to time.

#### 3. Duration of Licence

- 3. 1.** A licence for is valid from the date of purchase ('Licence Date') at the end of the relevant period in the below table:

Scope of Licence	Duration of Licence
Post on a website	12 months
Presentations	12 months
Books and journals	Lifetime of the edition in the language purchased

#### 4. Acknowledgement

**4. 1.** The Licensor's permission must be acknowledged next to the Licenced Material in print. In electronic form, this acknowledgement must be visible at the same time as the figures/tables/illustrations or abstract, and must be hyperlinked to the journal/book's homepage. Our required acknowledgement format is in the Appendix below.

#### 5. Restrictions on use

**5. 1.** Use of the Licensed Material may be permitted for incidental promotional use and minor editing privileges e.g. minor adaptations of single figures, changes of format, colour and/or style where the adaptation is credited as set out in Appendix 1 below. Any other changes including but not limited to, cropping, adapting, omitting material that affect the meaning, intention or moral rights of the author are strictly prohibited.

**5. 2.** You must not use any Licensed Material as part of any design or trademark.

**5. 3.** Licensed Material may be used in Open Access Publications (OAP) before publication by Springer Nature, but any Licensed Material must be removed from OAP sites prior to final publication.

#### 6. Ownership of Rights

**6. 1.** Licensed Material remains the property of either Licensor or the relevant third party and any rights not explicitly granted herein are expressly reserved.

#### 7. Warranty

IN NO EVENT SHALL LICENSOR BE LIABLE TO YOU OR ANY OTHER PARTY OR ANY OTHER PERSON OR FOR ANY SPECIAL, CONSEQUENTIAL, INCIDENTAL OR INDIRECT DAMAGES, HOWEVER CAUSED, ARISING OUT OF OR IN CONNECTION WITH THE DOWNLOADING, VIEWING OR USE OF THE MATERIALS REGARDLESS OF THE FORM OF ACTION, WHETHER FOR BREACH OF CONTRACT, BREACH OF WARRANTY, TORT, NEGLIGENCE, INFRINGEMENT OR OTHERWISE (INCLUDING, WITHOUT LIMITATION, DAMAGES BASED ON LOSS OF PROFITS, DATA, FILES, USE, BUSINESS OPPORTUNITY OR CLAIMS OF THIRD PARTIES), AND WHETHER OR NOT THE PARTY HAS BEEN ADVISED OF THE POSSIBILITY OF SUCH DAMAGES. THIS LIMITATION SHALL APPLY NOTWITHSTANDING ANY FAILURE OF ESSENTIAL PURPOSE OF ANY LIMITED REMEDY PROVIDED HEREIN.

#### 8. Limitations

**8. 1. BOOKS ONLY:** Where '**reuse in a dissertation/thesis**' has been selected the following terms apply: Print rights of the final author's accepted manuscript (for clarity, NOT the published version) for up to 100 copies, electronic rights for use only on a personal website or institutional repository as defined by the Sherpa guideline ([www.sherpa.ac.uk/romeo/](http://www.sherpa.ac.uk/romeo/)).

**9. Termination and Cancellation**

- 9. 1.** Licences will expire after the period shown in Clause 3 (above).
- 9. 2.** Licensee reserves the right to terminate the Licence in the event that payment is not received in full or if there has been a breach of this agreement by you.

**Appendix 1 – Acknowledgements:****For Journal Content:**

Reprinted by permission from [the Licensor]: [Journal Publisher (e.g. Nature/Springer/Palgrave)] [JOURNAL NAME] [REFERENCE CITATION (Article name, Author(s) Name), [COPYRIGHT] (year of publication)

**For Advance Online Publication papers:**

Reprinted by permission from [the Licensor]: [Journal Publisher (e.g. Nature/Springer/Palgrave)] [JOURNAL NAME] [REFERENCE CITATION (Article name, Author(s) Name), [COPYRIGHT] (year of publication), advance online publication, day month year (doi: 10.1038/sj.[JOURNAL ACRONYM].)

**For Adaptations/Translations:**

Adapted/Translated by permission from [the Licensor]: [Journal Publisher (e.g. Nature/Springer/Palgrave)] [JOURNAL NAME] [REFERENCE CITATION (Article name, Author(s) Name), [COPYRIGHT] (year of publication)

**Note: For any republication from the British Journal of Cancer, the following credit line style applies:**

Reprinted/adapted/translated by permission from [the Licensor]: on behalf of Cancer Research UK: : [Journal Publisher (e.g. Nature/Springer/Palgrave)] [JOURNAL NAME] [REFERENCE CITATION (Article name, Author(s) Name), [COPYRIGHT] (year of publication)

**For Advance Online Publication papers:**

Reprinted by permission from The [the Licensor]: on behalf of Cancer Research UK: [Journal Publisher (e.g. Nature/Springer/Palgrave)] [JOURNAL NAME] [REFERENCE CITATION (Article name, Author(s) Name), [COPYRIGHT] (year of publication), advance online publication, day month year (doi: 10.1038/sj.[JOURNAL ACRONYM])

**For Book content:**

Reprinted/adapted by permission from [the Licensor]: [Book Publisher (e.g. Palgrave Macmillan, Springer etc) [Book Title] by [Book author(s)] [COPYRIGHT] (year of publication)

**Other Conditions:**

Version 1.2

Questions? [customer@copyright.com](mailto:customer@copyright.com) or +1-855-239-3415 (toll free in the US) or +1-978-646-2777.





**JOHN WILEY AND SONS LICENSE  
TERMS AND CONDITIONS**

Jun 29, 2019

---

This Agreement between Imperial College London -- Anabela Areias ("You") and John Wiley and Sons ("John Wiley and Sons") consists of your license details and the terms and conditions provided by John Wiley and Sons and Copyright Clearance Center.

License Number	4616161385767
License date	Jun 25, 2019
Licensed Content Publisher	John Wiley and Sons
Licensed Content Publication	Cell Proliferation
Licensed Content Title	Mechanical compressive force inhibits adipogenesis of adipose stem cells
Licensed Content Author	Y. Lin, X. Cai, Y. Yao, et al
Licensed Content Date	Aug 29, 2013
Licensed Content Volume	46
Licensed Content Issue	5
Licensed Content Pages	9
Type of use	Dissertation/Thesis
Requestor type	University/Academic
Format	Electronic
Portion	Figure/table
Number of figures/tables	1
Original Wiley figure/table number(s)	Figure 1
Will you be translating?	No
Title of your thesis / dissertation	Mechanobiology of adipocytes
Expected completion date	Aug 2019
Expected size (number of pages)	1
Requestor Location	Imperial College London South Kensington Campus Prince Consort Road  London, SW7 2AZ United Kingdom Attn: Anabela Areias
Publisher Tax ID	EU826007151
Total	0.00 GBP
Terms and Conditions	

**TERMS AND CONDITIONS**

This copyrighted material is owned by or exclusively licensed to John Wiley & Sons, Inc. or one of its group companies (each a "Wiley Company") or handled on behalf of a society with which a Wiley Company has exclusive publishing rights in relation to a particular work

(collectively "WILEY"). By clicking "accept" in connection with completing this licensing transaction, you agree that the following terms and conditions apply to this transaction (along with the billing and payment terms and conditions established by the Copyright Clearance Center Inc., ("CCC's Billing and Payment terms and conditions"), at the time that you opened your RightsLink account (these are available at any time at <http://myaccount.copyright.com>).

### Terms and Conditions

- The materials you have requested permission to reproduce or reuse (the "Wiley Materials") are protected by copyright.
- You are hereby granted a personal, non-exclusive, non-sub licensable (on a stand-alone basis), non-transferable, worldwide, limited license to reproduce the Wiley Materials for the purpose specified in the licensing process. This license, **and any CONTENT (PDF or image file) purchased as part of your order**, is for a one-time use only and limited to any maximum distribution number specified in the license. The first instance of republication or reuse granted by this license must be completed within two years of the date of the grant of this license (although copies prepared before the end date may be distributed thereafter). The Wiley Materials shall not be used in any other manner or for any other purpose, beyond what is granted in the license. Permission is granted subject to an appropriate acknowledgement given to the author, title of the material/book/journal and the publisher. You shall also duplicate the copyright notice that appears in the Wiley publication in your use of the Wiley Material. Permission is also granted on the understanding that nowhere in the text is a previously published source acknowledged for all or part of this Wiley Material. Any third party content is expressly excluded from this permission.
- With respect to the Wiley Materials, all rights are reserved. Except as expressly granted by the terms of the license, no part of the Wiley Materials may be copied, modified, adapted (except for minor reformatting required by the new Publication), translated, reproduced, transferred or distributed, in any form or by any means, and no derivative works may be made based on the Wiley Materials without the prior permission of the respective copyright owner. **For STM Signatory Publishers clearing permission under the terms of the [STM Permissions Guidelines](#) only, the terms of the license are extended to include subsequent editions and for editions in other languages, provided such editions are for the work as a whole in situ and does not involve the separate exploitation of the permitted figures or extracts**, You may not alter, remove or suppress in any manner any copyright, trademark or other notices displayed by the Wiley Materials. You may not license, rent, sell, loan, lease, pledge, offer as security, transfer or assign the Wiley Materials on a stand-alone basis, or any of the rights granted to you hereunder to any other person.
- The Wiley Materials and all of the intellectual property rights therein shall at all times remain the exclusive property of John Wiley & Sons Inc, the Wiley Companies, or their respective licensors, and your interest therein is only that of having possession of and the right to reproduce the Wiley Materials pursuant to Section 2 herein during the continuance of this Agreement. You agree that you own no right, title or interest in or to the Wiley Materials or any of the intellectual property rights therein. You shall have no rights hereunder other than the license as provided for above in Section 2. No right, license or interest to any trademark, trade name, service mark or other branding ("Marks") of WILEY or its licensors is granted hereunder, and you agree that you shall not assert any such right, license or interest with respect thereto

- NEITHER WILEY NOR ITS LICENSORS MAKES ANY WARRANTY OR REPRESENTATION OF ANY KIND TO YOU OR ANY THIRD PARTY, EXPRESS, IMPLIED OR STATUTORY, WITH RESPECT TO THE MATERIALS OR THE ACCURACY OF ANY INFORMATION CONTAINED IN THE MATERIALS, INCLUDING, WITHOUT LIMITATION, ANY IMPLIED WARRANTY OF MERCHANTABILITY, ACCURACY, SATISFACTORY QUALITY, FITNESS FOR A PARTICULAR PURPOSE, USABILITY, INTEGRATION OR NON-INFRINGEMENT AND ALL SUCH WARRANTIES ARE HEREBY EXCLUDED BY WILEY AND ITS LICENSORS AND WAIVED BY YOU.
- WILEY shall have the right to terminate this Agreement immediately upon breach of this Agreement by you.
- You shall indemnify, defend and hold harmless WILEY, its Licensors and their respective directors, officers, agents and employees, from and against any actual or threatened claims, demands, causes of action or proceedings arising from any breach of this Agreement by you.
- IN NO EVENT SHALL WILEY OR ITS LICENSORS BE LIABLE TO YOU OR ANY OTHER PARTY OR ANY OTHER PERSON OR ENTITY FOR ANY SPECIAL, CONSEQUENTIAL, INCIDENTAL, INDIRECT, EXEMPLARY OR PUNITIVE DAMAGES, HOWEVER CAUSED, ARISING OUT OF OR IN CONNECTION WITH THE DOWNLOADING, PROVISIONING, VIEWING OR USE OF THE MATERIALS REGARDLESS OF THE FORM OF ACTION, WHETHER FOR BREACH OF CONTRACT, BREACH OF WARRANTY, TORT, NEGLIGENCE, INFRINGEMENT OR OTHERWISE (INCLUDING, WITHOUT LIMITATION, DAMAGES BASED ON LOSS OF PROFITS, DATA, FILES, USE, BUSINESS OPPORTUNITY OR CLAIMS OF THIRD PARTIES), AND WHETHER OR NOT THE PARTY HAS BEEN ADVISED OF THE POSSIBILITY OF SUCH DAMAGES. THIS LIMITATION SHALL APPLY NOTWITHSTANDING ANY FAILURE OF ESSENTIAL PURPOSE OF ANY LIMITED REMEDY PROVIDED HEREIN.
- Should any provision of this Agreement be held by a court of competent jurisdiction to be illegal, invalid, or unenforceable, that provision shall be deemed amended to achieve as nearly as possible the same economic effect as the original provision, and the legality, validity and enforceability of the remaining provisions of this Agreement shall not be affected or impaired thereby.
- The failure of either party to enforce any term or condition of this Agreement shall not constitute a waiver of either party's right to enforce each and every term and condition of this Agreement. No breach under this agreement shall be deemed waived or excused by either party unless such waiver or consent is in writing signed by the party granting such waiver or consent. The waiver by or consent of a party to a breach of any provision of this Agreement shall not operate or be construed as a waiver of or consent to any other or subsequent breach by such other party.
- This Agreement may not be assigned (including by operation of law or otherwise) by you without WILEY's prior written consent.
- Any fee required for this permission shall be non-refundable after thirty (30) days from receipt by the CCC.

- These terms and conditions together with CCC's Billing and Payment terms and conditions (which are incorporated herein) form the entire agreement between you and WILEY concerning this licensing transaction and (in the absence of fraud) supersedes all prior agreements and representations of the parties, oral or written. This Agreement may not be amended except in writing signed by both parties. This Agreement shall be binding upon and inure to the benefit of the parties' successors, legal representatives, and authorized assigns.
- In the event of any conflict between your obligations established by these terms and conditions and those established by CCC's Billing and Payment terms and conditions, these terms and conditions shall prevail.
- WILEY expressly reserves all rights not specifically granted in the combination of (i) the license details provided by you and accepted in the course of this licensing transaction, (ii) these terms and conditions and (iii) CCC's Billing and Payment terms and conditions.
- This Agreement will be void if the Type of Use, Format, Circulation, or Requestor Type was misrepresented during the licensing process.
- This Agreement shall be governed by and construed in accordance with the laws of the State of New York, USA, without regards to such state's conflict of law rules. Any legal action, suit or proceeding arising out of or relating to these Terms and Conditions or the breach thereof shall be instituted in a court of competent jurisdiction in New York County in the State of New York in the United States of America and each party hereby consents and submits to the personal jurisdiction of such court, waives any objection to venue in such court and consents to service of process by registered or certified mail, return receipt requested, at the last known address of such party.

#### **WILEY OPEN ACCESS TERMS AND CONDITIONS**

Wiley Publishes Open Access Articles in fully Open Access Journals and in Subscription journals offering Online Open. Although most of the fully Open Access journals publish open access articles under the terms of the Creative Commons Attribution (CC BY) License only, the subscription journals and a few of the Open Access Journals offer a choice of Creative Commons Licenses. The license type is clearly identified on the article.

##### **The Creative Commons Attribution License**

The [Creative Commons Attribution License \(CC-BY\)](#) allows users to copy, distribute and transmit an article, adapt the article and make commercial use of the article. The CC-BY license permits commercial and non-

##### **Creative Commons Attribution Non-Commercial License**

The [Creative Commons Attribution Non-Commercial \(CC-BY-NC\) License](#) permits use, distribution and reproduction in any medium, provided the original work is properly cited and is not used for commercial purposes. (see below)

##### **Creative Commons Attribution-Non-Commercial-NoDerivs License**

The [Creative Commons Attribution Non-Commercial-NoDerivs License \(CC-BY-NC-ND\)](#) permits use, distribution and reproduction in any medium, provided the original work is properly cited, is not used for commercial purposes and no modifications or adaptations are made. (see below)

##### **Use by commercial "for-profit" organizations**

Use of Wiley Open Access articles for commercial, promotional, or marketing purposes requires further explicit permission from Wiley and will be subject to a fee.

6/29/2019

RightsLink Printable License

Further details can be found on Wiley Online Library  
<http://olabout.wiley.com/WileyCDA/Section/id-410895.html>

**Other Terms and Conditions:**

**v1.10 Last updated September 2015**

Questions? [customercare@copyright.com](mailto:customercare@copyright.com) or +1-855-239-3415 (toll free in the US) or  
+1-978-646-2777.

---

---

**JOHN WILEY AND SONS LICENSE  
TERMS AND CONDITIONS**

Jun 29, 2019

---

This Agreement between Imperial College London -- Anabela Areias ("You") and John Wiley and Sons ("John Wiley and Sons") consists of your license details and the terms and conditions provided by John Wiley and Sons and Copyright Clearance Center.

License Number	4616170650637
License date	Jun 25, 2019
Licensed Content Publisher	John Wiley and Sons
Licensed Content Publication	Journal of Pathology
Licensed Content Title	Human adipocyte function is impacted by mechanical cues
Licensed Content Author	K Clément, D Lacasa, E Clément, et al
Licensed Content Date	May 14, 2014
Licensed Content Volume	233
Licensed Content Issue	2
Licensed Content Pages	13
Type of use	Dissertation/Thesis
Requestor type	University/Academic
Format	Electronic
Portion	Figure/table
Number of figures/tables	1
Original Wiley figure/table number(s)	Supplementary figure 2
Will you be translating?	No
Title of your thesis / dissertation	Mechanobiology of adipocytes
Expected completion date	Aug 2019
Expected size (number of pages)	1
Requestor Location	Imperial College London South Kensington Campus Prince Consort Road  London, SW7 2AZ United Kingdom Attn: Anabela Areias
Publisher Tax ID	EU826007151
Total	0.00 GBP
Terms and Conditions	

**TERMS AND CONDITIONS**

This copyrighted material is owned by or exclusively licensed to John Wiley & Sons, Inc. or one of its group companies (each a "Wiley Company") or handled on behalf of a society with which a Wiley Company has exclusive publishing rights in relation to a particular work

(collectively "WILEY"). By clicking "accept" in connection with completing this licensing transaction, you agree that the following terms and conditions apply to this transaction (along with the billing and payment terms and conditions established by the Copyright Clearance Center Inc., ("CCC's Billing and Payment terms and conditions"), at the time that you opened your RightsLink account (these are available at any time at <http://myaccount.copyright.com>).

### Terms and Conditions

- The materials you have requested permission to reproduce or reuse (the "Wiley Materials") are protected by copyright.
- You are hereby granted a personal, non-exclusive, non-sub licensable (on a stand-alone basis), non-transferable, worldwide, limited license to reproduce the Wiley Materials for the purpose specified in the licensing process. This license, **and any CONTENT (PDF or image file) purchased as part of your order**, is for a one-time use only and limited to any maximum distribution number specified in the license. The first instance of republication or reuse granted by this license must be completed within two years of the date of the grant of this license (although copies prepared before the end date may be distributed thereafter). The Wiley Materials shall not be used in any other manner or for any other purpose, beyond what is granted in the license. Permission is granted subject to an appropriate acknowledgement given to the author, title of the material/book/journal and the publisher. You shall also duplicate the copyright notice that appears in the Wiley publication in your use of the Wiley Material. Permission is also granted on the understanding that nowhere in the text is a previously published source acknowledged for all or part of this Wiley Material. Any third party content is expressly excluded from this permission.
- With respect to the Wiley Materials, all rights are reserved. Except as expressly granted by the terms of the license, no part of the Wiley Materials may be copied, modified, adapted (except for minor reformatting required by the new Publication), translated, reproduced, transferred or distributed, in any form or by any means, and no derivative works may be made based on the Wiley Materials without the prior permission of the respective copyright owner. **For STM Signatory Publishers clearing permission under the terms of the [STM Permissions Guidelines](#) only, the terms of the license are extended to include subsequent editions and for editions in other languages, provided such editions are for the work as a whole in situ and does not involve the separate exploitation of the permitted figures or extracts**, You may not alter, remove or suppress in any manner any copyright, trademark or other notices displayed by the Wiley Materials. You may not license, rent, sell, loan, lease, pledge, offer as security, transfer or assign the Wiley Materials on a stand-alone basis, or any of the rights granted to you hereunder to any other person.
- The Wiley Materials and all of the intellectual property rights therein shall at all times remain the exclusive property of John Wiley & Sons Inc, the Wiley Companies, or their respective licensors, and your interest therein is only that of having possession of and the right to reproduce the Wiley Materials pursuant to Section 2 herein during the continuance of this Agreement. You agree that you own no right, title or interest in or to the Wiley Materials or any of the intellectual property rights therein. You shall have no rights hereunder other than the license as provided for above in Section 2. No right, license or interest to any trademark, trade name, service mark or other branding ("Marks") of WILEY or its licensors is granted hereunder, and you agree that you shall not assert any such right, license or interest with respect thereto



- NEITHER WILEY NOR ITS LICENSORS MAKES ANY WARRANTY OR REPRESENTATION OF ANY KIND TO YOU OR ANY THIRD PARTY, EXPRESS, IMPLIED OR STATUTORY, WITH RESPECT TO THE MATERIALS OR THE ACCURACY OF ANY INFORMATION CONTAINED IN THE MATERIALS, INCLUDING, WITHOUT LIMITATION, ANY IMPLIED WARRANTY OF MERCHANTABILITY, ACCURACY, SATISFACTORY QUALITY, FITNESS FOR A PARTICULAR PURPOSE, USABILITY, INTEGRATION OR NON-INFRINGEMENT AND ALL SUCH WARRANTIES ARE HEREBY EXCLUDED BY WILEY AND ITS LICENSORS AND WAIVED BY YOU.
- WILEY shall have the right to terminate this Agreement immediately upon breach of this Agreement by you.
- You shall indemnify, defend and hold harmless WILEY, its Licensors and their respective directors, officers, agents and employees, from and against any actual or threatened claims, demands, causes of action or proceedings arising from any breach of this Agreement by you.
- IN NO EVENT SHALL WILEY OR ITS LICENSORS BE LIABLE TO YOU OR ANY OTHER PARTY OR ANY OTHER PERSON OR ENTITY FOR ANY SPECIAL, CONSEQUENTIAL, INCIDENTAL, INDIRECT, EXEMPLARY OR PUNITIVE DAMAGES, HOWEVER CAUSED, ARISING OUT OF OR IN CONNECTION WITH THE DOWNLOADING, PROVISIONING, VIEWING OR USE OF THE MATERIALS REGARDLESS OF THE FORM OF ACTION, WHETHER FOR BREACH OF CONTRACT, BREACH OF WARRANTY, TORT, NEGLIGENCE, INFRINGEMENT OR OTHERWISE (INCLUDING, WITHOUT LIMITATION, DAMAGES BASED ON LOSS OF PROFITS, DATA, FILES, USE, BUSINESS OPPORTUNITY OR CLAIMS OF THIRD PARTIES), AND WHETHER OR NOT THE PARTY HAS BEEN ADVISED OF THE POSSIBILITY OF SUCH DAMAGES. THIS LIMITATION SHALL APPLY NOTWITHSTANDING ANY FAILURE OF ESSENTIAL PURPOSE OF ANY LIMITED REMEDY PROVIDED HEREIN.
- Should any provision of this Agreement be held by a court of competent jurisdiction to be illegal, invalid, or unenforceable, that provision shall be deemed amended to achieve as nearly as possible the same economic effect as the original provision, and the legality, validity and enforceability of the remaining provisions of this Agreement shall not be affected or impaired thereby.
- The failure of either party to enforce any term or condition of this Agreement shall not constitute a waiver of either party's right to enforce each and every term and condition of this Agreement. No breach under this agreement shall be deemed waived or excused by either party unless such waiver or consent is in writing signed by the party granting such waiver or consent. The waiver by or consent of a party to a breach of any provision of this Agreement shall not operate or be construed as a waiver of or consent to any other or subsequent breach by such other party.
- This Agreement may not be assigned (including by operation of law or otherwise) by you without WILEY's prior written consent.
- Any fee required for this permission shall be non-refundable after thirty (30) days from receipt by the CCC.

- These terms and conditions together with CCC's Billing and Payment terms and conditions (which are incorporated herein) form the entire agreement between you and WILEY concerning this licensing transaction and (in the absence of fraud) supersedes all prior agreements and representations of the parties, oral or written. This Agreement may not be amended except in writing signed by both parties. This Agreement shall be binding upon and inure to the benefit of the parties' successors, legal representatives, and authorized assigns.
- In the event of any conflict between your obligations established by these terms and conditions and those established by CCC's Billing and Payment terms and conditions, these terms and conditions shall prevail.
- WILEY expressly reserves all rights not specifically granted in the combination of (i) the license details provided by you and accepted in the course of this licensing transaction, (ii) these terms and conditions and (iii) CCC's Billing and Payment terms and conditions.
- This Agreement will be void if the Type of Use, Format, Circulation, or Requestor Type was misrepresented during the licensing process.
- This Agreement shall be governed by and construed in accordance with the laws of the State of New York, USA, without regards to such state's conflict of law rules. Any legal action, suit or proceeding arising out of or relating to these Terms and Conditions or the breach thereof shall be instituted in a court of competent jurisdiction in New York County in the State of New York in the United States of America and each party hereby consents and submits to the personal jurisdiction of such court, waives any objection to venue in such court and consents to service of process by registered or certified mail, return receipt requested, at the last known address of such party.

#### **WILEY OPEN ACCESS TERMS AND CONDITIONS**

Wiley Publishes Open Access Articles in fully Open Access Journals and in Subscription journals offering Online Open. Although most of the fully Open Access journals publish open access articles under the terms of the Creative Commons Attribution (CC BY) License only, the subscription journals and a few of the Open Access Journals offer a choice of Creative Commons Licenses. The license type is clearly identified on the article.

##### **The Creative Commons Attribution License**

The [Creative Commons Attribution License \(CC-BY\)](#) allows users to copy, distribute and transmit an article, adapt the article and make commercial use of the article. The CC-BY license permits commercial and non-

##### **Creative Commons Attribution Non-Commercial License**

The [Creative Commons Attribution Non-Commercial \(CC-BY-NC\) License](#) permits use, distribution and reproduction in any medium, provided the original work is properly cited and is not used for commercial purposes.(see below)

##### **Creative Commons Attribution-Non-Commercial-NoDerivs License**

The [Creative Commons Attribution Non-Commercial-NoDerivs License \(CC-BY-NC-ND\)](#) permits use, distribution and reproduction in any medium, provided the original work is properly cited, is not used for commercial purposes and no modifications or adaptations are made. (see below)

##### **Use by commercial "for-profit" organizations**

Use of Wiley Open Access articles for commercial, promotional, or marketing purposes requires further explicit permission from Wiley and will be subject to a fee.

6/29/2019

RightsLink Printable License

Further details can be found on Wiley Online Library  
<http://olabout.wiley.com/WileyCDA/Section/id-410895.html>

**Other Terms and Conditions:**

**v1.10 Last updated September 2015**

Questions? [customercare@copyright.com](mailto:customercare@copyright.com) or +1-855-239-3415 (toll free in the US) or  
+1-978-646-2777.

---

---

<b>SPRINGER NATURE LICENSE TERMS AND CONDITIONS</b>	
Jun 29, 2019	
<p>This Agreement between Imperial College London -- Anabela Areias ("You") and Springer Nature ("Springer Nature") consists of your license details and the terms and conditions provided by Springer Nature and Copyright Clearance Center.</p>	
License Number	4618141148050
License date	Jun 29, 2019
Licensed Content Publisher	Springer Nature
Licensed Content Publication	Nature
Licensed Content Title	The different shades of fat
Licensed Content Author	Vivian Peirce, Stefania Carobbio, Antonio Vidal-Puig
Licensed Content Date	Jun 4, 2014
Licensed Content Volume	510
Licensed Content Issue	7503
Type of Use	Thesis/Dissertation
Requestor type	academic/university or research institute
Format	electronic
Portion	figures/tables/illustrations
Number of figures/tables/illustrations	1
High-res required	no
Will you be translating?	no
Circulation/distribution	<501
Author of this Springer Nature content	no
Title	Mechanobiology of adipocytes
Institution name	Imperial College London
Expected presentation date	Aug 2019
Portions	Figure 4
Requestor Location	Imperial College London South Kensington Campus Prince Consort Road  London, SW7 2AZ United Kingdom Attn: Anabela Areias
Total	0.00 GBP
Terms and Conditions	

## Springer Nature Customer Service Centre GmbH Terms and Conditions

This agreement sets out the terms and conditions of the licence (the **Licence**) between you and **Springer Nature Customer Service Centre GmbH** (the **Licensor**). By clicking 'accept' and completing the transaction for the material (**Licensed Material**), you also confirm your acceptance of these terms and conditions.

### 1. Grant of Licence

- 1. 1.** The Licensor grants you a personal, non-exclusive, non-transferable, world-wide licence to reproduce the Licensed Material for the purpose specified in your order only. Licences are granted for the specific use requested in the order and for no other use, subject to the conditions below.
- 1. 2.** The Licensor warrants that it has, to the best of its knowledge, the rights to license reuse of the Licensed Material. However, you should ensure that the material you are requesting is original to the Licensor and does not carry the copyright of another entity (as credited in the published version).
- 1. 3.** If the credit line on any part of the material you have requested indicates that it was reprinted or adapted with permission from another source, then you should also seek permission from that source to reuse the material.

### 2. Scope of Licence

- 2. 1.** You may only use the Licensed Content in the manner and to the extent permitted by these Ts&Cs and any applicable laws.
- 2. 2.** A separate licence may be required for any additional use of the Licensed Material, e.g. where a licence has been purchased for print only use, separate permission must be obtained for electronic re-use. Similarly, a licence is only valid in the language selected and does not apply for editions in other languages unless additional translation rights have been granted separately in the licence. Any content owned by third parties are expressly excluded from the licence.
- 2. 3.** Similarly, rights for additional components such as custom editions and derivatives require additional permission and may be subject to an additional fee. Please apply to [Journalpermissions@springernature.com](mailto:Journalpermissions@springernature.com)/[bookpermissions@springernature.com](mailto:bookpermissions@springernature.com) for these rights.
- 2. 4.** Where permission has been granted **free of charge** for material in print, permission may also be granted for any electronic version of that work, provided that the material is incidental to your work as a whole and that the electronic version is essentially equivalent to, or substitutes for, the print version.
- 2. 5.** An alternative scope of licence may apply to signatories of the [STM Permissions Guidelines](#), as amended from time to time.

### 3. Duration of Licence

- 3. 1.** A licence for is valid from the date of purchase ('Licence Date') at the end of the relevant period in the below table:

Scope of Licence	Duration of Licence
Post on a website	12 months
Presentations	12 months
Books and journals	Lifetime of the edition in the language purchased

#### 4. Acknowledgement

**4. 1.** The Licensor's permission must be acknowledged next to the Licenced Material in print. In electronic form, this acknowledgement must be visible at the same time as the figures/tables/illustrations or abstract, and must be hyperlinked to the journal/book's homepage. Our required acknowledgement format is in the Appendix below.

#### 5. Restrictions on use

**5. 1.** Use of the Licensed Material may be permitted for incidental promotional use and minor editing privileges e.g. minor adaptations of single figures, changes of format, colour and/or style where the adaptation is credited as set out in Appendix 1 below. Any other changes including but not limited to, cropping, adapting, omitting material that affect the meaning, intention or moral rights of the author are strictly prohibited.

**5. 2.** You must not use any Licensed Material as part of any design or trademark.

**5. 3.** Licensed Material may be used in Open Access Publications (OAP) before publication by Springer Nature, but any Licensed Material must be removed from OAP sites prior to final publication.

#### 6. Ownership of Rights

**6. 1.** Licensed Material remains the property of either Licensor or the relevant third party and any rights not explicitly granted herein are expressly reserved.

#### 7. Warranty

IN NO EVENT SHALL LICENSOR BE LIABLE TO YOU OR ANY OTHER PARTY OR ANY OTHER PERSON OR FOR ANY SPECIAL, CONSEQUENTIAL, INCIDENTAL OR INDIRECT DAMAGES, HOWEVER CAUSED, ARISING OUT OF OR IN CONNECTION WITH THE DOWNLOADING, VIEWING OR USE OF THE MATERIALS REGARDLESS OF THE FORM OF ACTION, WHETHER FOR BREACH OF CONTRACT, BREACH OF WARRANTY, TORT, NEGLIGENCE, INFRINGEMENT OR OTHERWISE (INCLUDING, WITHOUT LIMITATION, DAMAGES BASED ON LOSS OF PROFITS, DATA, FILES, USE, BUSINESS OPPORTUNITY OR CLAIMS OF THIRD PARTIES), AND WHETHER OR NOT THE PARTY HAS BEEN ADVISED OF THE POSSIBILITY OF SUCH DAMAGES. THIS LIMITATION SHALL APPLY NOTWITHSTANDING ANY FAILURE OF ESSENTIAL PURPOSE OF ANY LIMITED REMEDY PROVIDED HEREIN.

#### 8. Limitations

**8. 1. BOOKS ONLY:** Where '**reuse in a dissertation/thesis**' has been selected the following terms apply: Print rights of the final author's accepted manuscript (for clarity, NOT the published version) for up to 100 copies, electronic rights for use only on a personal website or institutional repository as defined by the Sherpa guideline ([www.sherpa.ac.uk/romeo/](http://www.sherpa.ac.uk/romeo/)).

**9. Termination and Cancellation**

- 9. 1.** Licences will expire after the period shown in Clause 3 (above).
- 9. 2.** Licensee reserves the right to terminate the Licence in the event that payment is not received in full or if there has been a breach of this agreement by you.

**Appendix 1 – Acknowledgements:****For Journal Content:**

Reprinted by permission from [the Licensor]: [Journal Publisher (e.g. Nature/Springer/Palgrave)] [JOURNAL NAME] [REFERENCE CITATION (Article name, Author(s) Name), [COPYRIGHT] (year of publication)

**For Advance Online Publication papers:**

Reprinted by permission from [the Licensor]: [Journal Publisher (e.g. Nature/Springer/Palgrave)] [JOURNAL NAME] [REFERENCE CITATION (Article name, Author(s) Name), [COPYRIGHT] (year of publication), advance online publication, day month year (doi: 10.1038/sj.[JOURNAL ACRONYM].)

**For Adaptations/Translations:**

Adapted/Translated by permission from [the Licensor]: [Journal Publisher (e.g. Nature/Springer/Palgrave)] [JOURNAL NAME] [REFERENCE CITATION (Article name, Author(s) Name), [COPYRIGHT] (year of publication)

**Note: For any republication from the British Journal of Cancer, the following credit line style applies:**

Reprinted/adapted/translated by permission from [the Licensor]: on behalf of Cancer Research UK: : [Journal Publisher (e.g. Nature/Springer/Palgrave)] [JOURNAL NAME] [REFERENCE CITATION (Article name, Author(s) Name), [COPYRIGHT] (year of publication)

**For Advance Online Publication papers:**

Reprinted by permission from The [the Licensor]: on behalf of Cancer Research UK: [Journal Publisher (e.g. Nature/Springer/Palgrave)] [JOURNAL NAME] [REFERENCE CITATION (Article name, Author(s) Name), [COPYRIGHT] (year of publication), advance online publication, day month year (doi: 10.1038/sj.[JOURNAL ACRONYM].)

**For Book content:**

Reprinted/adapted by permission from [the Licensor]: [Book Publisher (e.g. Palgrave Macmillan, Springer etc) [Book Title] by [Book author(s)] [COPYRIGHT] (year of publication)

**Other Conditions:**

Version 1.2

Questions? [customercare@copyright.com](mailto:customercare@copyright.com) or +1-855-239-3415 (toll free in the US) or +1-978-646-2777.

